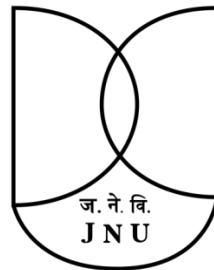


RECONSTRUCTING PALAEOCLIMATE OF LOWER BAITARANI BASIN, ODISHA

*Thesis submitted to the Jawaharlal Nehru University
in partial fulfillment of the requirement
for the award of the degree of*

DOCTOR OF PHILOSOPHY

UZMA PARVEEN



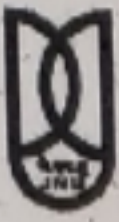
Centre for the Study of Regional Development

School of Social Sciences

Jawaharlal Nehru University

New Delhi-110067

2019



जवाहरलाल नेहरू विश्वविद्यालय
JAWAHARLAL NEHRU UNIVERSITY
Centre for the Study of Regional Development
School of Social Sciences
New Delhi-110067

DECLARATION

This is to certify that the thesis entitled "RECONSTRUCTING PALAEOCLIMATE OF LOWER BAITARANI BASIN, ODISHA" is my bonafide work for the degree of DOCTOR OF PHILOSOPHY and may be placed before the examiners for evaluation.

UZMA PARVEEN

Date: 15-07-2019


FORWARDED BY

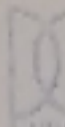
We recommend that thesis be placed the examiners for evaluation.

Dr. S. Sreekesh
(Supervisor)

15.07.19

Prof. Sachidanand Sinha
(Chairperson)

 Centre for the Study of Reg. Dev.
School of Social Sciences
Jawaharlal Nehru University
New Delhi - 110067

 Chairperson
Centre for the Study of Reg. Dev.
School of Social Sciences
Jawaharlal Nehru University
New Delhi - 110067

To My Lovely Family

Acknowledgments

This journey was never possible in the absence of valuable guidance and encouragement of my supervisor Dr. S. Sreekesh. He has always been very helpful and guided me in the right direction. I am not audacious enough to thank him by words. I am also deeply indebted to him for insightful supervision, constructive criticism, generous support and piece of advice throughout the work.

I would also like to thank all the faculty members and especially to Prof. Sachidanad Sinha, the Chairperson of the Centre for the Study of Regional Development for helping with all the facilities required for the present work. I also extend my sincere thanks to Prof. Milap Chand Sharma for his support. I am also very grateful to Prof. B.S. Butola for his encouraging words. I would also like to thank and Dr. Bikramaditya Chaudhary for boosting me since the graduation time.

This research would never have taken its true form in the absence of radiocarbon dates. For this I am very thankful to Dr. Sundeep Chopra, Scientist H, Dr. Pankaj Kumar, Research Scientist and Dr. Mukherji, Scientist, Inter-University Acceleration Centre (IUAC), New Delhi for giving permission for radiocarbon ¹⁴C dating using Accelerator Mass Facility. I will always be indebted to them for continuous help and supervision throughout the laboratory work as well as afterwards.

I am also very grateful to Mr. Sandeep Sarpal, Instruments in-charge, Advance Instrumentation Research Facility, (AIRF), Jawaharlal Nehru University, for his valuable support in sample preparation and analysis of sediment geochemistry using Energy Dispersive X-ray Fluorescence (EDXRF).

Many thanks to Prof. P. Raha, Laboratory in-charge Soil and Agricultural Science Institute, Banaras Hindu University, Varanasi, for allowing me to use the lab facilities for sediment carbon content determination. I would also

like to thank Mr. Sharma, Mr. Pathak for their help, support and approval during the TOC analysis at the lab.

This work would have not been contextualized in the absence of sub-surface sediment samples. For this, I will always be indebted to Sudama dada, Surendra dada, ajpur, Odisha, for assisting me with data collection through Borewelling. I would also like to thank Madan Dada, Ekan dada, and Madik data for digging trench for sample collection.

Let me also extend my gratitude my seniors, Dr. Kaushik Ghosh, Assistant Professor, Vidyasagar University and Dr. Prasenjit Acharya, Assistant Professor, Vidyasagar University for their continuous backing and advice throughout the research. I am also very thankful to all my dear friends and specially Nupoor, Padmaja, Anita, Shweta, Sonam di, Ratnesh and Divya for being major source of inspiration throughout this work. They have kept my spirit high and made this journey enriching. I thank each of them for every single thing they have done for me. I have also taken help of lots of workshops in order to carry this analysis. Hence, I am also grateful to the organizers of Geoscience Workshop and Paleo-link Workshop to provide crucial informations related to the field of geology and palaeoclimate. I am also equally thankful to Dr. Sebastian Wegner and Dr. Juan Jose Gomez Navarro for their instruction related to palaeoclimatic reconstructions.

Last but never the least; I would love to express my deep appreciation and affection to my lovely family. My Ph.D has been a dream of my father, Mohd. Murtuza. I am always grateful to him for his unconditional love and support that helped me materializing this research work. Many thanks to my mother Nasibun Nisha, who has always been a spiritual and health guide to me. I would also love to acknowledge my regards to my brainy sisters Nazia and Heena, brothers Danish and Sadique, who have always extended their unconditional support and boosted me up.

I am also very much grateful to ones who have played their special role in the most exemplar manner and contributed in this work directly or indirectly.

Date

UZMA PARVEEN

TABLE OF CONTENTS

Certificate

Acknowledgment

List of Figures

List of Tables

List of Plates

List of Abbreviations

Chapter 1 Introduction.....	1-41
1.1 Introduction.....	1
1.2 Literature Review.....	4
1.3 Rationale of the Study.....	25
1.4 Research Questions.....	25
1.5 Objectives.....	26
1.6 Data Base.....	26
1.7 Methodology.....	27
1.7.1 Sample collection and Pre-treatment.....	27
1.7.2 Colour and Textural Analysis.....	29
1.7.3 Geochemical Analysis.....	29
1.7.4 Total Organic Carbon (TOC).....	29
1.7.5 Geochronology.....	30
1.7.6 Geochemical Proxies.....	31
1.8 Area of Study.....	31
1.8.1 Geology and Stratigraphy.....	33
1.8.2 Physiography.....	35
1.8.3 Climate and Drainage.....	37
1.8.4 Soil and Vegetation.....	37
1.9 Classification of the Study Area.....	38
1.10 Scheme of Chapterization.....	39

Chapter 2 Physical Characteristics of Sub-Surface Sediments	42-72
2.1 Introduction.....	42
2.2 Methodology	45
2.2.1 Colour Determination	45
2.2.2 Texture Analysis	45
2.3 Analysis.....	48
2.3.1 Colour Determination	48
2.3.2 Textural Classification	53
2.4 Discussion and Conclusion	65
Chapter 3 Geochemical Characteristics of Sub-Surface Sediments	73-134
3.1 Introduction.....	73
3.2 Methodology	76
3.2.1 Concentration of Organic Carbon	76
3.2.2 Concentration of Major, Trace and Rare Earth Elements.....	77
3.2.3 Enrichment Factor (EF)	78
3.3 Analysis.....	80
3.3.1 Concentration of TOC and Major Elements	80
3.3.2 Concentration of selected Trace and Rare Earth Elements (REEs).....	98
3.3.3 Correlation among Major Elements.....	116
3.3.4 Correlation among Trace Elements and REEs.....	125
3.4 Discussion and Conclusion	131
Chapter 4 Assessment of Palaeoredox Environment using Geochemistry. 135-167	
4.1 Introduction.....	135
4.2 Methodology	137
4.3 Analysis.....	138
4.3.1 Variability of Redox-Sensitive Trace Elements	138
4.3.2 Variability of Redox-Sensitive Rare Earth Elements (REEs) and TOC	150
4.3.3 Correlation between TOC and Elemental Ratios.....	160
4.4 Discussion and Conclusion	165

Chapter 5 Chronology of Landforms.....	168-182
5.1 Introduction.....	168
5.2 Methodology	171
5.3 Analysis.....	174
5.3.1 Chronology of the Active Floodplain (SP).....	175
5.3.2 Chronology of the Older Beach Deposits	177
5.3.3 Chronology of the Palaeochannels.....	178
5.4 Discussion and Conclusion	181
Chapter 6 Reconstruction of Palaeoclimate using Geochemical Proxies and AMS	
¹⁴C dating	183-215
6.1 Introduction.....	183
6.2 Methodology	185
6.2.1 Geochemical Proxies	185
6.2.2 Radiocarbon (¹⁴ C) dating	188
6.3 Analysis.....	188
6.3.1 Reconstruction of Palaeoclimate in the Riverine Zone.....	188
6.3.2 Palaeoclimate Reconstruction in the Mixing Zone	199
6.5 Discussion and Conclusion	210
Chapter 7 Summary and Conclusion.....	216-226
7.1. Period of Enhanced Rainfall (till 7700 cal yr BP)	221
7.2 Period of Rainfall Weakening (between 7700 and 4736 cal yr BP)	222
7.3 Period of Enhanced Rainfall (between 4736 and 2700 cal yr BP)	223
7.4 Period of Rainfall weakening (since 2700 cal yr BP).....	224
Bibliography	227-248

LIST OF FIGURES

Figure 1.1 -Scheme of methodology applied in present study.....	27
Figure 1.2 -Location of the sample collection sites	33
Figure 1.3 - Geology and major landforms in area of study	33
Figure 1.4 - Geology and major landforms in area of study	35
Figure 1.5 - Relative height of the sample collection site.....	39
Figure 2.1 Particle size distribution in (a) EPL1, (b) EPL2, (c) EPL3, (d) EPL4, (e) EPL5, (f) EPL6 and (g) EPL7.....	54
Figure 2.2 Particle size distribution in (a) JPL1, (b) JPL2, (c) JPL3, (d) JPL4, (e) JPL5, (f) JPL6, (g) JPL7, (h) JPL8, (i) JPL9, (j) JPL10 and (k) JPL11	56
Figure 2.3 Particle size distribution in (a) KTIL1, (b) KTIL2, (c) KTIL3, (d) KTIL4 and (e) KTIL5.....	58
Figure 2.4 Particle size distribution in (a) KTIL1, (b) KTIL2, (c) KTIL3, (d) KTIL4, (e) KTIL5, (f) KTIL6, (g) KTIL7, (h) KTIL8 and (i) KTIL9.....	59
Figure 2.5 Particle size distribution in (a) SPL1, (b) SP, (c) SPL3, (d) SPL4, (e) SPL5 and (f) SPL6	61
Figure 2.6 Particle size distribution in (a) CBL1, (b) CBL2, (c) CBL3, (d) CBL4, (e) CBL5 and (f)CBL6	63
Figure 2.7 Particle size distribution in (a) AGL1, (b) AGL2, (c) AGL3, (d) AGL4 and (e) AGL5	64
Figure 2.8 Particle size distribution in (a) KKL1, (b) KKL2, (c) KKL3 and (d) KKL4.....	65
Figure 2.9 Facies classification of samples collected from the riverine zone and lateral association	68
Figure 2.10 Facies classification of samples collected from the mixing zone and lateral association	69
Figure 3.1 Concentration of selected major elements in facies of Ezapur.....	81
Figure 3.2 Concentration of selected major elements in facies of Jhumpuri.....	84
Figure 3.3 Concentration of selected major elements in facies of Katia I.....	86
Figure 3.4 Concentration of selected major elements in facies of Katia II.....	88

Figure 3.5 Concentration of selected major elements in facies of Sonpanki.....	91
Figure 3.6 Concentration of selected major elements in facies of Chandbali.....	93
Figure 3.7 Concentration of selected major elements in facies of Ambiligan.....	95
Figure 3.8 Concentration of selected major elements in facies of Kasturikaran	97
Figure 3.9 Concentration of selected trace elements and REEs in facies of Ezapur.....	100
Figure 3.10 Concentration of selected trace elements and REEs in facies of Jhumpuri.....	102
Figure 3.11 Concentration of selected trace elements and REEs in facies of Katia I.....	104
Figure 3.12 Concentration of selected trace elements and REEs in facies of Katia II.....	106
Figure 3.13 Concentration of selected trace elements and REEs in facies of Sonpanki.....	109
Figure 3.14 Concentration of selected trace elements and REEs in facies of Chandbali.....	111
Figure 3.15 Concentration of selected trace elements and REEs in facies of Ambiligan.....	113
Figure 3.16 Concentration of selected trace elements and REEs in facies of Kasturikaran	115
Figure 4.1 Variability of (a)) V/Cr, (b) V/Al (c) Fe/Al (d) Cu/Zn at Ezapur site	139
Figure 4.2 Variability of (a)) V/Cr, (b) V/Al (c) Fe/Al (d) Cu/Zn at Jhumpuri site	142
Figure 4.3 Variability of (a)) V/Cr, (b) V/Al (c) Fe/Al (d) Cu/Zn at Katia I sit	144
Figure 4.4 Variability of (a)) V/Cr, (b) V/Al (c) Fe/Al (d) Cu/Zn at Katia II site	145
Figure 4.5 Variability of (a)) V/Cr, (b) V/Al (c) Fe/Al (d) Cu/Zn at Sonpanki site	147
Figure 4.6 Variability of (a)) V/Cr, (b) V/Al (c) Fe/Al (d) Cu/Zn at Chandbali site	148
Figure 4.7 Variability of (a)) V/Cr, (b) V/Al (c) Fe/Al (d) Cu/Zn at Ambiligan site	149

Figure 4.8 Variability of (a) V/Cr, (b) V/Al (c) Fe/Al (d) Cu/Zn at Kasturikaran site.....	148
Figure 4.9 Variability of selected REEs (ppm) and TOC (%) in facies of Ezapur.....	151
Figure 4.10 Variability of selected REEs (ppm) and TOC (in %) in facies of Jhumpuri.....	152
Figure 4.11 Variability of selected REEs (ppm) in facies of KTI	153
Figure 4.12 Variability of selected REEs (ppm) in facies of KTII.....	154
Figure 4.13 Variability of selected REEs (ppm) and TOC (%) in facies of SP.....	155
Figure 4.14 Variability of selected REEs (ppm) and TOC (%) in CB.....	157
Figure 4.15 Variability of selected REEs (ppm) and TOC (%) in AG.....	158
Figure 4.16 Variability of selected REEs (ppm) and TOC (%) in KK.....	159
Figure 4.17 Correlation of between TOC and (a) V/Cr, b) V/Al (c) Fe/Al, (d) Cu/Zn at Ezapur site	160
Figure 4.18 Correlation of between TOC and (a) V/Cr, b) V/Al (c) Fe/Al, (d) Cu/Zn at Jhumpuri site	160
Figure 4.19 Correlation of between TOC and (a) V/Cr, b) V/Al (c) Fe/Al, (d) Cu/Zn at Katia I site	161
Figure 4.20 Correlation of between TOC and (a) V/Cr, b) V/Al (c) Fe/Al, (d) Cu/Zn at Katia II site	162
Figure 4.21 Correlation of between TOC and (a) V/Cr, b) V/Al (c) Fe/Al, (d) Cu/Zn at Sonpanki site	162
Figure 4.22 Correlation of between TOC and (a) V/Cr, b) V/Al (c) Fe/Al, (d) Cu/Zn at Chandbali site.....	163
Figure 4.23 Correlation of between TOC and (a) V/Cr, b) V/Al (c) Fe/Al, (d) Cu/Zn at Ambiligan site	163
Figure 4.24 Correlation between TOC and (a) V/Cr, b) V/Al (c) Fe/Al, (d) Cu/Zn at Kasturikaran site.....	164
Figure 5.1 Calibration of radiocarbon dates using OxCal 4.3	173
Figure 5.2 Stratigraphy and chronology of landforms (a) Active floodplain, (b) Older beach deposits, (c) Palaeochannel of AG and (d) paleochannel of KK.....	175

Figure 5.3 Lithostratigraph, age-depth curve and concentration of sand, silt and clay in the facies of active floodplain deposits collected from Sonpanki.....	176
Figure 5.4 Lithostratigraph, age-depth curve and concentration of sand, silt and clay in the facies of active floodplain deposits collected from Chandbali.....	178
Figure 5.5 Lithostratigraph, age-depth curve and concentration of sand, silt and clay in the facies of active floodplain deposits collected from Ambiligan.....	179
Figure 5.6 Lithostratigraph, age-depth curve and concentration of sand, silt and clay in the facies of active floodplain deposits collected from Kasturikaran	180
Figure 6.1 Variability in the proxies selected for terrestrial flux at the EP site.....	189
Figure 6.2 Variation in the proxies selected for paleoproductivity at EP site	189
Figure 6.3 Variability in the proxies of weathering and salinity at the EP site	190
Figure 6.4 Variability in the proxies indicating terrestrial flux at JP site	192
Figure 6.5 Variability in the proxies indicating paleoproductivity at JP site.....	193
Figure 6.6 Variability in the proxies indicating weathering and salinity at JP site	194
Figure 6.7 Variability in the proxies indicating terrestrial flux at KTI.....	195
Figure 6.8 Variability in the proxies indicating paleoproductivity at KTI site.....	196
Figure 6.9 Variability in the proxies indicating weathering and salinity at KTI site	196
Figure 6.10 Variability in the proxies indicating terrestrial flux at KTII site	197
Figure 6.11 Variability in the proxies indicating paleoproductivity at KTII site	198
Figure 6.12 Variability in the proxies indicating weathering and salinity at KTII site	198
Figure 6.13 Variability in the proxies indicating terrestrial flux at SP site	200
Figure 6.14 Variability in the proxies indicating paleoproductivity at SP site.....	201
Figure 6.15 Variability in the proxies indicating weathering and salinity at SP site	201
Figure 6.16 Variability in the proxies indicating terrestrial flux at CB site.....	202
Figure 6.17 Variability in the proxies indicating paleoproductivity at CB site	203

Figure 6.18 Variability in the proxies indicating weathering and salinity at CB site	204
Figure 6.19 Variability in the proxies indicating terrestrial flux at AG site	205
Figure 6.20 Variability in the proxies indicating paleoproductivity at AG site.....	206
Figure 6.21 Variability in the proxies indicating weathering and salinity at AG site.....	207
Figure 6.22 Variability in the proxies indicating terrestrial flux at KK site	208
Figure 6.23 Variability in the proxies indicating paleoproductivity at KK site.....	209
Figure 6.24 Variability in the proxies indicating weathering and salinity at KK site.....	209

LIST OF TABLES

Table 1.1 Geological history of the Earth since Cenozoic era	3
Table 1.2 Details of samples collection site in Lower Baitarani basin, Odisha	26
Table 1.3 Major geomorphic regimes and landforms identified in the area of study	40
Table 2.1 Classification of sediment sequences based on particle size	48
Table 2.2 Colour identification of subsurface sediment samples at EP site	49
Table 2.3 Colour identification of subsurface sediment samples at JP site	49
Table 2.4 Colour identification of subsurface sediment samples at Katia I site	50
Table 2.5 Colour identification of subsurface sediment samples at Katia II site.....	51
Table 2.6 Colour identification of sub-surface sediment samples at SP site	51
Table 2.7 Colour identification of sub-surface sediment samples at CB site	52
Table 2.8 Colour identification of sub-surface sediment samples at AG site.....	52
Table 2.9 Colour identification of subsurface sediment samples at KK site	53
Table 2.10 Textural classification of sediment layers at EP site.....	53
Table 2.11 Textural classification of subsurface sediments at JP site	57
Table 2.12 Textural classification of subsurface sediment at Katia I site.....	58
Table 2.13 Textural classification of subsurface sediments at Katia II	60
Table 2.14 Textural classification of subsurface sediments at SP site.....	61
Table 2.15 Textural classification of subsurface sediments at CB site.....	62
Table 2.16 Textural classification of subsurface sediments at AG site	63
Table 2.17 Textural classification of subsurface sediments at KK site	64
Table 3.1 Categorization of carbon concentration (%) in sub-surface samples.....	77
Table 3.2 Selected major, trace and rare earth elements (REEs)	78
Table 3.3 Concentration of TOC and selected major elements (%) in facies of Ezapur.....	80
Table 3.4 Concentration of TOC and major elements (%) in facies of Jhumpuri.....	83
Table 3.5 Concentration of TOC and selected major elements (%) in facies of Katia I	85
Table 3.6 Concentration of TOC and major elements (%) in facies of Katia II	87

Table 3.7 Concentration of TOC and major elements (%) in facies of Sonpanki	90
Table 3.8 Concentration of TOC and major elements (%) in facies of Chandbali.....	92
Table 3.9 Concentration of TOC and major elements (%) in facies of Ambiligan.....	94
Table 3.10 Concentration of TOC and major elements (%) in facies of Kasturikaran	96
Table 3.11 Concentration of selected trace and rare earth elements (ppm) in facies of Ezapur	99
Table 3.12 Concentration of selected trace and rare earth elements (ppm) in facies of Jhumpuri	101
Table 3.13 Concentration of selected trace and rare earth elements (ppm) in facies of Katia.....	103
Table 3.14 Concentration of selected trace and rare earth elements (ppm) in facies of Katia II	105
Table 3.15 Concentration of selected trace and rare earth elements (ppm) in facies of Sonpanki	108
Table 3.16 Concentration of selected trace and rare earth elements (ppm) in facies of CB	110
Table 3.17 Concentration of selected trace and rare earth elements (ppm) in facies of Ambiligan	112
Table 3.18 Concentration of trace and rare earth elements (ppm) in facies of Kasturikaran	114
Table 3.19 Correlation among TOC and major elements at Ezapur	117
Table 3.20 Correlation among TOC and major elements at Jhumpuri	118
Table 3.21 Correlation among TOC and major elements at Katia I	119
Table 3.22 Correlation among TOC and major elements at Katia II	120
Table 3.23 Correlation among TOC and major elements at Sonpanki	121
Table 3.24 Correlation among TOC and major elements at Chandbali	122
Table 3.25 Correlation among TOC and major elements at Ambiligan	123
Table 3.26 Correlation among TOC and major elements at Kasturikaran.....	124
Table 3.27 Correlation among trace elements and REEs at Ezapur.....	125
Table 3.28 Correlation among trace elements and REEs at Jhumpuri.....	126

Table 3.29 Correlation among trace elements and REEs at Katia I.....	126
Table 3.30 Correlation among trace elements and REEs at Katia II.....	127
Table 3.31 Correlation among trace elements and REEs at Sonpanki.....	128
Table 3.32 Correlation among trace elements and REEs at Chandbali	129
Table 3.33 Correlation among trace elements and REEs at Ambiligan.....	130
Table 3.34 Correlation among trace elements and REEs in Kasturikaran	130
Table 4.1 Selected redox-sensitive trace, rare earth elements (REEs) and ratios	137
Table 4.2 Distribution of selected trace elements (in ppm) and ratios in Ezapur site	139
Table 4.3 Distribution of selected trace elements (in ppm) and ratios at Jhumpuri site	140
Table 4.4 Distribution of selected trace elements (in ppm) and ratios at Katia I site	142
Table 4.5 Distribution of selected trace elements (in ppm) and ratios at Katia II site.....	143
Table 4.6 Distribution of selected trace elements (in ppm) and ratios at Sonpanki site	145
Table 4.7 Distribution of selected trace elements (in ppm) and ratios at Chandbali site	146
Table 4.8 Distribution of selected trace elements (in ppm) and ratios at Ambiligan site	148
Table 4.9 Distribution of selected trace elements (in ppm) and ratios at Kasturikaran site	149
Table 4.10 Distribution of selected REEs (in ppm) and TOC (in %) at Ezapur site	150
Table 4.11 Distribution of TOC and selected REEs in sub-surface facies of JP	152
Table 4.12 Distribution of TOC and selected REEs in sub-surface facies of KTI	153
Table 4.13 Distribution of TOC and selected REEs in sub-surface facies of KTII.....	154
Table 4.14 Distribution of TOC and selected REEs in sub-surface facies of SP.....	155
Table 4.15 Distribution of TOC and selected REEs in sub-surface facies of CB.....	156

Table 4.16 Distribution of TOC and selected REEs in sub-surface facies of AG	157
Table 4.17 Distribution of TOC and selected REEs in sub-surface facies of KK	158
Table 5.1 Reconstruction of sea level changes in the Indian Ocean region during the Holocene	168
Table 5.2 Palaeomonsoon reconstruction in Indian sub-continent during the Holocene.....	169
Table 5.3 Characteristics of different geomorphic regimes along the coast	171
Table 5.4 Details of ¹⁴ C AMS dates from the organic content of sediment samples	174
Table 6.1 Geochemical proxies used to analyze paleoclimate	186

LIST OF PLATES

Plate 1.1 Subsurface sample collected using bore-welling	28
Plate 1.2 Subsurface sample collected using trenching.....	28
Plate 1.3 Analysis of particle size distribution using hydrometer.....	29
Plate 1.4 Graphitization of sediment samples for radiocarbon dating using AMS	31
Plate 1.5 Landscape and vegetation in the riverine zone	38
Plate 1.6 Landscape and vegetation in the mixing zone	38

LIST OF ABBREVIATIONS

AG	Ambiligan
AIRF	Advanced Instrumentation Research Facility
Al ₂ O ₃	Aluminum dioxide
AMS	Accelerator Mass Spectrometry
Ba	Barium
CaO	Calcium
CB	Chandbali
Ce	Cerium
Co	Cobalt
Cr	Chromium
Cu	Copper
CV	Coefficient of Variation
EDXRF	Energy Dispersive X-Ray Fluorescence
EF	Enrichment Factor
EP	Ezapur
Fe ₂ O ₃	Iron dioxide
IUAC	Inter University Acceleration Centre
JP	Jhumpuri
K ₂ O	Potassium dioxide
KK	Kasturikaran
KTII	Katia I
KTII	Katia II
La	Lanthanum
LGM	Last Glacial Maximum
MgO	Magnesium dioxide
MnO	Manganese dioxide
Nd	Neodymium
P ₂ O ₅	Phosphorus dioxide
Pb	Lead
REEs	Rare Earth Elements
SiO ₂	Silicon dioxide

SP	Sonpanki
Sr	Strontium
TiO ₂	Titanium dioxide
TM	Terrestrial Mean
TOC	Total Organic Carbon
UCC	Upper Continental Crust
V	Vanadium
Zn	Zink
Zr	Zirconium

Chapter 1

Introduction

1.1 Introduction

“The present is the key to the past” postulated by Hutton is the premise of all palaeoclimate studies that intend to review the past climate. At present, climate change has become one of the most acute concerns for human on Earth. Concurrently, the ruckus about the magnitude of climatic change has raised the grave questions about the future of population under such oscillations (IPCC, 2007). In this backdrop, it is logical to inquire whether such perturbations have happened before or not. The geological archives disclose that a few hundred years ago, our planet was experiencing prolonged cold spell also known as the ‘little ice age’. Few thousand years before, a larger portion of the globe was covered under thick ice sheet whereas there existed no such phenomenon as the temperature was too high some million years before (Roberts, 1998; Anderson et al., 2007). These statistics enable us to compare and analyze deviations between the past and present climatic pattern. Such evidence has made the palaeoclimate analyses even more crucial as the reconstruction of the past climate is also utilized as a cornerstone for the climatic models predicting the future climate. Assessment of the palaeoclimate, however, not only meant to assemble the evidence of the past climate but is also intend to explore the processes underlying distinct climatic conditions.

The annals of palaeoclimate proclaim that climate has varied remarkably throughout the geological history and that the climate system on the Earth can transform dramatically at different time scales. These changes incorporate long term vagaries as well as short term deviations (Roberts, 1998; Banerji et al., 2017). Thus, the climate on the Earth has never been static and there are ample evidence and records confirming drastic changes in climate throughout the geological history (Roberts, 1998; Anderson et al., 2007). During the Permian-Triassic transition period, one of the greatest mass extinctions has been recorded in which more than 80 percent of the total species vanished (Stanley and Yang, 1994; Retallack, 1995). On the other hand, during the Quaternary, a larger part of the globe was covered under the thick ice sheet. The oscillations between glacial and interglacial climatic conditions have been characterized by the transfer of a large volume of water between the glaciers and the oceans manifesting into global sea level perturbations (Lambeck et al.,

2002). The Holocene has been marked with periods of enhanced humidity and aridity along with oscillations in sea level which are more pronounced at the regional and local scale.

The Quaternary has been considered a crucial period in the history of the Earth within the Cenozoic Era (Table 1.1). The 'Cenozoic' is the most recent Era which has been divided into Tertiary and Quaternary which are further categorized into different epochs. In the recent years, the study of climate during the Quaternary has achieved great significance as the environment and present day landscape have been largely shaped during this period through the geological processes and further instigated by climatic changes, sea level oscillations and tectonic activity. The Quaternary is comprised of Pleistocene and Holocene epochs constituting nearly 0.04 percent of the total (4600 million) years since the Earth was formed (Anderson et al., 2007). The Quaternary is regarded as a decisive period during which humans inhabited the Earth and developed great civilizations. Thus, it is rightly referred as Anthropogene due to the impactful presence as well as the development of human civilization. The vast majority of the Quaternary period is covered by Pleistocene while the period ranging around 11,500-10,000 years before present is recognized as the Holocene. The Holocene has been characterized as a period of climatic and eustatic changes at the local and regional scale. However, some events i.e. Little Ice Age during 1500 AD – 1850 have been marked globally (Anderson et al., 2007). The Holocene has been divided into early or Greenlandian (11,700 to ~8326 yr BP), mid or Northgrippian (~8326 to ~4200 yr BP) and late or Meghalayan (~4200 yr BP to recent) period as proposed by the International Commission on Stratigraphy (ICS).

The Holocene was usually viewed as a period of growth and development of human civilization without substantial change in the climate. Nevertheless, evidence derived from proxy records of terrestrial, glacial and marine environment across the world has refuted this opinion. However, during the Holocene, the global climate has appeared to become even more complex due to marked regional variability (Russ et al., 2000). During the Holocene significant changes in rainfall intensity and sea level has been experienced (Vaz and Banerjee, 1997; Jayalakshmi et al., 2004; Alappat et al., 2011; Jayangondaperumal et al., 2012; Tyagi et al., 2012; Srivastava and Farooqui, 2013; Quamar and Bera, 2014; Limaye et al., 2014; Tripathi et al., 2014; Malik et al., 2015; Rao et al., 2015; Govil et al., 2016; Banerji et al., 2017; Narayana et al., 2017; Resmi et al., 2017; Makwana et al., 2019).

Table 1.1 Geological history of the Earth since the Cenozoic Era

Era	Period	Epoch	
Cenozoic	Quaternary	Holocene	Late or Meghalayan
			Mid or Northgrippian
			Early or Greenlandian
		Pleistocene	
	Tertiary	Miocene	
		Oligocene	
		Eocene	
		Palaeocene	

Source: Based on Anderson et al., (2007)

Abrupt deviations in the climate during the past have influenced the coastal locations across the globe by causing sea level oscillations. Hence, coasts around the globe have been highly susceptible to climate and sea level perturbations (Warrick et al., 1993). Proxy sources indicate an uneven sea level across the globe. The rate of global sea level change, as per IPCC report (2007), between late nineteenth to early twentieth century has been unusually high in the last two millennia. The global mean sea level change on an average has been ranging from 1.7 to 0.2 mm/year during the twentieth century. In recent years, since 1993, the rate of sea level change has deviated between 2.8 and 3.6 mm/year (IPCC, 2007). However, the magnitude of sea level change has been much higher during the glacial and inter-glacial transition period. At that time, the sea level was nearly 5 m higher than the present (Roberts, 1998). Nevertheless, during the Holocene, the sea level has shown marked variations at the global and regional scale. Hanh and Furukawa (2007) have identified different components of sea level rise in their study. According to them, at the global scale, the sea level is influenced largely by the glacial melt and thermal expansion of the ocean water. In contrast, at the local or regional level, eustatic changes occur due to the vertical land movement arising from tectonics, isostatic adjustment, and sediment compaction. Thus, the climate has always remained dynamic on Earth.

The records of the past climate from instruments such as rain gauge, thermometer or satellite are often not more than 100 or 150 years old. This time period is too short to examine

climate change over a longer time scale going back hundreds and thousands of years. To avert this, it is critical to analyze climate change, employing natural or proxy sources. The proxy records also document archives of transition between various climatic phases as well as abrupt changes occurred in the climatic pattern. Reconstruction of past climate has relied upon the study of climate archives that extend our understanding of climate far beyond the instrumental records. These archives mainly include tree rings (Fritts, 1965; Fritts et al., 1971; LaMarche Jr, 1974; LaMarche Jr, 1978; Gebrekirstos et al., 2008; Barrett et al., 2019; Wang et al., 2019), pollen (Shaw et al., 2007; Khandelwal et al., 2008; Patnayak et al., 2009; Farooqui and Naidu, 2010; Andreu et al., 2012; Kumar and Chauhan, 2014; Limaye et al., 2014; Kumar and Bera, 2016) and sedimentary records (Damuth, 1974; Stanley and Yang, 1994; Vaz and Banerjee, 1997; Singh et al., 1998; Retallack, 1999; Allison et al., 2003; Juyal et al., 2003; Davies, 2006; Parker et al., 2006; Coltorti et al., 2010; Govil et al., 2011; Liu et al., 2011; Lyons et al., 2011; Sarkar et al., 2012; Tyagi et al., 2012; Saxena et al., 2015; Banerji et al., 2017; Limaye et al., 2017; Narayana et al., 2017; Resmi et al., 2017; Makwana et al., 2019).

The records of the Earth history have also been well archived in the coastal sedimentary environment (Vaz and Banerjee, 1997; Jayalaksmi et al., 2004; Coltorti et al., 2010; Nair et al., 2010; Alappat et al., 2011; Jayangondaperumal et al., 2012; Rao et al., 2012; Srivastava and Farooqui, 2013; Rao et al., 2015; Banerji et al., 2017; Limaye et al., 2017; Narayana et al., 2017; Resmi et al., 2017; Makwana et al., 2019). Thus, the coastal regions are the repository of thick sequencing of the Quaternary sediments. These records, therefore, provide an opportunity to investigate perturbations in the climate and sea level (Banerjee, 1993; Banerjee, 2000). Sedimentary colour, texture, and geochemical attributes have been analyzed extensively to inspect the depositional history, climate change and sea level oscillations in coastal regions (Narayana et al., 2017; Banerji et al., 2017).

In this backdrop, the present work is an attempt to reconstruct the palaeoclimate of lower Baitarni Basin, Odisha and encode the processes that have operated in the past based on the clues available in the sediment sequences. The study is aimed to apply a multi-proxy approach to derive inference about the palaeoclimate.

1.2 Literature Review

Extensive works have been carried around the world to reconstruct and interpret the palaeoclimate. As climate can vary from region to region resulting into distinct environments, the palaeoclimatic changes at global and regional scales have been reviewed in this segment to have a general outlook about the past climatic changes registered in different parts of the world. The studies based on the Indian subcontinent, in particular, have been categorized into the mainland, the west coast and the east coast of India. Lastly, the analyses based on the Odisha coast have been reviewed. Towards the end of this section, a review of different approaches and methodologies used for palaeoclimatic reconstruction is also presented.

The earliest efforts of reconstructing palaeoclimate and processes operating in the past from geological, palaeobiological, archaeological or chemical evidence started in the middle of the fourth century BC (Caran, 1998). One of the earliest empirical inspections of fluvial response to climate change can be attributed to the work of Penk and Bruckner (1909). Their investigation was based on relative approach considering terraces formation along the tributaries of Danube to examine the depositional history. This relative method used by them had dominated the world until the newer developments such as oxygen isotope records during the 1960s and 1970s (Blum and Tornqvist, 2000). Tucker and Benton (1982) have postulated that the equatorial humid belt was poorly developed during the Triassic period. This has indicated the existence of a relatively drier climate over the larger part of the globe. Nevertheless, the arid climate was interrupted by a humid phase during the mid-late Carnian times as indicated by the terrestrial sedimentary proxies, most probably resulting due to volcanism (Simms and Ruffell, 1990). During the Quaternary period incidence of five ice ages have been documented which are marked with severe glaciation during the glacial period and a relatively warmer phase during the inter-glacial episode (Warrick et al., 1993). The intensity of climatic changes, however, has varied enormously across the regions (Agrawal, 1987; Thompson et al., 1989; Warrick et al., 1993; deMenocal, 1995; Leeder et al., 1998; 2003; Kumaran et al., 2005; Beukema et al., 2011; Brook and Kirkbride, 2018). Ericson et al. (1956) have used Foraminifera of sediment cores from the Atlantic Ocean and adjacent areas to evaluate the Pleistocene climate. They have observed remarkably high temperature during the transition period between glacial and post-glacial. This change has been recorded around 11,000 years BP, also regarded as the advent of the Holocene. The

Quaternary climate has also been reconstructed by assessing fluctuation in the calcium carbonate retrieved from the equatorial Atlantic Ocean. The results have revealed a 20,000 years periodicity of warm-cold cycles recorded throughout the Quaternary. The ice core data from central Qinghai-Tibetan plateau of China has indicated that the late glacial stage was relatively cooler, wetter and dustier than the Holocene in the Tropics (Thompson et al., 1989).

The work of deMenocal (1995) using marine records has exhibited a shift towards more arid conditions after 2.8 million years ago in Africa. The climate in Africa became cooler and drier most probably as a result of glaciation in other parts of the globe. Around 1 million years before the aridity further increased owing to the prolonged glaciation. The enhanced aridity has been associated with the evolution of African Hominids and other vertebrates. Existence of wetter period in northern Africa has been established during the early Holocene period (Petit-Maire and Riser, 1983). It has been observed that around 10,000 to 5500 cal yr BP, level of lake water had increased leading to water surplus condition in the semi-arid Sahel and Sahara desert of Africa (Fontes and Gasse, 1991). However, since the mid-Holocene significant shift in vegetation from forest to arid has been observed in Africa (Lezine, 1989). The lakes became shallower in northern Africa between 7000 and 5700 cal yr BP suggesting enhanced aridity. These lakes completely dried and vanished during around 5100 cal yr BP illustrating further intensification of the arid climate.

McCarthy et al. (1995) have recorded warming around 10,000 BP followed by a decrease in temperature during the mid-Holocene. In contrast, an increase in precipitation has been recorded from mid-Holocene to the present. The work of Grette and Hopkins (1995) using palaeosols has revealed a higher sea level during the peak of the inter-glaciation in the region. It has also been inferred that the water masses off- the shore had been much warmer than the present. The chronologies have been derived from high resolution radiocarbon dates for Norway and from Oxygen isotope record for Switzerland by (Birks and Ammann (2000). They have found that Allerod in Switzerland was 4-4.5⁰C warmer than the western part of Norway. Contrary to this, the range of Holocene temperature rise has been similar in both the regions during the first 500 yr of Pleistocene-Holocene transition. Russ et al. (2000) have analyzed mid and late Holocene climate in Texas. based on past lichen activity on the rock surface as a proxy of the past climatic changes. They have recorded dry phases existing

during 6380-6030 cal yr BP, 4670-4500 cal yr BP, 3790-2840 cal yr BP, 2080 cal yr BP and 1360-680 cal yr BP marked by high lichen productivity. While reduced productivity during intervening periods has suggested wet and moist conditions.

Fukumoto et al. (2004) using bulk organic matter in marine sediments along the sedimentary column have indicated a rearrangement of the sedimentation in the region with increasing marine influence towards the present. The grain size data has also exhibited similar condition suggesting an energy increase over the last 1500 years. Davies (2006) has used multi-proxy approaches i.e. stratigraphy, geochemistry as well as investigation of highland peat and lacustrine sediments to study the palaeoclimate of Dhamar highlands, Yemen. This region has been considered as an ideal location for the analysis of the influence of Indian Ocean monsoon on the moisture history. AMS techniques have been used to analyze the chronology. The study has revealed that the climate of the region was wet in the past as compared to the present. An increase in the level of moisture has been established during the early-Holocene providing promising environment for the development of early human culture in this region. Parker et al. (2006) have attempted to develop a Holocene chronology of the palaeomonsoon rainfall from lacustrine sediment archives. They have suggested a strong correlation between cooler conditions in the North Atlantic and episodes of decreased monsoon activity and weakened winter rainfall in south-eastern Arabia. The study of Tamazelli and Dillenburg (2007) has been based on the facies analysis and stratigraphy on the exposed section of sandpits of South Brazil. As per the findings, the last interglacial sea transgression has been represented by a sandy coastal barrier, Barrier III. The sea has been a major source of sand for barrier aggradation. Based on the evidence they have concluded that the last interglacial sea level maxima in this coast had been around 7m above present day sea level. Thus, there are records that show a higher sea level in the geologic past.

Palaeosol as a high resolution proxy has been used to examine the palaeoclimate of Ebro Basin, Spain (Hamer et al., 2007). Through geochemical analysis, it was found mean annual precipitation has been the dominant control on the type of palaeosol. According to Sheldon et al. (2009) palaeosols well preserved in the terrestrial environments have increased the possibility of continuous, long term palaeoclimatic records and therefore can be used as one of the most powerful and reliable tools for the reconstruction of past climate. The study of Coltorti et al. (2010) has offered the results of stratigraphy, facies analysis and geomorphic

investigation along the coast of Sardinia, Italy. They have recognized two major synthems in this region. The evidence has indicated that the older sub-synthems could be correlated with higher sea level while the younger sub-synthems have been deposited during the rest of the Late Pleistocene. Lyons et al. (2011) have developed a stratigraphic framework for Lake Malawi, East Africa over the last ~150 ka by integrating several years of seismic reflection data along with drill cores. They have identified three lake level cycles in the region. As disclosed by the study, the lake level has dropped as much as 500 to 550 m on several occasions which have resulted in the reduction of nearly 97% water volume in the Lake Malawi. They have suggested a greater collaboration between the Earth sciences and statistical communities as there had appeared complexities in palaeoclimatic reconstruction from incomplete instrumental and climate proxies (Tingley et al., 2012). The study of Gattolin et al. (2015) has incorporated sedimentological evidence with changes in the geometry of carbonate bodies recognized in the Cartina area. Their work using facies analysis has enabled to reinterpret the patterns of progradation, basin infilling and ramp development at the end of the early Carnian. In East Antarctica climatic changes during Holocene have been analyzed using lake sediment core from Schirmacher region (Govil et al., 2016). The assessment of TOC, biogenic silica, grain size and elemental concentration such as Mg/Ca and Mn/Fe has yielded significant information about past climate. The result has suggested a warm phase between 11,600 and 10,000 yr BP during which a higher rate of accumulation has been observed. This had been followed by a cold phase during 10,000 and 3100 yr BP marked by a decline in aggradation rate. Enrichment of TOC and Mg/Ca ratio has indicated relatively warmer episode after 3100 yr BP. The climate of Florida has been analyzed using stalagmite from Brooksville ridge cave (Van et al., 2017). The oxygen and carbon isotope has indicated that the climate in central Florida was comparatively warm and wet during the glacial period rather than extremely cool and dry as in other parts of the country. Bufarale et al. (2017) have analyzed the influence of sea level perturbations, hydrodynamic condition and regional geomorphology along the Swan River, Australia. They have integrated high resolution seismic profile data with LiDAR data, sediment borehole analysis and available literature of geology and stratigraphy of the area to determine the formation of stratigraphic units as a response to the Late-Pleistocene and Holocene sea level fluctuations. This combination has aided to understand that the evolution of the estuary had occurred under the control of sea level oscillation. One of the recent

works has analyzed the utility of visible to short-wave infrared reflectance (VSWIR) spectroscopy as a tool to reconstruct past climate in place of traditional methods (Zhao et al., 2017). VSWIR has been used to examine properties of Quaternary soil sequence of Shengli in Sichuan Basin of South West China. The results obtained using 76 samples have indicated a warmer and seasonally drier palaeoclimate with a greater intensity of summer monsoon.

The study of Gayantha et al. (2017) has been based on multi-proxy analysis to inspect the late Holocene climate in Sri Lanka. They have assessed the grain size distribution, elemental concentration, TOC, mollusk shells along with C and N isotopes in the sediment core. The analysis has reported warm and humid climate with enhanced rainfall during 2941-2390 cal yr BP, a dry period marked with reduced rainfall during 2390-1780 cal yr BP, reoccurrence of intense precipitation under warm humid climate during 1780-1299 cal yr BP and prevalence of dry conditions since 1299 cal yr BP. Brooks and Kerkbride (2018) have utilized mountain glaciers as a proxy to reconstruct the past climate in New Zealand. They have observed that glaciation in North Island had been more extensive than the prior assumption. Palaeoclimate of eastern Anatolia has been assessed using elements i.e. Ca, Fe, K, Mn, Si, TOC and CaCO₃ (On and Ozeren, 2019). They have noted that the area was warm during the interglacial and was cold during the glacial period. The study has also suggested the region was not dry during this phase. The Holocene in the region was characterized by a wet period followed by dry intervals. Pennington et al. (2019) have based their analysis on XRF data. A gradual increase in Ca/Ni ratio between 5000-4000 cal yr BP in sediment core of Nile data has revealed hyper aridity in this region. This increase most likely has indicated elevated flux of aeolian material in the Nile river system.

In the context of the Indian subcontinent, one of the earliest studies on evaluating palaeoclimate includes the work of DeTerra and Paterson (1939). The studies based on reconstruction of palaeoclimate has been primarily concentrated in Himalayan region which is regarded as the major repository of past climate (Burbank and Fort, 1985; Stern et al., 1997; Owen, 2008; Beukema et al., 2011; Singh et al., 2014; Khatri et al., 2017; Rashid et al., 2017; Babeesh et al., 2019), desert of Rajasthan (Bryson and Swain, 1981; Swain et al., 1983; Andrews et al., 1998; Singhvi et al., 1998; Juyal, 2003; Prasad and Enzel, 2006), mainland (Srivastava et al., 2003; Durand et al., 2007), West coast (Agrawal and Guzder, 1972; Jayalakshmi et al., 2004; Kumaran et al., 2005; Singh et al., 2011; Kem et al., 2013;

Misra et al., 2014; Prasad et al., 2014; Singh et al., 2014; Alappat et al., 2015; Banerji et al., 2017; Narayana et al., 2017) and East coast (Rao, 1964; Babu, 1975; Rao and Vaidyanathan, 1978; Rao and Sadakata, 1985; Bikshan and Subramaniun, 1988; Chauhan et al., 1993; Murthy et al., 1995; Konhauser et al., 1997; Rao, 2001; Mohanty et al., 2003; Khandelwal et al., 2010; Rao et al., 2012; Bhattacharjee et al., 2013; Srivastava and Farooqui, 2013; Das, 2014; Tripathi et al., 2014).

Burbank and Fort (1985) have analyzed the extent of former glaciers as a proxy of the past climate variation in the Himalayas. In another study Stern et al. (1997) have examined oxygen isotope obtained from palaeosols in the Potwar plateau to assess the past precipitation intensity. The result have shown enhanced aridity or change in the source of precipitation from continental to marine during 8500 million years before (Ma) and 6500 Ma. Major advancement in the Himalayan glacier extent has been suggested during the late-Pleistocene and early-Holocene (Owen, 2008). The study has provided that since last glacial maximum (LGM), glaciers in the Himalaya and Tibet have responded to fluctuations in the south Asian monsoon regimes. Apart from this, lacustrine deposits have also been used to analyze the climatic history of Gori Ganga basin in central the Himalaya by Beukema et al., (2011). This has been done using lake stratigraphy in association with the radiocarbon and OSL dating. Singh et al. (2014) have explored the possible uses of stable isotope of non-pedogenic carbonates in palaeoclimatic and palaeoecological reconstruction of Ramnagar sub-basin of the Himalayas. The outcomes of the study have suggested that the stable $\delta^{13}\text{C}$ and $\delta^{18}\text{O}$ values unlike pedogenic carbonates have little significance in Palaeoclimatic studies. In Nepal Himalaya variation in Cenozoic climate has been has been investigated using pollen records (Khatri et al., 2017). Their study has indicated a gradual decrease in precipitation over the past 11 Ma as suggested by increase in oxygen isotope carbonate in fossil mollusks. This was followed by a stronger monsoon during 10.7 Ma. However, again during around 9 Ma, elevated aridity has been marked. They have reported existence of cold and very dry climate up to 26,000-19,000 yr BP and transformed to more humid and wet during 19,000 and 15,000 yr BP. Geochemistry has been used by Rashid et al. (2017) to investigate the provenance and palaeoclimatic conditions of Ordovician Thango formation in Spity Valley. A detailed petrographic and sedimentological analysis has suggested domination of three major depositional environment – fluvial, transitional and marine. It has

been confirmed that the climate has changed from humid during the early Ordovician (non-glacial) to cold (glacial) during the late Ordovician period. Babeesh et al. (2019) have used lake sediments to inspect the Holocene climate in Kashmir valley. Using grain size distribution, major and trace elements, TOC and C/N ratio along with diatom assemblage, the palaeoclimate has been constructed. They have identified several cold and arid phases during 3300-2500 and 1800-1300 yr BP. It was also reported that wet phases were associated with higher sand and silt content with less abundance of diatom and TOC and higher C/N ratio. Dry and cold periods have been identified between 3345-3300 yr BP and 2500-1800 yr BP in Kashmir valley.

Reconstruction techniques have also assisted in the analysis of palaeofloods. One of such studies has been conducted by Kale et al. (1997) for peninsular rivers. Their work has shown that in recent time the occurrence of high magnitude floods has increased significantly. Using oxygen and carbon isotopes in calcrete, the late Pleistocene climate has been investigated in the Thar Desert (Andrews et al., 1998). The study has demonstrated that the climate was predominantly arid before 10,000 yr BP. The aridity is proposed to be caused by the weakening of the summer monsoon associated with LGM. Singhvi et al. (1998) have attempted reconstruction of the late Pleistocene climate in India by evaluating oxygen and carbon stable isotopes in pedogenic calcrete of the Thar Desert. Chronology has been derived from thermoluminescence, infrared and green light stimulated luminescence dates. It has been found that Thar palaeoclimates were predominantly arid before 10,000 and after 25,000 yr BP. This has also been linked with the weakening of summer monsoon under the influence of LGM. They have also suggested widespread aridity in the Indian subcontinent during this time. Luminescence technique has also been used to examine the dune building activity in the southern part of the Thar Desert (Juyal, 2003). They have elucidated that the dune building has started around 26,000 yr BP which has continued until 5000 yr BP. An episode of landscape stability has also been recorded during 11,000-9000 yr BP which is the indirect indicator of strengthened southwest monsoon at this time. The geomorphic evolution of Ganga plain has been investigated by Srivastava et al. (2003) using luminescence dating. Their study has attempted to investigate palaeoenvironment using the alluvial deposits of Ganga plain which contains crucial records of the late Quaternary climate. In their study, Prasad and Enzel (2006) have examined variations in the monsoon

rainfall in the Indian desert using pollen records from lacustrine sediments. Durand et al. (2007) have studied calcrete in Alfisols on Precambrian silicate rocks to reconstruct palaeorainfall tendencies in semi-arid Karnataka. Their analysis has indicated stable semi-arid conditions around 200 ka with fluctuating annual rainfall closer to present day conditions. Due to its occurrence in a variety of climatic settings, calcrete has been considered an insignificant proxy for analysis of past climate variations. Existence of warm period has been indicated in Betul district of Madhya Pradesh during 1416 and 506 cal yr BP (Quamar and Chauhan, 2014). The climate shifted to more warm and humid during 506 and 120 cal yr BP followed by warm and less humid phase since 120 cal yr BP. The Quaternary climate has been analyzed using the geochemical proxy from a buried channel in Ghaggar Plain (Singh et al., 2016). A higher value of $\delta^{13}\text{C}$ has indicated elevated rainfall and temperature during the interglacial period. A negative value of $\delta^{13}\text{C}$, during the glacial period, has exhibited dry and cold climate. In east Khasi hills of Meghalaya climate during the Palaeocene-Eocene transition has been reconstructed (Prasad et al., 2018). This study has been based on multi-proxy archives recovered from Jathag section. During the Palaeocene warm and dry climate existed in the region. The climate shifted to warm and wet conditions during the late Palaeocene and early Eocene. Using Speleothem records from Kailash cave, central India, Gautam et al. (2019) have investigated the palaeomonsoon variability. They have reported intensified summer monsoon during 14,800 cal yr BP and 14,500 cal yr BP which stabilized gradually.

In the western coast of India, Agrawal and Guzder (1972) have documented a marine transgression around 5000 yr BP. Monsoon fluctuation along the West coast has been studied using oxygen isotope and pollen records by Campo (1986). A 20,000 year history has been reconstructed with two important phases of the advancement of the monsoon climate. These phases include an arid period between 22,000-18,000 yr BP correlating with lowest pollen representation followed by a humid phase around 11,000 yr BP corresponding with highest pollen appearance. The study has also disclosed a gradual extension of monsoon over Indian subcontinent after the last glacial maximum followed by the northward progression of the Intertropical Convergence Zone (ITCZ). Agrawal (1987) has done a comparison of $^{18}\text{O}/^{16}\text{O}$ measurement on *Globobulimina* *ruber* and *Globobulimina* *menardii* from the Andaman and Arabian sea cores. The obtained result shows that during 18,000 yr BP

(LGM) and at 10,000 yr BP the south-west monsoon was weaker than today whereas the north-east monsoon was stronger. Jayalakshmi et al. (2004) have reconstructed late Pleistocene-Holocene palaeoclimate of southern Kerala Basin. They have used a continuously cored borehole at Eruva (7.25 m) and Muthukulam (3 m) to analyze the depositional environment as well as palaeoclimate. The result has exhibited a marginal marine environment in earlier phase probably corresponding to a period of exceptionally high rainfall that had led to an ample supply of terrestrial sediments. This environment has continued however, there has appeared a significant reduction in the supply of terrestrial sediment showing a decline in rainfall. The study of Kumaran et al. (2005) based on radiocarbon dating has revealed the existence of two periods of abnormally high rainfall along the Kerala-Konkan basin. One of such events has been reported before LGM and another during early Holocene. However, the study has illustrated that between 22,000 and 18,000 year BP aridity had prevailed with reduced sea level and/or declined rainfall associated with LGM in this area. Singh et al. (2011) have included both macro and microfloral assemblage for palaeoclimatic analysis in Vagadkhol village, Gujarat. The results have shown the existence of tropical moist or wet forest with some deciduous vegetation during the Palaeocene- lower Eocene interval. Prasad et al. (2014) have conducted a multi-proxy analysis using Wadhvana lake sediments of sub-humid Gujarat in order to examine mid-Holocene climatic variability and its influence on Harappan culture. The study has indicated high lake level during 7500-5560 cal yr BP that probably have referred to a cool and moist condition which became less wet and dry later due to decreased rainfall and incidence of seasonally dry climate. This period resulted in the collapse of Harappan civilization during mid-Holocene period. A declining rainfall has resulted in low lake level during 4255 cal yr BP. However, after 3500 cal yr BP, a steady strengthening of southwest monsoon has appeared. Between 3238 and 2709 cal yr BP again a short period of dry climate has reappeared followed by a more or less present day climate. In their study, Kem et al. (2013) have analyzed sediments at Varkala cliff section to study the palaeoclimate. The succession has consisted of coastal marine sand alternation with fine grained, organic rich siliclastic. A palaeotemperature has also been constructed using Coexistence approach, which has shown similarity with present day temperature. In contrast to this, the precipitation was lower than present with marked seasonality pattern. Misra et al. (2014) have studied Holocene vegetation succession influenced by past climate and sea level

changes at Thrissur, Kerala. Their work is based on the combined use of pollen analysis derived from sediments and ^{14}C dating. The results have reported that before 7270 cal BP core mangroves of the intertidal zone grew in the area. With the continuation of warm and humid climate and monsoon at its peak, mangroves expanded between 7270 and 3530 cal BP in later period mangroves declined that may be the outcome of declined rainfall in the area. However, due to the shallow sediment profile (54 cm from the surface), the study has not been sufficient to understand the vegetation and climatic dynamics at high resolution during Holocene. The pollen signatures have demonstrated higher precipitation during 7220-3880 yr BP followed by drier climate since 3500 yr BP in south-west coast (Limaye et al., 2014), Based on combined use of geochemistry, magnetic parameters and sedimentation rate palaeoclimate has been studied by Singh et al. (2014). The sediments core have been obtained from mudflats of Kolamb creek (Maharashtra), Mandavi estuary (Panaji) and Todri creek (Karnataka) in order to study variability in sediment attributes over time. It has been observed that geology, geomorphology and anthropogenic activities have been the dominant controllers of spatio-temporal distribution of sediment composition. Alappat et al. (2015) in their work have, for the first time, attempted the luminescence chronology of beach ridges in central Kerala in order to reconstruct the past sea level and coastline progradation. The findings have indicated a stage of coastline progradation between 3 and 5 ka and formation of widespread beach ridges along the Kerala coast during this period. The results have also revealed that the sea level was between 3.5 and 4.5m above present mean sea level during the Late Holocene period which may also imply the emergence of the coast under the influence of neo-tectonic activity.

Narayana et al. (2017) have analyzed environmental changes during the Holocene from palaeodelta region of the south-west coast of India using geotechnical parameters and pollens. Sediment texture and geotechnical properties have exhibited a distinct change in depositional environment from marine to fluvial during the sea level fall after 7 ka to 5 ka. This might be attributed to neo-tectonics, sea level perturbation and monsoonal intensity in the region. Banerji et al. (2017) have examined sediment core from a mudflat of Diu Island using geochemical proxies and ^{14}C dating. This study has advocated warm and humid climatic conditions during 4105-2640 cal yr BP as a manifestation of intensifying Indian monsoon followed by an arid condition between 2640 and 1930 cal yr BP. They have

observed that around 1930-355 cal yr BP the region again started to experience warm and humid climate.

Basu et al. (2017) have used an integrated approach of isotopic ($\delta^{13}\text{C}_{\text{OM}}$) and biomarker (n-alkane) on soil, vegetation, lake surface as well as core sediments to construct shift in the palaeovegetation and hydrological regimes in the area of Lake Ennamangalam, southern India during the Holocene. They have retrieved a sediment core of 1.65 m spanning to 4800 cal BP. The n-alkane indices (i.e. Paq) and terrestrial vs aquatic ratio (TAR) have been used to infer the changes in the source of organic matter and to reconstruct past environmental changes. The trend in TAR values suggests fluctuating climatic condition during mid-late Holocene. The result has also indicated that although the intensity of monsoon varied, overall dry climate prevailed in the region during 4500-3000 cal BP. This has been considered the first of its kind study from the Peninsular India. However, the influence of climatic factors on n-alkane distribution is yet to be evaluated from the peninsula that receives rainfall from both south-west and north-east monsoon. Limaye et al. (2017) in their work conducted in Konkan-Kerala basin have reported the occurrence of swamps until Late Pleistocene which had been replaced by the riparian vegetation during the late Holocene. The analysis has exhibited elevated rainfall condition during 9000-6000 yr BP than the present. Migration of the palaeochannel in a response to climate change and tectonics has been analyzed for Palar river basin, Tamil Nadu (Resmi et al., 2017). Through the analysis of channel migration, they have suggested intensified monsoon rainfall during 3590-3260 yr BP. Using geochemistry, OSL and AMS dating, Makwana et al. (2019) have examined the mid-late Holocene climate in Banni plains of Kuchchh. They have reported a warm and humid climate from 2900 to 2000 yr BP along with higher sea level. It was observed that the sea level has declined since 2000 yr BP.

The study of past climate in the eastern coast is comparatively newer owing to the introduction of new and advanced dating techniques (Agrawal, 1987) whereas Arabian sea core has provided many of the complete and well-dated records and hence, has been examined intensively to analyze the climatic variability during the Holocene (Prasad and Enzel, 2006). The work of Rao (1964) can be considered among the earliest studies based on the east coast of India. His work has dealt with the sedimentary aspects of the continental shelf off the east coast. However, the majority of the researches along the east coast have

concentrated in Krishna–Godavari deltaic region (Babu, 1975; Rao and Vaidyanathan, 1978; Rao and Sadakata, 1985; Bikshan and Subramaniun, 1988; Murthy et al., 1995; Rao, 2001; Rao et al., 2012) as well as in Bay of Bengal (Chauhan et al., 1993; Bhattacharjee et al., 2013; Das, 2014). In contrast, the number of studies done along Odisha coast is very limited and confines mainly to geochemical analyses (Konhauser et al., 1997; Mohanty et al., 2003) and palynological investigations (Khandelwal et al., 2010; Srivastava and Farooqui, 2013; Tripathi et al., 2014).

The study of Vaidyanadhan and Ghosh (1993) has presented extensive details of the Quaternary history of the major river basins of the east coast. Their analysis has included deltas of Ganga, Subernrekha, Mahanadi-Brahmani-Baitarani, coastal Andhra Pradesh and Tamil Nadu. Two dominant arid phases and weak monsoon (73-110 cm) have been identified around last glacial maxima (LGM) at the Holocene-Pleistocene transition by Chauhan et al. (1993). However, clay mineral assemblage and their ratios, sediment texture, and absence of mineral have documented the prevalence of stronger monsoon since 10 ky⁻¹ BP along Bay of Bengal (Chauhan et al., 1993). Lagoons have been considered a significant repository of past changes in sea level. Vaz and Banerjee (1997) have reconstructed the Holocene sea level fluctuations in the eastern coast using palaeoclimatic imprints from Pulicut Lagoon. They have found subsequent cycles of regression that are reflected in three sets of dunes and beach ridges. The relative sea level changes, in the absence of signs indicating tectonic activity, have been interpreted as Late Holocene hydrostatic fluctuations.

The majority of the studies on the past climate in the coastal region have been based upon the palynological analysis (Blasco et al., 1996; Kumaran et al., 2005; Filho et al., 2006; Khandelwal et al., 2008; Bhattacharjee et al., 2013; Tripathi et al., 2014), as mangrove morphology and sedimentation have provided excellent register of the coastal modification as well as have indicated interaction between sea level fluctuation, coastal processes, and sediment supply. The study of Banerjee (2000) has provided evidence of minor sea level fall along the east and south Indian coasts. This fall has been attributed to LGM followed by strong aridity and fast retreat of the sea. Banerjee (2000) has also identified two oscillations in sea level using U series and ¹⁴C dating. As per the study, the secondary changes in relative sea level after mid-Holocene transgression are not unique to the east coast of India

as similar results have been found from the coasts of Mauritania, West Africa, and Recife Brazil.

Srivastav and Farooqui (2013) have used a high resolution multi-proxy approach including sedimentology, physio-chemistry and palynology to help construct a reliable chronology for the upper (5 m approx) sediments of north-east Cauvery delta. Samples have been collected from the South of Pichavaram estuary using a hand operated augur cum piston corer. The sediment color was determined using 'Munsell color chart' (2000) and the texture was examined on the basis of sand in the sediment following soil 'density method of USDA', 1992. Based on the changes in the depositional environment and pollen spectra palaeoclimate has been analyzed. There has appeared a warm and moist period from the base of the record (3630 cal yr BP – 3170 cal yr BP). Afterwards, an arid cold period has persisted between 3170 cal yr BP-1300 cal yr BP. A revival of the less warm and moist condition occurred after 1300 cal yr BP in addition, the record of sediment structure has indicated a series of late Holocene episode of increased aridity. Thus, it has become evident that during Holocene, the climate changed from warm and humid to cool and arid.

For palaeoclimatic reconstruction beach ridges which is a prominent geomorphic feature along tropical coast, have been considered as an important and reliable tool (Banerjee, 2000; Rao et al., 2005; Murray and Mohanty, 2006; Alappat et al., 2015). Along microtidal coast where tidal range varies between 0-2 m, it is considered to be a good indicator of palaeo sea level. However, its utilization as a tool has been debated (Thomas, 2009). Rao et al. (2005) have relied upon beach ridges to study the sedimentation process and development of Godavari delta. Using six borehole cores with varying depth of 3.0 m to 14.0 m they have analyzed the evolution of Godavari delta during the Holocene. Thomas (2009) in his study has attempted OSL dating of quartz grains extracted from beach rock on the south-east coast of India. The preliminary ages of beach rock has suggested that during the late Holocene around 3.6 to 2.1 ka, sea level was higher than present along this coast. This observation using OSL dating is broadly consistent with the existing records based on ^{14}C dating for the same region. However, the ^{14}C ages are slightly higher than OSL ages. The study has also provided an insight of using OSL dating on beach rock for tracing sea level chronology as well as shoreline evolution on the south-east coast of India.

Apart from beach ridges, beach rock, and sand dunes have also been recognized as reliable indicators of palaeoclimate and sea level oscillation. The work of Alappat et al. (2011) is one such attempt aimed to set up a detailed chronological framework to study the formation and reactivation history of coastal dunes of Tamil Nadu, in particular to the Cauvery delta region. The study has been done using OSL dating on eight subsurface sediment cores (depth up to 5 m from surface). This analysis has identified periodic formation and reactivation of dunes that has continued from the late Holocene to recent times. The periodicity in dune formation has resulted due to climatic variability and land use land cover change in the region. The study of Jayangondaperumal et al. (2012) has also explored the possibility and potential use of coastal dunes in the reconstruction of past climate along the south-east coast of India. They have observed the occurrence of stronger winter monsoon before 11400 yr BP. The work of Rao et al. (2012) has suggested a transgressive phase of the Godavari delta region in the early Holocene (8400 yr BP – 8000 yr BP) resulting from early Holocene sea level rise. Reddy et al. (2013) have tried to investigate changes in past climate based on stratigraphy OSL dating of sand dunes along the east coast of Andhra Pradesh. Their result is based on detailed analyses of 47 samples in total and 7 sediment cores for OSL dating with depth varying between 1 m to 7 m. The study has disclosed that the dunes were aeolian in origin with a long deposition history (9000 yr BP to 1700 yr BP). Das (2014) has attempted to analyze palaeoclimate on the basis of palynological evidence through ^{14}C dating in Garia, a suburb of Kolkata. The study based on biostratigraphy and palaeopalynological from the bore core samples (depth 21 m from the surface) obtained from the lower Bengal basin reflected a fluctuating environment between brackish and freshwater influenced by marine existence during 7000 yr BP - 2600 yr BP.

The study of Basavaiah et al. (2015) has been based on the mineral magnetic, geochemical and textural parameters as well as ^{14}C dating to analyze the Quaternary environment in Kolleru Lake. The result has revealed that the lake has been formed during Holocene. Using four borehole cores with a varying depth of 9.5 m to 12.5 m they have revealed the existence of an arid climatic regime during the Late Pleistocene period accompanied with a lower sea level than the present. Between 10000 yr BP and 9000 yr BP, a stronger monsoon has been marked with a sharp decline during 9000 yr BP and 8000 yr BP and rise during 7000 yr BP. This has suggested that during the early to middle Holocene a fluctuating climate has been marked resulting from stronger monsoon and probably a higher sea level. However, a

weakening in the monsoon and fall in sea level has been inferred between middle to late Holocene. Major tectonic subsidence also took place during 5500 yr BP that had led to submergence. The work of Rao et al. (2015) has investigated the evolution of Godavari delta during Holocene based on the analyses of landforms and 11 borehole cores retrieved from the delta plain using ^{14}C dating. The analyses of sediment facies and their ages have indicated a rapid rise in local sea level during 10000-8000 cal yr BP followed by a slow rise to its present level around 5000 cal yr BP. Successive changes in the main delta lobes have been revealed by spatio-temporal variation in sediment deposition and palaeo shorelines. They have also identified six stages of delta evolution during Holocene. However, due to the construction of dam and water divergence after 1970s Godavari delta plain has been reported to be shrinking. Rao et al. (2015) have carried an extensive study based on 11 undisturbed continuous cores whose depths have ranged from 15.5 m to 54.2 m. It has also been found that the recovery of sediment cores was better in muddy sediments while it was poor in sand layers. Mazumdar et al. (2015) have presented the first comprehensive analysis of the provenance of the Krishna-Godavari and Mahanadi offshore basin sediments using geochemical proxies. Geochemical composition and clay mineralogy of sediments have been used to find out the source region. It has appeared that the Mahanadi sediments have mainly come from the late Archean-early Proterozoic peninsular gneissic complex whereas the sediment of Krishna-Godavari has been primarily derived from mixing of late Archean-early Proterozoic peninsular gneissic complex and late Cretaceous Deccan basalt. As per the study, the use of clay mineralogical contents combined with weathering indices can be used for high resolution palaeoclimatic reconstruction.

In Odisha, Konhauser et al. (1997) have based their work on the geochemistry of river sediments from Odisha. They have collected samples manually from the surface of the rivers Mahanadi, Brahmani, and Baitarani as well as from their tributaries. The mineralogy of all the sediments has been examined using X-ray diffraction (XRD). It has been found that sediments of all the three river basins have higher elemental concentration than crustal abundances with some regional anomalies. In their investigation, Mohanty et al. (2003) have analyzed the geochemistry of monazite sands of Chhatrapur, Odisha and also have tried to trace the source of these sediment deposits. They have successfully utilized PIXE and EDXRF techniques to study the geochemistry of monazite sand. The Eastern Ghat

provenance, as found, has most probably been the major source of the heavy mineral assemblage of Chhatrapur placer deposits. In his study, Asa et al. (2013) have tried to assess the concentration of some selected trace metals in River Brahmani and Baitarani along the Dhamara Estuary. Different risk indices have been applied along with multivariate analysis for the quantification and interpretation of metal contamination in the sediments. This study has indicated that the concentration of metals like Cd, Co, Cr and Pb in the study region is higher than the World Surface Rock (WSR) average because of anthropogenic activities in the upper catchment area. It has also appeared that concentration of Zn, Cr, and Pb are present above the average of Indian rivers.

OSL technique has been used to examine the chronological development of the barrier spit separating Chilka Lake from Bay of Bengal (Murry and Mohanti, 2006). Lagoons, along the coast, provide remarkable sites for the reconstruction of relative sea level changes. Khandelwal et al. (2008) have attempted the reconstruction of late Quaternary vegetation history of Chilika Lake and inferred that the Holocene sea level variations from palynological analysis. They have collected extensive surface as well as short and long core samples from the lagoon. The lithological units have been described based on color, texture and organic content in the sediment. They have identified several transgressive and recessive episodes along the Odisha coast that, over time, led to the evolution of Chilika Lake around 500 years BP

The study of soil geochemistry and mineralogy can disclose substantial changes that occurred in past climate (Bandopadhyay et al., 2010 and Basavaiah et al., 2015). The interpretation of palaeoclimate based on palaeosol has been carried by Bandopadhyay et al. (2010). In their work done in Keonjhar, Odisha, the palaeosol analysis has unveiled their formation under a palaeoclimate marked by seasonal rainfall. Most probably the climate was sub-humid to sub-arid which has altered between very wet and very dry climatic cycle.

In their study, Tripathi et al. (2014) has rebuilt the palaeo-vegetation and climate in western Odisha based on pollen analysis. They have also tried to recognize the signature of climate change in the sediment sequence. Their study has concluded that during 5840-4380 yr BP there flourished dense tropical mixed deciduous forest in the region that can occur under a warm-humid climate with a highly active monsoon. Subsequently, there has appeared an

increase in the humid condition during 4380-3230 yr BP as evident from the increase in forest element. Between 3230 and 1860 BP mild climate with less humidity has existed as compared to the present. Afterwards, a more humid climate has returned between 1860 and 1300 BP. Since 1300 BP a strong signal of Little Ice Age can also be observed from the region that led to a drier climate. However, the study is not comprehensive as they have based their entire analysis on only one sediment core sample and thus the results cannot be verified. Palaeoclimatic records of continental shelves provide significant information but these are very scarce along Indian subcontinent. Yadav et al. (2017) have studied palaeomonsoon variability for Rushikuliya river mouth, coastal Odisha. They have performed elemental and grain size distribution analysis retrieved from sediment core of the continental shelf to quantify the palaeoclimatic changes along with radiocarbon dating. To understand sea floor morphology and sedimentary processes spatial distribution of grain size (clay vs sand) and geochemistry (TiO_2 vs Al_2O_3) has been carried out. These analyses have helped to interpret the changes in terrigenous supply. The results have indicated a period of increased surface water runoff from 6800 to 3100 cal BP followed by a drier environment during 3100 cal BP to present that can be the manifestation of declining monsoon. The weakening of monsoon has been reported from other locations also showing the response of Indian monsoon to changing solar insolation during the late Holocene.

Reconstruction of past climate has been based on both relative and absolute approaches. The development of sequence stratigraphy has been associated with the publication of Vail and colleagues in AAPG Memoir (Blum and Tornqvist, 2000). Their work has initiated a wave of research reviewing the reactions of depositional systems to sea level change (Blum and Tornqvist, 2000). And to date, it is still one of the most preferred tools to analyze palaeoclimate. Studies of continental stratigraphic records, Quaternary and ancient were further energized in the final decade of the twentieth century.

The number of studies using tree ring as a proxy tool has appeared to be quite limited for the purpose of palaeoclimatic reconstruction in coastal areas (Ramesh et al., 1985). The use of cross dating now a day, however, has made it possible to stretch back tree ring records for thousands of years. The isotopic composition of tree cellulose can also be used as it is believed to be less influenced by ecological as well as biological parameters. On the other hand, geochemical properties of sediments have been frequently evaluated to understand and

interpret the palaeoclimate in coastal locations (Francine et al., 1995; Lone et al., 2018; Pennington et al., 2019;).

The sediment geochemistry has also been regarded as a crucial tool to analyze the palaeo-redox environment. The abundance and depletion of oxygen in the depositional setting has been assessed using Al, Fe, Mg, Ca, Mn, Zn, U, V, Y, Th, Mo, Sb and TOC along with various ratios as Fe/Al, La/Sc, La/Co, V/At etc. (Poulichet et al., 1997; Morford and Emerson, 1999; Ferrat et al., 2011; Pi et al., 2013; O'Connor et al., 2015; Coynel et al., 2016; Goldberg and Humayun, 2016; Madhavaraju et al., 2016; Kumar et al., 2017; Natali and Bianchini, 2017; Costa et al., 2018; Eltom et al., 2018).

Ferrat et al. (2011) have investigated monsoonal changes in Tibetan plateau using Sc, Y, Th, and REEs. Oceanic redox condition has been studied in Guizhou province of South China (Pi et al., 2013). The enrichment of U, V, and Mo in the lower black shale has been linked with euxinic conditions. Assessment of variation in the depositional setting has been conducted for Permian Irati formation in Brazil on the basis of Ti, Al, Ca, Mg, Fe, Mn, TOC and Fe/Al (Goldberg and Humayun, 2016). The study of Madhavaraju et al., (2016) has examined the history of sedimentation and palaeoredox environment in Baja California using SiO₂, CaO, and ratios of La/Sc and La/Co. History of sedimentation in Guryul ravines located in Jammu and Kashmir has been detected on the basis of selected trace and REEs (Kumar et al., 2017). They found that the enrichment of Co, Ni, Cu, V, and Zn has revealed reducing condition during sediment deposition in. Costa et al. (2018) have observed that Mn and Ni are the indicators of enhanced oxygen availability whereas Zn, V, and U are the indicators of oxygen depletion. Increase in oxygen abundance in Juan de Fuca Ridge, North Pacific Ocean has been linked with better ventilation during the glacial period. Change in the environment of deposition has been examined in Saudi Arabia using redox-sensitive trace and rare earth elements (Eltom et al., 2018).

Arcellacean or Thecamoebian with pollen succession has been used to study palaeoclimate of Atlantic Canada (Francine et al., 1995). They have been considered as a significant indicator of past climate due to their quick response to environmental changes. They can also record short term phenomena as Mid-Holocene Hypsithermal.

Apart from animal and plant remains and geochemistry, fossil soil or palaeosols have also been helpful to recognize past climate and processes as the reconstruction of the most general indices like maximum and minimum temperature and mean annual precipitation can

be done using palaeosols (Hopkins, 1995; Morozova, 1995; Stern et al., 1997; Sheldon et al., 2009; Bandopadhyay et al., 2010).

Radiocarbon dating, as a tool of palaeoclimatic has been generally applied to all types of environment where organic matters are available. Nevertheless, the palaeoclimatic reconstruction in the costal environment has been mostly conducted using radiocarbon dates (Hughen, 2007; Rao, 2012; Alexanderson et al., 2014; Basavaiah et al., 2015). ^{14}C dating has been the most common methods used for dating organic materials (Rao, 2012; Alexanderson et al., 2014; Basavaiah et al., 2015). Along with this, ^{14}C has been considered to be a powerful tool for accurate dating of marine sediments that can also be used as a geochemical tracer of climate change (Hughen, 2007). However, areas with low organic products and/or lack of preservation capacity restrict the utility of ^{14}C dating. Limited sample size can also manifest into large standard deviation and ^{14}C dating becomes less reliable when the targeted age range is above 30,000 years BP as the result can be strongly affected by even minor contamination. Thus, a more reliable method is required to establish chronology in coastal areas.

Recently the use of luminescence dating has opened new horizons in the field of palaeoclimate. Luminescence dating has gained more prominence presently (Srivastava et al., 2003; Murari et al., 2007; Jayangondaperumal et al., 2012; Alexanderson et al., 2014; Alappat et al., 2015). It includes optically stimulated luminescence (OSL), infrared stimulated luminescence (IRSL), and thermo luminescence (TL) inferred using quartz and feldspar. A key factor in luminescence dating is resetting or zeroing or bleaching of the luminescence clock during or immediately before the event to be dated, i.e. whether the quartz or feldspar grains were exposed to sufficient light or heat at the deposition time (Alexanderson et al., 2014). Zeroing is comparatively faster for OSL than for IRSL and TL. Generally, glacio-fluvial, shallow marine, littoral, and Aeolian sediments are well bleached. It has been recognized that age overestimation due to incomplete bleaching is less than a few thousand years which is meager for dating Pleistocene but it will be significant for younger deposits i.e. Holocene. However, even in such challenging environments, reliable outcomes have been achieved using luminescence techniques through the dating of single grains or small aliquots (Alappat et al., 2015). One of the researches, based on OSL dating has examined the ancient settlement of Angkor Borei near southern Mekong delta in Cambodia by Bishop et al. (2004). They have tried to examine the pattern of settlement development

along Angkorian canals based on the sedimentation pattern as well as have tried to understand the cause that has transformed this area by the mid-first millennium. The evidence of re-digging in stratigraphic and luminescence samples along with disturbed canal sediment probably represent the issue of swamping and shallowing of the canal or a bank collapse. The study has found a correlation between the decline in the intensity of land use and demise of canal which, however, may not be the appropriate cause behind regional depopulation.

Most of the dating methods have problems related to the availability and quality of materials to be dated i.e. scarcity of organic material for radiocarbon dating. But new developments in dating techniques have provided a wider range of datable materials. This includes a smaller amount of organic material and lower detection limits for ^{14}C dating as well as single grain analysis and new analytical protocols in luminescence dating. The AMS ^{14}C dating, however, has solved some of these issues as it requires a very little amount of sample for dating.

The main purpose of the literature review was to examine the palaeoclimatic changes as reported across the globe using distinct proxy sources- sediments, pollen, tree rings, geochemistry, etc. It has become apparent that the climate has varied significantly at the global and local scale. The regional changes may not always be associated with global perturbations as these can be highly influenced by the local oscillations in sea level and tectonics. However, some events such as hot-humid early Holocene and relatively drier mid-Holocene are experienced at a larger scale, may be at slightly different time intervals. It has also become obvious that in coastal regions, mainly for sub-surface sediment deposits, radiocarbon dating is the most favoured as other techniques i.e. OSL, might not yield the desired results.

The findings of the studies have also demonstrated a cyclic pattern of climatic oscillations, varying from humid to dry and vice versa throughout geological history.

1.3 Rationale of the Study

The present work deals with the global issue of climate change with an emphasis on palaeoclimate. The recent uproar regarding the rate and magnitude of climate change has provided an edge to this study as the palaeoclimate analysis offers a comprehensive

understanding of the climatic dynamism which is impossible through direct instrument based data assessment. The palaeoclimatic studies have also enriched the understanding of climate at a broader time scale. Apart from these, there has appeared a complete absence of studies based on reconstructing past climate along the lower reaches of river Baitarani. Nonetheless, there are works available on geochemical analyses of sediment but their number is very limited for the area. In this context, this work is first of its kind to attempt the reconstruction of the palaeoclimate in the Lower Baitarani Basin. Subsequently, there exists scattered account of palaeoclimate data of the Odisha coast. Some studies have been done using pollen as proxies. Even more importantly, efforts to integrate geochemistry and dating techniques to reconstruct palaeoclimate are insignificant and scanty in number, especially for this region. In this backdrop, the present study has been aimed to reconstruct the palaeoclimate along the lower Baitarani basin, Odisha and to examine the processes that have prevailed in the region during the Holocene. In addition, this research is also intended to serve as a link for reconstructing of palaeoclimate of the eastern coast.

1.4 Research Questions

During the commencement of this work, numerous questions have emerged while surveying the area and reviewing the literature. These were basically oriented towards the applicability of the methodology and probable outcomes. An attempt, in this regard, has been made to answer a few fundamental questions, which have encouraged the analysis throughout. The analysis is intended to answer the following research questions-

1. How variation in physical and geochemical characteristics of sediment can provide clues to the past climate?
2. Whether these information can be applied to deduce the dominant processes which have operated in the past?
3. How aptly these proxies can be utilized to reconstruct the past climate in the region?

1.5 Objectives

The basic goal of this research is to reconstruct the palaeoclimate of the study area during Holocene. To fulfill this purpose, the following objectives have been incorporated in this work-

1. To investigate the utility of geochemistry of sediment deposits in unraveling the palaeoclimate.
2. To construct the chronology of landforms.
3. To reconstruct the palaeoclimate and analyze the processes which have operated in the area of study.

1.6 Data Base

The present work is based on 53 samples retrieved from subsurface cores up to the depth of 1000 cm (Table 1.2). These samples were obtained from eight sites along the lower reaches of river Baitarani. These are located in Jajpur and Bhadrak district of Odisha, East coast of India. The elevation of the sample collection site has varied considerably. The height of palaeochannels, EP and KTI are relatively lower than the inter-channel region from where JP and KTII were collected. The deviation in general elevation is likely to manifest in the stratigraphy.

Table 1.2 Details of samples collection site in Lower Baitarani basin, Odisha

Sample ID	Lat/long	Location	Elevation (m) AMSL	Depth (cm)	Sub-samples	Distance from the Coast (km)
EP	20°50'33.3"/ 86°24'49.5"	Ezapur, Jajpur	08	0-1000	07	59
JP	20°49'52.5"/ 86°26'40.5"	Jhumpuri, Jajpur	10	0-1000	11	55
KTI	20°49'30.5"/ 86°28'15.2"	Katia, Jajpur	06	0-140	05	52.8
KTII	20°49'20.2"/ 86°28'08.2"	Katia, Jajpur	07	0-165	09	52
SP	20°47'29.6"/ 86°40'36.6"	Sanpanki, Bhadrak	02	0-1000	06	31
CB	20°46'42.7"/ 86°44'50.1"	Chandbali, Bhadrak	07	0-1000	06	24
AG	20°45'46.6"/ 86°46'23.6"	Ambiligan, Bhadrak	05	0-1000	05	21
KK	20°45'38.1"/ 86°48'31.4"	Kasturikan, Bhadrak	02	0-1000	04	17.5

1.7 Methodology

The study has incorporated a multi-proxy approach using sedimentary sequence and ¹⁴C dating to evaluate the past climate. This includes both the relative approach including the physical attributes, geochemistry, geochemical proxies as well as absolute approach

including geochronology of sediment deposits to infer the palaeoclimate and processes that have operated in the past in the study region (Figure 1.1). This study has been carried out in the following steps-

1.7.1 Sample collection and Pre-treatment

The area has been classified into two distinct zones, riverine and mixing, based on the present geomorphic regime (Table 1.3). In existing circumstances, in the riverine zone, fluvial processes are more effective whereas in the mixing zone the environment of deposition has been marked by both fluvial and tidal processes. A fault line also runs almost parallel to the Baitarani River bank, separating the sample collection sites into southern and northern transects. The samples obtained from the riverine zone fall in the southern transect while those collected from mixing zone are situated in the northern transect of this fault line (Figure 1.3).

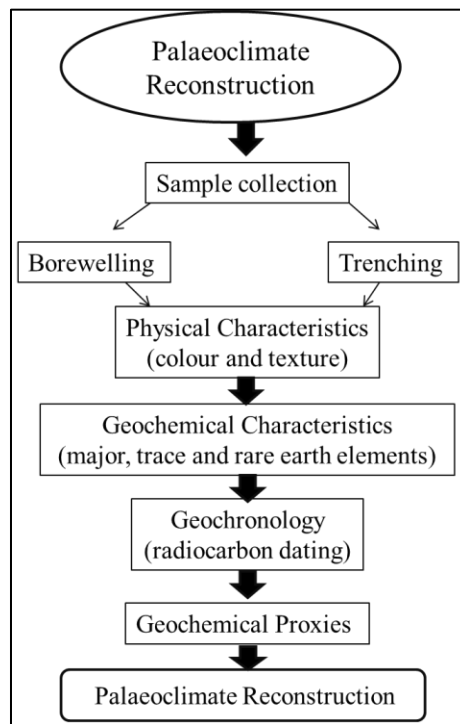


Figure 1.1 Scheme of methodology applied in present study

A total number of eight subsurface sediment samples up to the depth of 1000 cm have been obtained from riverine (EP, JP, KTI, and KTII) and mixing (SP, CB, AG and KK) zones. Sample EP has been collected from Ezapur, JP from Jhumpuri, SP from Sonpanki, CB from

Chandbali, AG from Ambiligan and KK from Kasturikaran villages through bore-welling up to the depth of 1000 cm (Plate 1.1). In addition, KTI and KTII from Katia village have been collected by trenching to a depth of 140 and 165 cm (Plate 1.2).

The facies have been identified for each site at different intervals depending on the specific colour and textural characteristics. Each of these samples has been treated for colour, texture, geochemical and radiocarbon dating according to the requirements.



Plate 1.1 Subsurface sample collected using bore-welling

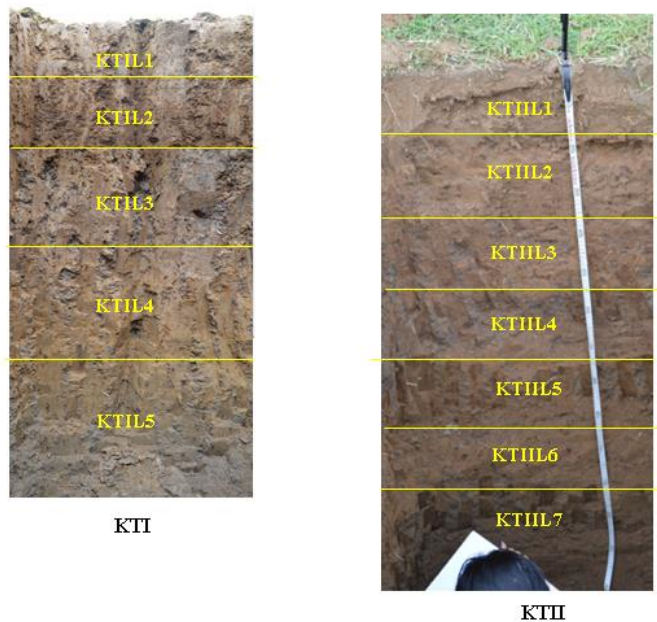


Plate 1.2 Subsurface sample collected using trenching

1.7.2 Colour and Textural Analysis

The idea behind colour and textural determination was first to identify distinct sub-surface sedimentary facies as the colour and texture are the most common physical attributes of the sediments. Subsequently, the colour and particle size distribution have been considered as significant tracers of the past climate and depositional environment. Hence, down core variability in colour and texture has also been used to differentiate between depositional environment. The analysis has been done using the Munsell colour chart and hydrometer (Plate 1.3). The details have been provided in Chapter 2 (Section 2.2).

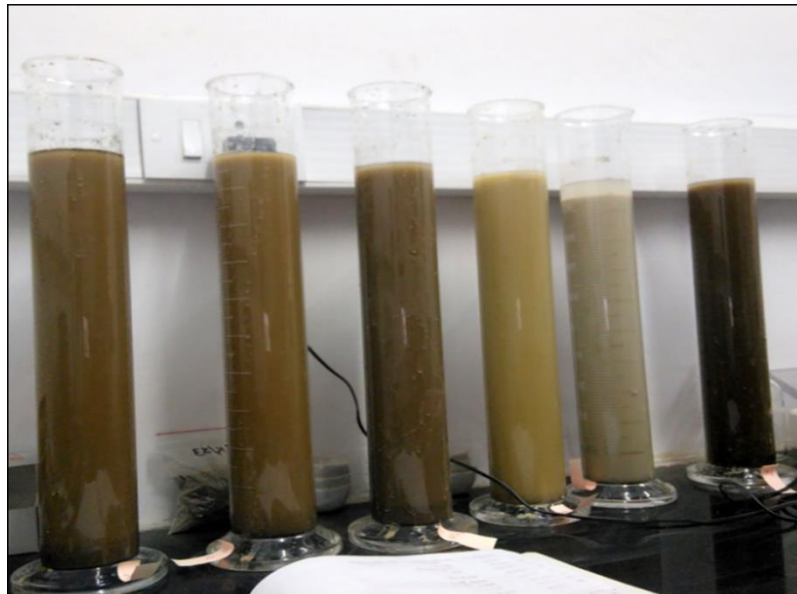


Plate 1.3 Analysis of particle size distribution using hydrometer

1.7.3 Geochemical Analysis

The geochemical characteristics of the sub-surface sediments have been investigated to review the existing climate during the time of sediment aggradation along with colour and texture. Under a distinct climate, certain metals are enriched while other gets depleted. These also assist in distinguishing the fluvial and marine processes in coastal regions. Thus, the distribution of major, trace and rare earth elements also provide clues to the past climate and processes.

The geochemical analysis is based on Energy Dispersive X-ray Fluorescence (EDXRF) techniques. The EDXRF employs rather simple preparation of samples and also offer a fast multi-elemental analysis in a broad concentration range from percentage to ppm

(Bounakhla, et al. 2008). Therefore, for the present study concentration of major in percentage (%), trace and rare earth elements (REEs) in parts per million (ppm) has been reviewed using EDXRF. The enrichment factor of the elements in comparison to the Upper Continental Crust value is also examined to assess their enrichment and depletion across the facies. A more detailed discussion has been given in Chapter 3 (Section 3.2).

Furthermore, the analysis of palaeoredox environment has been carried on the basis of enrichment and depletion of selected redox-sensitive elements. A detailed discussion of the methodology has been provided in Chapter 4 (Section 4.2)

1.7.4 Total Organic Carbon (TOC)

The concentration of total organic carbon (TOC) is determined to analyse the palaeo-environmental conditions of deposition. TOC is also one of the most crucial tracers of primary productivity. Hence, it has been used as a proxy to examine the palaeoproductivity. The percentage concentration of TOC has been examined using the Walkley-Black titration method (Chapter 3).

1.7.5 Geochronology

The chronology of deposition and the process involved in sediment aggradation has been determined through direct and indirect methods. A combination of absolute and relative technique has been used to determine the geochronology and also to reconstruct the palaeoclimate.

The analysis of chronology and palaeoclimate reconstruction has relied on radiocarbon (^{14}C) dating. It was done using Accelerator Mass Spectrometry (AMS) conducted at Inter-University Acceleration Centre (IUAC), New Delhi, India (Plate 1.4). Samples with carbon content above 0.5 % have been selected for AMS radiocarbon dating. The details about the method have been provided in Chapter 6.

It has been observed that radiocarbon dating has been the most often used method for palaeoclimate reconstruction in coastal locations. It is based on the law of radioactive decay. ^{14}C isotope is continuously formed in the atmosphere by the action of cosmic rays. The ^{14}C ions combine with oxygen to form Carbon-di-oxide (CO_2) and enter in the Earth's

carbon cycle. The age range of ^{14}C dating is limited to ~50,000 years with a half -life of 5730 years.



Plate 1.4 Steps involved in graphitization of sediment samples for AMS ^{14}C dating (a) ABA treatment, (b), determination of percentage carbon content in soil (filling samples in aluminium foil and), (c), graphitization of samples (d) samples after ^{14}C dating using AMS

The ^{14}C dating has relied on the concept of –

- How much radiocarbon (carboneous material) would have been in the organism when it was alive?
- What is the rate of radiocarbon decay?
- How much radiocarbon is remaining?

1.7.6 Geochemical Proxies

In this study, the geochemical proxies have been used as the relative method of palaeoclimatic reconstruction. With the help of geochemical proxies the processes were analyzed and even in those locations where radiocarbon dating could not be performed (i.e. the riverine zone). Through the assessment of terrestrial flux, palaeoproductivity, weathering and salinity using these proxies the changes in rainfall intensity has been assessed which has been used to infer the past climate. An increase or decline in these indicators have been associated with enhanced fluvial activity or marine influence. Thus, the geochemical proxies suggest the past climate and dominant processes operational at that time. These have also

indicated changes in sea level in the study area. Along with geochemistry, as mentioned earlier, ^{14}C dates have been used to provide a temporal context to past climatic events. The details are discussed in chapter 6 (section 6.2)

1.8 Area of Study

The proposed study has been carried out in the selected locations of the Lower Baitarani Basin. These are located in the coastal plains of Jajpur and Bhadrak districts of Odisha (Figure 1.2). The sample sites were identified based on the landform types present in the fluvial and coastal environments.

Odisha has been categorized into two broader geographic divisions – 1) Odisha highland region towards the West and 2) Coastal plain towards the East (Singh, 1971). The 75 meter contour line delineates the coastal plain from western highlands. The coastal plain of Odisha or Utkal Plain is a low lying stretch of land. The Utkal Plain extends between the River Subarnarekha (West Bengal) in the north and the River Rushikulya in the south having the maximum width near the Middle Coastal Plain close to Mahanadi Delta. It is the narrowest in the Southern Coastal Plain near Ganjam Plain. These coastal plains are primarily depositional in nature and of recent origin (Singh, 1971).

In order to investigate the past climate and processes, comprehensive knowledge of the study region in the form of its geology, geomorphology, existing climate and soil is imperative. Thus, these attributed will be discussed in the following sections-

1.8.1 Geology and Stratigraphy

Odisha is located on the eastern periphery of Peninsular India. A larger part of the total area (>70%) is occupied by Precambrian metamorphic rocks of Archaean and Proterozoic Eras (Figure 1.3). These are the major sources of minerals found in the state. Around 30 % of the total area is occupied by the Tertiary and Quaternary formations considered as the source of aluminous/nickeliferous laterite and heavy metals in the sand found in coastal areas. The spots of Gondwana supergroup are represented in coal bearing formations. In the northern region, the Archaean formations are characterized by the gneisses, granite, and Migmatite (Mahalik, 2013). In between, some patches of mafic/ultramafic intrusions are also observed. These are the sources of Chromite, Titaniferous, Vanadiferous Magnetite. In the western

part, the Archaean group includes Gnesses, Granite, Migmatite and Sartonium bearing strata.

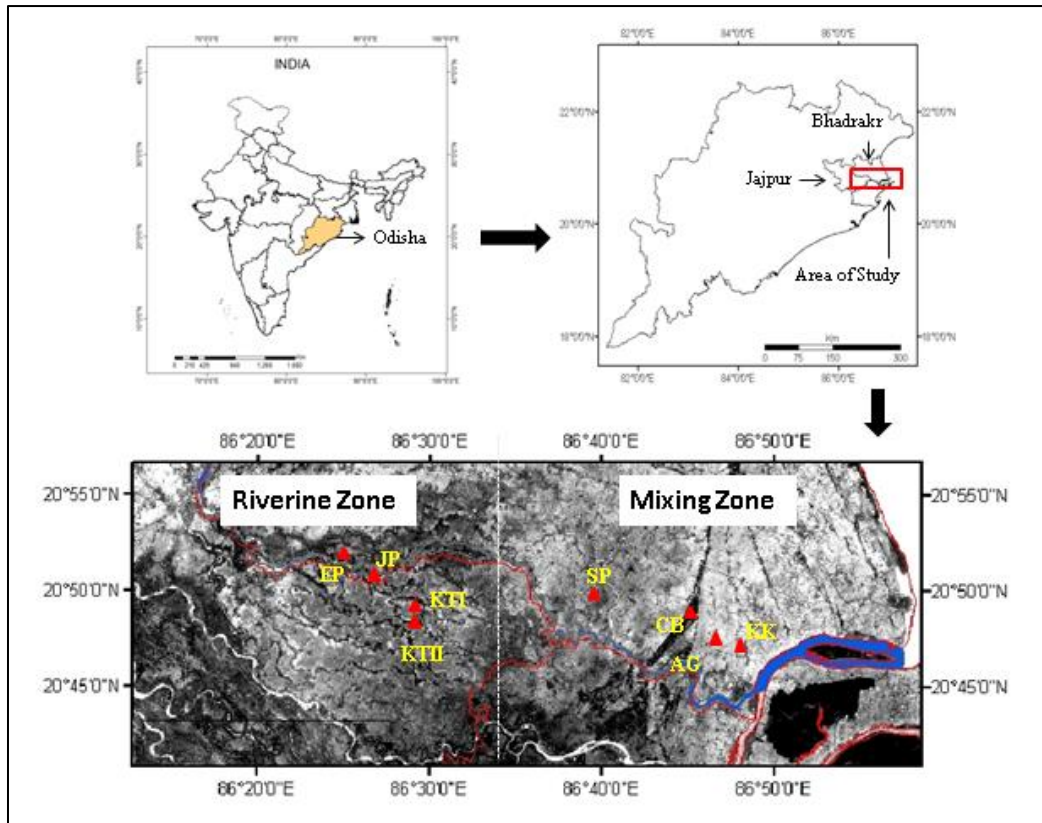


Figure 1.2 Location of the sample collection sites

Note: EP=Ezapur, JP=Jhumpuri, KTI=Katia I, KTII=Katia II, SP=Sonpanki, CB=Chandbali, AG=Ambiligan, KK=Kasturikaran

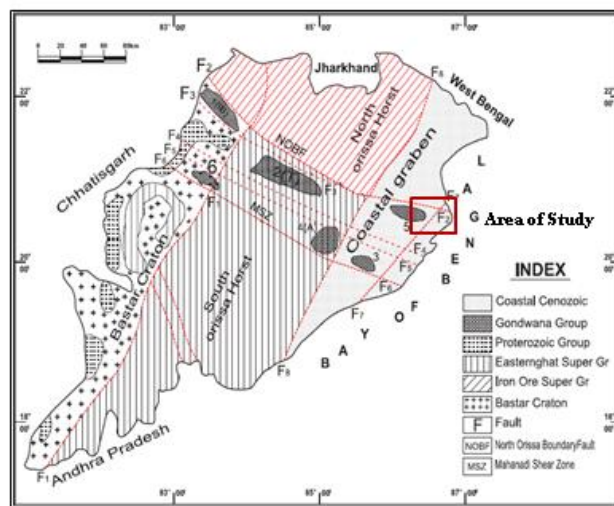


Figure 1.3 Geology and major landforms in area of study based on Mahalik (2013)

Proterozoic rocks in western Odisha are found in the form of sedimentary formations. These are associated with limestone deposits. In north-western part, these are classified as Gangapur group containing Manganese, limestone, and lead-zinc deposits. In central and southern Odisha, these formations are represented by the Eastern Ghat containing Khondolite, Charnockite, Migmite, and alkaline rocks.

The eastern coastal plains are occupied by the formations of Cenozoic age (Vaidyanadhan and Ghosh, 1993) These are observed in the form of sand, ash beds and low level laterites. River Baitarani and Brahmani along with the Mahanadi form the middle coastal plain. Geologically the Utkal plain belongs to the Post-Tertiary Period. Stratigraphically, as described by Vaidyanadhan and Ghosh (1993), Precambrian Khondalites, Charnockites, and Anorthosite occur as the discontinuous hills and mounds in the combined basin of Mahanadi, Brahamani, and Baitarani. The laterites have been found on the Pleistocene boulder conglomerate. These sediments are clearly fluvial in origin and have been called as Khurda formation and Belgarh formation. This Pleistocene formation has created the base of the younger sediments constituting the delta. Younger than the Belagarh formation has been recognized as alluvial deposits along the valleys forming the oldest terrace in the upper part of the delta region. These sediment deposits have identified to be of the late Pleistocene to early Holocene age. These have been known as Belipada formation. The Belipada formation has been covered by the laterite wash and hill wash that have been underlain by laterites. The Holocene sedimentation under fluvial dominance has occurred along the basin margin creating a young terrace along major drainage channels. These terrace sediments have been recognized as Bankigarh formation of middle the Holocene period. The sediment consists of alternate layers of brownish silt and very fine sand with silty clay in between. The sedimentation pattern is very complex in nature. This has been formed due to fluvial, fluvio-marine, marine and aeolian influences. These have been accumulated on the deltaic plain and coastal tract (Singh, 1971).

1.8.2 Physiography

The respective basins are marked by conspicuous variation in physiography consisting of hills, isolated hillocks, undulating plains and alluvial tracts (Figure 1.4). In Baitarani basin,

particularly, highly resistant rocks such as quartzites, banded hematite quartzites, and dolorites constitute the hill range; the undulating terrain bordering the hills comprises laterite zones forms the uplands, and flat alluvial terrain on Late Pleistocene to recent sediments occurs in the flood plains. This alluvial tract occupies lower elevation and is located at a height of around 20-35 m above mean sea level. The coastal areas are covered with deltaic sediments, formed in recent times.

The area presents gently undulating to flat topography without major altitudinal variation. The general slope is towards east and south-east. The entire area can be broadly divided into four distinct geomorphic units-

(a) Coastal Plain

It is a gently sloping plain occurring parallel to the coast. These have been formed by fluvio-marine action and intersected by a network of creeks, which are basically saline due to tidal action. The area is marshy with shrubby vegetation. The width of the plain varies from 5 to 25 km. The coastal plain encompasses a series of beach ridges characterized by sand dunes running almost parallel to the coast.

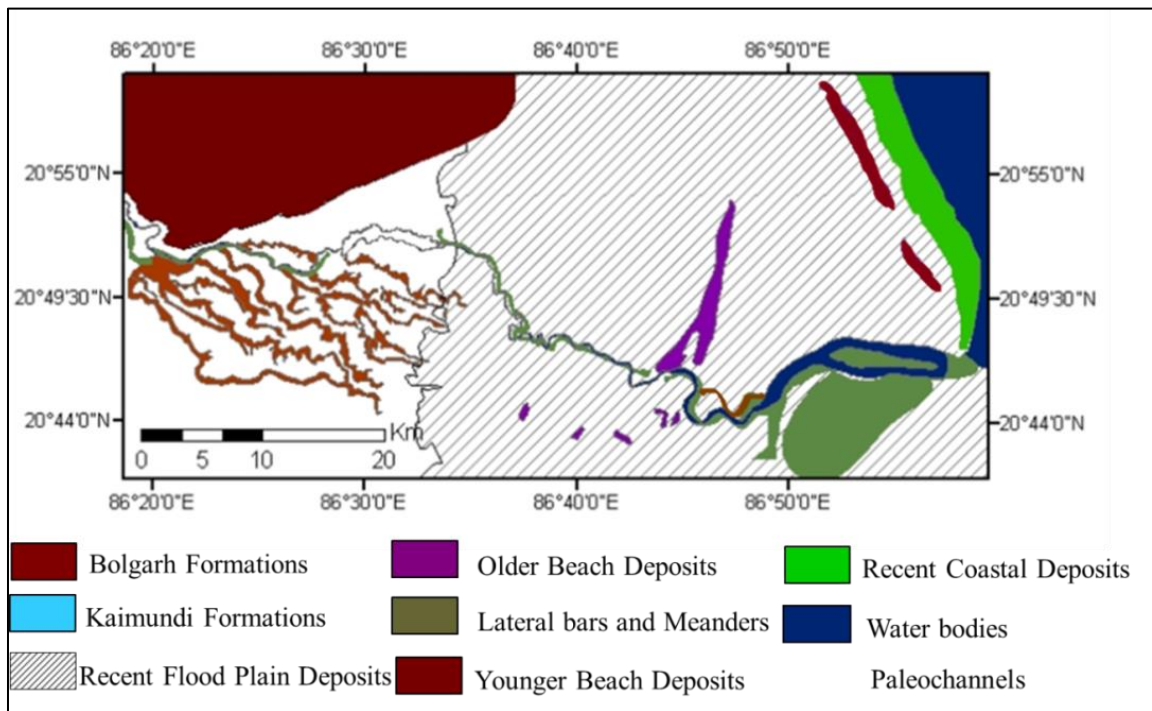


Figure 1.4 Geology and major landforms in area of study

Source: Geological survey of India map

(b) Alluvial Plain

Gently sloping alluvial plain occurs to the west of the coastal plain and forms the most fertile area of this region. It can be further divided as-

Older Alluvial plain: The north-west part of the region forms older alluvial plain. This has been attributed mostly due to the earlier cycle of deposition of sediments carried by streams and constitutes gravel, sand, and clay. At places, lateritisation at the top down to a depth of few meters has also occurred.

Younger Alluvial plain: It represents the major part of the area near river channels. This has been developed due to depositional activities of the major rivers in the fluvial environment. Several geomorphic units like palaeochannels, meander scars, oxbow lakes are also found.

(c) The Older Beach Deposits

The older beach deposits of coastal Odisha indicate the emergence of the coast (Singh, 1971). Along the coast, there are many sandbars generally near the river mouths. Coastal islands also occur frequently. The plain of marine and aeolian deposits found up to 10 km inland. It has been recognized as a zone of sand dunes (Geological Survey of India Map). These have developed mainly by wind action. In Odisha plain, parallel sand dune ridges composed of granites, zircon, etc. by brought by ocean currents. These are supposed to be originated due to uplift. Each of these hills marks an old sea coast indicating the recession of sea. The coast forms a monotonous plain rising gently westwards to the foot of the Eastern Ghats. The plains are marked by deltas and lower course of mature rivers forming broad shallow valleys.

1.8.3 Climate and Drainage

The basin enjoys a subtropical monsoon climate with marked seasons of summer, winter, and monsoon. Bay of Bengal which forms the eastern boundary plays a significant role in controlling the climate of the region. The relative humidity is high varying from 40-90% during the year. It is recorded to be more during monsoon season and during winters minimum humidity has been found. Rainfall is mainly caused by the south-west monsoon.

Baitarani is the third largest river of Odisha after Mahanadi and Brahmani. It originates from the Gonasika hills. After originating, it flows underground for about half a kilometer as

Gupta Baitarani. The river finally drains into the Bay of Bengal after joining Brahmani and Dhamara mouth near the coast. Baitarani has a drainage basin of 8570 km², a length of 365 km and peak discharge of 14150m³s⁻¹. The major tributaries of the river include Deo, Kanjhari, Kusei, and Salanadi. The river Baitarani drains the North-East plateaus of Odisha with a varying height from 300 m to 1200 m and dominated by a flat topography. The upland of Baitarani forms the Eastern flank of Brahmani- Baitarani divide. The basin of Baitarani has been developed with the joint operation of Baitarani and Salnadi (Singh, 1971). Baitarani is an inter-state river flowing in the states of Jharkhand and Odisha. The lower part of the basin lies in Odisha completely and constitutes a part of the eastern coastal plain. The river is characterized by regular floods and destruction to life and livelihood.

1.8.4 Soil and Vegetation

Variety of soils is found in the area of study, which includes- Alfisols, Aridsols, Entisols, Ulisols, and Vertisols. Alfisols include deltaic and older alluvium soils. The deltaic soils are found along the course of the Baitarani river while older alluvium occurs in the extreme north-west part. The deltaic alluvial soils are generally deficient in phosphate and nitrogen whereas potassium is adequately available. The pH of the soil varies from 6.5 to 7.3. Aridsols are saline and saline-alkali soils occurring along the coast. These are rich in calcium, magnesium and also consist of half decomposed organic matter. Entisols include coastal alluvial soils which are deficient in nitrogen, phosphoric acid, and humus, but not in potash and lime. The soil texture varies from loam to clayey loam. It is alkaline in nature and most fertile soil of the area. Utisols include lateritic soils which are found in the western upland areas and poor in nitrogen, phosphorus, potassium and organic matter. Vertisols are medium black soils occurring in the northern regions and are rich in iron, calcium, magnesium, potash, and lime.

It the riverine zone the soil is less saline and hence, the agricultural activities are extensively performed (Plate 1.5). In contrast, in the mixing zone, the soil is not suitable for agriculture due to high salinity. Here, mainly pisciculture is done along with agriculture (Plate 1.6).



Plate 1.5 Landscape and vegetation in the riverine zone (a) Ezaphur, (b) Jhumpuri, (c) Katia I and (d) Katia II



Plate 1.6 Landscape and vegetation in the mixing zone (a) Sonpanki, (b) Chandbali, (c,d) Ambiligan

1.9 Classification of the Study Area

The coastal regions represent the amalgamation of various landforms having both depositional and erosional features, e.g. older beach ridges, deltaic plains, and shallow continental shelf, palaeochannels that are the repository of thick sequencing of the Quaternary sediments (Figure 1.4).

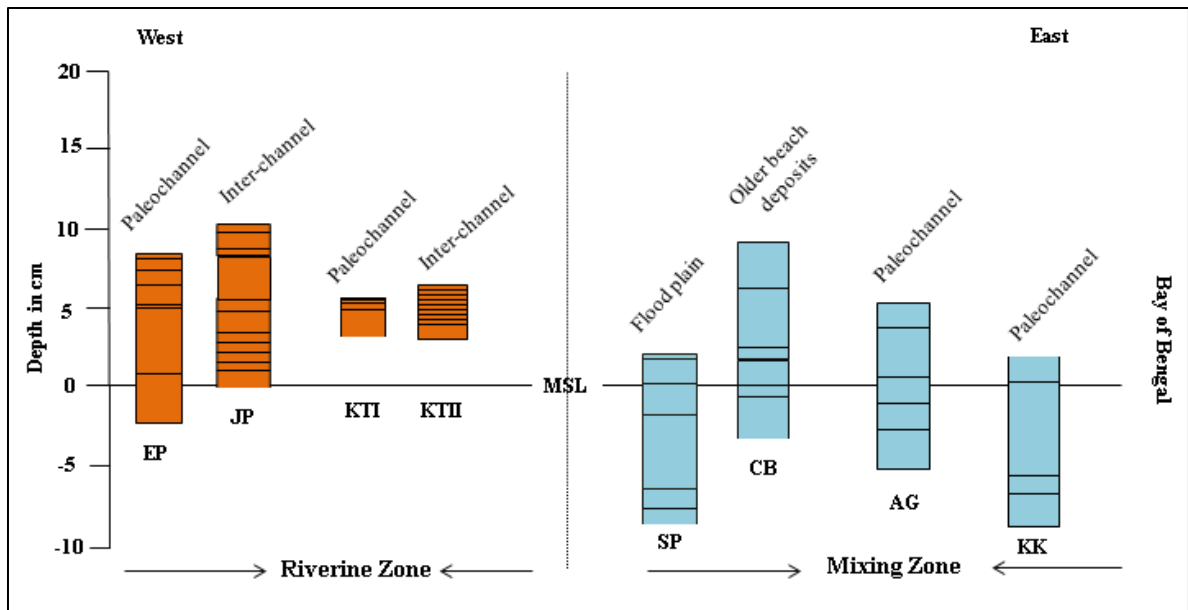


Figure 1.5 Relative height of the sample collection site

Note: The orange colour is showing samples collected from the riverine zone while blue colour is showing samples collected from the mixing zone

The study area has been divided into two characteristic zones- riverine and mixing zone (Figure 1.5). The basis of this classification is the governing geomorphic process at present. For instance, the riverine zone is dominated by the fluvial process; the mixing zone is affected by both fluvial and tidal processes. The samples, EP, JP, KTI, and KTII have been collected from river dominated area while SP, CB, AG and KK have been collected from mixing region of coastal Odisha (Table 1.3).

It is also significant to note that the sample EP and KTI have been collected from the palaeochannels of river Baitarani located in the riverine zone that also appears to be a portion of palaeo-delta. On the other hand, JP and KTII have been obtained from flood plains situated between two palaeochannels of Baitarani in the riverine region. Therefore, these have been considered as least affected by the tidal processes being located in relict landform. From mixing zone, SP has been obtained from the active flood plain near the confluence of Salnadi and Baitarani. CB has been collected from the beach ridge that traversed the region. The beach ridges are generally aggraded due to aeolian action along the coast. Thus, the existence of beach ridge has signified that in the past the sea level would have been higher. The samples AG and KK have been retrieved from the palaeochannels of

Baitarani near the Dhamara estuary approximately 18 km from the coast revealing dominance of tidal activity (Figure 1.5).

The sub-surface samples of EP, JP, SP, CB, AG, and KK have been collected through bore-welling up to a depth of 10 m along the lower reaches of Baitarani. The KTI and KTII samples, on the other hand, have been collected by digging the trench to a depth of 140 and 165 cm respectively from fluvial dominated area. Sediment facies for each location have been determined on the basis of colour and textural variability and representative samples from each facie have been collected at different depths. These sub-samples have been used for geochemical and radiocarbon dating.

Table 1.3 Major geomorphic regimes and landforms identified in the area of study

Geomorphic Regime/Landforms	Riverine Zone (Southern Transect)	Mixing Zone (Northern Transect)
Palaeochannels	EP, KTI	AG, KK
Flood plain or inter-palaeochannel region	JP, KTII	-
Active Flood plain	-	SP
Beach ridge	-	CB

1.10 Scheme of Chapterization

This thesis has been categorized into distinguish parts, general description of which has been provided below-

Chapter 1 introduces the study and reviews the existing literature. The database and methodology is also discussed along with the area of study.

Chapter 2 is based on the description of colour and textural properties of the subsurface samples on which basis facies have been determined. Along with this, it is also attempted to examine the past depositional conditions providing each facie distinct colour and texture. The grain size distribution has also been associated with probable processes influencing sediment transportation and aggradation.

Chapter 3 analyses down core deviation of selected major, trace and rare earth elements (REEs). Variation of each of these elements is discussed in comparison to the terrestrial

mean reflecting enrichment and selective mobilization of different elements. The relationship between major and trace elements has also been discussed.

Chapter 4 examines palaeoredox environment using selected trace elements and REEs. The fluctuation in the concentration of redox-sensitive elements has yielded crucial information about the availability of oxygen during the deposition in past.

Chapter 5 reviews the chronology of landforms aggradation during Holocene. The analysis can be only carried for the sites of mixing zone (SP, CB, AG, and KK) as radiocarbon ages are not available for the riverine zone. The geochronology has been discussed based on AMS radiocarbon dates.

Chapter 6 interprets and reconstructs the palaeoclimate using relative approach i.e. geochemical proxies along with radiocarbon dates. Based on perturbations in geochemical proxies the analysis of terrestrial flux, palaeoproductivity, weathering, and salinity condition has been conducted. The results have demonstrated distinct periods of enhancement and weakening of precipitation in the region.

Chapter 7 discusses the major findings and concludes the present work.

Chapter 2

Physical Characteristics of Sub- surface Sediments

2.1 Introduction

Prime physical properties of sediments comprise their colour and texture. These characteristics are the manifestations of the environment of deposition. The physical attributes also demonstrate the nature and rate of geomorphic processes that have operated in the region throughout geological history. Colour is one of the first observed features of the sediments. Discrepancies in colour across the stratigraphic sequences provide information about the water depth, diagenesis, and disposal of certain elements (Kobayashi et al. 2016). For instance, red, yellow and gray colours indicate the presence of iron in its various forms i.e. hematite, magnetite. Colour of the sediments is also modified by the abundance of organic carbon. A higher concentration of organic matter provides the sediments a black colour. Black and dark gray colour can also be attributed to partial oxidation of organic carbon due to low oxygen availability. Hence, an inquiry of colour scheme can yield vital information about the past depositional setting along with the key elements i.e. iron. These characteristics indirectly illustrate the palaeoclimate (Jakobsson et al. 2000; Sayem et al., 2018).

The sediments are also interspersed by organic matter during the deposition stage. Organic matter in diverse quantity is accumulated in addition to the sand, silt, and clay (clastic particles). The occurrence of organic carbon contributes to the palaeoclimatic analyses (Meyers, 1994). Along with clastic particles and organic carbon, the void spaces comprise of water. The water in the sediment profile carries dissolved ions and gasses that interact constantly with the metals and carbon. Lower concentration of organic matter and/or well-oxygenated environment allows complete decay of all the organic carbon. The remaining oxygen is used to oxidize other elements like iron. Subsequently, the oxidized iron gets converted into the mineral hematite (Fe_2O_3) which gives the sediment red colour. Thus, red color of sediments indicates an abundance of iron under the dry or well-oxygenated environment such as flood plains or shallow marine depositional conditions (Koukina et al., 2017). Dark red colour of sediments is associated with warm-humid environment while light red colour is considered as the representative of semi-arid to sub-humid depositional environment (Sayem et al., 2018). The formation of iron in a reducing sedimentary environment generated by the elevated flux of organic carbon can lead generate red colour

(Kobayashi et al., 2016). Furthermore, red and yellow colours also exhibit high primary productivity (Springer et al., 1996). Orange-brown colour of sediments indicates the higher supply of iron (Fe) and manganese (Mn) oxides (Koukina et al., 2017). The prime ingredient of dark brown to black colour sediments is the organic matter that is inadequately oxygenated or was under deep water and/or swampy environment. At the same time, it can also be the outcome of excessive accretion of organic carbon which was not decomposed properly due to insufficient availability of oxygen. Average oxygen and moisture availability provides sediments a yellow colour. In contrast, gray colour illustrates the deficiency of oxygen under prolonged waterlogged or swampy conditions. Grayish colour in deeper facies deposited during the Holocene has been attributed to reducing environment (Kobayashi et al., 2016). The white or grayish-white colour of sediment sequence with excessive fine sand specifies the presence of calcium carbonate. These are also indicative of excess leaching. Thus, it is apparent that colour can be considered as one of the proxy indicators of the past depositional environment and hydrology indirectly pointing towards the palaeoclimate.

The aggradation of sediments is initiated by the physical disintegration and chemical decomposition of source rocks. A portion of this weathered product may accumulate in situ forming palaeosols while the remaining are removed from the original site and transported to distant locations. These weathered materials are deposited as gravel, cobble, sand, silt, and mud when the transporting agent ceases to carry them. In the lower reaches of a river basin basically finer particles are deposited by the river channel. Relatively coarser sediments are delivered to the coastal environment from weathered rocks primarily with heavy rainfall and river runoff (Milliman and Farnsworth, 2011). Moreover, the properties and thickness of sediment sequences are largely governed by the bedrock, lithology, and climate (Faure and Volkoff, 1998). These factors also influence the intensity of weathering in the catchment and determine which minerals survive to become a part of the stratigraphy. A decline in sediment transportation and rate of accumulation can also lead migration of coastline towards the land whereas an increase in sediment supply can cause lengthening of river course (Krishna, 2017). Hence, in coastal areas the textural characteristics of the sediments are also be affected by the shoreline changes. Consequently, the textural

composition of the sediments bears the marks of the past climate and changes in the depositional processes.

The texture of sediment sequences illustrates the distribution of primary particles, mainly sand, silt, and clay (Briggs, 1977; Dyer 1986; Kettler et al., 2001; Butola, 2013). Particle size distribution (PSD) is one of the most fundamental physical attributes of sediment (Esmaelnejad et al. 2016). The analysis of PSD is a measurement of the size distribution of individual particles in a sample. It also influences chemical properties of the sediments such as absorption of chemicals and their cation exchange capacity (Erashin et al. 2006; Rizea et al 2009). Variations in the gradation of sediment particles reflect the mode of transportation and deposition which are the manifestations of changes in the geomorphic processes over time and space (Gui et al. 2010; Bedaiwy 2012). These clues are preserved in the form of a stratigraphic sequence and thereby, a cautious inspection of the stratigraphic sequences can yield significant information about the past climate (Warrier et al. 2016; Krishna, 2017). Furthermore, the analysis of particle size distribution reflects the intensity of transporting agents such as rivers, wind, and waves (Gui et al. 2010). It also reveals the competence of geomorphic agents to carry the sediments load as well as fall-in-velocity of the sediments below which they cannot persist in the transportation system.

The physical characteristics, therefore, are one of the commonly used approaches for facies classification (Amorosi et al., 2003). Earlier, these were also utilized to identify the similarities in the depositional environment at distant locations. The similar looking facies were supposed to be deposited under similar climatic and geomorphic setting (Krishna, 2017). However, this may not always be the case (Alexanderson et al., 2007). Sedimentary facies are considered a distinct layer having unique physical, geochemical or biological properties. Lithofacies are recognized mainly on the basis of unique colour and textural characteristics. It has been recognized that facies association and horizontal succession depends largely upon interconnected controls. The most important being sedimentary processes, sediment supply, climate, earth movements or tectonics, sea level changes, water chemistry, etc. (Kettler et al. 2001).

In this backdrop, the present chapter attempts to analyze the physical attributes (colour and texture) of the sub-surface sediment sequences of lower Baitarani basin, coastal Odisha.

This information is used to determine subsurface facies at each location. Subsequently, it is also intended to analyze the predominant geomorphic processes, riverine or marine which has operated in the past in the area of study on the basis of physical characteristics of the subsurface sediments.

2.2 Methodology

For this study, first of all colour of the sub-surface samples was determined. Thereafter, the textural analysis of sediment samples was done to identify the concentration of sand, silt and clay. Based on the distinctiveness of colour and texture, sub-surface sedimentary facies were identified. These physical properties were utilized as the tracers of changes in the depositional environment.

2.2.1 Colour Determination

Colour of the sediment reveals the concentration of metals and organic matter. Furthermore, it reflects the past climate that to a large extent controls the environment of deposition. In present analysis, Munsell colour chart has been utilized for sediments colour identification (Munsell, 1947). This colour chart incorporates three principal attributes of colours- hue, value and chroma also known as HVC (Cochrane, 2014). Hue is the colour i.e. red, yellow or brown, etc. The value represents the darkness or lightness of the colour such as pure black to pure white. Chroma is the brightness of colour. By combining the HVC exact colour of the sediment has been determined.

2.2.2 Texture Analysis

The concentration of sand, silt, and clay particles has been determined to classify the sub-surface sediment profile into distinct texture category. The texture of the sediments also offers crucial indications of the processes that corrode, transport and finally accumulate the sediments in the distinct depositional settings. The texture has been identified using 151 H-hydrometer method. The scale of this hydrometer ranges from 1.000 to 1.038. It measures the specific gravity of the suspension. Depending on the settlement duration, particle size has been determined. The steps of the textural analysis are as follows-

(a) Blank Preparation

Blank was prepared for the calibration of samples. For this 50 g of Sodium Hexa Metaphosphate ((NaPO₃)₆) was mixed with 1000 ml of deionized water in measuring cylinder. The temperature and viscosity readings were taken using thermometer and hydrometer after the interval of 30 and 60 seconds (average of three readings is taken into consideration), 10 minutes, 1.5 hours, 4 hours, 8 hours and 24 hours.

(b) Sample Preparation

Each of the samples was oven-dried at 105⁰ C for 24 hours. Thereafter, it is passed through 2 mm sieve to extract coarser particles, wood or shells from the sample. Afterward, it was ground using agate mortar. 50 g of this sample (clay) is used for hydrometer analysis. In the case of sand, approximately 100 g of sample is required.

(c) Hydrometer Analysis

Sodium Hexa Metaphosphate (NaPO₃)₆ solution was required to suspend the particles in solution. This solution was prepared by mixing 50 g of (NaPO₃)₆ with 1000 ml deionized water. 100 ml of this solution and 250 ml of deionized water were mixed with oven-dried samples. This mixture was kept undisturbed for 24 hours. Afterward, it was mixed properly using a mixing machine for around 5 minutes. This mixture (350 ml) along with deionized water (650 ml) was then poured in a 1000 ml measuring cylinder. This solution was mixed well and after 30 seconds first temperature and hydrometer readings were taken. An average of three readings has been used for further calculations. Subsequently, temperature and hydrometer readings were repeated at the intervals of 60 seconds, 10 minutes, 1.5 hours, 4 hours, 8 hours and 24 hours. The reading intervals of blank and sediment samples were kept uniform for calibration purpose. The particle diameter, particle size, and percent finer have been calculated using the laboratory manual (provided by the manufacturer for 151 H-hydrometer). The particle diameter and particle size have been calculated using the following equations-

i. Particle diameter (in mm) $D = K\sqrt{\frac{L}{T}}$ (equation 1)

Where K = Constant (as in laboratory manual)
 L = Effective depth of Hydrometer (in cm)
 T = Time elapsed (in minutes)

ii. Particle size
$$V = \frac{1}{18} \left(\frac{G_s - G_w}{n} \right) \times D^2 \dots\dots\dots(\text{equation 2})$$

Where V = terminal velocity of soil particles (cm/s)
 G_s = Specific gravity of soil particles (cm)
 G_w = Specific gravity of water
 n = viscosity of water (g-s/cm²)
 D = diameter of soil particle (m)

iii. Percentage finer in suspension
$$N = \left(\frac{G_s}{G_s - G_1} \times \frac{100000}{W_s} \right) \times R - 1 \dots\dots\dots(\text{equation 3})$$

Where N = percentage of finer particles in suspension
 R = Hydrometer reading with a composite correction factor applied
 W_s = Oven-dried weight of soil
 G_s = Specific gravity of soil particles
 G₁ = Specific gravity of the suspending liquid (1.000 for water)

Hydrometer method of texture analysis implies the Stokes law according to which the velocity, at which particles settle out of suspension, all other factors being equal, is dependent upon the shape, weight, and size of the grain (Bedaiwy, 2012). In the case of sediment, it is assumed that the particles are spherical and have the same specific gravity. Consequently, it is inferred that in a soil-water suspension, the coarser particles would settle more rapidly than the finers.

Sediment particles span a wide size range from coarse sand (4.75-2 mm diameter) to fine clay (<0.001 mm diameter). In this study, particles smaller than 4.75 mm diameter are categorized into three major factions -sand, silt, and clay (Table 2.1).

PSD was evaluated through the particle size distribution curve. In this graph, the percentage of particles less than a given particle size is plotted against the logarithm of effective particle diameter. This delivers a frequency distribution curve for various particle sizes. The peak or

peaks of the particle size distribution curve specify the most prevalent grain sizes in a given sample. The shape of the curve indicates gradation of sediment whether it is well graded, poorly graded or gap graded. In a well graded sediment sequence, the particles are uniformly distributed while in a gap graded profile concentration of some particles are high in comparison to other.

Table 2.1 Classification of sediment sequences based on particle size

Indian Standard Soil Classification System (ISSCS)		Particle Diameter (mm)	
Very Coarse Soil	Boulder Size	>300	
	Cobble Size	80-300	
	Gravel Size (G)	80-20	Coarse
20-4.75		Fine	
Coarse Soil	Sand Size (S)	4.75-2	Coarse
		2-0.425	Medium
		0.425-0.075	Fine
Fine Soils	Silt Size (c)	0.075-0.002	
	Clay Size (M)	<0.002	

Identification of facies, at each location, is based on down core deviation in colour and texture of the sediments.

2.3 Analysis

2.3.1 Colour Determination

2.3.1.1 Riverine Zone

Ezapur (EP)

Colour of the sediments retrieved from EP site has varied from dark reddish-brown in the surface sequence to palae yellow in the bottom of stratigraphy (Table 2.2). The EPL1 was dark reddish brown displaying the abundance of iron and organic carbon. In EPL2, colour of the sediments has altered to reddish brown which can be due to the enrichment of iron. The yellow colour in EPL3 has exposed poor drainage conditions. The yellowish-brown colour of EPL4 probably has demonstrated depletion of iron and organic carbon. The EPL5 was reddish brown suggesting relative enrichment in iron and carbon content. The colour has changed to dull orange in EPL6 revealing the abundance of iron and oxygen. The palae

yellow colour of the deepest facie, EPL7 has indicated poor drainage condition during its deposition.

Table 2.2 Colour identification of subsurface sediment samples at EP site

Samples	EPL1	EPL2	EPL3	EPL4	EPL5	EPL6	EPL7
Depth (cm)	0-30	30-90	90-180	180-300	300-320	320-700	700-1000
Colour	Dark Reddish Brown	Dull Reddish Brown	Yellow	Yellowish Brown	Reddish Brown	Dull Orange	Palae Yellow

Jhumpuri (JP)

At this location, most of the sub-surface sequences have exhibited a specific colour ranging from grayish-white to reddish-brown (Table 2.3). The dark reddish-brown colour of JPL1 has indicated a higher content of iron and carbon. JPL2 was dull reddish-brown revealing enrichment of iron under well-oxygenated conditions. The colour has abruptly altered to yellow in the succeeding facie JPL3, depicting deficient drainage. The JPL4 was reddish-gray indicating the existence of a stagnated environment during accumulation.

Table 2.3 Colour identification of subsurface sediment samples at JP site

Sample s	JPL1	JPL2	JPL3	JPL4	JPL5	JPL6	JPL7	JPL8	JPL9	JPL10	JPL11
Depth (cm)	0-60	60-160	160-200	200-460	460-540	540-670	670-730	730-790	790-850	850-900	900-1000
Colour	Dark Reddish Brown	Dull Reddish Brown	Yellow	Reddish Gray	Reddish Black	Grayish Red	Brownish Black	Grayish yellow	Palae Reddish Orange	Dull Orange	Grayish white

The colour of the sediments has changed to reddish black in JPL5 indicating an increase in iron and organic carbon concentration. The colour of JPL6 was grayish-red exhibiting the revival of the damp environment of deposition. The JPL7 was brownish-black which could have been due to partial oxidation of organic carbon. The colour has modified to grayish-yellow in JPL8 suggesting deposition under poor drainage condition. Palae-reddish-orange colour of JPL9 has indicated well-oxygenated condition. The JPL10 was dull orange revealing the abundance of iron under a persistent well-oxidized environment. In the basal

facie shown as JPL11, grayish-white colour has suggested excessive leaching condition which can be possible under enhanced humidity.

Katia I (KTI)

The colour of the samples collected from KTI location has fluctuated from reddish-gray in the lowermost sequence to reddish-brown in the surface facie (Table 2.4). The KTIL1 was reddish-brown which can be due to the presence of humus and iron in the surface sequence. Reddish-gray colour of KTIL2 has indicated the reduction of organic carbon and most probably deposition under a damp environment. The colour has transformed into grayish-brown in KTIL3 suggesting the rise in carbon concentration as well as the persistence of anoxic conditions. The KTIL4 was palae yellow which is the manifestation of elevated oxygen availability. The reddish-gray colour of KTIL5 has demonstrated the revival of reducing condition during its sedimentation.

Table 2.4 Colour identification of subsurface sediment samples at Katia I site

Samples	KTIL1	KTIL2	KTIL3	KTIL4	KTIL5
Depth (cm)	0-8	8-10	10-18	18-45	45-140
Colour	Reddish Brown	Reddish Gray	Redish Brown	Palae Yellow	Reddish Gray

Katia II (KTII)

Substantial colour variation has appeared in the samples obtained from the Katia II site (Figure 2.5). The KTIIIL1 was brown indicating the presence of humus in the surface sequence. the reddish-brown colour of KTIIIL2 has depicted the abundance of iron and humus. The KTIIIL3 was dull yellow suggesting depletion in iron and carbon concentration and poor drainage. The KTIIIL4 was dull orange indicating enrichment of iron and well-oxygenated conditions. The grayish red colour in KTIIIL5 has demonstrated the abundance of iron and reduced oxygen availability. The colour has again changed to dull orange in KTIIIL6 suggesting relative depletion of iron. The colour has revised to brown in KTIIIL7 advocating enrichment of organic carbon during sedimentation. The dull orange colour of KTIIIL8 has illustrated the reduction in iron concentration. The KTIIIL9 was reddish-gray indicating the higher concentration of iron and expectedly reducing environment.

Table 2.5 Colour identification of subsurface sediment samples at Katia II site

Samples	KTIL1	KTIL2	KTIL3	KTIL4	KTIL5	KTIL6	KTIL7	KTIL8	KTIL9
Depth (cm)	0-15	15-30	30-45	45-60	60-75	75-90	90-105	105-120	120-160
Colour	Reddish Brown	Reddish Gray	Dull Yellow	Dull Orange	Grayish Red	Dull Orange	Brown	Dull Orange	Reddish Gray

2.3.3.2 Mixing Zone

Sonpanki (SP)

The colour scheme has deviated from reddish-brown in the upper-most stratigraphic sequence to grayish-white in the bottom (Table 2.6). The colour of SPL1 was reddish-brown revealing higher content of humus along with iron. This sequence has been followed by the red coloured SPL2 which most likely reveals the relative enrichment in iron content while depletion in organic carbon. The colour of SPL3 was reddish-brown which has exhibited a higher content of organic matter. In SPL4, the colour has modified to reddish-gray exhibiting poor oxygenation of organic carbon. In SPL5, gray colour has been associated with reducing environment of sediment accumulation. The grayish-white colour of SPL6 can be attributed to the excessive leaching of metals during the deposition of this facie which is possible under elevated weathering. Thus, at this site, the upper three sequences (SPL1, SPL2, and SPL3) have demonstrated the well-oxygenated depositional conditions whereas colours of deeper facies (SPL4, SPL5, and SPL6) have demonstrated damp and reducing conditions.

Table 2.6 Colour identification of sub-surface sediment samples at SP site

Samples	SPL1	SPL2	SPL3	SPL4	SPL5	SPL6
Depth (cm)	0-30	30-180	180-360	360-790	790-900	900-1000
Color	Reddish Brown	Red	Reddish Brown	Reddish Gray	Gray	Grayish White

Chandbali (CB)

Majority of the stratigraphic sequences at CB location were gray. This has indicated the predominance of damp environment and a prolonged saturated condition during aggradation of most of the sequences (Table 2.7). The CBL1 was reddish-gray which can be attributed to iron abundance under low oxygen availability. The colour has changed to brownish gray in

CBL2 indicating relatively higher concentration of organic carbon. The black colour of CBL3 has suggested a substantial increase in organic carbon. In this facie, wood pieces have also been observed yielding higher organic matter concentration. The colour has altered to brownish-gray in CBL4 indicating reducing environment. The CBL5 was reddish-gray which can be associated with prolongation of damp conditions. In contrast, the palae yellow colour of the lower-most sequence CBL6, has signified a major shift in the depositional setting. The colour has suggested poor drainage conditions during its sedimentation.

Table 2.7 Colour identification of sub-surface sediment samples at CB site

Samples	CBL1	CBL2	CBL3	CBL4	CBL5	CBL6
Depth (cm)	0-240	240-540	540-600	600-730	730-790	790-1000
Colour	Reddish Gray	Brownish Gray	Black	Brownish Gray	Reddish Gray	Palae Yellow

Ambiligan (AG)

The colour of the sediments has changed considerably at AG site. However, at this location also gray has been recognized as the most pronounced colour across the sedimentary sequences (Table 2.8). The reddish-gray colour of AGL1 has indicated higher iron concentration and lower oxygen availability most probably revealing anoxic environment of deposition. The colour of AGL2 was reddish-brown that might have been the manifestation of higher iron concentration under the oxic conditions.

Table 2.8 Colour identification of sub-surface sediment samples at AG site

Layers	AGL1	AGL2	AGL3	AGL4	AGL5
Depth (cm)	0-150	150-450	450-600	600-760	760-1000
Colour	Reddish Gray	Reddish Brown	Brownish Gray	Black	Brownish Gray

The brownish-gray colour of AGL3 has suggested increase in the concentration of organic carbon under reducing environment. The colour of AGL4 was black suggesting further enrichment of organic carbon or lower oxygen availability due to which carbon was less-oxidized. The brownish gray colour of AGL5 has depicted relative reduction in the organic carbon or increase in its oxydation during the sediment aggradation.

Kasturikaran (KK)

At this location, a total of four sequences with distinct colour were marked (Table 2.9). The colour of KKL1 was palae yellow, indicating poor drainage. This was followed by the reddish-brown KKL2. The color of this sequence has suggested the abundance of iron and carbon under well-oxygentaed depositional setting. The colour of KKL3 was gray which has illustrated a swampy environment of deposition. The colour of the lower-most facie, KKL4 was reddish-gray. This has demonstrated a higher iron content under a stagnated environment.

Table 2.9 Colour identification of subsurface sediment samples at KK site

Layers	KKL1	KKL2	KKL3	KKL4
Depth (cm)	0-150	150-700	700-800	800-1000
Colour	Palae Yellow	Reddish Brown	Gray	Reddish Gray

2.3.2 Textural Classification

2.3.2.1 Riverine Zone

Ezapur (EP)

In EPL1 approximately 68% of the particles were finer than 0.1 mm diameter providing it a finer clayey texture (Table 2.10). The order of particle concentration was- clay> sand >silt. It was a well-graded sequence containing a wide range of particle sizes (Figure 2.1a). The distribution of particles was quite uniforms. In EPL2 above 70% of the particles were finer than 0.1 mm diameter and the order of occurrence was clay> sand> silt. It was also classified as clay. It has also shown a uniform gradation of the grain sizes (Figure 2.1b).

Table 2.10 Textural classification of sediment layers at EP site

Samples	EPL1	EPL2	EPL3	EPL4	EPL5	EPL6	EPL7
Depth (cm)	0-30	30-90	90-180	180-300	300-320	320-700	700-1000
Texture	Clay	Clay	Clay	Loamy Fine Sand	Clay	Sandy Clay Loam	Clay

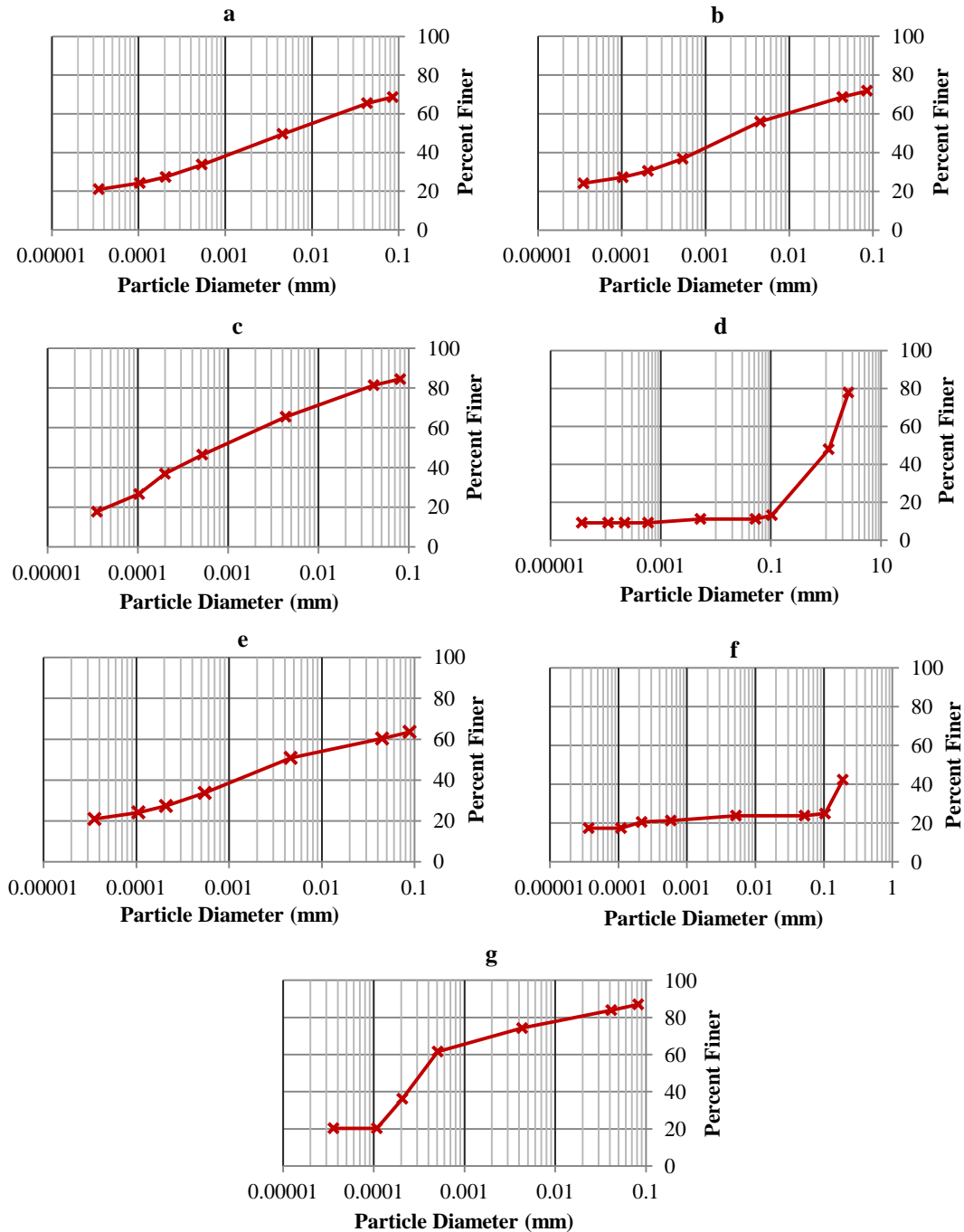


Figure 2.1 Particle size distribution in (a) EPL1, (b) EPL2, (c) EPL3, (d) EPL4, (e) EPL5, (f) EPL6 and (g) EPL7

Nearly 85% of the particles were finer than 0.1 mm in EPL3 exhibiting a downward fining pattern. The EPL3 was also identified as clay and the order of particle concentration was clay>silt>sand. This was also well-graded with the predominance of clay particles (Figure 2.1c). The abundance of finer particles has been associated with low energy of depositional

process. The EPL4 was coarser as most of the particles were above 0.75 mm diameter such as sand> silt> clay. It was identified as loamy fine sand in which fine particles were present in lower ratio showing a gap graded distribution (Figure 2.1d). This sandy sequence suggest a remarkable change in the depositional process. It might be associated with a high magnitude of river flow or deposition under marine influence. In EPL5 nearly 64% of particles were below 0.10 mm diameter. Clay was the predominant ingredient of this facie.

The order of particle distribution was clay> sand> silt and hence, it was classified under clay category. This sequence was also a well-graded with relatively higher clay concentration (Figure 2.1e). An increase in finer particle has indicated another shift in the depositional process which might be due to low flow conditions under reduced tidal influence. The EPL6 is categorized as sandy clay loam in which majority of the particles were above 0.10 mm diameter. The order of particle distribution was sand> clay> silt. It was gap graded sequence as the concentration of sand and clay particles were higher than silt (Figure 2.1f). This sequence has also demonstrated a change in the depositional process. The lower-most sequence, shown as EPL7, was categorized as clay in which the distribution order was clay> silt> sand. It has exhibited a gap-graded distribution as the concentration of some grain sizes is very low (Figure 2.1g). The dominance of fine particles has suggested subsequent change in the depositional process which can be attributed to enhanced river flow under reduced tidal activity.

Jhumpuri (JP)

At this location, JPL1 and JPL2 were well-graded with the abundance of clay and silt particles (Figure 2.2a, 2.2b). JPL1 has been identified as clay (Table 2.11). In this sequence the order of particle concentration was clay> silt> sand. The JPL2 was silty clay (silt> clay> sand) suggesting a marginal increase in the energy of fluvial process. The JPL3 was clay with gap-graded suggesting higher concentration of some of the particle sizes (Figure 2.2c). In JPL4, however, coarser particles were the most abundant (Figure 2.2d). The scheme of concentration was sand> clay> silt. Due to the dominance of sandy particles, it has been classified into loamy fine sand. The coarser texture of this sequence indicates a change in the depositional process which might be associated with elevated tidal activity.

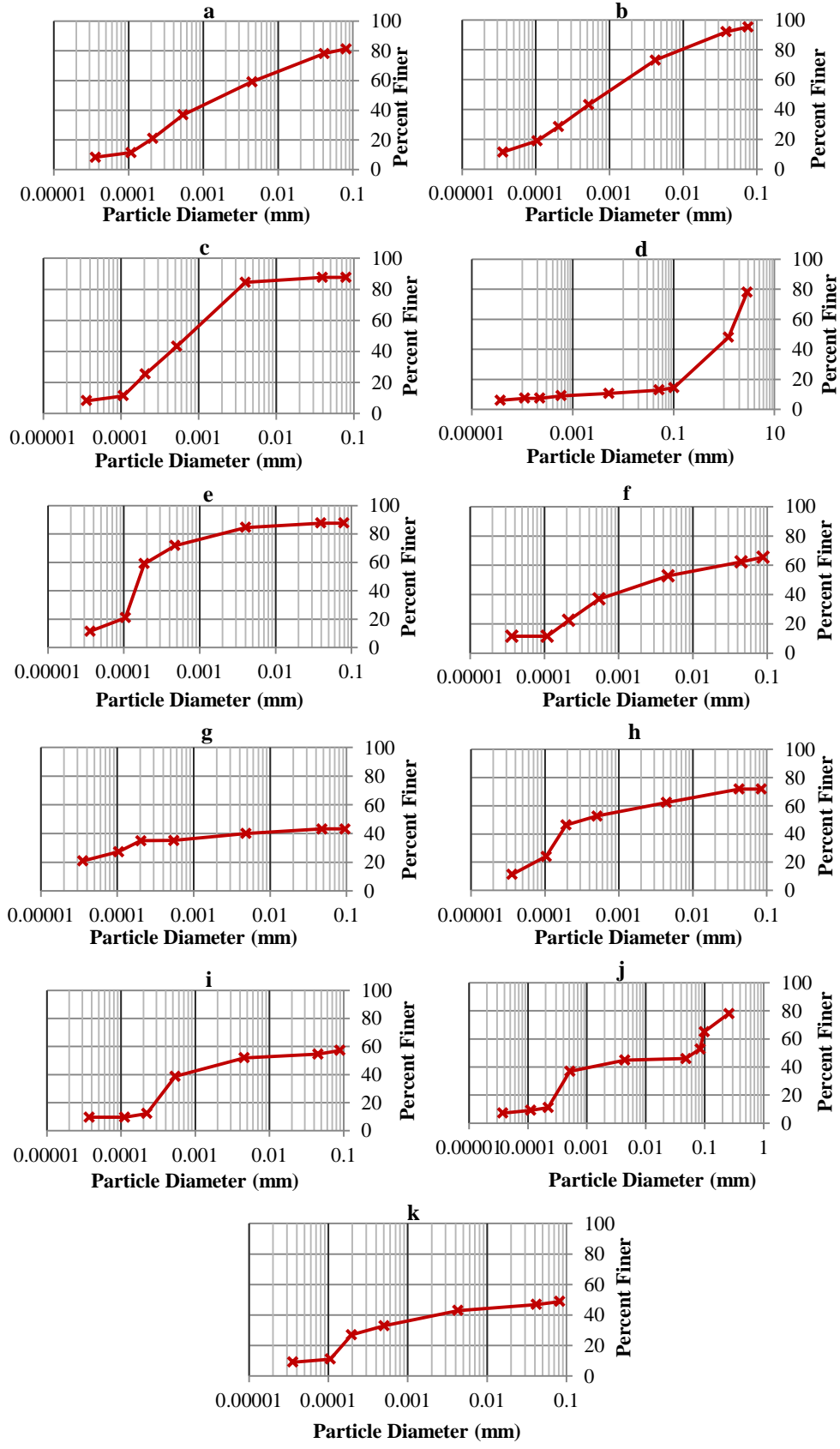


Figure 2.1 Particle size distribution in (a) JPL1, (b) JPL2, (c) JPL3, (d) JPL4, (e) JPL5, (f) JPL6, (g) JPL7, (h) JPL8, (i) JPL9, (j) JPL10 and (k) JPL11

In JPL4, the particles have been poorly graded (Figure 2.2d). In the succeeding facies, JPL5 and JPL6 the fine particles were most abundant suggesting another shift in depositional activity (Figure 2.2e, Figure 2.2f). In both facies, the order of particle distribution was clay> sand> silt. The sand and clay particles (sand> clay> silt) were the main constituents of JPL7 and thus, it has been identified as sandy clay. It was also gap-graded containing higher ratios of sand and clay (Figure 2.2g). On the other hand, in JPL8 concentration of finer particles were high providing it a clayey texture. The order of occurrence was clay> sand> silt. The particles were relatively well-graded (Figure 2.2h). The JPL9, JPL10, and JPL11 were primarily constituted of sand and clay. The order of particle concentration was sand> clay> silt. These facies were categorized as sandy clay. The gap graded distribution curve has revealed higher concentration of sand and clay in comparison to silt (Figure 2.2g).

Table 2.11 Textural classification of subsurface sediments at JP site

Sample	JPL1	JPL2	JPL3	JPL4	JPL5	JPL6	JPL7	JPL8	JPL9	JPL10	JPL11
Depth (cm)	0-60	60-160	160-200	200-460	460-540	540-670	670-730	730-790	790-850	850-900	900-1000
Texture	Clay	Silty Clay	Clay	Loamy Fine Sand	Clay	Clay	Sandy Clay	Clay	Sandy Clay	Sandy Clay	Sandy Clay

Katia I (KTI)

In KTIL1 the distribution of particle sizes was considerably uniform with relatively higher concentration of fine particles (Figure 2.3a). The order of grain size distribution was clay> silt> sand. Therefore, it was identified as clay (Table 2.12). The KTIL2 was also well graded, however, particles were comparatively coarser. The order of particle concentration was sand> clay> silt (Figure 2.3b). It was categorized as sandy clay loam indicating higher energy of transporting agent. In KTIL3 and KTIL4 fine grains were predominant providing them clayey texture. In KTIL3, the order of particle concentration was clay> silt> sand while in KTIL4, clay> sand> silt. These sequences have exhibited the well-gradation of particles (Figure 2.3c and Figure 2.3d). The percentage of coarser grains was relatively higher in KTIL5 offering it a clay loam texture (clay> silt> sand). It has shown a uniform distribution of grain sizes (Figure 2.3e).

Table 2.12 Textural classification of subsurface sediment at Katia I site

Sample	KTIL1	KTIL2	KTIL3	KTIL4	KTIL5
Depth (cm)	0-8	8-10	10-18	18-45	45-150
Texture	Clay	Sandy Clay Loam	Clay	Clay	Clay Loam

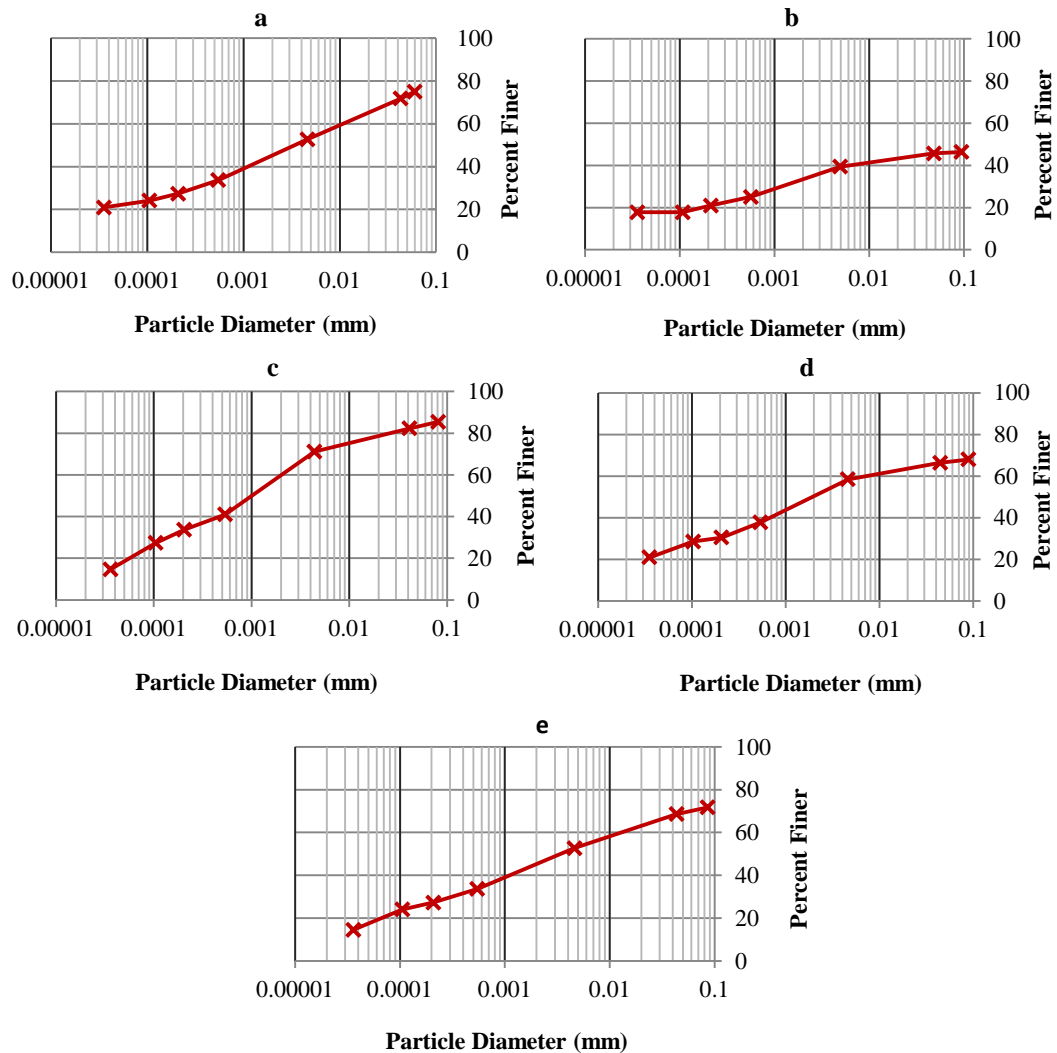


Figure 2.3 Particle size distribution in (a) KTIL1, (b) KTIL2, (c) KTIL3, (d) KTIL4 and (e) KTIL5

Katia II (KTII)

The distribution of particles in KTII1 was substantially uniform (Figure 2.4a). The clay particles, however, were the most abundant (0.002 to 0.06 mm diameter). The order of concentration was clay > sand > silt.

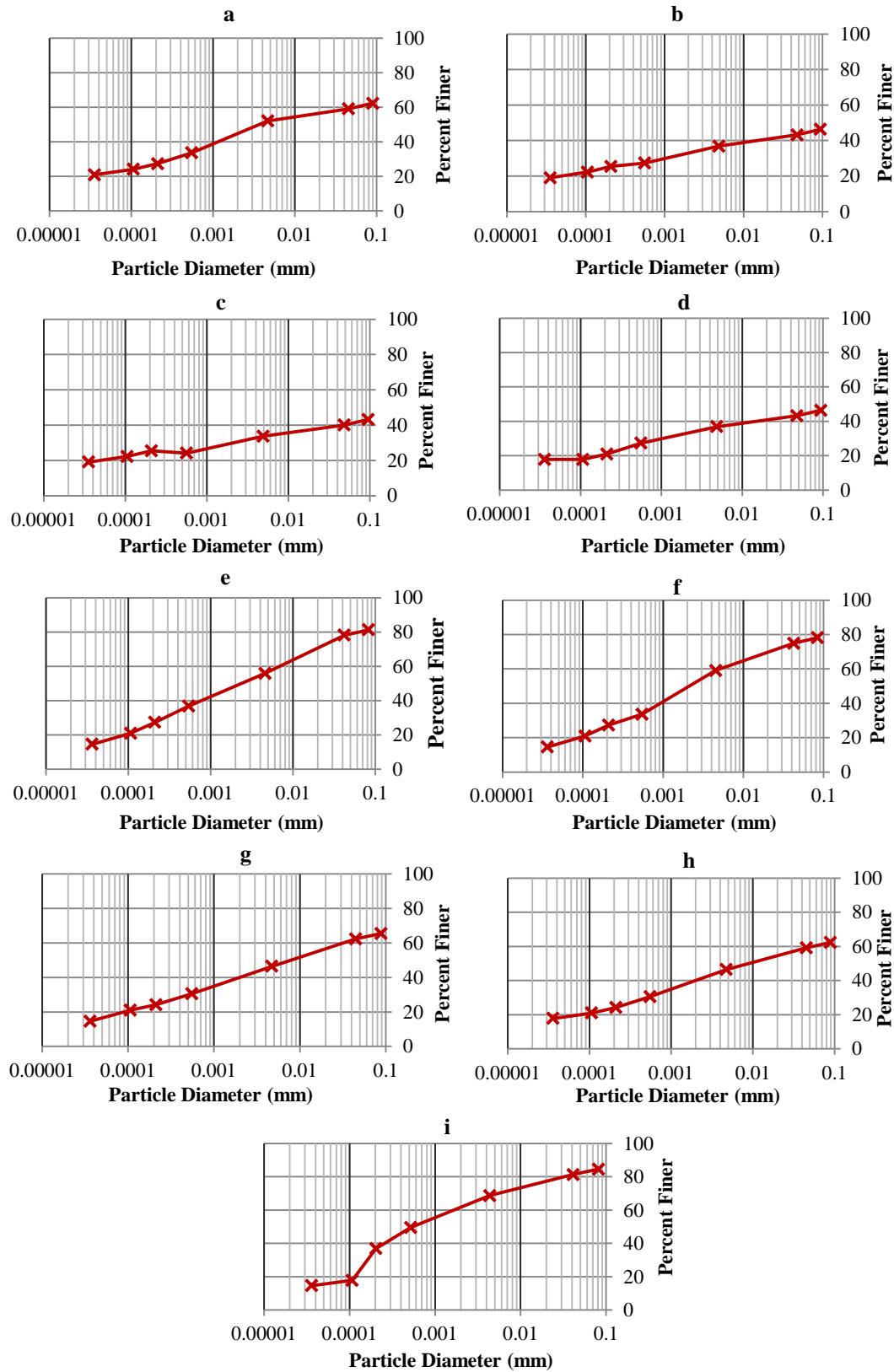


Figure 2.4 Particle size distribution in (a) KTIL1, (b) KTIL2, (c) KTIL3, (d) KTIL4, (e) KTIL5, (f) KTIL6, (g) KTIL7, (h) KTIL8 and (i) KTIL9

In KTII2, KTII3 and KTII4 particles were comparatively coarser giving these sequences sandy clay loam texture (Table 2.13). In these sequences, the order of particle concentration was sand > clay > silt. They were gap-graded in which higher concentration of coarser grains (Figure 2.4b, 2.4c, 2.4d). In KTII5 silt and clay were the most abundant. The scheme of particle concentration was silt > clay > sand and hence it was kept under the silty clay category. It has also revealed the well-gradation of particles (Figure 2.4e). The KTII6, however, was predominantly clay wherein other grain sizes were present in rather smaller portions (Figure 2.4f). The order of concentration was clay > silt > sand. In KTII7 and KTII8 relatively coarser particles were observed (sand > clay > silt) with a well-graded distribution curve (Figure 2.4g and Figure 2.4h). Hence, these were classified as clay loam. The lower-most sequence, KTII9 was clay with the abundance of fine grains. The order of particle concentration was clay > silt > sand. It has revealed a well-graded structure (Figure 2.4i).

Table 2.13 Textural classification of subsurface sediments at Katia II

Sample	KTII1	KTII2	KTII3	KTII4	KTII5	KTII6	KTII7	KTII8	KTII9
Depth (cm)	0-15	15-30	30-45	45-60	60-75	75-90	90-105	105-120	120-160
Texture	Clay	Sandy Clay Loam	Sandy Clay Loam	Sandy Clay Loam	Silty Clay	Clay	Clay Loam	Clay Loam	Clay

The analysis has indicated significant changes in the process of sediment transportation and deposition. It has been inferred that variation in the concentration of finer and coarser particles in different sequences has been caused by the action of distinct geomorphic processes, fluvial and marine.

2.3.2.2 *Mixing Zone*

Sonapanki (SP)

The SPL1 has shown a higher concentration of fine grain sizes ranging from 0.002 to 0.06 mm diameter where clay=silt > sand. It was, therefore kept under the silty clay texture category (Table 2.14). The particles were uniformly distributed (Figure 2.5a). The following sequence, SPL2 was also well-graded although the concentration of finers (<0.005 mm) has increased giving it a clayey texture (Figure 2.5b). The order of concentration was clay > silt > sand. The dominance of silt and clay in these stratigraphic sequences has indicated

deposition through fluvial activity. The SPL3 has been categorized as clay loam. In this sequence also the particles are uniformly distributed (Figure 2.5c). The order of particle distribution was clay=silt> sand. The SPL4 was well-graded clay with the prevalence of fine particles (Figure 2.5d).

Table 2.14 Textural classification of subsurface sediments at SP site

Sample	SPL1	SPL2	SPL3	SPL4	SPL5	SPL6
Depth (cm)	0-30	30-180	180-360	360-790	790-900	900-1000
Texture	Silty Clay	Clay	Clay Loam	Clay	Clay	Clay Loam

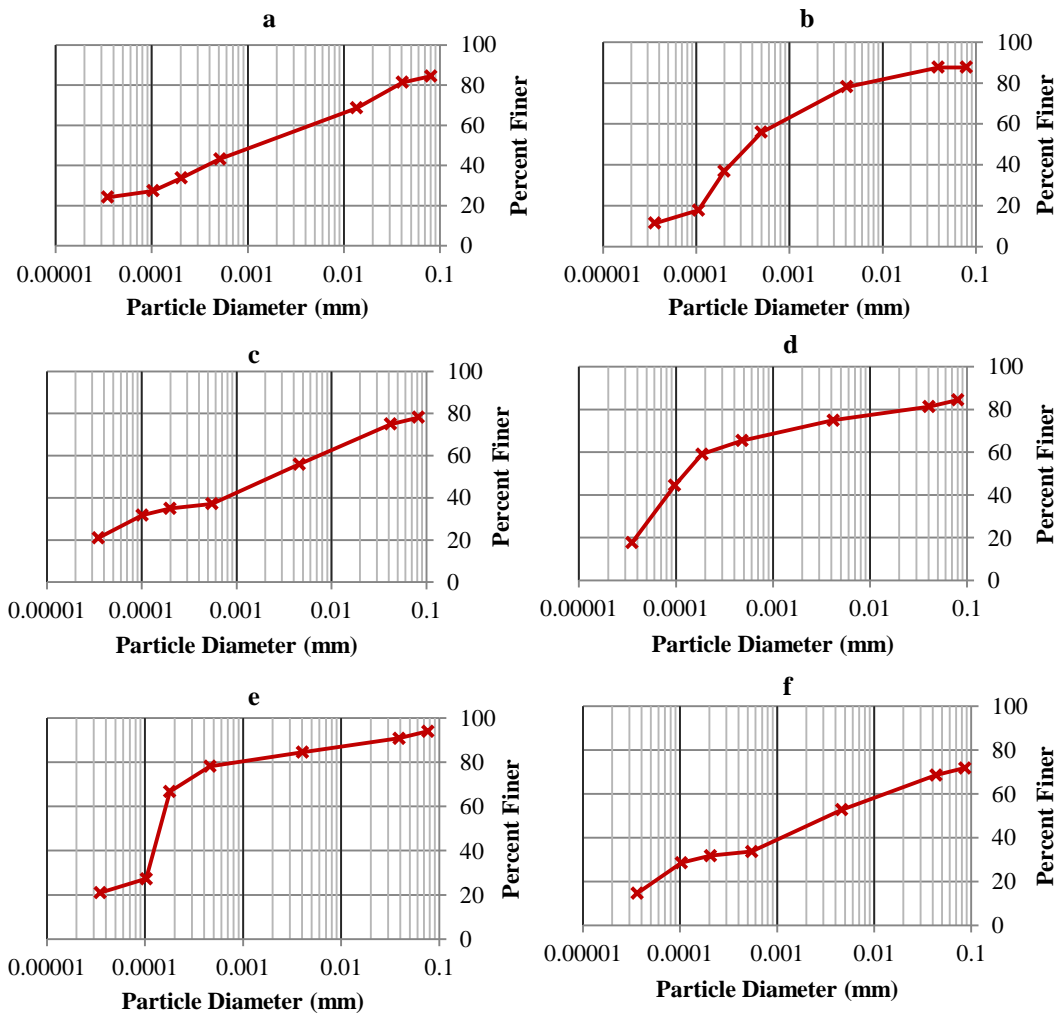


Figure 2.5 Particle size distribution in (a) SPL1, (b) SP, (c) SPL3, (d) SPL4, (e) SPL5 and (f) SPL6

The order of occurrence was clay> silt> sand. The SPL5 has been identified as clay with the well-graded curve (Figure 2.5e) in which. The lower-most stratigraphic sequence shown as SPL6 was well graded with an abundance of clay and silt size particles (Figure 2.5f). It was classified as clay loam.

Chandbali (CB)

In CBL1 coarser grains were the most abundant. The particle sizes ranging from sand (2.00 mm) to clay (0.002 mm) were present in the order of sand> clay> silt. The higher concentration of coarse grains has given it a sandy loam texture (Table 2.15). It has a gap-graded distribution of particles in which coarser grains were present in higher ratio (Figure 2.6a). In CBL2, sand and clay particles were abundant (sand> clay> silt) and hence it was classified as sandy clay loam. It has shown a well-graded structure where the particles were present in relatively uniform ratio (Figure 2.6b). The abundance of coarser particles has been associated with high energy of the depositional process.

The CBL3, CBL4, CBL5, and CBL6 were also well-graded (Figure 2.6c, Figure 2.6d, 2.6e, 2.6f). These had a higher percentage of clay particles in order of clay> sand> silt providing them a clayey texture indicating relative reduction in the energy of transporting agent or a shift in the process of deposition.

Table 2.15 Textural classification of subsurface sediments at CB site

Samples	CBL1	CBL2	CBL3	CBL4	CBL5	CBL6
Depth (cm)	0-240	240-540	540-600	600-730	730-790	790-1000
Texture	Sandy Loam	Sandy Clay Loam	Clay	Clay	Clay	Clay

Ambiligan (AG)

Fine particles were chief constituent of samples obtained from AG site and thus most of the sediment sequences were categorized as clay (Table 2.16). The AGL1 and AGL2 were clay with higher proportion of fine particles ranging between 0.002 and 0.06 mm diameter (Figure 2.7a, Figure 2.7b). The order of particle concentration was clay> silt> sand in both of the facies. In contrast, AGL3 had fair concentration of coarser particles (>0.1 mm) in order of sand> clay> silt giving it clay loam texture. These were well graded containing

variety of particle sizes (Figure 2.7c). The AGL4 and AGL5 were primarily constituted of fine grains with higher percentage of clay (Figure 2.7d, 2.7e). The concentration scheme in these facies was clay> silt> sand. Thus, these two basal sequences were categorized as clay.

Table 2.16 Textural classification of subsurface sediments at AG site

Samples	AGL1	AGL2	AGL3	AGL4	AGL5
Depth (cm)	0-150	150-450	450-600	600-760	760-1000
Texture	Clay	Clay	Clay Loam	Clay	Clay

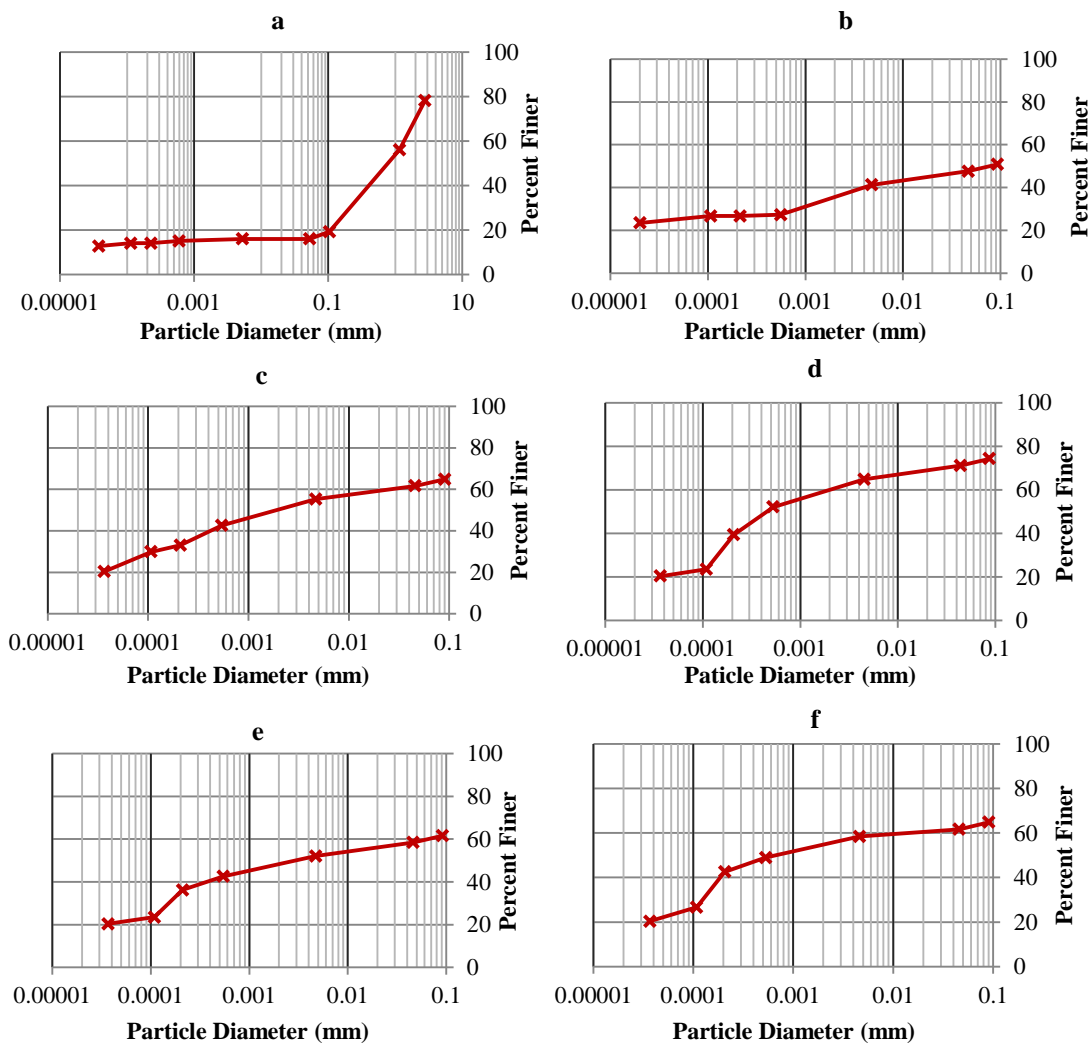


Figure 2.6 Particle size distribution in (a) CBL1, (b) CBL2, (c) CBL3, (d) CBL4, (e) CBL5 and (f) CBL6

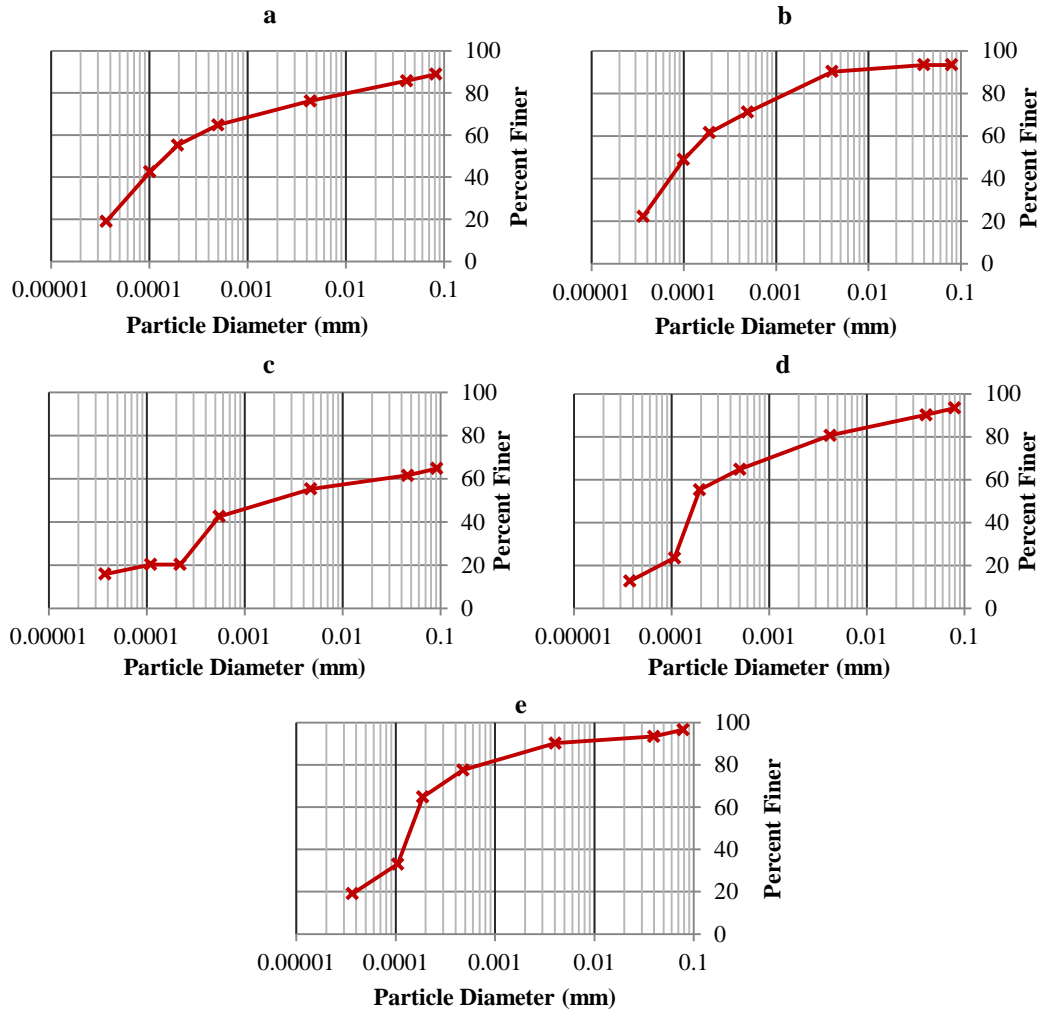


Figure 2.7 Particle size distribution in (a) AGL1, (b) AGL2, (c) AGL3, (d) AGL4 and (e) AGL5

Kasturikaran (KK)

It can be stated by observing Figure 2.8a, that the sediments in KKL1 were well graded. The fine particles were the most abundant (clay > sand > silt) offering it a clayey texture. The succeeding facie, KKL2 was also clay with a fairly uniform distribution of particles (Figure 2.8b). Nevertheless, in KKL1 the percentage of coarser particles was comparatively high.

Table 2.17 Textural classification of subsurface sediments at KK site

Samples	KKL1	KKL2	KKL3	KKL4
Depth (cm)	0-150	150-700	700-800	800-1000
Texture	Clay	Clay	Fine Sand	Clay Loam

The order of particle concentration in KKL2 was clay > silt > sand. A considerably high concentration of coarser grains was present in KKL3 in which the distribution was in the order of sand > clay > silt. Therefore, it was identified as fine sand (Table 2.17). It was gap-graded with a lower concentration of finers (Figure 2.8c). The KKL4 was relatively finer and hence it was categorized as clay loam. This facie was also well-graded in which particles were uniformly distributed (Figure 2.8d).

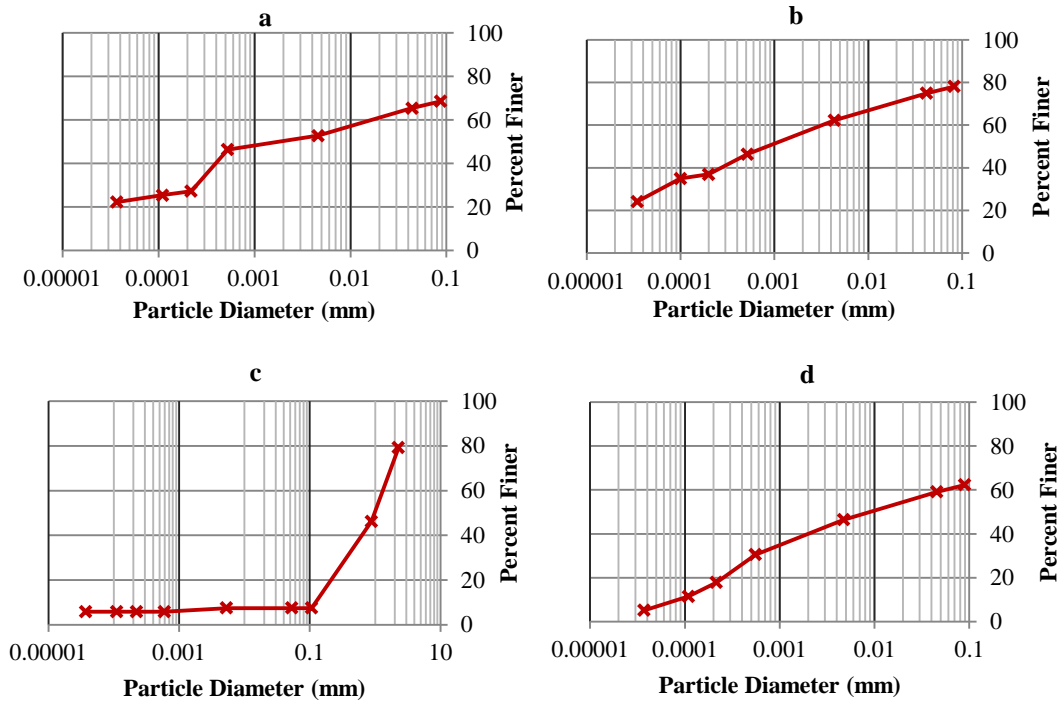


Figure 2.8 Particle size distribution in (a) KKL1, (b) KKL2, (c) KKL3 and (d) KKL4

Thus, the analysis done so far has indicated that the occurrence of stratigraphic sequences containing clay is more common in the Mixing Zone. At CB site, collected from the older beach deposits, the coarser particles are more abundant than in SP (active floodplain), AG and KK (palaeochannels).

2.4 Discussion and Conclusion

Down-core variability in physical properties of sediments i.e. colour and texture has been discussed in the present chapter. These variations have been utilized to identify the sub-surface sedimentary facies at each location.

The sample EP was collected from the palaeochannel of river Baitarani in the Riverine Zone. The basal part has been marked as EPL7 (Figure 2.9a). It has a total thickness of 300 cm and mainly constituted by the fine-grained clay of palae yellow colour. A major part of this facie is below the mean sea level (MSL). The dominance of fine particles has suggested that the deposition of this sequence was through the fluvial process as, towards the mouth region, the river mainly transports fine particles. The colour has revealed poor drainage conditions during the deposition. The succeeding facie, EPL6 has a thickness of 400 cm. It is identified as a coarser sequence of dull orange colour (Figure 2.9e). In this facie, the sorting of sediment particles is very poor. An abundance of coarser particles has indicated sedimentation under changed circumstances. Most probably the sand has been derived from the marine sources during enhanced tidal activity in the region. The following facie EPL5 is comparatively thinner (20 cm). This fine-grained clayey sequence has been marked between the two sandy facies, illustrating abrupt change in the provenance and environment of deposition. Facie EPL4 is 120 cm thick and yellowish-brown in colour. The concentration of sand has increased considerably in this facie. However, the size of sand is smaller than in EPL6. These properties have illustrated an elevated energy of the transporting agent during the sediment aggradation. The sandy texture has also been associated with transformation in the depositional environment. The EPL3 is yellow clay with a thickness of 90 cm. The fine texture of this facie has indicated the governance of the riverine process at this time. The EPL2 is 60 cm thick dull reddish-brown clay. The content of fine particles has reduced in this facie with a marginal surge in the coarser grains. Facie EPL1 has been represented by the 30 cm thick upper-most sequence. It is dark reddish-brown clay wherein the concentration of sand has further increased. The colour scheme, in general, has illustrated the existence of oxic environment.

The number of facies has increased considerably in JP which is located in the flood plain between two palaeochannels of Baitarani (Figure 2.9b). Facie JPL11 has been identified in the lower-most sequence having a total thickness of about 100 cm. The JPL11 is sandy clay with an abundance of coarser particles. A shell was also collected in this facie. The colour and textural characteristics have indicated an increase in the tidal influence during sedimentation. Facie JPL10 is dull orange having sandy clay texture. Similar to the preceding facie, coarser particles are the predominant however, its thickness has reduced to

50 cm. The JPL9 is a 60 cm thick palae reddish-orange. Here also sand and clay particles are the most abundant. The succeeding facie, JPL8 is grayish-yellow clay indicating sediment accumulation through fluvial action. Facie JPL7 is 60 cm thick, brownish-black sandy clay. The elevated concentration of coarser particles has indicated a shift in the environment of sedimentation. The JPL6 has been identified as 130 cm thick facie of grayish red colour. This is predominantly clay locally known as 'kelu'. The concentration of coarser particles is lower than the preceding facie though it is higher than the succeeding facie suggesting a transition episode. Between 540 and 460 cm, facie JPL5 (80 cm thick) has been identified. It is reddish black clay with the predominance of the fine particles illustrating deposition through fluvial action. The JPL4 is represented by 260 cm thick facie of reddish-gray colour. It is constituted by loamy fine sand. The dominance of coarser particles has depicted the persistence of tidal influence. The JPL3 has been identified as 40 cm thick yellow clay suggesting deposition through riverine action. Facie JPL2 (100 cm thick) is observed between 160 and 60 cm depth. Its colour is dull reddish-brown. It has a silty clay texture. The JPL1 is represented by the upper-most sequence of stratigraphy with a total thickness of 60 cm. It is dark reddish-brown clay indicating aggradation through fluvial processes.

A total of five facies have been identified at KTI site, which is obtained from another palaeochannel of Baitarani in the riverine zone (Figure 2.9c). The KTIL5 has been identified as 100 cm thick reddish-gray clay loam. The succeeding facie, KTIL4 has been represented by a thin sequence (32 cm) of palae yellow clay. The clayey texture has suggested the dominance of the fluvial process during their accumulation. The KTIL3 has been identified between 18 and 10 cm depth. It is reddish-brown clay with a dominance of fine particles indicating the persistence of riverine influence. The KTIL2 has been marked as a thin sequence (2 cm thick) of reddish-gray sandy clay loam. A marginal increase in coarser grains has suggested a minor rise in tidal influence. The KTIL1 is an 8 cm thick reddish-brown facie with clayey texture. The texture has demonstrated the revival of the fluvial process. The number of facies identified in KTI has increased owing to its location in the flood plain (Figure 2.9d). The lower-most facie, KTIIL9 between 165 and 120 cm is reddish-gray clay indicating deposition under riverine and stagnated environment. The KTIIL8 is dull orange clay loam where coarser particles have increased suggesting a marginal rise in tidal influence. The KTIIL7 is brown clay loam while KTIIL6 is dull orange

clay showing a decline in flow intensity. Facie KTII5 is a grayish red silty clay revealing the increase in river flow during its deposition. The KTII4 is dull orange sandy clay loam. The KTII3 is dull yellow sandy clay loam and KTII2 is reddish-gray sandy clay loam. The texture of these facies has suggested the increase in flow intensity however; colour of KTII2 has indicated the existence of anoxic environment during sedimentation. The KTII1 is reddish-brown clay suggesting deposition through the fluvial process.

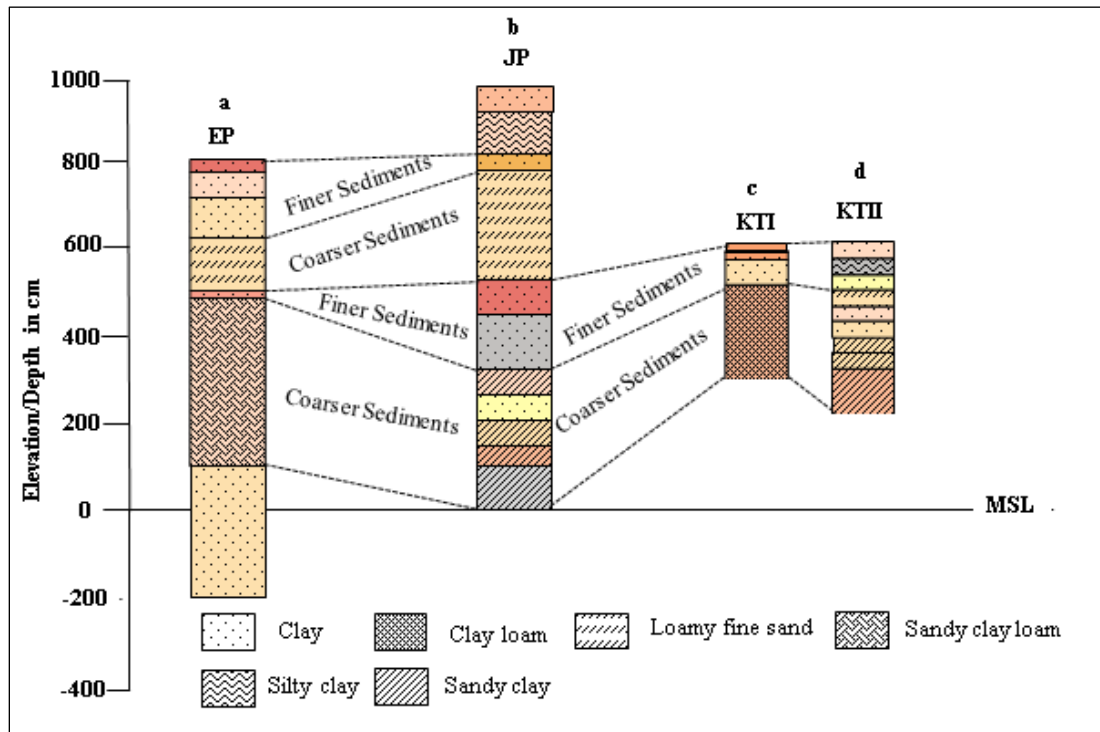


Figure 2.9 Facies classification of samples collected from the riverine zone and lateral association

Note: The index is showing textural classification

2.3.3.2 Mixing Zone

From the active flood plain located at the confluence of Baitarani and Salnadi, SP has been collected. The lower-most facie, SPL6 has been identified as a 100 cm thick sequence of grayish-white colour (Figure 2.10a). It has clay loam texture also known as ‘white genguti’. The texture has indicated that during the deposition fluvial activity has prevailed. The SPL5 has a total thickness of 110 cm. It is gray facie with clayey texture exhibiting deposition through the riverine process. The succeeding facie SPL4 (430 cm thick) is reddish-gray clay locally known as ‘pantal mitti’. The texture has suggested the persistence of the fluvial process. The SPL3 is 180 cm thick reddish-brown clay loam. The colour has revealed well-

oxygenated condition during deposition while texture has indicated a shift in the depositional environment. Between 180 and 30 cm, SPL2 has been marked. It is red clay with an abundance of fine particles. Fine texture has revealed sedimentation under fluvial dominance. Facie SPL1 is a 30 cm thick reddish-brown sequence having silty clay texture illustrating marginal transformation in depositional condition.

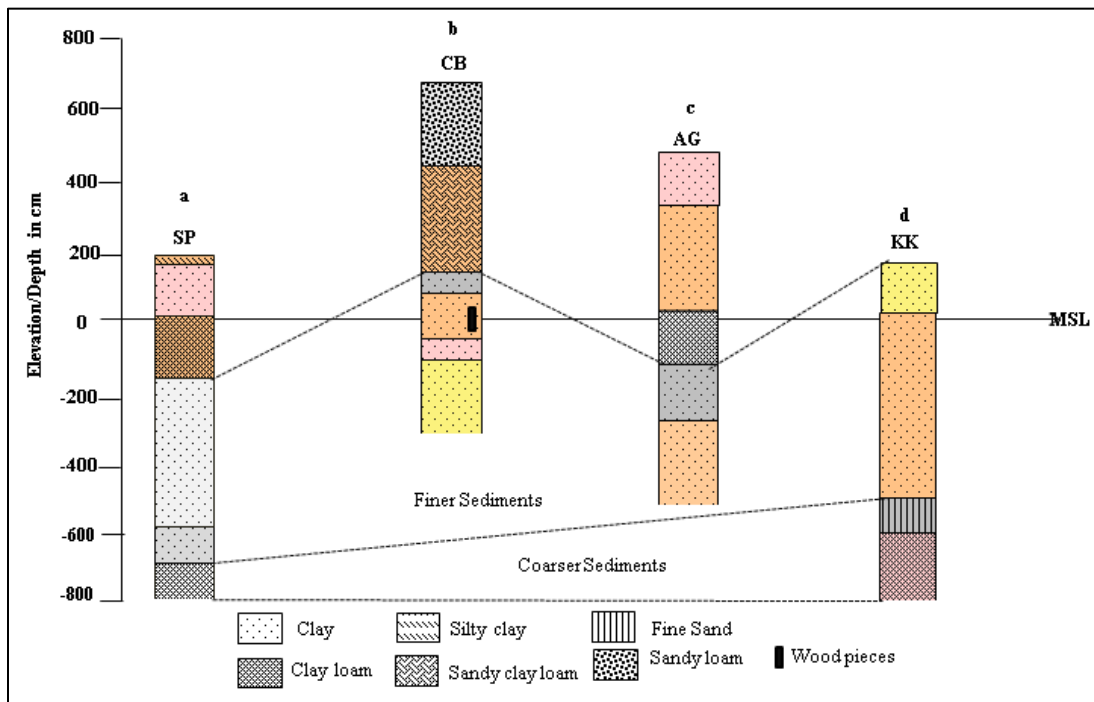


Figure 2.10 Facies classification of samples collected from the mixing zone and lateral association

Note: The index is showing textural classification

The CB was obtained from the older beach deposits located in the mixing zone. The CBL6 has been represented by the 210 cm thick basal sequence of CB (Figure 2.10b). This is palae yellow clay indicating poor drainage conditions. The texture has revealed, most expectedly aggradation due to aeolian action. The succeeding facie, CBL5 is a thin sequence of reddish-gray clay indicating the stagnated or marshy environment of deposition. The CBL4 is 130 cm thick brownish gray clay indicating the increase in carbon content under persisting marshy or swampy conditions. The CBL3 is 60 cm thick black clay revealing an abundance of organic carbon. These facies suggest deposition under the riverine influence. The gray colour has been associated with the increased influence of marine activity which may have resulted in stagnation. Facie CBL2 is 300 cm thick, brownish gray sandy clay loam. The

increase in coarser particles has indicated a shift in the environment of deposition most probably from riverine to marine. At CB site, from surface to 240 depths a sequence of reddish-gray sandy loam has been observed. The texture of this facie has been attributed to the continuation of tidal influence at the time of sediment aggradation.

The AG was collected from the palaeochannel of Baitarani in the mixing zone. The AGL5 has been shown by the lower-most sequence having a total thickness of 240 cm (Figure 2.10c). It is brownish-gray clay indicating low deposition under riverine action and existence of the stagnated environment. The AGL4 with a thickness of 40 cm is black clay demonstrating a considerable enrichment of organic carbon. Succeeding facie AGL3 is a 150 cm thick sequence of brownish-gray clay loam. Its relative coarser texture has revealed a change in the depositional environment. Facie AGL2 is 300 cm thick, reddish-brown clay suggesting deposition under the fluvial influence. The AGL1 is 150 cm thick, reddish-gray having clayey texture signifying the influence of fluvial action during deposition.

Another sample collected from the palaeochannel of Baitarani is KK. The KKL4, with a total thickness of 200 cm is reddish-gray clay loam (Figure 2.10d). The KKL3 is 100 cm thick gray fine sand indicating the reduction in river flow. However, it has also appeared that this has been deposited through tidal action. Facie KKL2 has been marked between 700 and 150 cm depth. It is reddish-brown clay indicating the reduced river flow condition. KKL1 is 150 cm thick palae yellow clay showing a continued reduction in river flow.

The occurrence of red and brown colours, in this study, has been related to the well-oxygenated environment of deposition. The well-oxygenated depositional environment is the representatives of oxygen abundance under humid and warm climatic conditions (Sayem et al., 2018). Under drier conditions the sediments are highly oxidized and the red colour is faded (Sayem et al., 2018). The brown colour of the sediments can be associated with higher carbon concentration (Springer et al. 1996). The shades of gray, in contrast, has been attributed to the anoxic and stagnated environment where oxygen is depleted (Kobayashi et al. 2016). Hence, it is apparent that in the riverine zone, usually, the well-oxygenated environment has prevailed during aggradation suggested by the dominance of Red, brown and yellow colours. However, in some of the cases i.e. between 460-730 cm depth in JP, gray colour is also observed revealing the reducing environment. In contrast, in the mixing

zone, shades of gray are recognized as the most abundant revealing prevalence of anoxic environment.

The texture of the samples collected from the Riverine Zone is predominantly silt and clay. In coastal and estuarine areas, finer sediments are likely to be deposited through terrestrial supply (Harris and Collins, 1985). However, in deeper facies of the Riverine Zone, coarser particles have been observed i.e. in EP between 300 and 700 cm, in JP between 200 and 460 cm, 850 and 900 cm, in Katia II between 30 and 45 cm depth. On the other hand, coarser sequences are more common in the mixing zone such as SPL1, SPL5, CBL1, CBL2, AGL3, and KKL4.

Most of the sediments are delivered to the coastal environment from weathered rocks primarily with heavy precipitation and runoff (Milliman and Farnsworth, 2011). Sand particles are usually transported as bed loads and fair weather flow is not able to move the particles over long distances (Liu et al., 2019). Rodriguez et al. (2018) have explained that linear sand deposits formed by the tidal action near the coast were formed during the Holocene transgression. The occurrence of linear beach deposits such as CB, in this area indicates a period of sea transgression. In coastal regions, the textural variations can also be instigated by modifications brought in the depositional process due to sea level fluctuations. The eustatic changes led to the predominance of riverine or marine activities during sediment accumulation. In coastal areas, the course of the river is extended during the sea regression phase (Krishna, 2018). At this time, primarily fluvial processes dominate. In contrast, a rise in the sea level curtails the river length rejuvenating the marine processes. Marine current and tide imprint their directional flow on the distribution and spatial trend of sediments. With wind or tide, nearshore sediment is transported landward in a narrow zone parallel to the coastline (Li et al., 2019). The estuarine transport is determined by the interplay of freshwater outflow and salt water inflow.

Here, the textural variations of the sediments have revealed significant changes in the mode of transportation at different instances. It has been inferred that deviation in the texture has been caused by the changes in the provenance and prevalent geomorphic process, fluvial or marine. The facies with finer sediments are supposed to be deposited from source region through fluvial action. On the other hand, the coarser particles are derived from marine

sources under enhanced tidal influence and lower fluvial activity. Thus, the assessment of the physical properties of the sub-surface sediment sequences has provided the basis for the inspection and interpretation of the palaeoclimate in the selected region. Therefore, it can be concluded that the physical characteristics, colour and texture, propose significant clues to the environment under which the sedimentation has occurred which can be utilized to unravel the palaeoclimate (Jakobsson et al. 2000; Warriar et al. 2016; Sayem et al. 2018). However, it is crucial to note that the reconstruction of palaeoclimate should not be done only on the basis of physical appearance (colour and texture). It has to be validated and cross-checked using other indicators i.e. geochemistry, geochronology. The geochemistry is considered one of such crucial indicators that would be discussed in the preceding chapters (Chapter 3 and 4) to further analyze the past depositional environment and palaeoclimate. Nevertheless, the geochemical characteristics of the sediments such as absorption and removal of certain metals, are also influenced by the colour and texture.

Chapter 3

Geochemical Characteristics of Sub- surface Sediments

3.1 Introduction

Geochemistry is the science based on analyzing the chemistry of the Earth as a whole and its parts (Goldschmidt, 1954). It also meant to examine the concentration and transportation of the elements over space and time. In a specific geographic setting, the behavior of an element is governed by the established laws and principles. Geochemistry of sediments, in general, is dominated by source area geology (Koukina et al., 2017). The chemicals that are released from the catchment area into the aquatic system are generally bound to particulate matters which eventually settle and become part of the depositional system (Zwolsman et al., 1997; Pan et al., 2014; Koukina et al., 2017). Hence, sediments in a coastal location commonly act as a sink for terrestrial elements (Belhadj et al., 2017).

The geochemistry of sedimentary processes is based on the reactions taking place between elements and existing environment and more specifically with oxygen. Henderson (1984) has argued that the place of deposition of an element during the sediment aggradation is largely governed by the ionic potential of the element. Subsequently, the ionic potential of the elements clarifies for the similar behavior of dissimilar elements and vice-versa during the sedimentation process in similar environments. For instance, elements with low ionic potential i.e. sodium (Na), calcium (Ca), magnesium (Mg), lithium (Li), barium (Ba) and strontium (Sr) called as soluble cations, remain in solution during the weathering and transportation. On the other hand, elements of hydrolysis with intermediate ionic potential such as aluminum (Al), titanium (Ti), zircon (Zr) and rare earth elements (REEs) are precipitated from aqueous solution. The elements with higher ionic potentials or soluble complex anions constitute anions containing oxygen which are again soluble.

Henderson (1984) has found that minerals that are resistant to chemical and mechanical breakdown are deposited as granular material. The most common example is quartz showing a marked enrichment of silica. Deposition of the products of chemical disintegration of aluminosilicates provides a mud consisting of the clay minerals. This results in the concentration of aluminum and potassium by absorption. Iron is precipitated as ferric hydroxide. Sometimes, a high concentration of iron is the result of the formation of iron ores. Calcium is precipitated as calcium carbonate either by purely inorganic process or by the action of organisms. The bases that remain in solution are deposited in the ocean. The

most important of these bases are sodium, potassium, and magnesium. Therefore, silica concentrates in the resistate sediments, alumina in the hydrolystates, iron and manganese in the oxides and calcium and magnesium in carbonates. It is also reported that the common sedimentary rocks seldom show high enrichment of trace elements over the amount present in igneous rocks. Most trace elements are generally concentrated in shales than in other types of sedimentary environment. The resistates i.e. quartz (SiO_2) forms the important group of sand. Zircon (Zr) is another important persistent mineral deposited in the sand.

It is apparent that chemical elements naturally occur in the Earth crust. These ingredients of the Earth crust are unstable and are highly susceptible to weathering process. As sediments are derived from the parent rock, their constitution also bears a relationship of the composition of their source rock. Studies, however, reveal that chemical characteristics of sediments may vary significantly from their parent rocks as some minerals get transformed into new and chemically stable elements (Henderson, 1984). Geochemical elements are readily modified by the action of oxygen, carbonic acid, and water. After formation, these are transported to different places by the action of water, wind or ice and re-deposited (Henderson, 1984). Most commonly, deposition takes place in standing water condition such as lake and sea. The deposition involves two mechanisms, biochemical fixing of solutes by aquatic or marine or direct chemical precipitation from the saline water.

Generally, in coastal zones, there are two main sources of sediment deposition- terrestrial materials transported by river and marine biogenous sediments (Liu et al., 2011; Dou et al., 2013). In addition, coastal and estuarine environment receive contaminants via local anthropogenic activities and river inputs (Eggleton and Thomas, 2004). Nevertheless, anthropogenic activities have introduced high loads of these constituents in the environment making it difficult to differentiate between natural and human contribution (Belhadj et al., 2017). Trace metals, cadmium (Cd) and lead (Pb) are considered the most critical pollutant in the environment (Belhadj et al., 2017). Trace metal contamination in estuarine and coastal areas has recently received increasing attention (Belhadj et al., 2017; Liu et al., 2019). Consequently, sediment-associated contaminants can further influence the concentration of trace metals if they are desorbed or become available to benthic organisms (Diaz de Alba et al., 2011).

The grain size of the sediment also influences the concentration of elements (Liu et al., 2016). The amount of absorption increases as the grain size of the absorbent decreases (Henderson, 1984). The clay minerals show marked absorbed capacity. Sufficient amount of elements such as copper, arsenic, and lead have been supplied by weathering and erosion during the geological time to cause serious poisoning of the ocean. Nevertheless, some processes of elimination are active that ingest these substances. Hence, the distribution of elements is not only controlled by the processes operating in the source region but also at the place of deposition. The productivity of organic carbon also influences the distribution of major, trace and rare earth elements.

The concentration of organic carbon is associated with the biogeochemical cycle of the elements. The relationship between organic carbon concentration, sedimentation rate, and oxygen availability is well established (Hartnett et al., 1998). The elements which are strongly bound to the organic carbon i.e. Zr, Ti, and Br are least mobile over space and time (Biester et al., 2012). Along with this, a strong correlation exists between Fe, Al, and TOC (Pokrovsky et al., 2005).

The TOC and specific elements are suitable environmental indicators. Variations in TOC distribution suggests the synthesis of organic carbon in the sediment sequences providing crucial clues about the past environment (Banerji et al., 2017). Similarly, the fraction of the total metal contents direct towards their origin (Hass and Fine, 2010; Romano et al., 2012). Consequently, geochemical analyses of sediment sequences yield essential information about the evolution of the landscape throughout geological time under distinctive geomorphic and climatic backdrop. Thus, in this chapter an assessment of spatial and temporal variability of major, trace and rare earth elements (REEs) is done by analyzing their enrichment and depletion in each face obtained from riverine and mixing zones. This enrichment and depleted has been examined in respect to their upper continental crust (UCC) value.

3.2 Methodology

3.2.2 Concentration of Organic Carbon

Estimation of percentage total organic carbon (TOC) concentration in different facies has been based on Walkley and Black titration method (1934). This experiment has been conducted at the soil laboratory of the Institute of Agricultural Sciences, Banaras Hindu University, Varanasi. The experiment was conducted in the following steps-

(a) Blank Preparation

First of all, for calibration, a blank sample was prepared by mixing Potassium Dichromate ($K_2Cr_2O_7$) and 20 ml of Sulphuric Acid (H_2SO_4) in 500 ml conical flask. Further, deionized water was added to make a solution. It was added with Sodium Fluoride (NaF) and 4-5 drops of DPA (Diphenyl Amine). Thereafter, it was titrated against 0.5 N Ferrus Ammonium Sulphate (FAS). When the colour of the solution turned to light green, the point is noted and used for sample calibration.

(b) Walkley-Black Titration

First of all, each sample was air dried completely prior to the analysis. These were finely grinded using agate mortar in the lab. Thereafter, 1 g of this dried and powdered sample was kept in 500 ml conical flask, mixed with 10 ml Potassium Dichromate ($K_2Cr_2O_7$) and 20 ml of Sulphuric Acid (H_2SO_4). This mixture was kept in dark place undisturbed for digestion about half an hour. Afterwards, 200 ml of deionized water was added to this mixture to make a solution. 1 pinch of Sodium Fluoride (NaF) and 4-5 drops of DPA (Diphenyl Amine) indicator was added to this solution. The solution was, thereafter titrated against 0.5 N Ferrus Ammonium Sulphate (FAS). The point, at which the solution turned to light green colour, was noted down. These statistics were used to calculate TOC concentration. The total concentration of TOC in sediment sequences has been classified into high, medium and low categories based on its availability (Table 3.1). The TOC concentration in percentage, was determined as-

$$\text{Percentage of Total Organic Carbon (TOC)} = (B - S) \times \frac{0.003 \times 100 \times 0.50}{W} \dots\dots\dots(\text{equation 1})$$

Where, B =Blank reading
 S =Sample reading
 W = dried weight of soil (in gram)

Table 3.1 Categorization of carbon concentration (%) in sub-surface samples

Carbon Concentration (TOC in %) in sediments	Carbon Concentration Category
<0.5	Low
0.5 – 0.75	Medium
>0.75	High

3.2.1 Concentration of Major, Trace and Rare Earth Elements

Elemental concentration in sub-surface sediment samples has been analyzed using Energy Dispersive X-ray Fluorescence (EDXRF) spectrometry made by PANalytical Epsilon 5' at Advanced Instrumentation Research Facility (AIRF), Jawaharlal Nehru University, New Delhi.

EDXRF provides a wide range of analysis as an element can be determined from ppm to percentage level. Due to this, EDXRF has become one of the most favorable approaches for determining elemental concentration. This technique has several merits including non-destructive nature due to which samples can be recovered after the analysis. It is capable of multi-elemental analysis with good precision and speed. The testing has been conducted in following stages-

(a) Sample Preparation

Caution in sample preparation is vital for EDXRF analysis. The sample layer subjected to primary radiation has to be very homogenous because only this layer (0.01-0.1 mm) is to release fluorescence spectrum. Each sample has been oven dried over night before the analysis to oxidize or desiccate the organic matter. Thereafter, they have been finely grinded using pestle mortar. 2 g of this powdered sample has been mixed with 2 g of boric acid. Boric acid has been used to provide a homogenous layer to the sample which ensures that X-ray penetrates to a homogenous depth and no refraction takes place. A Pallet Pressure machine presses the sample so that there is no air between boric acid powder and sediment layer.

(b) EDXRF Analysis

Major elements in their oxidized state have been determined as percentage (%) of the total composition in sediment samples. Selected major elements contribute to about 95% of the total concentration. Content of trace and rare earth elements (REEs) has remained quite low, thereby these are obtained in parts per million (ppm). In this study, selection of trace elements and REEs has been done on the basis of their abundance in each facie and notable variation across the sediment sequences. The selected major, trace and rare earth elements have been listed in Table 3.2.

Table 3.2 Selected major, trace and rare earth elements (REEs)

Major Elements (in %)	Aluminum (Al ₂ O ₃), Silicon (SiO ₂), Phosphorus (P ₂ O ₅), Potassium (K ₂ O), Calcium (CaO), Titanium (TiO ₂), Manganese (MnO) and Iron (Fe ₂ O ₃) and Magnesium (MgO).
Trace Elements (in ppm)	Vanadium (V), Chromium (Cr), Cobalt (Co), Copper (Cu), Zinc (Zn), Lead (Pb), Strontium (Sr), Zirconium (Zr) and Barium (Ba)
Rare Earth Elements (REEs in ppm)	Lanthanum (La), Cerium (Ce) and Neodymium (Nd)

The down core variability of selected elements has been shown through coefficient of variation (CV). It has been calculated as-

$$\text{Coefficient of Variation in percentage (CV \%)} = \frac{SD}{Mean} \times 100 \dots\dots\dots(\text{equation 2})$$

A CV of 50% and above has been regarded as high variability; 20-50% as moderate variability and below 20% has been considered as low variability. Along with this, enrichment and depletion of elements have been analyzed based on enrichment factor.

3.2.3 Enrichment Factor (EF)

Elements behave differently during the weathering process. The elements resistant to weathering usually gain mass and get enriched. The non-resistant and less resistant elements are depleted and lose mass. Enrichment and depletion of elements differ depending on source rock composition and climate. Enrichment factor is used to estimate the sediment elemental source (Bahloul et al., 2018; Nagarajan et al., 2018). This index is calculated

based on normalization element (Fe or Al) which moderates the variation generated by heterogeneous sedimentation (Landsberger et al., 1982). In the present work, Fe is used as the normalization element to calculate Enrichment Factor (EF). Fe in marine sediments is mainly derived from natural weathering process so it is generally utilized to normalize the metal concentration (Covelli and Fantolan, 1997; Zhang et al., 2007; Nagarajan et al., 2018). As sediment chemistry is dominated by the geology of source area, the enrichment and depletion of elements in terms of enrichment factor has been examined in relation to their upper continental crust (UCC) mean provide by Rudnick and Gao (2014). They have provided an updated and improved value for the average concentration of different metals.

EF is calculated using the following equation based on Ergin et al. (1991):

$$\text{Enrichment factor (EF)} = \frac{(C_X/C_{Fe}) \text{ Sample}}{(C_X/C_{Fe}) \text{ Crust}} \dots\dots\dots(\text{equation 3})$$

Where,

- (C_X/C_{Fe})_{Sample} = is the ratio between concentration of the element X and that of Fe in the sediment sample
- (C_X/C_{Fe})_{Crust} = is the ratio between concentration of the element X and that of Fe in the reference base (Rudnick and Gao, 2014)
- Fe = Selected natural element of reference

In this study, Fe is selected as the element for normalization because anthropogenic sources of iron are insignificant. Several other works have also preferred Fe as normalizing element for the calculation of enrichment factor (Ergin et al. 1991; Zhang et al., 2007; Asa et al., 2013).

The background value of each element has been derived from the upper continental crust (UCC) mean suggested by Rudnick and Gao (2014). They have provided their own estimate after a comprehensive discussion of the merits and demerits of earlier studies (Cole et al., 2017). Tribovillard et al. (2006) have considered that the element is depleted if EF is below < 1; element is considered as stable if EF = 1; element is considered as enriched if EF > 1. This scheme has been followed in this study to analyse depletion and enrichment of the elements.

3.3 Analysis

The distribution of TOC, major and trace elements along with REEs have been discussed for the riverine and mixing zone. The assessment of enrichment and depletion of elements is based on EF. The concentration of certain elements influences the availability of other metals, hence to assess their relationship, correlation among major and trace elements have also been analyzed. The correlation also discloses similarity in the source of metal origin. Elements which are closely related are supposed to be derived from the same sources while those who disclose opposite pattern are considered to be delivered from a distinct environment (Koukina et al., 2017).

3.3.1 Concentration of TOC and Major Elements

3.3.1.1 Riverine Zone

Ezapur (EP)

Distribution of TOC (%) at this site is ranging between low and medium. TOC content is low (<0.5%) in EPL1, EPL2, EPL3, EPL6 and EPL7 whereas it is medium (0.5-0.75%) in EPL4 and EPL5 (Table 3.3). Average distribution of TOC at EP remains 0.31% with moderate variability across the facies (CV=42.33%). Among major elements, SiO₂ is the most abundant across the sediment sequences. This is followed by Al₂O₃, Fe₂O₃, N₂O, CaO, and MgO constituting about 90% of the total elemental composition at this location (Table 3.3).

Table 3.3 Concentration of TOC and selected major elements (%) in facies of Ezapur

Elements/ Facies	TOC	Na ₂ O	MgO	Al ₂ O ₃	SiO ₂	P ₂ O ₅	K ₂ O	CaO	TiO ₂	MnO	Fe ₂ O ₃
EPL1	0.18	3.68	2.42	11.8	60.86	0.16	1.95	2.87	0.75	0.51	10.95
EPL2	0.36	3.68	2.41	11.9	59.97	0.15	1.99	2.82	0.73	0.50	11.33
EPL3	0.11	4.11	2.34	12.46	57.97	0.18	2.20	2.47	0.81	0.49	11.26
EPL4	0.53	4.19	2.65	10.16	60.95	0.02	2.28	2.39	0.25	0.45	8.73
EPL5	0.48	4.05	2.41	11.9	58.71	0.11	2.13	2.59	0.72	0.58	12.48
EPL6	0.24	4.16	2.65	10.15	60.89	0.02	2.41	2.35	0.19	0.27	5.46
EPL7	0.30	4.07	2.45	11.6	59.03	0.14	1.64	3.30	0.89	0.32	8.67
Mean	0.31	3.99	2.48	11.42	59.77	0.11	2.09	2.68	0.62	0.45	9.84
CV (%)	42.33	4.73	4.32	6.86	1.75	51.25	10.51	10.9	39.09	21.54	21.02
TM*	-	3.27	2.48	15.4	66.62	0.15	2.8	3.59	0.64	0.1	5.04

*Terrestrial mean is based on values suggested by Rudnick and Gao (2014)

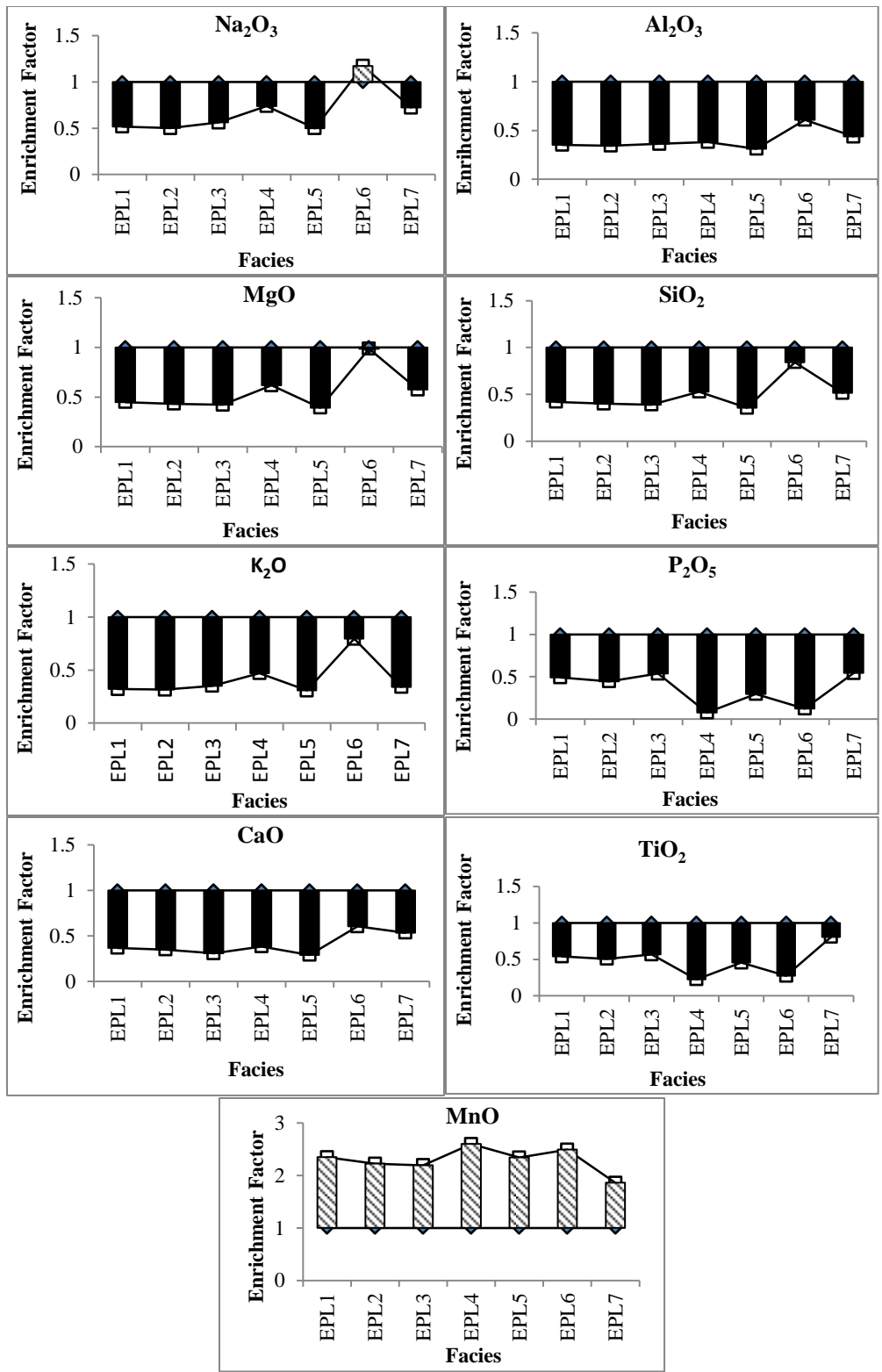


Figure 3.1 Concentration of selected major elements in facies of Ezapur

Concentration of Na_2O is enriched in EPL6 ($\text{EF} > 1$) whereas in other facies it is depleted (Figure 3.1). The average content of Na_2O has remained 3.99%. It, however, has shown low

variability across the sediment facies (CV=4.73%). The content of MgO has shown resistant (EF< 1) in EPL6. In contrast, it is depleted in all the other sediment sequences (EF<1). Mean distribution is 2.48%. It has exhibited low variation (CV=4.32%). In each facie, Al₂O₃ is depleted (EF<1). In EPL3 it is relatively high than other facies. The total concentration of Al₂O₃ has deviating between 10.15 and 12.46% with low coefficient of variation (6.86%). Distribution of SiO₂ is also depleted across the facies (EF<1). However, in EPL1, EPL4 and EPL6 its content is comparatively high. The average concentration has been recorded as 59.77%. It has shown low deviation (CV=1.75%) at this site. Similarly, the concentration of P₂O₅ is depleted. It is comparatively high in EPL1 and EPL3. Average concentration of P₂O₅ is 0.11% with high variability across the sediment sequence (51.25 %). Mean content of K₂O is 2.09%. It is also depleted at this location (EF<1). Nevertheless, in EPL3, EPL4, EPL5, EPL6 and EPL7 its concentration is relatively high than other facies. Low fluctuation of K₂O is recorded across the sediment sequence (CV= 10.51%). Concentration of CaO has remained around 2.68%. In all the facies it is depleted (EF<1). Its content in EPL1 and EPL2 is higher than the other facies. The CaO has shown low variation across the sediment sequence (CV=10.90 %). Concentration of TiO₂ is also depleted in each facie of this site. In EPL1, EPL2, EPL3, EPL5 and EPL7, the TiO₂ concentration is relatively high. Its average concentration is 0.62% with moderate variability (CV=39.1%) across the sediment sequences. Concentration of MnO has shown enrichment in all the facies (EF>1). The mean content of MnO is 0.45%. It has varied moderately (CV=21.5%) at EP. The Fe₂O₃ content is comparatively high in EPL1, EPL2, EPL3 and EPL5. Mean concentration is 9.84% with moderate (CV=21.0%) deviation across the sediment sequences.

Jhumpuri (JP)

Concentration of TOC at JP has varied from low to medium. Average concentration of TOC is 0.34% with medium concentration (0.5 - 0.75%) in JPL5, JPL7, JPL8 and JPL9 and low (<0.5%) in remaining facies (Table 3.4). It has shown high variation across the sediment sequences (58.82%). The order of abundance of major elements at this site are SiO₂> Al₂O₃> Fe₂O₃> Na₂O> CaO and MgO. These elements have constituted nearly 90% of the total elemental concentration.

The Na₂O has shown resistance (EF=1) in JPL4 and JPL7 whereas in other facies its content is depleted (Figure 3.2). Mean concentration of Na₂O is 3.77%. It has shown low variability

(CV=5.27%) across the sediment sequence. Contrary to this, MgO is depleted in all the facies with average concentration being 2.93%. It has exhibited low fluctuation (CV=4.76) across the facies. It is relatively high in JPL4 and JPL8 in comparison to other facies. Concentration of Al₂O₃ is also depleted in all the facies of JP. The average content of Al₂O₃ is 12.06% with low variability (CV=7.46%) across the sediment sequences. Similarly, the SiO₂ is depleted in each facie. Its average concentration has remained 58.2%. In JPL2, JPL4, JPL7 and JPL8 it is higher than the other facies. The down core variability of SiO₂ is low (CV=2.14%). Average distribution of P₂O₅ is 0.10 %. It is also depleted across the sediment sequences (EF<1).

Table 3.4 Concentration of TOC and major elements (%) in facies of Jhumpuri

Elements/ Facies	TOC	Na ₂ O	MgO	Al ₂ O ₃	SiO ₂	P ₂ O ₅	K ₂ O	CaO	TiO ₂	MnO	Fe ₂ O ₃
JPL1	0.33	3.63	2.42	11.7	58.56	0.14	1.87	2.95	0.88	0.75	16.4
JPL2	0.11	3.64	2.48	11.29	59.23	0.13	1.85	2.96	0.90	0.76	16.47
JPL3	0.06	3.66	2.37	12.13	57.15	0.09	1.84	2.97	0.96	0.79	17.36
JPL4	0.26	3.73	2.51	11.19	59.15	0.02	2.28	2.48	0.24	0.25	5.82
JPL5	0.63	3.48	2.17	13.74	55.07	0.07	1.80	3.06	0.92	0.69	15.49
JPL6	0.33	3.62	2.19	13.62	57.76	0.15	1.86	2.95	0.74	0.35	8.63
JPL7	0.75	4.10	2.42	11.79	59.62	0.07	1.77	3.10	0.53	0.30	7.13
JPL8	0.56	3.68	2.54	10.74	59.30	0.11	1.74	3.56	0.79	0.45	10.81
JPL9	0.54	4.09	2.33	12.44	57.68	0.10	1.83	3.05	0.75	0.57	12.82
JPL10	0.08	3.98	2.44	11.69	57.68	0.07	1.91	2.97	0.52	0.50	12.03
JPL11	0.09	3.89	2.37	12.30	58.62	0.15	1.86	3	0.67	0.22	5.83
Mean	0.34	3.77	2.39	12.1	58.2	0.10	1.87	3	0.72	0.51	11.7
CV	58.8	5.27	4.76	7.46	2.14	39.1	7.28	7.83	28.8	39.9	35.8
TM*	-	3.27	2.48	15.4	66.62	0.15	2.8	3.59	0.64	0.10	5.04

*Terrestrial mean is based on values suggested by Rudnick and Gao (2014)

In JPL6 and JPL11 its concentration is comparatively high than in other facies. Likewise, the K₂O is depleted (EF<1) across the sediment sequences. It is comparatively high in JPL4 and JPL10. Average distribution of K₂O is 1.87% with low variation (CV=7.28 %). Mean concentration of CaO is 3% with low deviation across the sediment sequences (CV=7.83). It is depleted below the continental mean of in all the facies. Its concentration is relatively high in JPL5, JPL7, JPL8, JPL9 and JPL11. Average content of TiO₂ is 0.72% with moderate variability across the facies (CV=28.81%). It is also depleted (EF<1) in all the facies. MnO, on the other hand, is enriched (EF>1) across the sediment sequences.

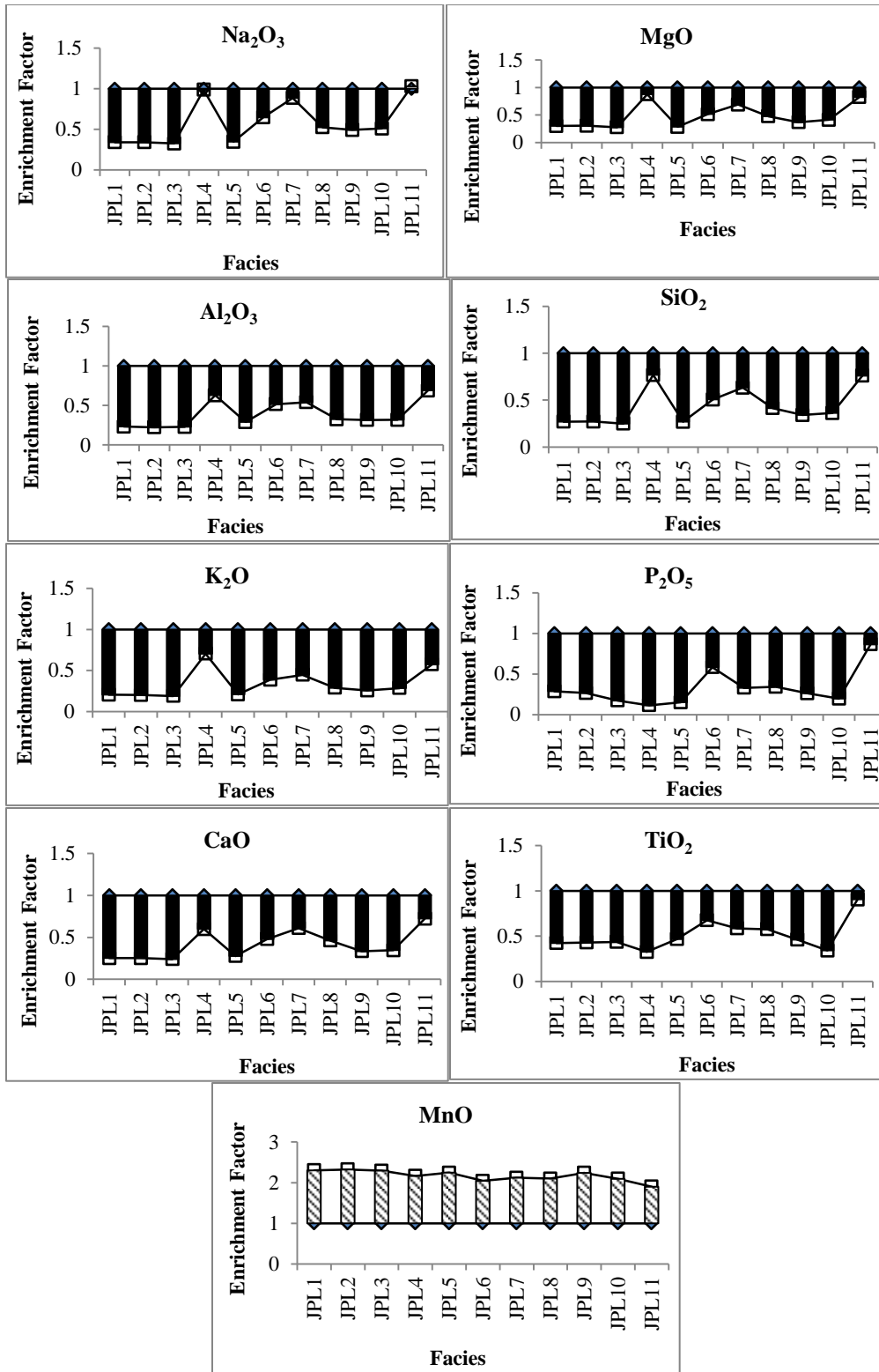


Figure 3.2 Concentration of selected major elements in facies of Jhumpuri

In JPL1, JPL2 and JPL3 its concentration is even higher. Average distribution of MnO is 0.51% with moderate variability (CV=39.94%) at this site. The concentration of Fe₂O₃ is relatively high in JPL1, JPL2, JPL3 and JPL5. Mean concentration of Fe₂O₃ is 11.71%. It has varied moderately at this location (CV=35.75%).

Katia I (KTI I)

Distribution of TOC has deviated from low to medium at KTI site. It is low (<0.5%) in KTIL2, KTIL3 and KTIL5 while medium (0.5 - 0.75 %) in KTIL1 and KTIL4 (Table 3.5). The average concentration of TOC is relatively high, 0.44% as compared to the previous locations. Its concentration has fluctuated moderately across the facies (CV=27.27%). Among all the major elements SiO₂ is the most abundant followed by Fe₂O₃, Al₂O₃, Na₂O and CaO (Table 3.5).

Table 3.5 Concentration of TOC and selected major elements (%) in facies of Katia I

Elements/ Facies	TOC	Na₂O	MgO	Al₂O₃	SiO₂	P₂O₅	K₂O	CaO	TiO₂	MnO	Fe₂O₃
KTIL1	0.59	3.56	2.59	10.42	61.38	0.19	1.83	2.98	0.86	0.41	10.32
KTIL2	0.26	3.85	2.37	12.27	57.65	0.13	1.90	2.94	0.79	0.70	14.59
KTIL3	0.42	3.72	2.50	11.12	59.02	0.11	1.87	2.93	0.96	0.75	16.55
KTIL4	0.51	3.64	2.35	12.39	57.74	0.12	1.85	2.97	0.91	0.73	16.15
KTIL5	0.24	4.15	2.41	11.90	57.95	0.13	1.87	2.95	0.86	0.65	14.83
Mean	0.44	3.78	2.44	11.62	58.75	0.14	1.86	2.95	0.88	0.65	14.49
CV (%)	27.27	5.46	3.66	6.42	2.39	20.6	1.25	0.63	6.48	19.1	15.28
TM*	-	3.27	2.48	15.4	66.62	0.15	2.8	3.59	0.64	0.10	5.04

*Terrestrial mean is based on values suggested by Rudnick and Gao (2014)

Average distribution of Na₂O is 3.78%. It is depleted in all the facies (EF<1). Its concentration is comparatively high in KTIL5 (Figure 3.3). The Na₂O has demonstrated low fluctuation (CV=5.46%). The MgO is also depleted. Its mean concentration is 2.44% with low variability (CV=3.66%) across the sediment sequences. Concentration of Al₂O₃ is depleted in each facies. Its mean content is 11.62%. It has exhibited low deviation across the facies. In KTIL2 and KTIL4 it is higher in comparison to the other facies. Similarly, the SiO₂ is depleted (EF<1). The mean concentration is 58.57% and low fluctuation across the sediment sequences. Its content is comparatively high in KTIL1 and KTIL3. The P₂O₅ is

also depleted at this site. Mean concentration has remained around 0.14%. It has exhibited moderate variation at this location (CV=20.59%) where in KTIL1 it is higher than the other facies. In each sediment sequence, the K_2O is depleted (EF<1). Its average concentration has remained 2.95% with very low variability (CV=1.25%).

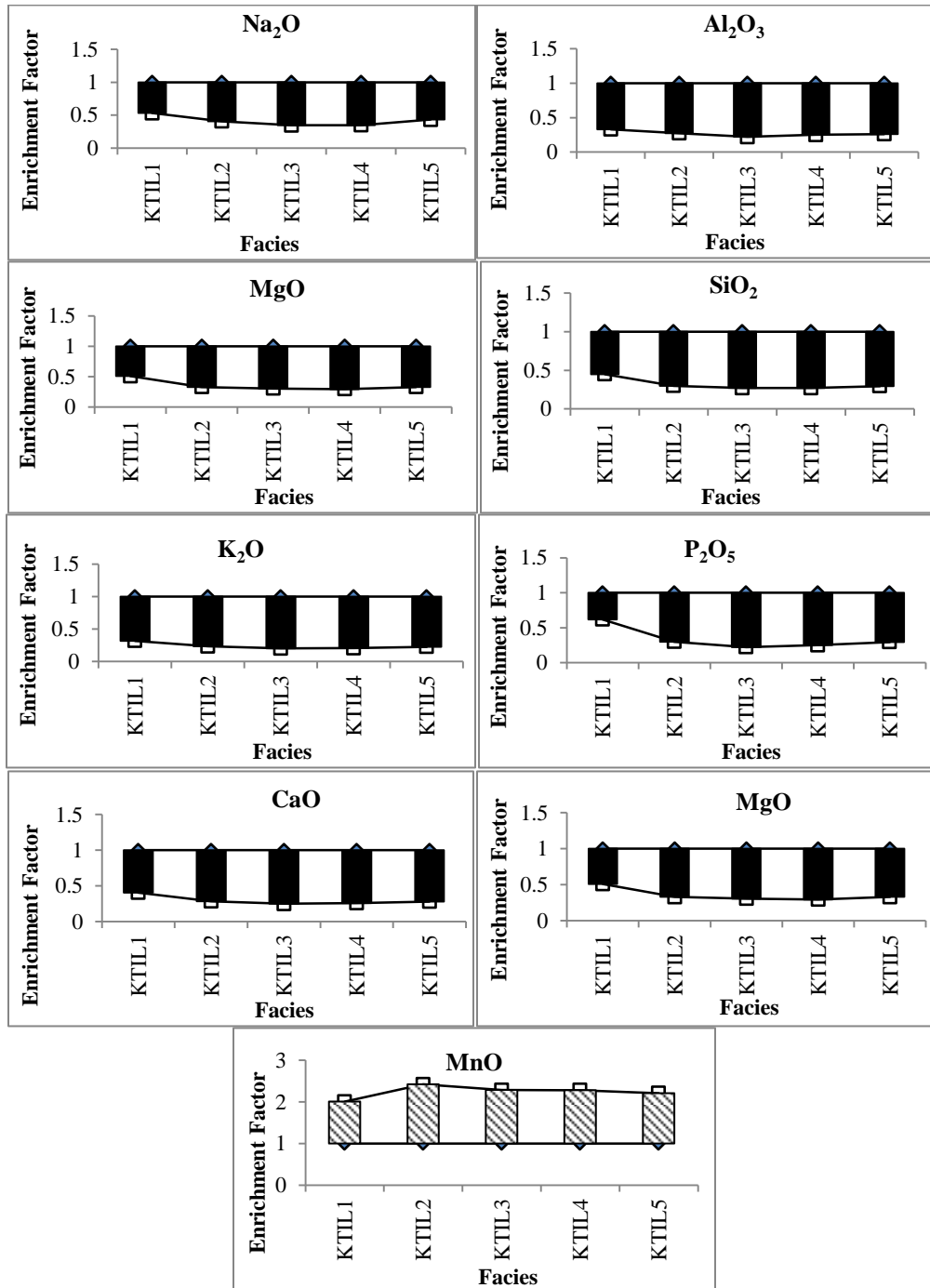


Figure 3.3 Concentration of selected major elements in facies of Katia I

Similarly, the concentration of TiO₂ is depleted in all the facies of KTI with average content of 0.88%. However, in KTIL3 and KTIL4 its content is relatively high. In contrast, the MnO is enriched in all the facies. Its average concentration is 0.65%. MnO has shown low variability (CV=19.1%). The Fe₂O₃ is relatively high in KTIL3 and KTIL4. The average content is 14.49% with low down core variability and Fe₂O₃ (CV=15.28 %).

Katia II (KTII)

At this site the TOC value has ranged from low (<0.5%) to high (>0.75%). Higher concentration of TOC (>0.75%) was recorded in KTIL5 and KTIL7 suggesting increased productivity of organic carbon. Contrary to this, in KTIL1 TOC is medium (0.5 - 0.75%) while in all the other facies TOC is low (Table 3.6). Average concentration of TOC is 0.49 % with very high variability across the facies (CV=93.9%).

Table 3.6 Concentration of TOC and major elements (%) in facies of Katia II

Elements/ Facies	TOC	Na ₂ O	MgO	Al ₂ O ₃	SiO ₂	P ₂ O ₅	K ₂ O	CaO	TiO ₂	MnO	Fe ₂ O ₃
KTIL1	0.50	3.70	2.30	12.73	58.22	0.17	1.87	2.95	0.89	0.58	13.23
KTIL2	0.32	4.00	2.49	11.20	59.29	0.14	1.89	2.96	0.78	0.60	13.19
KTIL3	0.20	3.68	2.30	12.82	57.22	0.13	2.02	2.81	0.68	0.54	11.94
KTIL4	0.29	3.80	2.43	11.69	58.50	0.14	1.96	2.87	0.71	0.58	12.62
KTIL5	1.38	3.45	2.25	13.15	56.68	0.12	1.84	2.98	0.95	0.92	18.71
KTIL6	0.08	3.72	2.53	10.86	59.52	0.15	1.89	2.93	0.85	0.56	12.96
KTIL7	1.28	3.67	2.38	12.12	58.51	0.16	1.91	2.89	0.82	0.48	11.52
KTIL8	0.24	3.58	2.35	12.36	58.04	0.17	1.93	2.88	0.79	0.55	12.24
KTIL9	0.15	3.40	2.46	11.42	58.04	0.10	1.84	2.99	0.88	0.71	16.12
Mean	0.49	3.67	2.39	12.04	58.22	0.14	1.91	2.92	0.82	0.61	13.61
CV (%)	93.9	4.62	3.79	6.21	1.45	15.47	2.88	1.92	10.03	20.03	16.07
TM*	-	3.27	2.48	15.4	66.62	0.15	2.8	3.59	0.64	0.10	5.04

*Terrestrial mean is based on values suggested by Rudnick and Gao (2014)

The SiO₂ is the most significant constituent of KTII similar to the other locations in riverine zone. The order of concentration is as follows- Fe₂O₃ > Al₂O₃ > Na₂O > CaO > MgO. Together these elements constitute for nearly 93% of the total metal concentration at this location. Low variability has been observed in the content of Na₂O, MgO, Al₂O₃, SiO₂, K₂O and CaO at this site (CV<10%).

The Na₂O is depleted (EF<1) in each facie (Figure 3.4). Mean concentration of Na₂O is 4.62%. It is relatively high in KTIL2 and KTIL4. The MgO is also depleted across the facies. Its concentration is comparatively high in KTIL2, KTIL6 and KTIL9. Mean

distribution of Al_2O_3 is 12.04%. It is depleted across the sediment sequences. Its concentration is comparatively high in KTIL1, KTIL3, KTIL5, KTIL7 and KTIL8.

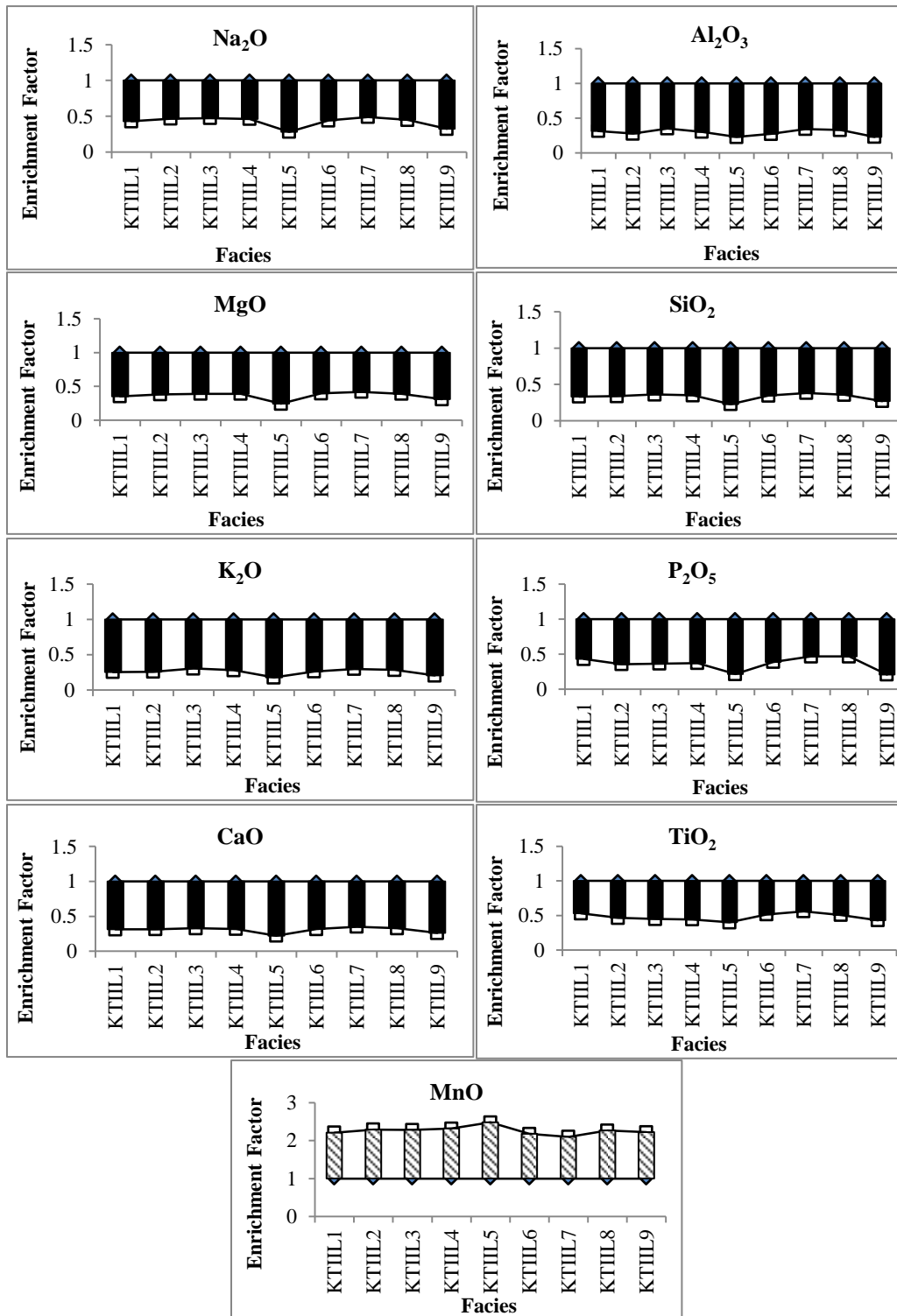


Figure 3.4 Concentration of selected major elements in facies of Katia II

Similarly, the SiO_2 is depleted in each facie. Relatively higher concentration of SiO_2 is in KTII2. K_2O is also depleted across the sediment sequences. Its mean availability is around 1.91%. The content of K_2O is higher in KTII3 than other facies. The P_2O_5 is depleted at this location. It is relatively high in KTII1, KTII7 and KTII8. The average concentration of P_2O_5 is 0.14%. It has exhibited low variability in KTII (CV=15.47%). The TiO_2 is depleted as well with mean availability of 0.82%. The content of MnO , in contrast, is enriched across the facies with an average of 0.61%. The Fe_2O_3 is relatively high in KTII5 and KTII9.

On the basis of above analysis it can be stated that there has been significant down core variation in the distribution of TOC and major elements. TOC has shown high deviation at EP and KTI while at JP and KTII it has exhibited high fluctuation. The TiO_2 , MnO and Fe_2O_3 have been moderately variable at EP and JP. Only MnO is enriched in comparison to the UCC whereas all the other elements are depleted at each location. The Na_2O and MgO are comparatively high in EPL6, JPL4 and JPL11.

3.3.3.2 Mixing Zone

Average concentration of TOC has increased remarkably in the facies of mixing zone which can be due to high availability of organic carbon or insufficient oxygen to oxidize the carbon (Liu et al., 2019).

Sonpanki (SP)

At this site of mixing zone, average TOC concentration was recorded as 0.71 %. It has varied from low to high. TOC remains high (>0.75%) in SPL1 and SPL3 whereas in SPL4 it is medium (0.5-0.75%). Concentration of TOC is low (<0.5%) in SPL2, SPL5 and SPL6 (Table 3.7). The coefficient of variation (45.30%) has suggested moderate variability across the facies. This implies that in some facies (SPL1 and SPL3) the TOC concentration is significantly high than rest of the facies.

The most important constituents of SP are in the following order- $\text{SiO}_2 > \text{Al}_2\text{O}_3, > \text{Fe}_2\text{O}_3 > \text{Na}_2\text{O} > \text{MgO} > \text{CaO} > \text{K}_2\text{O}$. These metals have constituted approximately 92.6 % of the total elemental concentration.

Table 3.7 Concentration of TOC and major elements (%) in facies of Sonpanki

Elements/ Facies	TOC	Na ₂ O	MgO	Al ₂ O ₃	SiO ₂	P ₂ O ₅	K ₂ O	CaO	TiO ₂	MnO	Fe ₂ O ₃
SPL1	0.99	3.36	2.28	12.83	57.18	0.15	2.25	2.37	0.84	0.63	14.11
SPL2	0.33	3.57	2.19	13.52	55.68	0.09	2.33	2.25	0.9	0.65	16.0
SPL3	1.16	3.45	2.19	13.51	56.58	0.16	2.25	2.37	0.87	0.46	11.26
SPL4	0.71	3.52	2.28	12.83	57.29	0.15	2.26	2.39	0.81	0.53	12.48
SPL5	0.39	3.72	2.26	12.99	57.39	0.2	2.4	2.16	0.9	0.24	7.40
SPL6	0.42	3.79	2.52	11.12	60.33	0.01	2.54	2.22	0.13	0.16	4.31
Mean	0.71	3.52	2.24	13.14	56.82	0.15	2.3	2.31	0.86	0.5	12.25
CV (%)	45.3	3.43	1.85	2.4	1.12	23.5	2.57	3.86	4.05	29.5	23.7
TM*	-	3.27	2.48	15.4	66.62	0.15	2.8	3.59	0.64	0.1	5.04

*Terrestrial mean is based on values suggested by Rudnick and Gao (2014)

The distribution of Na₂O is enriched (EF>1) in the basal sequence, SPL6 while it is depleted (EF<1) in all the other facies (Figure 3.5). Average concentration of Na₂O is 3.52% with low variability (CV=3.42%) across the sediment sequences. The MgO is also enriched in SPL6 while it is depleted in other facies. The mean concentration of MgO has remained 2.24%. It has shown low variability (CV=1.85%). The Al₂O₃, on the other hand, is depleted in all the facies. However, in SPL2 and SPL3 it is comparatively high. The average concentration of Al₂O₃ is 13.14%. The SiO₂ is enriched in SPL6 whereas it is depleted in other sequences.

The mean concentration of SiO₂ is 56.82 % with low down core variation (CV=1.12%). The P₂O₅ is depleted in all the facies with average concentration of 0.15%. Concentration of P₂O₅ has varied moderately (CV=23.5%). The K₂O is enriched in SPL6 (EF>1). Its average content is 2.30% with low deviation (CV=2.57%) across the facies. Concentration of CaO is depleted in each facie. Its mean concentration is 2.31% with low variation (CV=3.86%) across the sediment sequences. Average concentration of TiO₂ is 0.86%. It is enriched in SPL5 whereas in other facies it is depleted. The MnO is enriched (EF>1) across the sediment sequences. It has remained moderately variable (CV=29.48%). The Fe₂O₃

concentration is relatively high in SPL1, SPL2, SPL3 and SPL4. It has shown moderate variability across the sediment sequences (CV=23.68%).

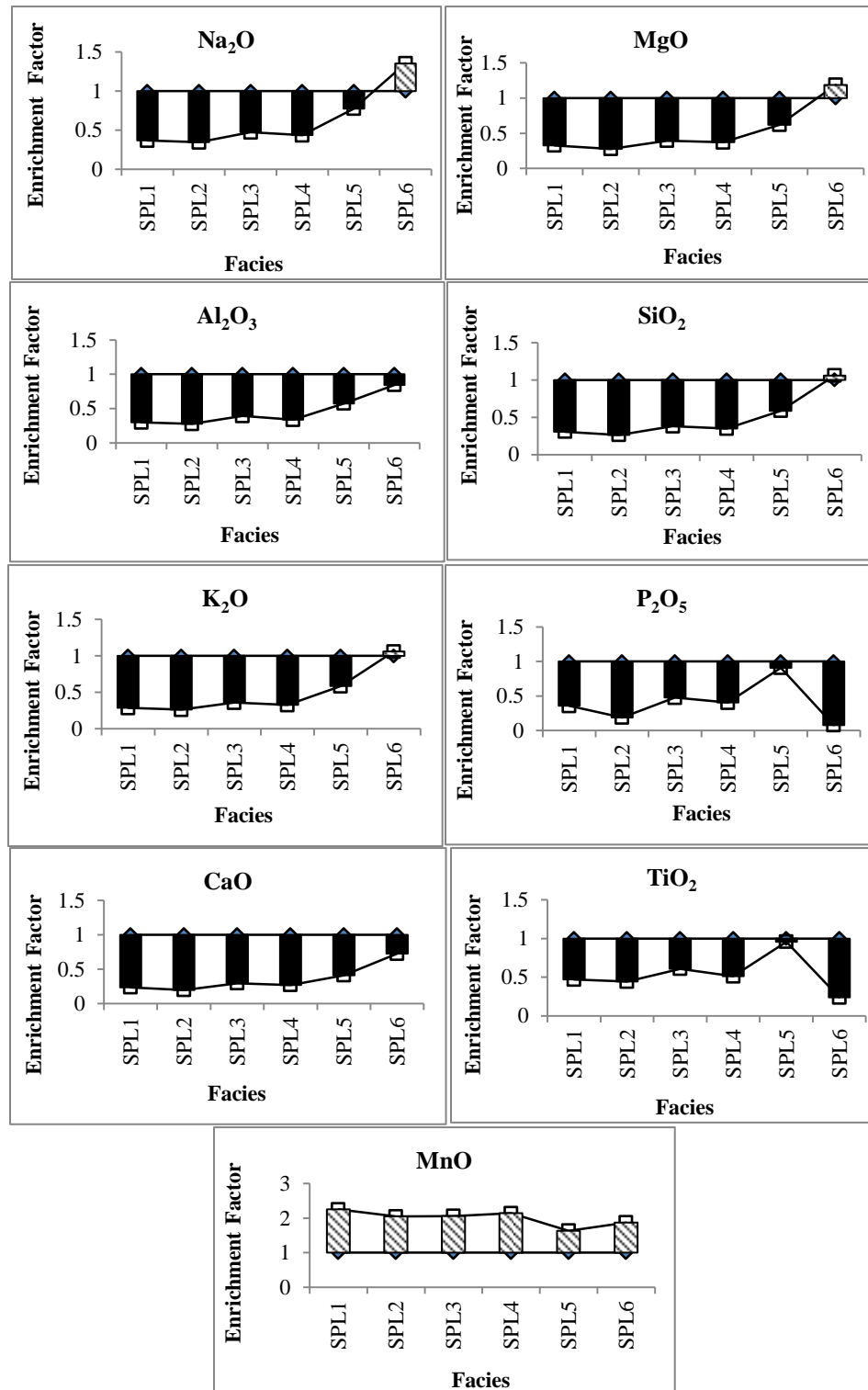


Figure 3.5 Concentration of selected major elements in facies of Sonpanki

Chandbali (CB)

The organic carbon or TOC has deviated from low (<0.5%) to high (>0.75%) at this site (Table 3.8). Its concentration is significantly high in CBL3 (>3%). It is medium in CBL2 and CBL4 (0.5-0.75%) while low (<0.5%) in CBL1, CBL5 and CBL6. Mean concentration of TOC is markedly high (0.91%) at this location. It has exhibited high (CV=149%) variability across the facies. The order of abundance of major elements in CB is similar to the other sites, $\text{SiO}_2 > \text{Al}_2\text{O}_3 > \text{Fe}_2\text{O}_3 > \text{Na}_2\text{O} > \text{CaO} > \text{MgO}$. These comprise for around 90% of the total elemental concentration.

Table 3.8 Concentration of TOC and major elements (%) in facies of Chandbali

Elements/ Facies	TOC	Na ₂ O	MgO	Al ₂ O ₃	SiO ₂	P ₂ O ₅	K ₂ O	CaO	TiO ₂	MnO	Fe ₂ O ₃
CBL1	0.11	3.74	2.56	10.85	60.09	0.12	2.7	1.92	0.57	0.68	11.88
CBL2	0.65	3.62	2.51	10.92	63.97	0.15	2.51	2.1	0.65	0.24	7.45
CBL3	3.9	3.96	2.36	12.27	59.91	0.27	2.06	2.63	0.78	0.11	3.79
CBL4	0.56	3.83	2.46	11.44	58.37	0.14	2.24	2.34	0.75	0.36	9.39
CBL5	0.2	4.06	2.91	7.46	63.56	0.11	2.15	4.85	0.59	0.54	10.69
CBL6	0.06	3.85	2.31	12.61	57.74	0.18	2.27	2.34	0.86	0.32	8.68
Mean	0.91	3.84	2.52	10.93	60.61	0.16	2.32	2.7	0.7	0.38	8.65
CV (%)	149	3.7	7.73	15.37	3.93	33.01	9.4	36.63	14.98	50.1	29.94
TM*	-	3.27	2.48	15.4	66.62	0.15	2.8	3.59	0.64	0.1	5.04

*Terrestrial mean is based on values suggested by Rudnick and Gao (2014)

The Na₂O, MgO, Al₂O₃, SiO₂, K₂O, P₂O₅, CaO and TiO₂ are enriched (EF>1) in CBL3 while in other facies these are depleted (Figure 3.6). This pattern has demonstrated that during the deposition of CBL3 distinct processes might have operated at this beach ridge and during weathering these elements might have gain weight. Mean concentration of Na₂O is 3.84% and it has shown low variability across the sediment sequences (CV=3.7%). Average concentration of MgO is 2.52% at CB which is significantly high than the other locations. Higher MgO content might be due to its location at beach ridge. It has exhibited low fluctuation (CV=7.73%) across the sediment sequences. Average abundance of Al₂O₃ is around 11% and it has shown low variability (CV=15.4%) at this location.

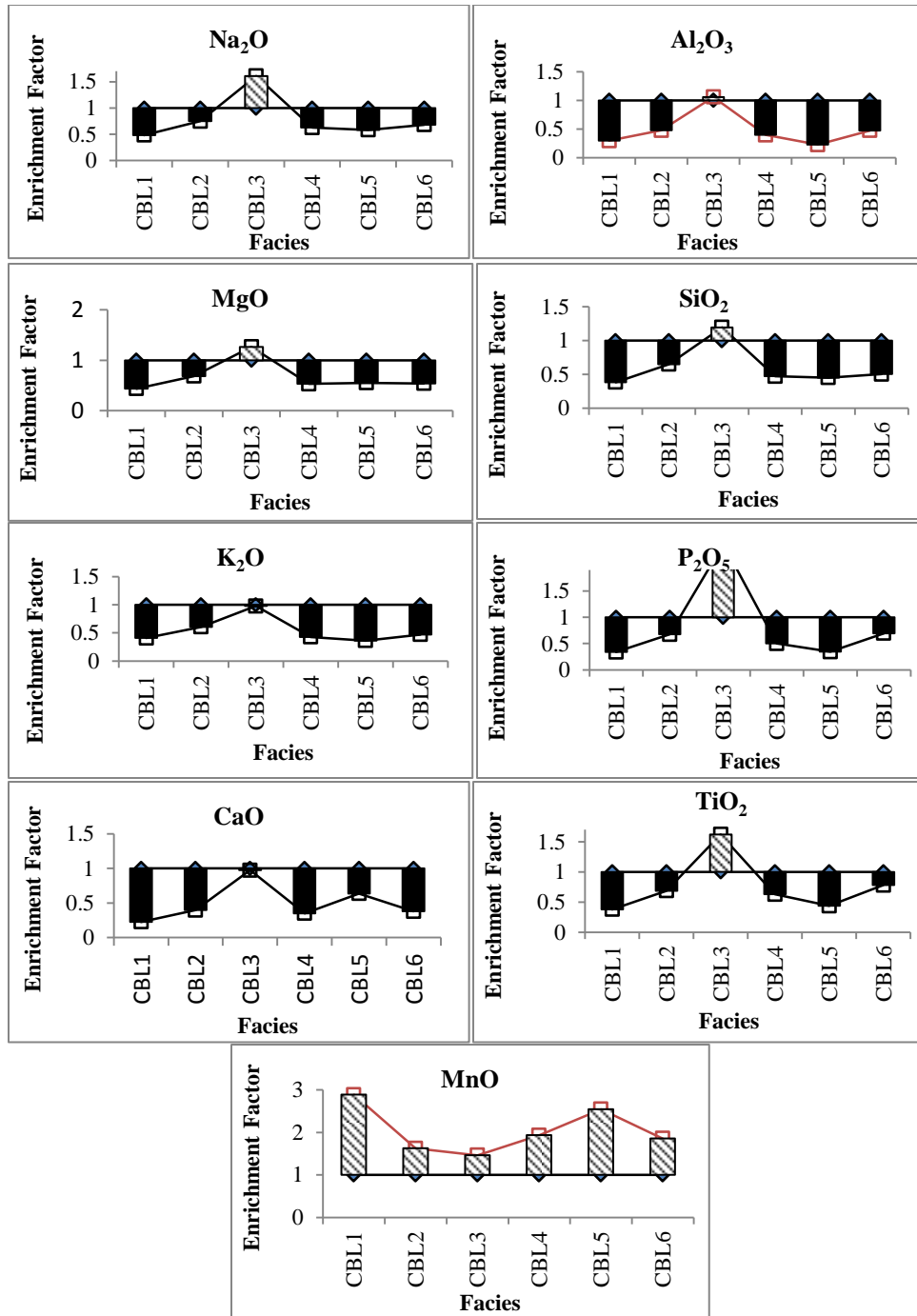


Figure 3.6 Concentration of selected major elements in facies of Chandbali

Mean concentration of SiO₂ is 60.61% which is significantly high than in other locations. It has revealed low variation (CV=3.93%) across the facies. Average availability of P₂O₅ is 0.16%. It has shown moderate deviation across the sediment sequences (CV=33%). Average concentration of K₂O is 2.32% with low variation (CV=9.40%). Mean content of CaO is

2.70% and it has exhibited moderate variation at this site (CV=36.6%). Average concentration of TiO₂ is 0.70% with low down core variability (CV=15%). Contrary to these, the concentration of MnO is enriched in all the facies. However, it has shown high variability (CV=50.1%). The availability of Fe₂O₃ is relatively high in CBL1, CBL2, CBL4, CBL5 and CBL6 than in other facies. Mean content of Fe₂O₃ is 8.65% with moderate variability at this site (CV=29.9%).

Ambiligan (AG)

Concentration of TOC has deviated between low (<0.5%) to high (>0.75%). It is high in AGL2, AGL3, AGL4 and AGL5 whereas in surface facie represented as AGL1, TOC concentration is low (Table 3.9). The average concentration of TOC at this location is considerably high (2.22%). It has revealed high variation (CV=101.3%) across the sediment sequences (Table 3.9). The most abundant element is SiO₂ followed by Al₂O₃, Fe₂O₃, Na₂O, K₂O and MgO contributing nearly 88% of the bulk elemental constituents.

Table 3.9 Concentration of TOC and major elements (%) in facies of Ambiligan

Elements/ Facies	TOC	Na ₂ O	MgO	Al ₂ O ₃	SiO ₂	P ₂ O ₅	K ₂ O	CaO	TiO ₂	MnO	Fe ₂ O ₃
AGL1	0.18	3.43	2.18	13.63	55.66	0.09	2.49	2.0	0.9	0.5	13.26
AGL2	1.65	3.28	2.07	14.43	53.61	0.05	2.48	2.02	0.78	0.46	12.45
AGL3	1.68	4.13	2.48	11.24	60.64	0.22	2.36	2.25	0.76	0.22	6.3
AGL4	6.6	3.72	2.42	11.62	58.97	0.11	2.37	2.27	0.71	0.31	8.82
AGL5	1.02	3.83	2.23	13.19	55.97	0.09	2.31	2.26	0.8	0.32	9.56
Mean	2.22	3.67	2.27	12.82	56.97	0.11	2.4	2.16	0.79	0.36	10.08
CV (%)	101	8.15	6.7	9.44	4.4	51.3	2.95	5.69	7.93	28.5	25.1
TM*	-	3.27	2.48	15.4	66.62	0.15	2.8	3.59	0.64	0.1	5.04

*Terrestrial mean is based on values suggested by Rudnick and Gao (2014)

The Na₂O has shown resistance (EF=1) in AGL3 (Figure 3.7). The average concentration is 3.67% with low fluctuation across the sediment sequences (CV=8.15%). On the contrary, MgO, Al₂O₃, SiO₂, P₂O₅, K₂O, CaO and TiO₂ are depleted in all the facies (EF<1). Average distribution of MgO is 2.27%. It has exhibited low variability across the facies (CV=6.7%). Mean concentration of Al₂O₃ is 12.12% with low down core variability (CV=9.44%). Average content of SiO₂ is 56.97% with low deviation across the facies (CV=4.40%).

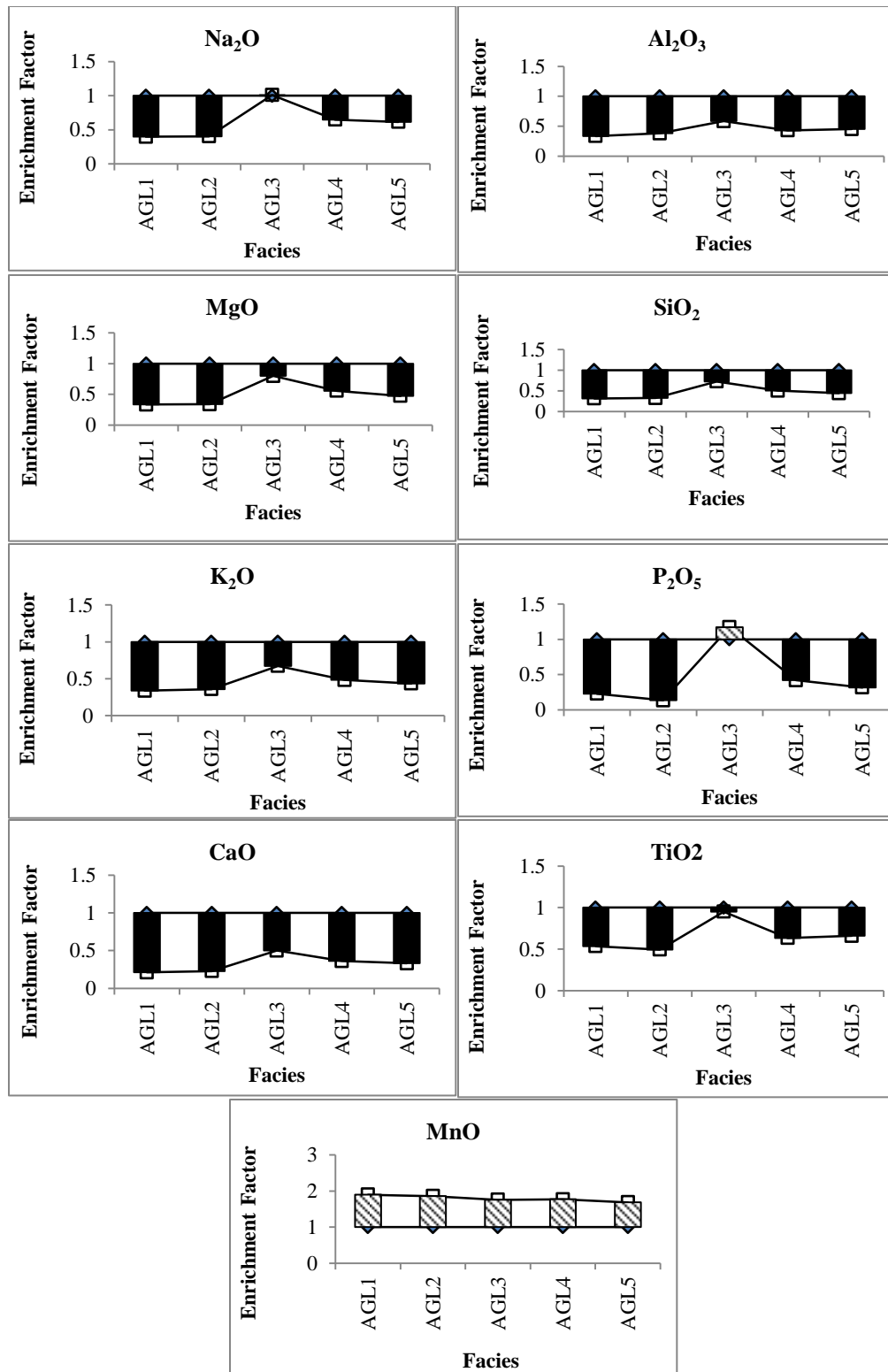


Figure 3.7 Concentration of selected major elements in facies of Ambiligan

The average distribution of P₂O₅ is around 0.11%. It has varied significantly (CV=51.1%) at this location. Concentration of K₂O has shown low variability across the facies (CV=2.95%) with mean of 2.4%. Average concentration of CaO is 2.16%. It has also exhibited low variation across the sediment sequences (CV=5.69%). The average distribution of TiO₂ is 0.79% which is considerably high. It has shown low variation (CV=7.93%) across the Facies. The MnO is enriched across the facies (EF>1). Its concentration is markedly high in AGL1. Mean concentration of MnO is 0.36%. It has varied moderately (CV=28.5%) at AG. Average concentration of Fe₂O₃ is 10.08% and it has shown moderate deviation across the facies (CV=25.1%).

Kasturikaran (KK)

In general, the concentration of TOC has declined at this location. It has deviated between low (<0.5%) and medium (0.5-0.75%). In KKL2 and KKL4 it was medium whereas it was low in KKL1 and KKL3 (Table 3.10). Average concentration of TOC is 0.36% which is relatively low. The variability across sediment sequences is high (CV=50.1%).

The order of concentration of major elements is as follows- SiO₂> Al₂O₃> Fe₂O₃> Na₂O> K₂O> MgO> CaO. These constitute nearly 90% of the total elemental concentration at KK.

Table 3.10 Concentration of TOC and major elements (%) in facies of Kasturikaran

Elements/ Facies	TOC	Na ₂ O	MgO	Al ₂ O ₃	SiO ₂	P ₂ O ₅	K ₂ O	CaO	TiO ₂	MnO	Fe ₂ O ₃
KKL1	0.33	3.34	2.18	13.59	56.01	0.15	2.58	1.91	0.82	0.37	9.99
KKL2	0.53	3.42	2.31	12.55	56.59	0.1	2.41	2.18	0.75	0.45	11.78
KKL3	0.08	4.08	2.59	10.54	60.97	0.13	2.13	2.78	0.63	0.38	7.78
KKL4	0.5	3.45	2.21	13.24	56.2	0.09	2.56	2.03	0.69	0.44	11.12
Mean	0.36	3.57	2.32	12.48	57.44	0.11	2.42	2.22	0.72	0.41	10.16
CV (%)	50.1	8.28	6.97	9.46	3.56	20.3	7.43	15.03	9.76	8.62	14.95
TM*	-	3.27	2.48	15.4	66.62	0.15	2.8	3.59	0.64	0.1	5.04

*Terrestrial mean is based on values suggested by Rudnick and Gao (2014)

The Na₂O is depleted (EF<1) in each facies at this location (Figure 3.8). Its average concentration is 3.57%. It has exhibited low variability (CV=8.28%) across the sediment sequences. The MgO is also depleted in each facie. Mean concentration is 2.32% with low down core deviation (CV=6.97%).

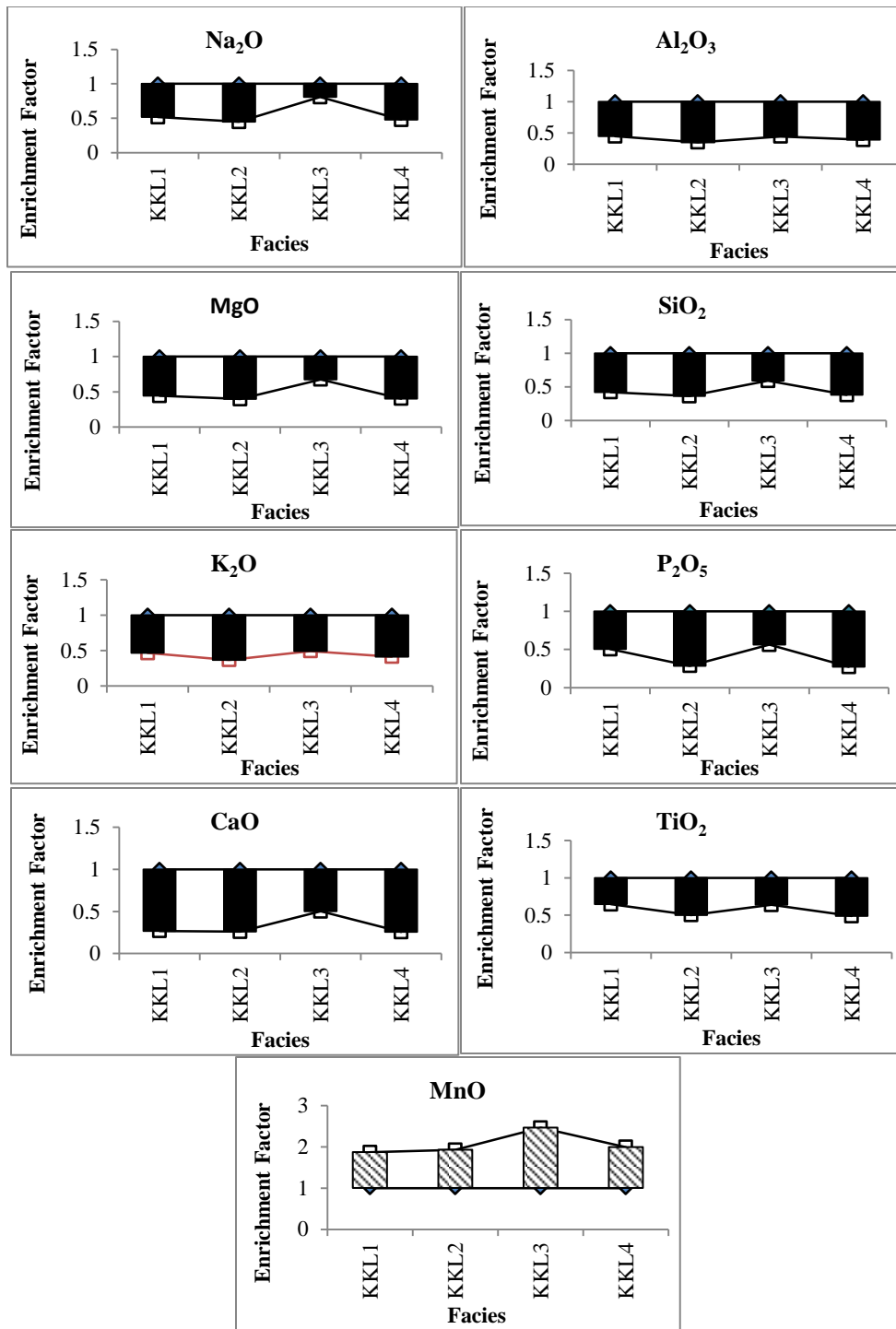


Figure 3.8 Concentration of selected major elements in facies of Kasturikaran

The Al₂O₃ is also depleted across the sediment sequences. Mean distribution of Al₂O₃ is 12.48%. It has exhibited low variability (CV=9.46%) at this site. The SiO₂ is also depleted in each facie. Average concentration of SiO₂ is 57.44%. It has shown low variability

(CV=3.56 %) across the sediment sequences. The P_2O_5 is depleted as well across the facies with mean concentration of 0.11%. It has varied moderately at this site (CV=20.30%). The concentration of K_2O is also depleted. Its mean concentration is 2.42% with low variation across the sediment sequences (CV=7.43%). Similarly, the CaO is depleted in each facie. Mean concentration is 2.22% with low variability (CV=15.03%). Concentration of TiO_2 is depleted in each facie. Average availability is observed around 0.72% with low down core deviation (CV=9.76%). On the contrary, the MnO is enriched across the facies. Average concentration MnO is 0.41% with low variation (8.62%) across the sediment sequences. Average content of Fe_2O_3 is 10.16%. It has exhibited low fluctuation (CV=15%) across the sediment sequences.

It has become obvious that at SP site Na_2O , MgO, SiO_2 and MnO are enriched in SPL6. At CB the concentration of Na_2O , Al_2O_3 , MgO, SiO_2 , K_2O , P_2O_5 , CaO and TiO_2 are enriched in CBL3. In AGL3, the Na_2O , P_2O_5 and TiO_2 are enriched. Similar to riverine zone, the concentration of MnO is enriched at each location of mixing zone.

3.3.2 Concentration of selected Trace and Rare Earth Elements (REEs)

3.3.2.1 Riverine Zone

Ezapur (EP)

The most abundant among trace and REEs are Ba, Zr, Cr, Sr, Ce and V. Concentration of V is depleted (EF<1) in each facie (Figure 3.9). Mean concentration of V is 64.71 ppm. It is relatively high in EPL1 and EPL3 than in other facies (Table 3.11). It has exhibited low deviation across the sediment sequences (CV=13.5%). Contrary to this, Cr is enriched (EF>1) in EPL4 and EPL6 while in EPL5 it has exhibited resistance to weathering (EF=1). In other facies it is depleted. Its average concentration is 182.57 ppm which is significantly high. It has shown moderate variation (CV=26%). Distribution of Co is depleted across the facies. Its content is higher in EPL2, EPL5 and EPL7 in comparison to other facies. Average concentration of Co is 16.29 ppm. It has exhibited low deviation across the sediment sequences (CV=7.9%). The Cu is also depleted in all the facies. The mean content of Cu is 32.86 ppm with moderate variation in sediment sequences (CV=37.5%). Concentration of Zn is also depleted at this location of palaeochannel. Average concentration of Zn is 22.72 ppm with high variability across the sediment sequences (CV=67%).

Table 3.11 Concentration of selected trace and rare earth elements (ppm) in facies of Ezapur

Elements/ Facies	V	Cr	Co	Cu	Zn	Sr	Zr	Ba	Pb	La	Ce	Nd
EPL1	72	159	16	46	60	90	381	521	16	31	90	24
EPL2	67	148	18	46	62	108	381	475	22	37	79	27
EPL3	74	156	15	37	6	132	418	522	34	44	83	34
EPL4	54	249	15	16	0	57	59	477	26	16	50	12
EPL5	69	217	17	35	9	108	271	501	13	31	63	24
EPL6	49	236	15	13	0	52	55	453	0	10	28	8
EPL7	68	113	18	37	22	31	332	444	14	40	73	32
Mean	64.7	183	16.3	32.9	22.7	82.6	271	484.7	17.9	29.9	67	23
CV (%)	13.5	26	7.9	37.5	110	41	52.4	5.9	56.2	38.9	30	39.1
TM*	97	92	17.3	28	67	320	193	624	17	31	63	27

*Terrestrial mean is based on values suggested by Rudnick and Gao (2014)

Similarly, distribution of Sr is depleted across the sediment sequences. Mean content of Sr is 82.57 ppm. It has exhibited high fluctuation across the sediment sequences (CV=320%). Contrary to this, Zr is enriched in EPL1, EPL2, EPL3 and EPL7 while in EPL4 and EPL5 it is depleted. Average availability of Zr is 271 ppm at this location which is considerably high. It has shown high variability across the facies (CV=192%). Ba is also depleted across the sediment sequences. Mean Concentration of Ba is 484 ppm with low deviation across the sediment sequences (CV=5.93%). Concentration of Pb is depleted in all the facies (EF<1). The average distribution of Pb is 17.86 ppm. It has exhibited high deviation at this site (CV=56.2%).

Average concentration of La is 29.86 ppm and it is depleted in each facie. It has shown moderate variability across the facies (CV=38.9%). The Ce is also depleted with mean content being 29.9 ppm. It has exhibited moderate variability (CV=30%) at this location. Similarly, concentration of Nd is depleted. Its average content is 23 ppm with moderate variation across the facies (CV=39.1%).

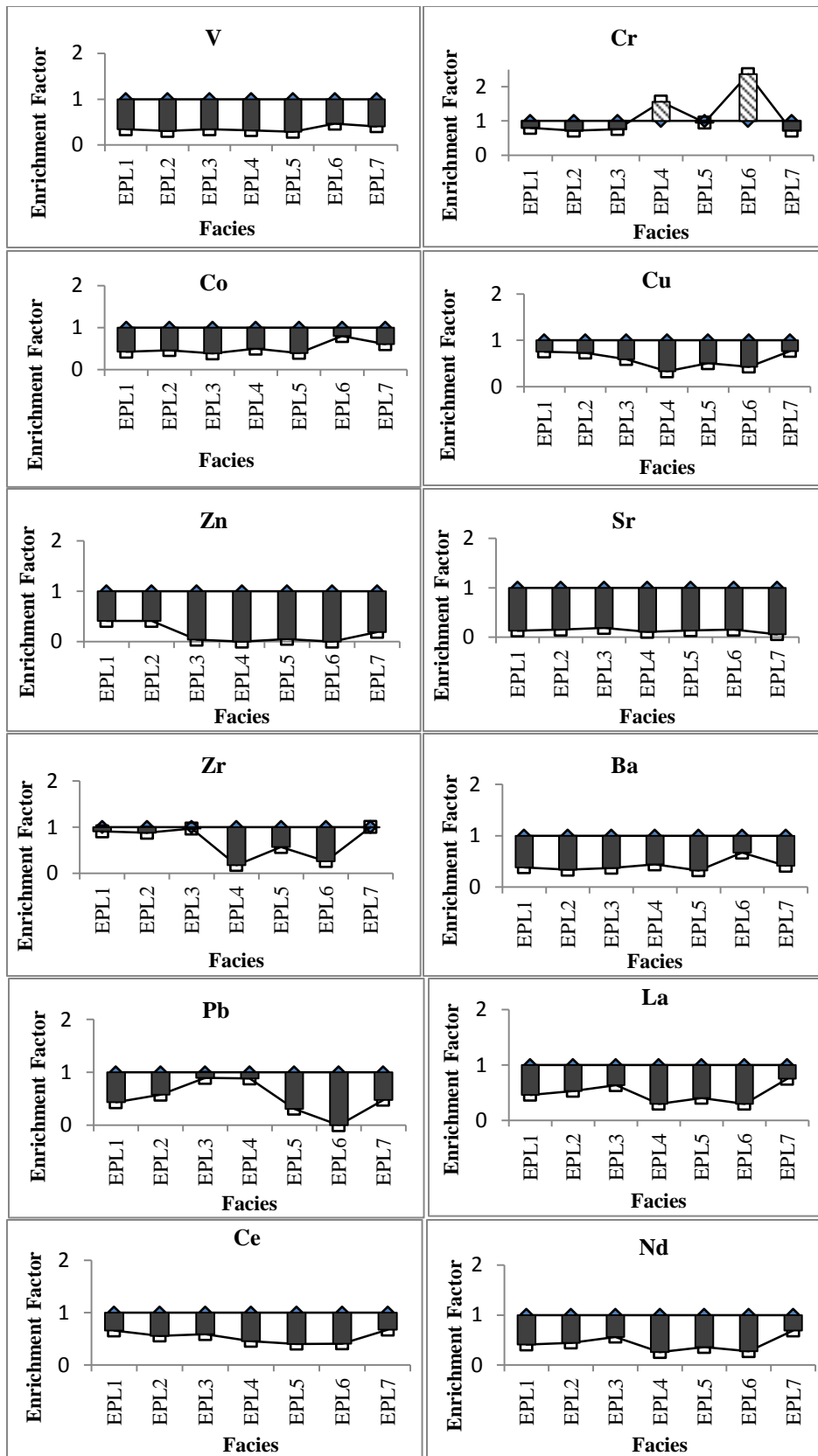


Figure 3.9 Concentration of selected trace elements and REEs in facies of Ezapur

Jhumpuri (JP)

The most abundant element at JP is Ba. The order of concentration of the trace elements and REEs is as follows- Ba > Zr > Cr > Sr > Ce > V. The concentration of V is depleted in each facie (Figure 3.10). Average distribution of V is 61.3 ppm. It has exhibited low fluctuation (CV=18.6%) across the sediment sequences. The Cr, on the other hand, is enriched in JPL4, JPL7 and JPL11 while in other facies it is depleted. Mean content of Cr is 189 ppm with low down core variability (CV=11.6%). The concentration of Co is depleted across the facies (EF<1). Its average concentration is 19.2 ppm with low variation (CV=19.7%) across the facies. The Cu is enriched in JPL4, JPL6 and JPL11 whereas in all the other facies it is depleted. Mean concentration of Cu is 44.1 ppm with moderate deviation (CV=26.6%).

Table 3.12 Concentration of selected trace and rare earth elements (ppm) in facies of Jhumpuri

Element/ Facies	V	Cr	Co	Cu	Zn	Sr	Zr	Ba	Pb	La	Ce	Nd
JPL1	70	214	23	53	66	111	333	466	27	50	84	31
JPL2	74	190	21	49	73	105	314	496	65	53	108	38
JPL3	76	185	23	56	79	107	222	497	67	49	101	39
JPL4	43	233	17	37	23	78	66	385	3	10	25	10
JPL5	63	187	25	67	103	87	172	393	92	45	84	30
JPL6	56	198	21	51	63	44	347	384	14	52	91	30
JPL7	44	192	17	30	11	7	171	324	12	38	64	19
JPL8	73	191	21	41	60	74	271	520	27	24	60	17
JPL9	68	153	14	41	7	92	250	479	0	35	60	22
JPL10	52	155	13	34	3	99	182	385	0	25	48	13
JPL11	55	177	16	26	13	52	346	386	37	20	47	15
Mean	61.3	189	19.2	44.1	45.6	77.8	243	428.6	31.3	36.5	70.2	24
CV (%)	18.6	11.6	19.7	26.6	73	39.3	35.3	14.3	94.5	38.7	34.7	40
TM*	97	92	17.3	28	67	320	193	624	17	31	63	27

*Terrestrial mean is based on values suggested by Rudnick and Gao (2014)

Zn, however, is depleted in each facie. Mean concentration of Zn is 45.6 ppm. It has shown high variability (CV=73%) across the facies. Similarly, the Sr is depleted in all the facies with mean content of 77.8 ppm. It has indicated moderate variation (CV=39.3%) at this site. The Zr is enriched in JPL6 and JPL11 while it is depleted in all the other facies. Its average distribution is markedly high, 243 ppm with moderate variability across the facies (CV=35.3%). Contrary to this, Ba is depleted in all the facies with average concentration of 428 ppm. It has shown low variability (CV=14.3%).

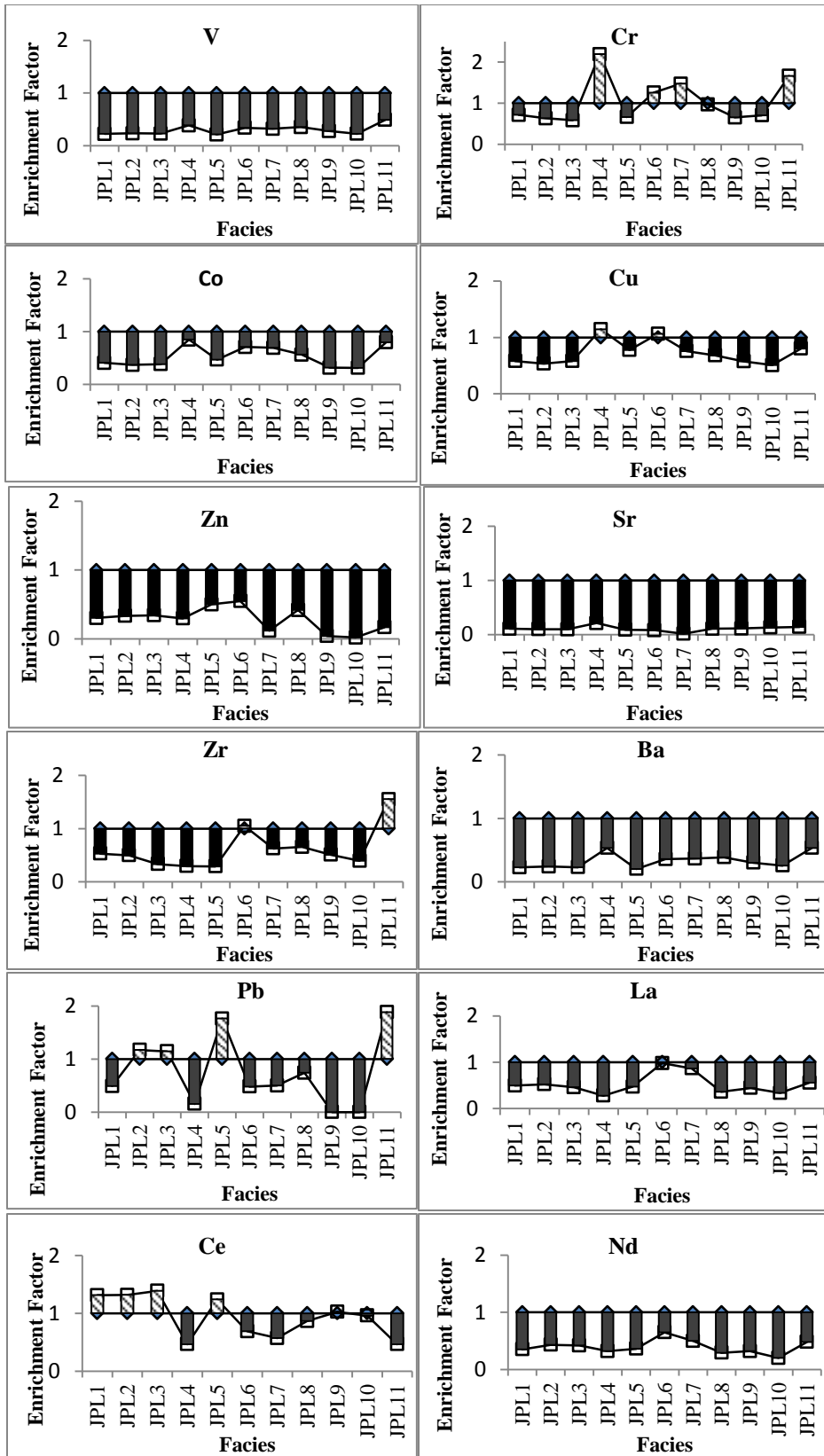


Figure 3.10 Concentration of selected trace elements and REEs in facies of Jhumpuri

At this site the distribution of Pb is enriched in JPL2, JPL3, JPL5 and JPL11. Average content of Pb is 31.3 ppm with high variability (CV=94.5%) across the sediment sequences.

Among REEs, the La is depleted in all the facies except in JPL7 where it has shown resistance. Average concentration of La is 36.5 ppm with moderate variability across the sediment sequences (CV=38.7%). Concentration of Ce is enriched in JPL1, JPL2, JPL3 and JPL5. It has shown resistance in JPL9 and JPL10. Mean concentration of Ce is 70.2 ppm with moderate variability (34.7%). In contrast, Nd is depleted in every facie. Average concentration of Nd is 24 ppm. It has exhibited moderate variability (CV=40%) at this location.

Katia I (KTI)

The most abundant element at this location is Ba followed by Zr, Cr, Sr, Ce and V (Table 3.13). The V, Cr, Co, Cu, Zn, Sr and Ba are depleted in each facie (Figure 3.11) as the EF is below 1. Average concentration of V is 72 ppm with low down core variability (CV=4.97%). Mean distribution of Cr is 169 ppm with low variation (CV=14.43%). Mean content of Co is 18.80 ppm and it has also revealed low variability across the facies (CV=14.03%). Average concentration of Cu is 43.80 ppm with low down core deviation (CV=15.17%). Mean concentration of Zn is 47 ppm. It has exhibited moderate variation (40.55%). Mean content has been 109.6 ppm. Sr has shown low deviation in KTI (CV=9.3%). The Zr, however, is enriched in KTIL1 whereas in other facies it is depleted.

Table 3.13 Concentration of selected trace and rare earth elements (ppm) in facies of Katia I

Elements/ Facies	V	Cr	Co	Cu	Zn	Sr	Zr	Ba	Pb	La	Ce	Nd
KTIL1	71	148	16	36	60	100	430	476	68	52	95	35
KTIL2	68	215	16	36	48	121	315	468	34	34	69	24
KTIL3	79	165	20	52	61	101	275	522	70	54	97	35
KTIL4	73	168	23	49	56	103	291	486	63	48	96	32
KTIL5	72	149	19	46	10	123	316	481	54	50	84	33
Mean	73	169	18.8	44	47	110	325	487	58	48	88	31.8
CV (%)	4.9	14.4	14.0	15	41	9.3	16.8	3.84	23	15	12	12.8
TM*	97	92	17.3	28	67	320	193	624	17	31	63	27

*Terrestrial mean is based on values suggested by Rudnick and Gao (2014)

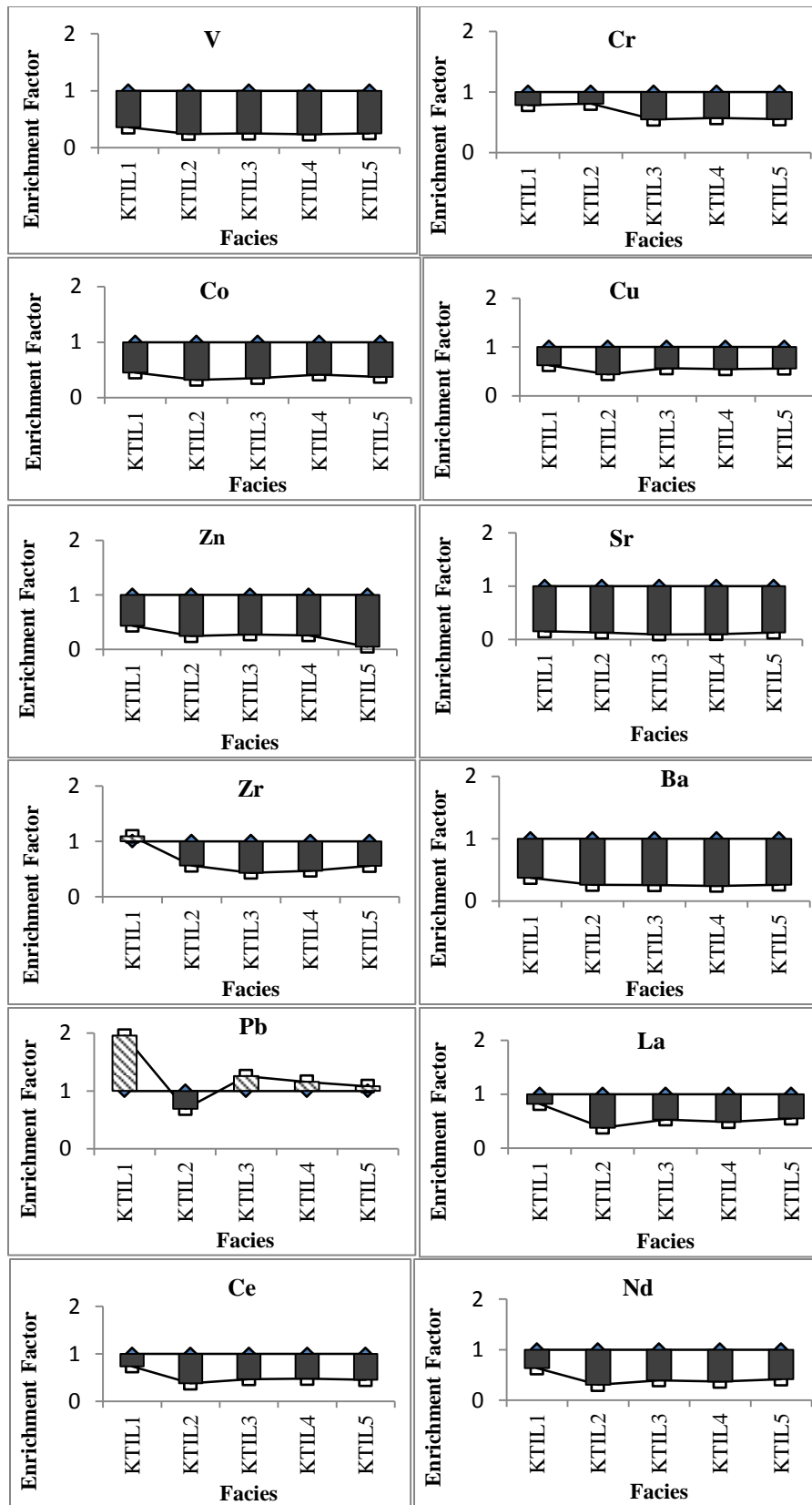


Figure 3.11 Concentration of selected trace elements and REEs in facies of Katia I

Average concentration of Zr has remained 325 ppm. The Ba is depleted across the facies. Average concentration of Ba is quite low (486 ppm) with low deviation (CV=3.84%). Concentration of Pb is enriched in most of the facies. Only in KTIL2 it is depleted. Mean content of Pb is 57.8 ppm and it has exhibited moderate variation at this site (CV=22.7%).

The REEs are also depleted in each facie of this location. Mean distribution of La is 47.6 ppm with low down core variability (CV=12%). Average content of Ce is 88.2 ppm. It has exhibited low fluctuation. Average concentration of Nd is 31.8 ppm with low vertical deviation (CV=12.8%).

Katia II (KTII)

The most abundant elements at this site are Ba, Zr, Cr, Sr, Ce and V. The concentration of V is enriched (EF>1) in KTIL1, KTIL6, KTIL7 and KTIL8 (Figure 3.12). It has remained persistent (EF=1) in KTIL2, KTIL3 and KTIL4 while it is depleted (EF<1) in KTIL9. The average content of V is 69.33 ppm (Table 3.14). It has exhibited low of variation (CV=9.6%) across the facies. The Cr has remained unchanged in KTIL3, KTIL4 and KTIL8 while in other facies it is depleted. Its mean distribution is 179 ppm with low down core deviation (CV=15.4 %). The Co, Cu, Zn, Sr, Zr and Ba are depleted in each facie. Average availability of Co is 18.6 ppm. It has shown low variability (CV=12.7%).

Table 3.14 Concentration of selected trace and rare earth elements (ppm) in facies of Katia II

Element/ Facies	V	Cr	Co	Cu	Zn	Sr	Zr	Ba	Pb	La	Ce	Nd
KTIL1	71	159	16	44	44	108	388	467	65	47	88	31
KTIL2	66	165	18	34	15	114	330	455	19	32	65	23
KTIL3	60	213	18	32	52	124	305	429	19	31	60	19
KTIL4	63	213	15	31	42	130	340	444	36	40	65	22
KTIL5	85	146	23	46	71	116	295	584	87	53	187	38
KTIL6	73	147	19	42	55	115	352	496	85	49	127	33
KTIL7	69	171	17	35	62	118	371	471	40	45	74	31
KTIL8	69	221	20	38	56	125	391	486	24	38	71	27
KTIL9	68	182	21	48	81	113	239	445	73	45	82	30
Mean	69	180	18.6	38.9	53	118	334.6	475	49.8	42.2	91	28.2
CV (%)	9.6	15.4	12.7	15.3	34	5.52	13.84	9.12	53	16.8	43	20.1
TM*	97	92	17.3	28	67	320	193	624	17	31	63	27

*Terrestrial mean is based on values suggested by Rudnick and Gao (2014)

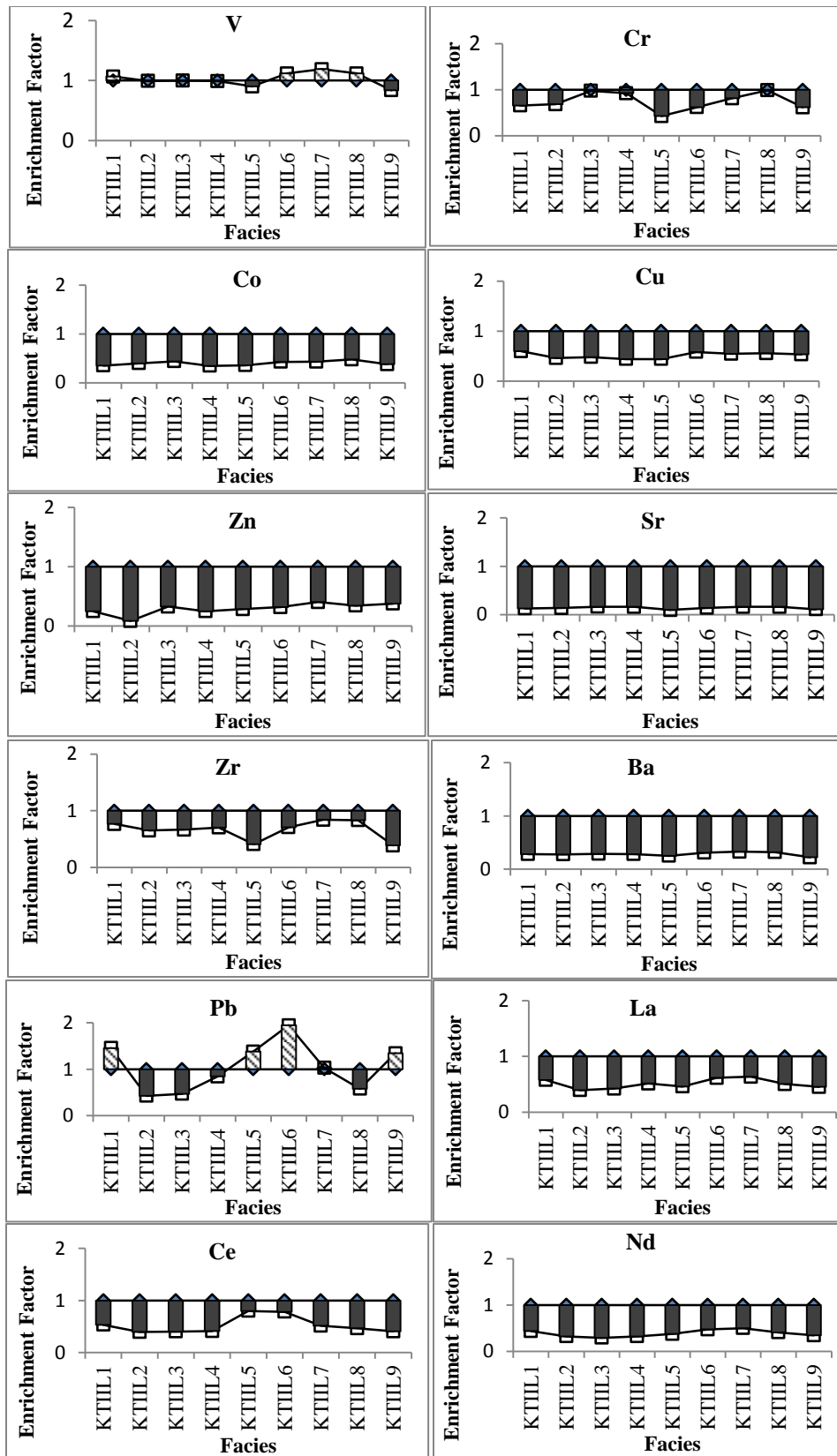


Figure 3.12 Concentration of selected trace elements and REEs in facies of Katia II

Average distribution of Cu is 38.9 ppm with low fluctuation across the facies (CV=15.3%). Mean distribution of Zn is 53.1 ppm with moderate variation (CV=33.5%). The Sr has remained around 118 ppm. It has exhibited low variability across the facies (CV=5.52%). Mean concentration of Zr is 334.6 ppm with low deviation (CV=13.8%). The average content of Ba is 475.2 ppm. It has revealed low deviation across the facies (CV=9.12%). On the contrary, Pb is enriched in KTII1, KTII5, KTII6 and KTII9. It has remained consistent in KTII7 while in other facies it is depleted. Average distribution of Pb is 49.78 ppm with high fluctuation (CV=52.9%).

Concentration of La, Ce and Nd is also depleted at KTII. The average distribution of La is 42.2 ppm with low down core variation (CV=16.8%). Overall concentration of Ce is around 91 ppm with moderate fluctuation across the sediment sequences (CV=43%). Mean concentration of Nd is 28.2 ppm. It has varied moderately at this location (20.1%).

It can be summarized that Cr, Cu, Sr, La, Ce and Nd has shown moderated variation at EP which is collected from palaeochannel. In contrast, Zn and Zr has been highly variable. The concentration of Cr is enriched in EPL4 and EPL6 while in EPL5 it has shown resistance. The Zr content has been persistent in EPL3 and EPL7. On the other hand, V, Co, Cu, Zn, Sr, Ba, Pb, La, Ce and Nd are depleted. At JP which is located in flood plain between two palaeochannels Pb has exhibited high fluctuation. Cu, Zr, La, Ce and Nd have been moderately variable. The Cr is enriched in JPL4, JPL6, JPL7 and JPL11 while depleted in other facies. The Cu is enriched in JPL4 and JPL6. The Zr is enriched in JPL6 and JPL11. In JPL2, JPL3, JPL5 and JPL11 the content of Pb is enriched. Among REEs, La is enriched in JPL6. The Ce is enriched in JPL1, JPL2, JPL3, JPL5, JPL9 and JPL10. Other trace and REES are depleted. At KTI the distribution of V, Cr, Co, Cu, Ba, La, Ce and Nd is depleted. On the contrary, Zr is enriched in KTIL1 while in KTIL1, KTIL3, KTIL4 and KTIL5 Pb is enriched. At KTII, however, V is enriched in KTII1, KTII2, KTII3, KTII4, KTII7 and KTII8. The concentration of Cr is enriched in KTII3 and KTII8 whereas Pb is enriched in KTII1, KTII5, KTII6, KTII7 and KTII9. All the other elements are depleted in this inter-channel region.

3.3.2.2 Mixing Zone

Sonpanki (SP)

The order of concentration of trace elements and REEs is Ba>Zr> Cr> Sr> Ce> V. The V is depleted (EF<1) in all the facies (Figure 3.13). Its mean concentration is 73.8 ppm. The down core variability is low for V (CV=6.14%). In contrast, the Cr is enriched in SPL6. It has shown resistance during the sedimentation of SPL5 while in other facies it is depleted. The average concentration of Cr is 159 ppm with low variation (CV=9.3%) across the sediment sequences. The Co is also depleted with average content of 23.2 ppm. Its down core deviation is also low (CV=3.23%). The Cu, however, is enriched in SPL6 whereas in other facies it is depleted. Mean distribution of Cu is 36.8 ppm. It has shown low fluctuation across the facies (CV=9.32%). The Zn, Sr and Ba are depleted in all the facies. Average concentration of Zn is 74.6 ppm with low down core variability (CV=3.85%). Mean availability of Sr is 97.6 ppm. It has exhibited low fluctuation at this location (CV=11%).

Table 3.15 Concentration of selected trace and rare earth elements (ppm) in facies of Sonpanki

Elements/	V	Cr	Co	Cu	Zn	Sr	Zr	Ba	Pb	La	Ce	Nd
SPL1	69	177	24	38	72	96	347	472	63	42	91	32
SPL2	72	134	23	39	79	116	222	470	91	50	94	33
SPL3	75	157	22	39	76	90	380	513	72	55	104	38
SPL4	71	169	24	38	75	101	362	493	64	49	95	34
SPL5	82	158	23	30	71	85	457	577	31	42	88	31
SPL6	33	218	19	37	18	56	33	326	39	7	29	6
Mean	73.8	159	23.2	36.8	74.6	97.6	353.6	505	64.2	47.6	94.4	33.6
CV (%)	6.14	9.13	3.23	9.32	3.85	11	21.5	7.8	30.2	10.5	5.71	7.19
TM*	97	92	17.3	28	67	320	193	624	17	31	63	27

*Terrestrial mean is based on values suggested by Rudnick and Gao (2014)

On the contrary, Zr is enriched in SPL5 while in other facies it is depleted. Its remains around 353.6 ppm with moderate variability (CV=21.5%). The average concentration of Ba is 505 ppm. It has shown low variability across (CV=7.8%). In contrast, the Pb is enriched in all the facies of active floodplain. The mean concentration of Pb is 64.2 ppm and it has varied moderately (CV=30.2%). The average distribution of La remains 47.6 ppm with low variation (CV=10.5%). Mean availability of Ce is 94.4 ppm. It has shown low variability (CV=5.71%). The average concentration of Nd is 33.6 ppm with low deviation (CV=7.19%) across the sediment sequences.

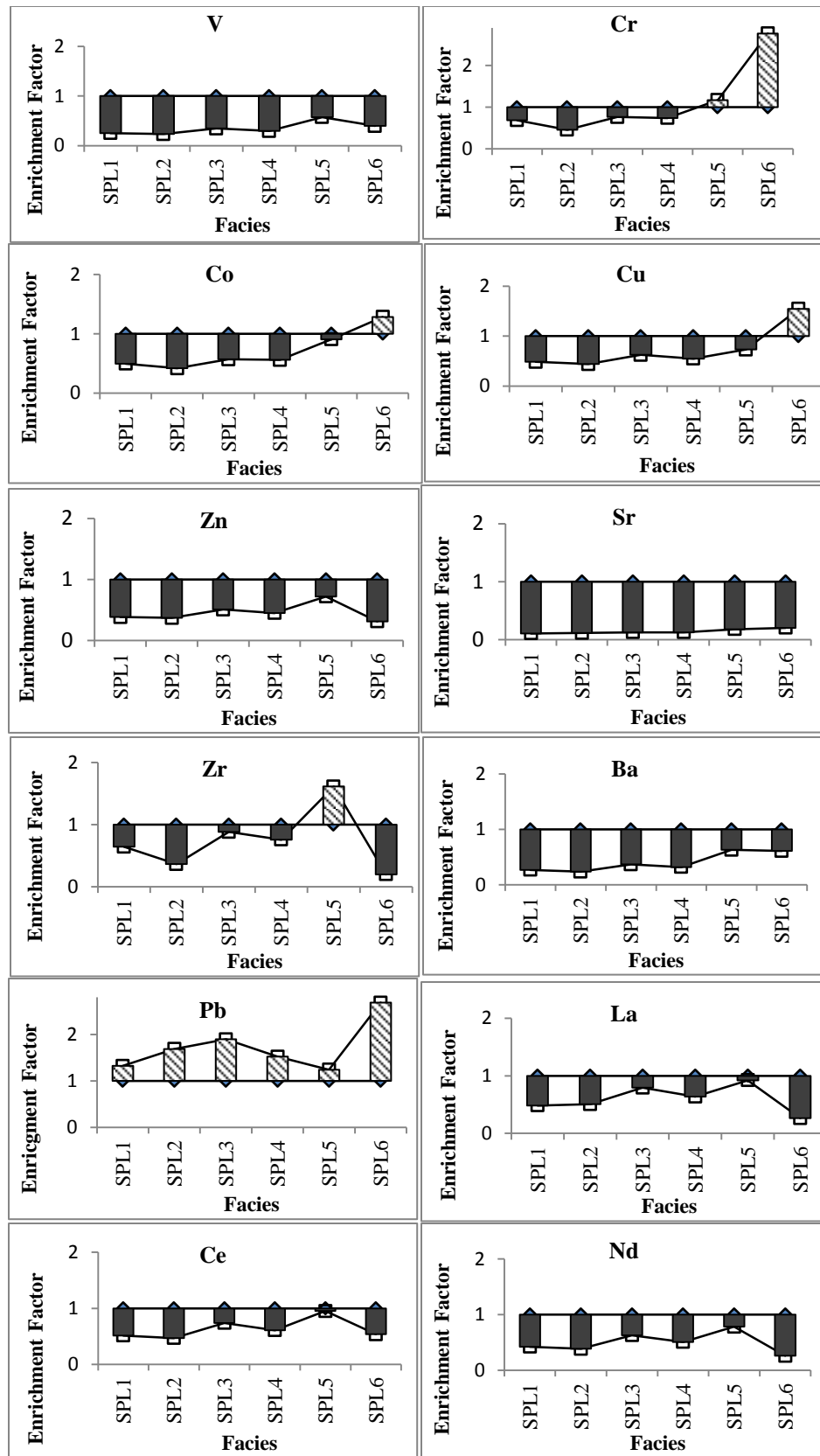


Figure 3.13 Concentration of selected trace elements and REEs in facies of Sonpanki

Chandbali (CB)

The order of occurrence of most significant elements is Ba > Zr > Cr > Sr > V and Ce. The V is enriched ($EF > 1$) in each facie of beach ridge (Figure 3.14). Its average concentration is 74.3 ppm. It has exhibited low deviation ($CV = 12.1\%$) across the facies. The Cr is enriched in CBL1, CBL3, CBL5 and CBL6 while in other facies it is depleted. Average concentration of Cr is 209.3 ppm. It has shown low down core variability ($CV = 38.5\%$). The Co is enriched in CBL3 whereas in other facies it is depleted. Mean content has remained 20.8 ppm with low variation across the facies ($CV = 11.9\%$). The Cu similarly, is enriched in CBL3 while it is depleted in other facies. Average distribution of Cu is 31.3 ppm and low variation across the sediment sequences ($CV = 18.58\%$). In contrast, the concentration of Zn and Sr is depleted in every facie of CB. Average concentration of Zn is 46.3 ppm. It has exhibited low fluctuation at this site ($CV = 36.2\%$). Mean concentration of Sr is 75.8 ppm. However, it has shown high deviation across the facies ($CV = 77.9\%$). The concentration of Zr is enriched in CBL2, CBL3 and CBL6 while it is depleted in other facies. Average distribution of Zr is 371 ppm with moderate deviation ($CV = 30.9\%$). The Ba has remained constant in CBL3 while in other facies it is depleted. Its average concentration is 558 ppm with low variability ($CV = 16.4\%$). The Pb, on the other hand, is enriched in CBL1, CBL3, CBL4 and CBL6 whereas in CBL2 and CBL5 it is depleted. Average distribution is 58.7 ppm with high variation across the facies ($CV = 82\%$).

Table 3.16 Concentration of selected trace and rare earth elements (ppm) in facies of CB

Elements/	V	Cr	Co	Cu	Zn	Sr	Zr	Ba	Pb	La	Ce	Nd
CBL1	88	368	18	21	28	59	277	723	116	17	43	15
CBL2	66	115	22	40	74	83	335	480	16	43	87	34
CBL3	68	199	20	34	40	3	604	489	29	29	66	23
CBL4	66	154	25	34	59	49	338	467	125	32	82	25
CBL5	73	240	18	29	27	196	263	574	0	20	55	20
CBL6	85	180	22	30	50	65	410	617	66	24	69	20
Mean	74.3	209.3	20.8	31.3	46.3	75.8	371.2	558.3	58.7	27.5	67	22.8
CV (%)	12.1	38.5	11.9	18.6	36.2	77.9	30.9	16.36	82	31.2	22.4	25.7
TM*	97	92	17.3	28	67	320	193	624	17	31	63	27

*Terrestrial mean is based on values suggested by Rudnick and Gao (2014)

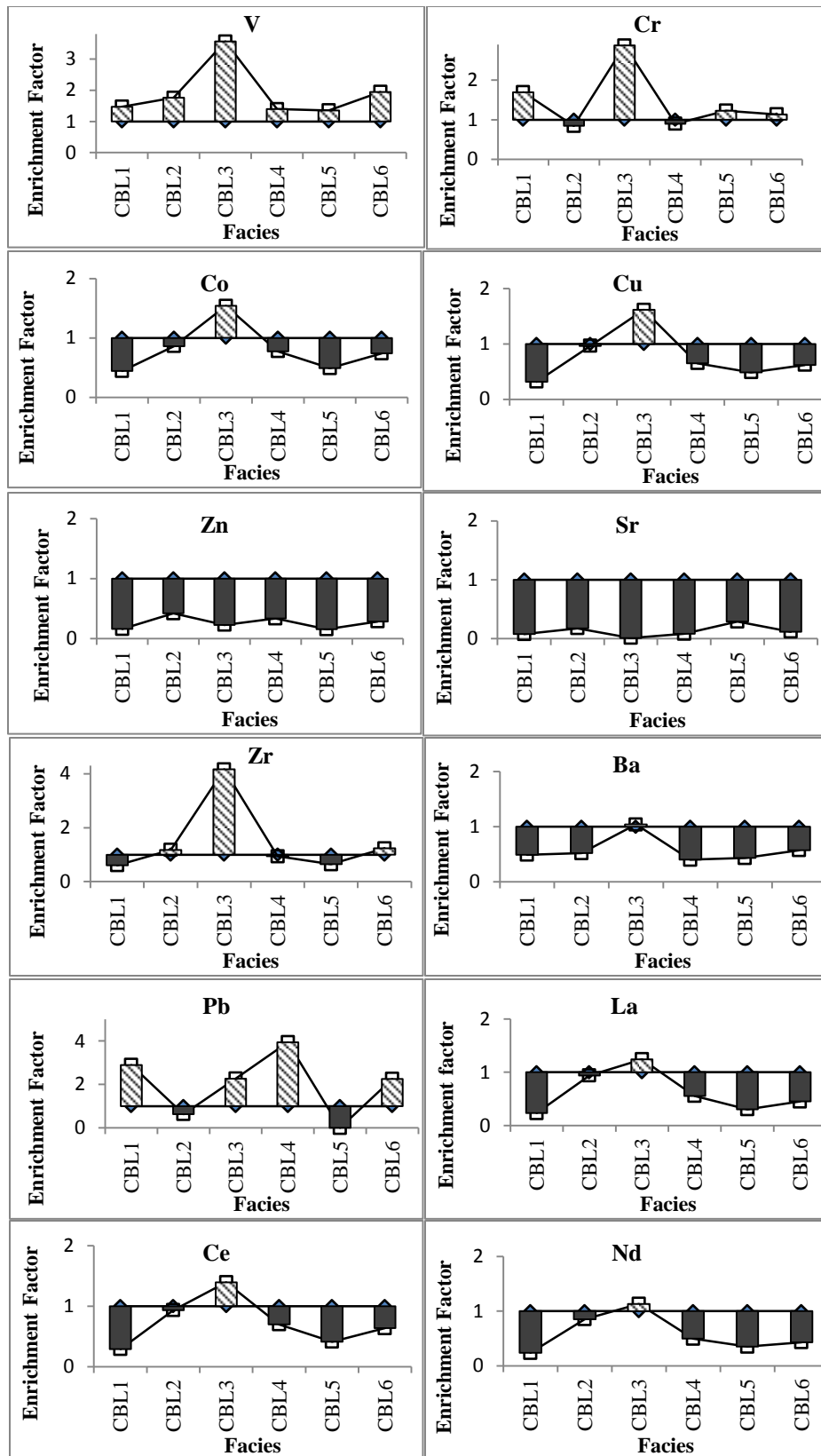


Figure 3.14 Concentration of selected trace elements and REEs in facies of Chandbali

Concentration of La is enriched in CBL3 while it is persistent in CBL2. In all the other facies it is depleted. Its average content is 27.5 ppm with moderate variability (CV=31.2%). The Ce, similarly is enriched in CBL3 whereas constant in CBL3. It is depleted in other facies. Mean distribution of Ce is 67 ppm. It varies moderately across the facies (CV=22.4%). The Nd is also enriched in CBL3 while in all the other facies it is depleted. Its mean concentration is 22.8 ppm. It has shown low down core variability (CV=25.7%).

Ambiligan (AG)

The most abundant among the trace elements and REEs are Ba, Zr, Cr, Sr, Ce, V and Pb. Concentration of V is enriched (EF>1) in each facie of this palaeochannel (Figure 3.15). Average content is 71.4 ppm with low down core variability (CV=8.24%). The Cr, however, is enriched only in AGL3 while in other facies it is depleted (CV<1). Its mean distribution is 115.2 ppm with moderate variability across the sediment sequences (CV=23.3%).

Table 3.17 Concentration of selected trace and rare earth elements (ppm) in facies of Ambiligan

Elements/	V	Cr	Co	Cu	Zn	Sr	Zr	Ba	Pb	La	Ce	Nd
AGL1	79	153	26	41	76	109	231	549	67	49	103	42
AGL2	68	92	24	49	108	105	148	459	141	50	96	36
AGL3	78	139	16	23	25	66	512	578	44	46	93	34
AGL4	67	109	20	28	34	121	273	476	48	47	93	35
AGL5	65	83	22	28	39	80	234	431	57	34	74	28
Mean	71.4	115.2	21.6	33.8	56.4	96.2	279.6	498.6	71.4	45.2	91.8	35
CV (%)	8.24	23.3	15.9	28.6	55.2	21	44.0	11.2	50	12.8	10.5	12.5
TM*	97	92	17.3	28	67	320	193	624	17	31	63	27

*Terrestrial mean is based on values suggested by Rudnick and Gao (2014)

The Co, Cu, Zn, Sr and Ba are depleted in each facie. The mean availability of Co is 21.6 ppm with low deviation (CV=15.9%). The distribution of Cu lays around 33.8 ppm. It has exhibited moderate variability across the facies (CV=28.6%). The average concentration of Zn is 56.4 ppm with high fluctuation (CV=55.2%). The mean content of Sr is 96.2 ppm. It has shown low deviation across the sediment sequences (CV=21%). The mean distribution of Ba is 498.6 ppm with low variation (CV=11.2%). The Zr is enriched in AGL3 while in other facies it is depleted. Average content of Zr is 279 ppm. It has exhibited moderate fluctuation at this site (CV=44%). The Pb, in contrast, is enriched in each facies of AG. It has shown high deviation (CV=50%).

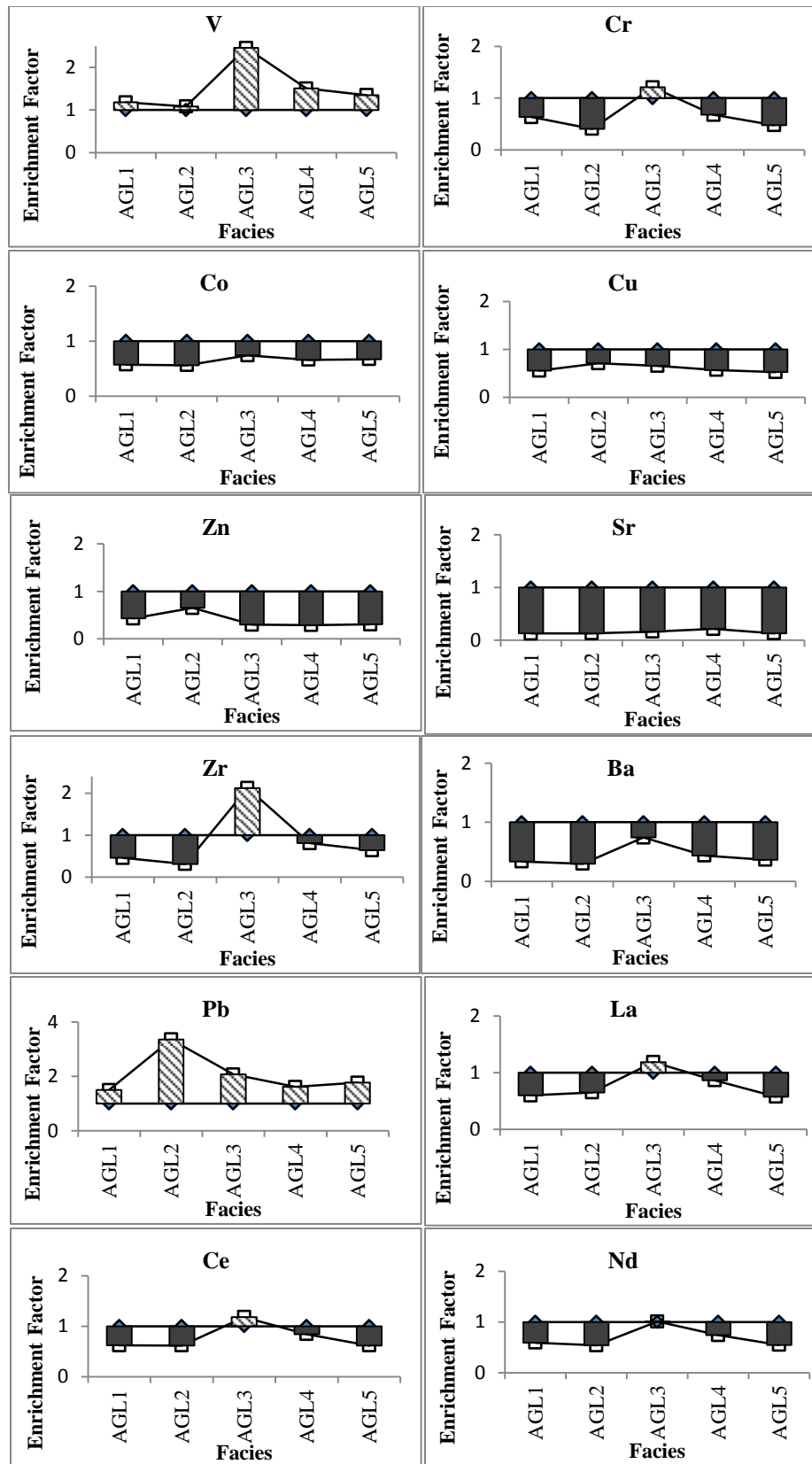


Figure 3.15 Concentration of selected trace elements and REEs in facies of Ambiligan

The La and Ce are enriched in AGL3 while these are depleted in all the other facies. Average content of La is 45.2 ppm with low deviation across the facies. Mean concentration of Ce is 91.8 ppm. It has exhibited low deviation across the sediment sequences (CV=10.5%). The Nd is constant in AGL3 whereas it is depleted in other facies. Its average concentration has remained 35 ppm with moderate down core variation (CV=12.5%).

Kasturikaran (KK)

Across the sediment sequences, the order of abundance is Ba > Zr > Cr > Sr > Ce > Zn and V. Mean distribution of V is 66.75 ppm with low variability (CV=2.7%) across the facies (Table 3.18). It is enriched (EF>1) in all the facies (Figure 3.8). The Cr is enriched in KKL3 while in other facies it is depleted. Its mean availability is 187 ppm. It has shown moderate deviation (CV=25.3%). The Co, Cu, Zn, Sr and Ba are depleted (EF<1) in each facie of this palaeochannel. The mean content of Co is 23 ppm across the facies. It has exhibited low deviation at this site (CV=6.15%). Average concentration of Cu is 35 ppm and it has exhibited low down core variability (CV=12%). Average concentration of Zn is 72.3 ppm. It has exhibited moderate variability (CV=38.7%). Average availability of Sr is 83.8 ppm. It has shown moderate variability across the facies (CV=38.8%). On the contrary, the Zr is enriched in KKL1, KKL2 and KKL4 whereas it is persistent in KKL3. The average concentration of Pb is 280 ppm with low fluctuation (CV=39.5%).

Table 3.18 Concentration of trace and rare earth elements (ppm) in facies of Kasturikaran

Elements/	V	Cr	Co	Cu	Zn	Sr	Zr	Ba	Pb	La	Ce	Nd
KKL1	68	168	23	36	98	88	345	476	27	50	95	35
KKL2	67	150	23	37	82	119	242	481	63	46	92	35
KKL3	64	268	21	28	25	31	315	488	24	32	71	26
KKL4	64	162	25	39	84	97	221	465	43	38	81	27
Mean	65.8	187	23	35	72.3	83.8	280	477.5	39.3	41.5	84.8	30.8
CV (%)	2.7	25.3	6.2	12	38.7	38.8	18.1	1.76	39.5	16.8	11.2	13.9
TM*	97	92	17.3	28	67	320	193	624	17	31	63	27

*Terrestrial mean is based on values suggested by Rudnick and Gao (2014)

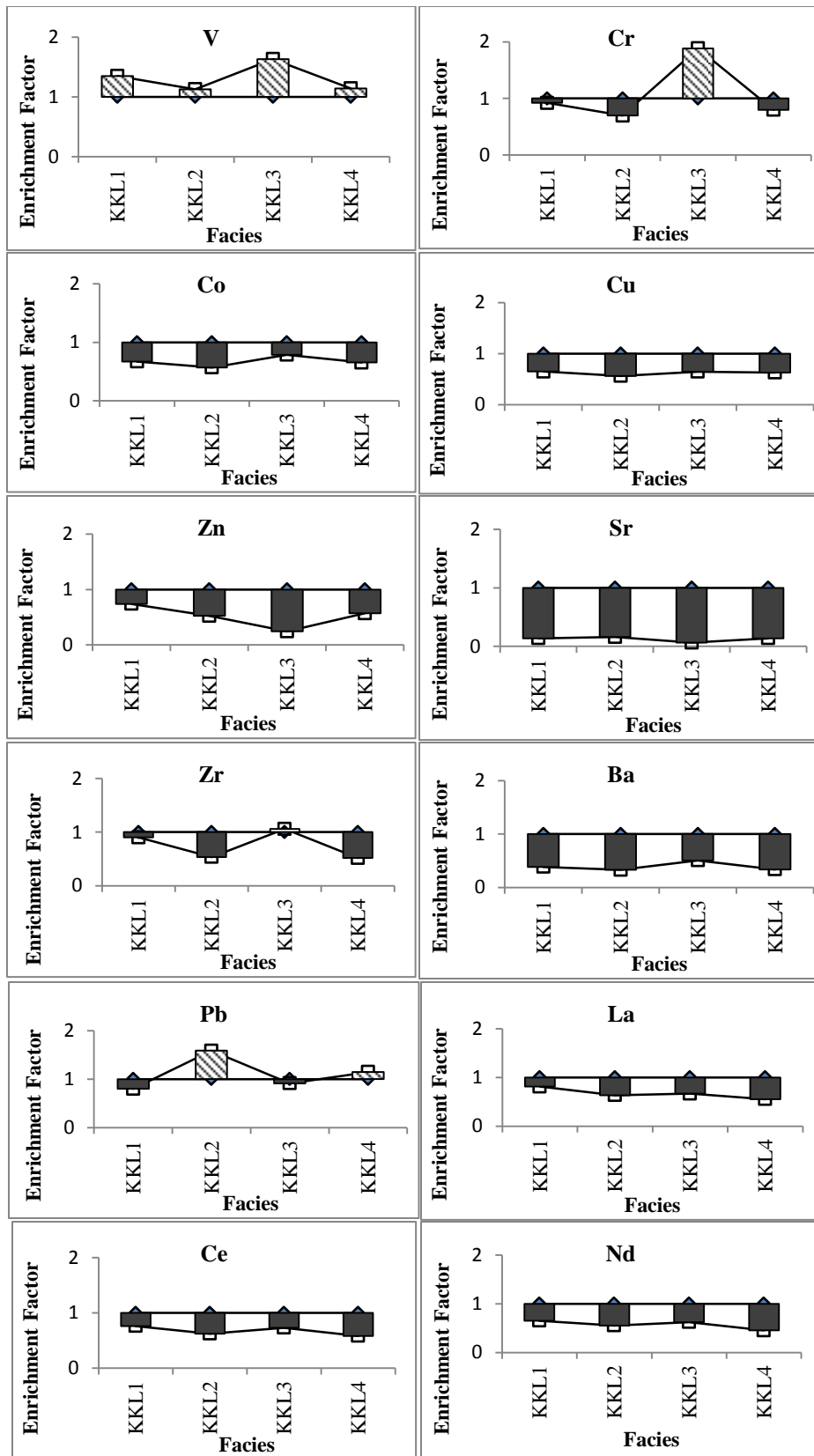


Figure 3.16 Concentration of selected trace elements and REEs in facies of Kasturikaran

The La, Ce and Nd are depleted in all the facies. The La content is has remained around 41.5 ppm. It has exhibited low deviation (CV=16.8%). Mean concentration of Ce is 84.8 ppm with low down core variability (CV=11.2%). Average content of Nd is 30.8 ppm. It has shown low deviation across the facies (CV=13.9%).

From the above analysis it is clear that in flood plain of SP the V, Zn, Sr, Ba and Nd are depleted. In contrast, the Cr is enriched in the basal facies of SPL5 and SPL6. The Co and Cu are also enriched in SPL6. The Zr is enriched in SPL5 while Pb is enriched in all the facies. The La and Ce have exhibited resistance to enrichment or depletion in SPL5. At CB site which is obtained from a beach ridge, the concentration of V, Cr, Zr and Pb is enriched in each facie. The Co, Cu, Ba and La are enriched in CBL3. At AG which is located in the palaeochannel of mixing zone, the V and Pb are enriched across the facies. In addition, the Cr, Zr, La, Ce and Nd are enriched in AGL3. Similarly, in KK which is also collected from a palaeochannel of Baitarani, the content of V and Pb is enriched in each facie while Cr and Zr in KKL3.

3.3.3 Correlation among Major Elements

3.3.3.1 Riverine Zone

Ezapur (EP)

Positively correlation of TOC was observed with Na₂O, MgO, SiO₂, K₂O, MnO and Fe₂O₃ while with Al₂O₃, P₂O₅, CaO and TiO₂ it has shown negative correlation. However, strong correlation of TOC was only recorded with P₂O₅ (Table 3.19). The Na₂O has exhibited positive correlation with MgO and K₂O. It has been negatively associated with P₂O₅, Al₂O₃, Fe₂O₃. The concentration of MgO was positively associated with SiO₂ and K₂O whereas it has negative correlation with all the other major elements. Strong negative correlation of MgO has been recorded with Al₂O₃. Down core distribution of Al₂O₃ was positively influenced by P₂O₅, CaO, TiO₂, MnO and Fe₂O₃. In contrast, it has exhibited negative correlation with Na₂O, MgO, SiO₂ and K₂O. The SiO₂ has shown positive correlation with MgO and K₂O, while with other major elements it has revealed negative connection. The P₂O₅ distribution was positively correlated with TOC, Al₂O₃, CaO, TiO₂, MnO and Fe₂O₃ whereas with other elements it was negatively correlated. The K₂O has shown positive correlation with the distribution of Na₂O₃, MgO and SiO₂ while negative correlation with

Al₂O₃, P₂O₅, CaO, TiO₂ and Fe₂O₃. The CaO content was positively correlated with Al₂O₃, P₂O₅ and TiO₂. On the contrary, it has shown negative association with Na₂O, MgO and K₂O and no correlation with other major elements. The TiO₂ has revealed positive connection with concentration of Al₂O₃, P₂O₅, CaO, MnO and Fe₂O₃ whereas negative correlation with other elements. The MnO concentration has shown positive relationship with Al₂O₃, P₂O₅, TiO₂ and Fe₂O₃. It was negatively correlated with Na₂O, MgO and SiO₂. With K₂O and CaO, it has exhibited no strong correlation. Distribution of Fe₂O₃ was positively linked with Al₂O₃, TiO₂, P₂O₅ and MnO. On the other hand, it has shown negative correlation with other elements.

Table 3.19 Correlation among TOC and major elements at Ezapur

	TOC	Na ₂ O	MgO	Al ₂ O ₃	SiO ₂	P ₂ O ₅	K ₂ O	CaO	TiO ₂	MnO	Fe ₂ O ₃
TOC	1										
Na ₂ O	0.21	1									
MgO	0.41	0.49	1								
Al ₂ O ₃	-0.41	-0.48	-1.00	1							
SiO ₂	0.21	-0.20	0.74	-0.75	1						
P ₂ O ₅	-0.53	-0.58	-0.96	0.96	-0.61	1					
K ₂ O	0.09	0.44	0.52	-0.51	0.27	-0.63	1				
CaO	-0.12	-0.45	-0.44	0.42	-0.19	0.56	-0.99	1			
TiO ₂	-0.34	-0.47	-0.93	0.93	-0.69	0.94	-0.79	0.72	1		
MnO	0.22	-0.43	-0.59	0.59	-0.30	0.46	-0.02	-0.10	0.41	1	
Fe ₂ O ₃	0.08	-0.49	-0.82	0.82	-0.53	0.71	-0.31	0.19	0.70	0.93	1

Jhumpuri (JP)

In this sample as well, no strong correlation was observed between TOC and major elements (Table 3.20). The distribution of Na₂O was positively correlated with MgO and SiO₂ while negative correlation was detected with Al₂O₃, TiO₂, MnO and Fe₂O₃. However, it has shown strong correlation only with TiO₂. The MgO was positively correlated with Na₂O, SiO₂ and K₂O while with Al₂O₃, P₂O₅ and TiO₂ it has exhibited negative relationship. With Al₂O₃ and MgO it has shown strong negative correlation. The Al₂O₃ was negatively correlated with most of the major elements such as MgO, SiO₂ and K₂O while with P₂O₅ and TiO₂ it has shown positive correlation. The concentration of SiO₂ was positively associated with Na₂O and MgO. In contrast, it has exhibited negative correlation with Al₂O₃, TiO₂, MnO and Fe₂O₃. The P₂O₅ has exhibited positive connection with the distribution of Al₂O₃, CaO and TiO₂ whereas negative correlation with MgO and K₂O. The concentration of K₂O has shown

positive correlation with MgO whereas with Al₂O₃, P₂O₅, CaO, TiO₂, MnO and Fe₂O₃ it was negatively correlated. The CaO was positively linked with P₂O₅ and TiO₂. Contrary, to this, it has shown negative correlation with the distribution of K₂O. With other elements no correlation was observed. The content of TiO₂ has revealed positive association with Al₂O₃, P₂O₅, CaO, MnO and Fe₂O₃ while with Na₂O, MgO, SiO₂ and K₂O negative correlation was found. The MnO concentration has been positively association with TiO₂ and Fe₂O₃. It was, on the other hand, negatively correlated with Na₂O, SiO₂ and K₂O. With other elements it has shown no strong correlation. The distribution of Fe₂O₃ has shown positive influence of TiO₂ and MnO whereas with Na₂O, SiO₂ and K₂O negative correlation has been observed.

Table 3.20 Correlation among TOC and major elements at Jhumpuri

	TOC	Na ₂ O	MgO	Al ₂ O ₃	SiO ₂	P ₂ O ₅	K ₂ O	CaO	TiO ₂	MnO	Fe ₂ O ₃
TOC	1										
Na ₂ O	0.15	1									
MgO	-0.21	0.24	1								
Al ₂ O ₃	0.18	-0.22	-1.00	1							
SiO ₂	-0.05	0.37	0.78	-0.77	1						
P ₂ O ₅	-0.22	-0.18	-0.22	0.20	0.11	1					
K ₂ O	-0.36	-0.05	0.28	-0.23	0.18	-0.54	1				
CaO	0.43	0.04	0.04	-0.09	0.02	0.37	-0.85	1			
TiO ₂	-0.01	-0.49	-0.37	0.31	-0.43	0.59	-0.71	0.50	1		
MnO	-0.14	-0.44	-0.11	0.06	-0.43	0.15	-0.33	0.14	0.78	1	
Fe ₂ O ₃	-0.15	-0.44	-0.13	0.07	-0.45	0.17	-0.37	0.18	0.79	1.00	1

Katia I (KTI)

The distribution of TOC was positively associated with MgO, SiO₂, P₂O₅, CaO and TiO₂ whereas with Na₂O, Al₂O₃, K₂O, MnO and Fe₂O₃, it has shown negative correlation (Table 3.21). The Na₂O has exhibited positive correlation with Al₂O₃, K₂O, MnO and Fe₂O₃ while with MgO, SiO₂, P₂O₅, CaO and TiO₂ negative correlation has been observed. The concentration of MgO was positively linked with SiO₂, P₂O₅, CaO and TiO₂. It has exhibited negative correlation with Na₂O, Al₂O₃, K₂O, MnO and Fe₂O₃. MgO has shown strong negative correlation with Al₂O₃ and MnO. The Al₂O₃ content was positively influenced by the distribution of Na₂O, K₂O, MnO and Fe₂O₃ while negative correlation was observed with MgO, SiO₂, P₂O₅, CaO and TiO₂. The SiO₂ has illustrated positive correlation with MgO, P₂O₅ and CaO. In contrast, it was negatively correlated with Na₂O, Al₂O₃, K₂O, MnO

and Fe₂O₃. The TiO₂ was positively associated with the concentration of MgO, MnO and Fe₂O₃ whereas with Na₂O, Al₂O₃, P₂O₅ and K₂O negative correlation exists. The MnO exposes positive correlation with Na₂O, Al₂O₃, K₂O, TiO₂ and Fe₂O₃. It has shown negative correlation with the distribution of MgO, SiO₂, P₂O₅ and CaO. The distribution of Fe₂O₃ was positively linked with Na₂O, Al₂O₃, K₂O, TiO₂ and MnO whereas negative correlation has been marked with MgO, SiO₂, P₂O₅ and CaO.

Table 3.21 Correlation among TOC and major elements at Katia I

	TOC	Na ₂ O	MgO	Al ₂ O ₃	SiO ₂	P ₂ O ₅	K ₂ O	CaO	TiO ₂	MnO	Fe ₂ O ₃
TOC	1										
Na ₂ O	-0.90	1									
MgO	0.56	-0.43	1								
Al ₂ O ₃	-0.57	0.44	-1.00	1							
SiO ₂	0.70	-0.57	0.96	-0.96	1						
P ₂ O ₅	0.51	-0.37	0.69	-0.67	0.83	1					
K ₂ O	-0.87	0.57	-0.59	0.60	-0.72	-0.62	1				
CaO	0.69	-0.47	0.26	-0.25	0.49	0.72	-0.82	1			
TiO ₂	0.44	-0.31	0.24	-0.27	0.13	-0.37	-0.40	-0.12	1		
MnO	-0.49	0.31	-0.74	0.72	-0.85	-0.99	0.65	-0.70	0.30	1	
Fe ₂ O ₃	-0.42	0.30	-0.68	0.66	-0.80	-0.99	0.53	-0.65	0.45	0.98	1

Katia II (KTII)

Concentration of TOC has shown positive correlation with Al₂O₃, CaO, TiO₂, MnO and Fe₂O₃ whereas negative correlation has been marked with Na₂O, MgO, SiO₂ and K₂O (Table 3.22). The Na₂O has exhibited positive correlation with MgO, SiO₂, P₂O₅ and K₂O. Contrary to this, it was negatively correlated with Al₂O₃, CaO, TiO₂, MnO and Fe₂O₃. Concentration of MgO was positively associated with Na₂O, SiO₂ and CaO while with Al₂O₃, MnO and Fe₂O₃, it has shown negative correlation. Contrary to the previous samples, the distribution of Al₂O₃ has exhibited positive correlation with TOC along with MnO and Fe₂O₃ while negative correlation has been observed with Na₂O, MgO, SiO₂ and CaO. The concentration of SiO₂ was positively correlated with Na₂O, MgO and P₂O₅. It has shown negative correlation with Al₂O₃, MnO and Fe₂O₃ whereas with other major elements no significant correlation was found. The P₂O₅ was positively correlated with Na₂O, SiO₂ and K₂O. It has revealed negative correlation with CaO, MnO and Fe₂O₃; however, with other elements there was no significant correlation. The distribution of K₂O has exhibited positive correlation with Na₂O and P₂O₅ whereas with CaO, TiO₂, MnO and Fe₂O₃, it was negatively

correlated. The CaO distribution was positively correlated with MgO, TiO₂, MnO and Fe₂O₃. It has shown negative correlation with Na₂O, Al₂O₃, P₂O₅ and K₂O. Concentration of TiO₂ has revealed positive influence of CaO, MnO and Fe₂O₃. Contrary to this, Na₂O and K₂O have negative influence on TiO₂ distribution. There has been no significant influence of other major element. The MnO content was positively correlated with Al₂O₃, CaO, TiO₂ and Fe₂O₃ whereas negative correlation was observed with Na₂O, MgO, SiO₂, P₂O₅ and K₂O. The distribution of Fe₂O₃ has exhibited positive correlation with Al₂O₃, CaO, TiO₂ and MnO. It has shown negative correlation with Na₂O, MgO, SiO₂, P₂O₅ and K₂O.

Table 3.22 Correlation among TOC and major elements at Katia II

	TOC	Na ₂ O	MgO	Al ₂ O ₃	SiO ₂	P ₂ O ₅	K ₂ O	CaO	TiO ₂	MnO	Fe ₂ O ₃
TOC	1										
Na ₂ O	-0.27	1									
MgO	-0.54	0.41	1								
Al ₂ O ₃	0.53	-0.40	-1.00	1							
SiO ₂	-0.43	0.66	0.87	-0.87	1						
P ₂ O ₅	0.03	0.41	-0.10	0.10	0.37	1					
K ₂ O	-0.33	0.37	-0.11	0.14	-0.06	0.22	1				
CaO	0.20	-0.25	0.20	-0.23	0.11	-0.33	-0.97	1			
TiO ₂	0.47	-0.54	-0.16	0.13	-0.16	-0.13	-0.93	0.84	1		
MnO	0.40	-0.54	-0.33	0.31	-0.57	-0.63	-0.60	0.64	0.64	1	
Fe ₂ O ₃	0.37	-0.60	-0.25	0.23	-0.51	-0.66	-0.70	0.72	0.72	0.98	1

3.3.3.2 Mixing Zone

Sonpanki (SP)

The concentration of TOC has been positively correlated with Al₂O₃, P₂O₅, CaO, TiO₂, MnO and Fe₂O₃ whereas with Na₂O, MgO, SiO₂ and K₂O, it has shown negative correlation (Table 3.23). The Na₂O distribution has exhibited positive correlation with MgO, SiO₂ and K₂O while with Al₂O₃, P₂O₅, CaO, TiO₂, MnO and Fe₂O₃ negative correlation has been observed. The MgO was positively associated with Na₂O, SiO₂, and K₂O. In contrast, it has shown negative correlation with Al₂O₃, P₂O₅, CaO, TiO₂, MnO and Fe₂O₃. Content of Al₂O₃ was positively connected with P₂O₅, CaO, TiO₂, MnO and Fe₂O₃ whereas negatively correlated with Na₂O, MgO, SiO₂ and K₂O. The SiO₂ has shown positive association with Na₂O, MgO and K₂O. Negative correlation of SiO₂ has been marked with Al₂O₃, P₂O₅, CaO, TiO₂, MnO and Fe₂O₃. The content of P₂O₅ has shown positive relationship with Al₂O₃, CaO, TiO₂, MnO and Fe₂O₃. It was negatively correlated with Na₂O, MgO, SiO₂ and K₂O.

The K₂O has exhibited positive association with Na₂O, MgO and SiO₂ while negative correlation with Al₂O₃, P₂O₅, CaO, TiO₂, MnO and Fe₂O₃. The CaO has shown positive influence with the concentration of Al₂O₃, P₂O₅, CaO, MnO and Fe₂O₃. In contrast, it has negative relationship with Na₂O, MgO, SiO₂ and K₂O. The TiO₂ was positively correlated with Al₂O₃, P₂O₅, CaO, MnO and Fe₂O₃ while negative correlation with Na₂O, MgO, SiO₂ and K₂O has been observed. The concentration of MnO has shown positive influence of Al₂O₃, P₂O₅, CaO, TiO₂ and Fe₂O₃ whereas it was negatively correlated with Na₂O, MgO, SiO₂ and K₂O. The Fe₂O₃ distribution has shown positive association with Al₂O₃, P₂O₅, CaO, TiO₂ and MnO while it has negative influence of Na₂O, MgO, SiO₂ and K₂O.

Table 3.23 Correlation among TOC and major elements at Sonpanki

	TOC	Na ₂ O	MgO	Al ₂ O ₃	SiO ₂	P ₂ O ₅	K ₂ O	CaO	TiO ₂	MnO	Fe ₂ O ₃
TOC	1										
Na ₂ O	-0.80	1									
MgO	-0.32	0.61	1								
Al ₂ O ₃	0.31	-0.61	-1.00	1							
SiO ₂	-0.23	0.62	0.98	-0.98	1						
P ₂ O ₅	0.39	-0.45	-0.71	0.71	-0.60	1					
K ₂ O	-0.70	0.93	0.80	-0.79	0.78	-0.66	1				
CaO	0.82	-0.85	-0.31	0.30	-0.30	0.22	-0.79	1			
TiO ₂	0.29	-0.61	-0.96	0.95	-0.93	0.84	-0.81	0.28	1		
MnO	0.37	-0.84	-0.68	0.68	-0.78	0.26	-0.82	0.64	0.65	1	
Fe ₂ O ₃	0.29	-0.78	-0.76	0.76	-0.86	0.31	-0.81	0.55	0.72	0.99	1

Chandbali (CB)

The TOC concentration has been positively associated with Na₂O, Al₂O₃ and P₂O₅ whereas it has negative correlation with MgO, SiO₂, K₂O, CaO, MnO and Fe₂O₃ (Table 3.24). The distribution of Na₂O has shown positive correlation with MgO and CaO, whereas with Al₂O₃ and K₂O it has negative correlation. The MgO has exhibited positive correlation with Na₂O, SiO₂, CaO, MnO and Fe₂O₃. In contrast, it negative correlation with Al₂O₃, P₂O₅ and TiO₂ has been marked. With other major elements there has been no significant correlation. The distribution of Al₂O₃ was positively correlated with P₂O₅ and TiO₂ while with Na₂O, MgO, SiO₂, CaO, MnO and Fe₂O₃, it has negative association. The concentration of SiO₂ has exhibited positive correlation with MgO, P₂O₅ and TiO₂. On the contrary, it was negatively correlated with the distribution of Al₂O₃, P₂O₅ and TiO₂. However; with other

major elements no significant correlation has been observed. The P_2O_5 was positively correlated with all the terrestrial elements i.e. Al_2O_3 and TiO_2 whereas with MgO , SiO_2 , K_2O , CaO , MnO and Fe_2O_3 , it was negatively correlated. The distribution of K_2O has revealed positive association with elements like MnO and Fe_2O_3 while with Na_2O , P_2O_5 , CaO and TiO_2 , negative correlation has been detected. The down core variability of CaO has shown positive association with of Na_2O , MgO , SiO_2 and MnO . In contrast, the Al_2O_3 , P_2O_5 , K_2O and TiO_2 have negative influence on the distribution of CaO . The TiO_2 concentration has shown positive influence of Al_2O_3 and P_2O_5 whereas the elements such as MgO , SiO_2 , K_2O , CaO , MnO and Fe_2O_3 have negative effect. The MnO was positively correlated with MgO , K_2O , CaO and Fe_2O_3 . It has exhibited negative effect of changes in concentration of Al_2O_3 , P_2O_5 and TiO_2 . The concentration of MgO , K_2O and MnO has positive influenced on Fe_2O_3 while TOC , Al_2O_3 , P_2O_5 and TiO_2 has negative effect on the distribution of Fe_2O_3 at this location.

Table 3.24 Correlation among TOC and major elements at Chandbali

	TOC	Na ₂ O	MgO	Al ₂ O ₃	SiO ₂	P ₂ O ₅	K ₂ O	CaO	TiO ₂	MnO	Fe ₂ O ₃
TOC	1										
Na ₂ O	0.29	1									
MgO	-0.37	0.38	1								
Al ₂ O ₃	0.36	-0.41	-1.00	1							
SiO ₂	-0.07	-0.06	0.70	-0.71	1						
P ₂ O ₅	0.90	0.19	-0.67	0.65	-0.33	1					
K ₂ O	-0.53	-0.80	0.02	0.04	0.14	-0.52	1				
CaO	-0.07	0.80	0.80	-0.83	0.47	-0.25	-0.55	1			
TiO ₂	0.33	0.12	-0.79	0.75	-0.70	0.66	-0.53	-0.30	1		
MnO	-0.70	0.02	0.61	-0.55	0.09	-0.82	0.55	0.22	-0.69	1	
Fe ₂ O ₃	-0.88	-0.09	0.55	-0.51	0.05	-0.93	0.55	0.17	-0.57	0.95	1

Ambiligan (AG)

The distribution of TOC has been positively associated with enrichment and depletion of MgO , SiO_2 and CaO while it has been negatively correlated with Al_2O_3 , K_2O , TiO_2 , MnO and Fe_2O_3 (Table 3.25). The Na_2O has shown positive correlation with MgO , SiO_2 , P_2O_5 and CaO . It was negatively correlated with Al_2O_3 , K_2O , TiO_2 , MnO and Fe_2O_3 . The distribution of MgO has exhibited positive influence of Na_2O , SiO_2 , P_2O_5 and CaO whereas with Al_2O_3 , K_2O , TiO_2 , MnO and Fe_2O_3 it has shown negative correlation. The Al_2O_3 was positively

correlated with K₂O, TiO₂, MnO and Fe₂O₃; however, with Na₂O, MgO, SiO₂, P₂O₅ and CaO it has negative correlation. Concentration of SiO₂ was positively associated with the distribution of Na₂O, and MgO whereas it has negative correlation with Al₂O₃, K₂O, TiO₂, MnO and Fe₂O₃. P₂O₅ has shown positive correlation with the concentration of Na₂O, MgO, SiO₂ and CaO. In contrast, it has exhibited negative correlation with Al₂O₃, K₂O, TiO₂, MnO and Fe₂O₃. The K₂O was positively correlated with Al₂O₃, TiO₂, MnO and Fe₂O₃ while with other elements negative correlation has been observed. The CaO content was influenced positively with changes in the concentration of Na₂O, MgO, SiO₂ and P₂O₅. Contrary to this, Al₂O₃, K₂O, TiO₂, MnO and Fe₂O₃ have negatively influenced the distribution of CaO at AG. The distribution of TiO₂ has exhibited positive connection with Al₂O₃, K₂O, MnO and Fe₂O₃ while it was negatively correlated with other major elements. The MnO has shown positive correlation with Al₂O₃, K₂O and TiO₂ whereas with Na₂O, MgO, SiO₂, P₂O₅ and CaO, negative relationship has been marked. The concentration of Fe₂O₃ has exhibited positive influence of Al₂O₃, K₂O, TiO₂ and MnO whereas it has negative correlation with Na₂O, MgO, SiO₂, P₂O₅ and CaO.

Table 3.25 Correlation among TOC and major elements at Ambiligan

	TOC	Na ₂ O	MgO	Al ₂ O ₃	SiO ₂	P ₂ O ₅	K ₂ O	CaO	TiO ₂	MnO	Fe ₂ O ₃
TOC	1										
Na ₂ O	0.15	1									
MgO	<i>0.52</i>	<i>0.86</i>	1								
Al ₂ O ₃	<i>-0.54</i>	<i>-0.85</i>	<i>-1.00</i>	1							
SiO ₂	0.44	<i>0.87</i>	<i>0.99</i>	<i>-0.99</i>	1						
P ₂ O ₅	0.06	<i>0.88</i>	<i>0.86</i>	<i>-0.85</i>	<i>0.90</i>	1					
K ₂ O	-0.29	<i>-0.82</i>	<i>-0.62</i>	<i>0.62</i>	<i>-0.57</i>	-0.45	1				
CaO	<i>0.52</i>	<i>0.85</i>	<i>0.79</i>	<i>-0.80</i>	<i>0.73</i>	<i>0.55</i>	<i>-0.95</i>	1			
TiO ₂	<i>-0.80</i>	-0.41	<i>-0.56</i>	<i>0.58</i>	<i>-0.50</i>	-0.28	<i>0.53</i>	<i>-0.69</i>	1		
MnO	-0.38	<i>-0.94</i>	<i>-0.86</i>	<i>0.87</i>	<i>-0.84</i>	<i>-0.79</i>	<i>0.86</i>	<i>-0.92</i>	<i>0.69</i>	1	
Fe ₂ O ₃	-0.38	<i>-0.94</i>	<i>-0.90</i>	<i>0.90</i>	<i>-0.88</i>	<i>-0.84</i>	<i>0.80</i>	<i>-0.88</i>	<i>0.68</i>	<i>0.99</i>	1

Kasturikaran (KK)

The TOC concentration has shown positive influence of Al₂O₃, TiO₂, MnO and Fe₂O₃ (Table 3.26). It has shown negative correlation with Na₂O, MgO, SiO₂, P₂O₅ and CaO. The Na₂O content has exhibited positive correlation with MgO, P₂O₅ and CaO whereas it was negatively correlated with Na₂O, Al₂O₃, K₂O, TiO₂, MnO and Fe₂O₃. The MgO has shown

positive association with Na₂O, SiO₂ and CaO while it has negative correlation with Al₂O₃, K₂O, TiO₂, MnO and Fe₂O₃. The Al₂O₃ was positively affected by the enrichment and depletion of K₂O, TiO₂, MnO and Fe₂O₃ while with other major elements it has shown negative correlation. The concentration of SiO₂ was positively correlated with Na₂O, MgO, P₂O₅ and CaO. It has exhibited negative association with Al₂O₃, K₂O, TiO₂, MnO and Fe₂O₃. The distribution of P₂O₅ was positively associated with SiO₂ and TiO₂. In contrast, negative correlation has been observed with MnO and Fe₂O₃. The K₂O content has shown positive relationship with Al₂O₃, TiO₂, MnO and Fe₂O₃ while with other elements it was negatively correlated. Concentration of CaO has exhibited positive influence of Na₂O, MgO and SiO₂. Contrary to this, it has shown negative correlation with all the other major elements. The TiO₂ was positively correlated with Al₂O₃, P₂O₅, K₂O and Fe₂O₃, while it has exhibited negative correlation with other elements. The MnO distribution has revealed positive influence of Al₂O₃, K₂O and Fe₂O₃ while with Na₂O, MgO, SiO₂, P₂O₅ and CaO negative association has been marked. Similarly, The Fe₂O₃ was positively correlated with Al₂O₃, K₂O, TiO₂ and MnO. On the other hand, it has shown negative correlation with Na₂O, MgO, SiO₂, P₂O₅ and CaO.

Table 3.26 Correlation among TOC and major elements at Kasturikaran

	TOC	Na ₂ O	MgO	Al ₂ O ₃	SiO ₂	P ₂ O ₅	K ₂ O	CaO	TiO ₂	MnO	Fe ₂ O ₃
TOC	1										
Na ₂ O	<i>-0.85</i>	1									
MgO	<i>-0.77</i>	<i>0.96</i>	1								
Al ₂ O ₃	<i>0.75</i>	<i>-0.96</i>	<i>-1.00</i>	1							
SiO ₂	<i>-0.87</i>	<i>0.99</i>	<i>0.98</i>	<i>-0.98</i>	1						
P ₂ O ₅	<i>-0.65</i>	0.17	0.13	-0.09	0.24	1					
K ₂ O	<i>0.74</i>	<i>-0.94</i>	<i>-1.00</i>	<i>1.00</i>	<i>-0.96</i>	-0.12	1				
CaO	<i>-0.76</i>	<i>0.97</i>	<i>1.00</i>	<i>-1.00</i>	<i>0.98</i>	0.09	<i>-0.99</i>	1			
TiO ₂	0.47	<i>-0.84</i>	<i>-0.77</i>	<i>0.80</i>	<i>-0.78</i>	0.36	<i>0.74</i>	<i>-0.82</i>	1		
MnO	<i>0.81</i>	-0.38	-0.27	0.24	-0.41	<i>-0.95</i>	0.24	-0.25	-0.10	1	
Fe ₂ O ₃	<i>1.00</i>	<i>-0.85</i>	<i>-0.75</i>	<i>0.73</i>	<i>-0.86</i>	<i>-0.62</i>	<i>0.71</i>	<i>-0.75</i>	<i>0.51</i>	<i>0.80</i>	1

3.3.3 Correlation among Trace Elements and REEs

3.3.4.1 Riverine Zone

Ezapur (EP)

The distribution of most of the elements such as V, Cu, Zn, Sr, Zr, La, Ce and Nd has shown positive correlation with each other (Table 3.27). In contrast, the concentration of Cr was negatively correlated with most of the trace elements and REEs. However, no significant correlation of Cr has been observed with Sr and Ba. Similarly, the Co was positively influenced by the concentration of most of the elements though with Sr and Pb it has shown no correlation.

Table 3.27 Correlation among trace elements and REEs at Ezapur

	V	Cr	Co	Cu	Zn	Sr	Zr	Ba	Pb	La	Ce	Nd
V	1											
Cr	-0.73	1										
Co	0.42	-0.63	1									
Cu	0.90	-0.80	0.63	1								
Zn	0.48	-0.59	0.56	0.80	1							
Sr	0.61	-0.11	-0.07	0.52	0.24	1						
Zr	0.95	-0.85	0.49	0.95	0.63	0.59	1					
Ba	0.63	-0.03	-0.32	0.46	0.21	0.81	0.50	1				
Pb	0.50	-0.25	-0.12	0.33	0.06	0.55	0.45	0.53	1			
La	0.92	-0.86	0.53	0.84	0.41	0.49	0.94	0.36	0.56	1		
Ce	0.93	-0.78	0.41	0.93	0.68	0.52	0.94	0.59	0.58	0.87	1	
Nd	0.92	-0.86	0.52	0.82	0.37	0.45	0.93	0.34	0.52	1.00	0.85	1

Jhumpuri (JP)

The concentration of V has shown positive correlation with all the trace elements and REEs except Cr (Table 3.28). On the other hand, the distribution of Cr has been negatively influenced by changes in the concentration of most of the elements. Though, with Co, Cu and Zn it has shown positive correlation. The Co, Cu and Zn have exhibited positive correlation with all the elements. The distribution of Sr, Zr, Ba, Pb, La, Ce and Nd has revealed positive correlation with all the elements except Cr

Table 3.28 Correlation among trace elements and REEs at Jhumpuri

	V	Cr	Co	Cu	Zn	Sr	Zr	Ba	Pb	La	Ce	Nd
V	1											
Cr	-0.21	1										
Co	0.54	0.46	1									
Cu	0.57	0.18	0.84	1								
Zn	0.61	0.33	0.97	0.91	1							
Sr	0.65	-0.10	0.24	0.50	0.37	1						
Zr	0.51	-0.19	0.22	0.08	0.21	0.04	1					
Ba	0.92	-0.10	0.34	0.37	0.41	0.69	0.36	1				
Pb	0.53	0.04	0.76	0.69	0.82	0.31	0.13	0.28	1			
La	0.54	-0.03	0.63	0.70	0.65	0.19	0.48	0.26	0.50	1		
Ce	0.68	-0.04	0.71	0.72	0.75	0.28	0.50	0.42	0.65	0.95	1	
Nd	0.70	0.03	0.73	0.77	0.77	0.39	0.43	0.46	0.68	0.93	0.97	1

Katia I (KTI)

The V, Co and Sr have exhibited positive correlation with most of the elements. However, these have been negatively correlated with Cr, Sr and Zr (Table 3.29). In contrast, the Cr has shown positive association with Zr and Sr while with other elements negative correlation has been observed. The concentration of Cu was also positively correlated with most of the trace elements and REEs except with Cr, Zn, Sr and Zr.

Table 3.29 Correlation among trace elements and REEs at Katia I

	V	Cr	Co	Cu	Zn	Sr	Zr	Ba	Pb	La	Ce	Nd
V	1											
Cr	-0.44	1										
Co	0.56	-0.26	1									
Cu	0.85	-0.34	0.86	1								
Zn	0.26	0.19	0.03	-0.05	1							
Sr	-0.56	0.40	-0.30	-0.26	-0.81	1						
Zr	-0.46	-0.34	-0.65	-0.74	0.13	-0.21	1					
Ba	0.99	-0.29	0.49	0.81	0.30	-0.51	-0.52	1				
Pb	0.74	-0.80	0.43	0.52	0.37	-0.84	0.16	0.64	1			
La	0.74	-0.92	0.38	0.56	0.07	-0.62	0.13	0.63	0.95	1		
Ce	0.72	-0.76	0.55	0.56	0.41	-0.86	0.08	0.62	0.98	0.90	1	
Nd	0.69	-0.93	0.33	0.49	0.09	-0.64	0.21	0.57	0.95	1.00	0.90	1

The distribution of Zn has positive influence of V, Cr, Zr, Nb, Ba and Pb whereas with Cu and Sr it was negatively correlated. The Zn has shown no correlation with Co, La and Nd. The concentration of Zr was positively correlated with all the elements except Nd while no strong correlation was found with Zn, Pb, La and Ce. The Ba has revealed positive effect of

enrichment or depletion in most of the trace elements and REEs; however, it has shown negative influence of changes in Cr, Sr and Zr. The distributions of Pb and Ce have been positively correlated with most of the elements whereas with Zr there was no strong correlation. The Nd also has shown positive correlation with all the elements except Cr and Sr.

Katia II (KTII)

At Katia II as well, the concentration of V, Co and Cu has been positively linked with changes in most of the trace elements and REEs (Table 3.30). The Cr and Sr however, have shown negative influence while Zr has no strong effect on the distribution of these elements. The Cr was negatively correlated with most of the elements except Sr. The distribution of Zn was positively correlated with most of the trace elements and REEs except Zr. It has no significant correlation with Cr and Sr. The Sr content, in contrast, has shown positive correlation with Cr while with other elements it was negatively associated. Nevertheless, Zr has exhibited negative correlation with most of the elements while with V, Cr, Ba, La and Nd no strong correlation has been observed. The Nb and Ba have exhibited positive association with changes in most of the elements except Cr and Sr while with Zr no such influence has been observed. The concentration of Hf, Pb, La, Ce and Nd has revealed positive relationship with most of the trace elements and REEs whereas no correlation was observed with Cr, Sr and Zr.

Table 3.30 Correlation among trace elements and REEs at Katia II

	V	Cr	Co	Cu	Zn	Sr	Zr	Ba	Pb	La	Ce	Nd
V	1											
Cr	-0.70	1										
Co	0.66	-0.27	1									
Cu	0.70	-0.57	0.64	1								
Zn	0.41	-0.05	0.59	0.61	1							
Sr	-0.44	0.81	-0.22	-0.70	-0.05	1						
Zr	-0.04	0.06	-0.52	-0.34	-0.43	0.10	1					
Ba	0.96	-0.56	0.66	0.51	0.34	-0.21	0.01	1				
Pb	0.75	-0.72	0.46	0.85	0.58	-0.55	-0.28	0.60	1			
La	0.82	-0.67	0.36	0.75	0.60	-0.45	-0.03	0.70	0.92	1		
Ce	0.94	-0.68	0.67	0.64	0.43	-0.33	-0.21	0.93	0.80	0.78	1	
Nd	0.92	-0.75	0.55	0.80	0.56	-0.57	-0.01	0.81	0.86	0.94	0.83	1

3.3.4.2 Mixing Zone

Sonpanki (SP)

The distribution of V has shown positive correlation with most of the trace elements and REEs (Table 3.31). Though, with Cr and Cu it has negative association. The Cr, on the other hand, has negatively correlated with all the elements. The concentration of Cu was positively influenced by the changes in Sr and Pb. However, negative correlation has been observed with V and Cr distribution. The Co, Zn, Sr, Zr, Pb, La, Ce and Nd were also positively correlated. In contrast, with Cr, these have shown negative correlation.

Table 3.31 Correlation among trace elements and REEs at Sonpanki

	V	Cr	Co	Cu	Zn	Sr	Zr	Ba	Pb	La	Ce	Nd
V	1											
Cr	-0.86	1										
Co	0.83	-0.67	1									
Cu	-0.25	-0.02	-0.02	1								
Zn	0.95	-0.90	0.89	0.06	1							
Sr	0.73	-0.88	0.83	0.30	0.89	1						
Zr	0.92	-0.60	0.78	-0.38	0.81	0.48	1					
Ba	0.97	-0.75	0.74	-0.44	0.84	0.55	0.96	1				
Pb	0.29	-0.62	0.38	0.79	0.56	0.78	0.00	0.06	1			
La	0.91	-0.88	0.81	0.16	0.98	0.85	0.78	0.81	0.61	1		
Ce	0.93	-0.85	0.85	0.11	0.99	0.83	0.83	0.84	0.55	0.99	1	
Nd	0.93	-0.85	0.84	0.10	0.98	0.82	0.84	0.84	0.54	0.99	1.00	1

Chandbali (CB)

The pattern of correlation among trace and rare earth elements is quite distinct at CB (collected from beach ridge) in comparison to the observations made before (Table 3.32). The concentration of V has exhibited positive association with enrichment and depletion of Cr, Ba and Pb whereas there has appeared negative correlation with all the other elements. Similarly, the Cr was positively correlated with V and Pb while with all the other elements it has shown negative correlation. The Cu has exhibited positive association with most of the elements. In contrast, with V, Cr, Ba and Pb negative correlation has been marked. The Co, Zn and Zr were positively correlated most of the trace elements and REEs. However, the distribution of V, Cr, Sr and Ba has negative influence on the concentration of these elements. The Sr, on the contrary has shown negative correlation with most of the elements while with V, Cr, Cu, Ba and Nd there was no significant correlation. The concentration of

Ba has exhibited positive correlation with the content of V and Cr. On the other hand, with other elements negative correlation has been observed. The distribution of Pb has shown positive influence of V, Cr, Co and Ba, however, it has negative association with Cu, Sr, La and Nd. The REEs have been positively correlated with most of the elements except V, Cr, Sr, Ba and Pb.

Table 3.32 Correlation among trace elements and REEs at Chandbali

	V	Cr	Co	Cu	Zn	Sr	Zr	Ba	Pb	La	Ce	Nd
V	1											
Cr	0.72	1										
Co	-0.46	-0.75	1									
Cu	-0.84	-0.95	0.62	1								
Zn	-0.53	-0.84	0.81	0.83	1							
Sr	0.04	0.10	-0.40	-0.14	-0.29	1						
Zr	-0.26	-0.30	0.14	0.35	0.09	-0.69	1					
Ba	0.96	0.86	-0.63	-0.92	-0.65	0.17	-0.40	1				
Pb	0.36	0.33	0.37	-0.44	-0.01	-0.47	-0.19	0.31	1			
La	-0.75	-0.85	0.65	0.94	0.93	-0.27	0.22	-0.80	-0.24	1		
Ce	-0.71	-0.96	0.86	0.92	0.95	-0.23	0.21	-0.84	-0.11	0.92	1	
Nd	-0.78	-0.85	0.56	0.95	0.89	-0.08	0.12	-0.80	-0.38	0.98	0.89	1

Ambiligan (AG)

Similar to CB, at AG the V has shown positive correlation with the Cr along with Zr, Ba, La, Ce and Nd (Table 3.33). With other elements no significant correlation has been observed. The Co has exhibited positive influence of Cu, Zn, Sr, Pb and Nd while no strong correlation with other trace elements and REEs. The Cu has been positively associated with Zn, Sr, Pb and REEs while no strong correlation has been observed with other elements. The Zn, Sr and Nb have been positively correlated with changes in Co, Cu, Pb and REEs. The Zr has shown positive association with V, Cr and Ba whereas negatively correlated with Co, Cu, Zn, Sr, Ba and Pb. The Ba has exhibited positive correlation with V, Cr, Zr and REEs. The Pb, likewise, was positively correlated with Co, Cu, Zn and La. With Zr it has been negatively correlated. The REEs have shown positive correlation with all the trace elements except Zr with which no strong correlation was observed.

Table 3.33 Correlation among trace elements and REEs at Ambiligan

	V	Cr	Co	Cu	Zn	Sr	Zr	Ba	Pb	La	Ce	Nd
V	1											
Cr	0.96	1										
Co	-0.07	-0.06	1									
Cu	-0.02	-0.09	0.82	1								
Zn	-0.03	-0.12	0.78	1.00	1							
Sr	-0.23	-0.03	0.58	0.52	0.44	1						
Zr	0.53	0.50	-0.87	-0.77	-0.74	-0.66	1					
Ba	0.96	0.94	-0.32	-0.21	-0.22	-0.28	0.71	1				
Pb	-0.24	-0.38	0.54	0.89	0.93	0.29	-0.66	-0.37	1			
La	0.48	0.52	0.17	0.52	0.50	0.50	-0.04	0.49	0.40	1		
Ce	0.66	0.71	0.26	0.49	0.46	0.48	0.00	0.62	0.26	0.95	1	
Nd	0.67	0.74	0.47	0.54	0.49	0.54	-0.14	0.57	0.21	0.84	0.96	1

Kasturikaran (KK)

As apparent from Table 3.34, the concentration of V (similar to SP), was positively correlated with most of the trace elements and REEs excluding Cr. On the contrary, Cr has shown negative correlation with all the elements except Zr and Ba. The distribution of Co has positive influence of changes in Cu, Zn and Sr while negative effect of Cr, Zr and Ba.

Table 3.34 Correlation among trace elements and REEs in Kasturikaran

	V	Cr	Co	Cu	Zn	Sr	Zr	Ba	Pb	La	Ce	Nd
V	1											
Cr	-0.55	1										
Co	0.00	-0.79	1									
Cu	0.33	-0.96	0.93	1								
Zn	0.66	-0.94	0.75	0.90	1							
Sr	0.53	-0.98	0.72	0.91	0.85	1						
Zr	0.39	0.47	-0.65	-0.58	-0.18	-0.56	1					
Ba	0.08	0.67	-0.97	-0.84	-0.69	-0.55	0.51	1				
Pb	0.20	-0.67	0.43	0.61	0.39	0.81	-0.78	-0.20	1			
La	0.95	-0.77	0.30	0.60	0.86	0.72	0.18	-0.23	0.31	1		
Ce	0.93	-0.83	0.37	0.67	0.89	0.79	0.07	-0.27	0.41	0.99	1	
Nd	0.98	-0.66	0.08	0.43	0.69	0.67	0.20	0.04	0.41	0.95	0.95	1

The Cu along with REEs has been positively correlated with Co, Zn and Sr whereas with Cr, Zr and Ba it has shown negative connection. The concentration of Zn and Sr has exhibited positive association with all the trace elements and REEs except Cr, Zr and Ba. The Zr was positively linked with Cr, Nb and Ba. However, with Co, Cu, Sr and Pb negative correlation

has been observed. The distribution of Ba has exhibited negative correlated with most of the elements excluding Cr and Zr. The Pb was positively correlated with the distribution of Cu, Zn and Sr. In contrast, negative correlation has been observed with Cr and Zr. The REEs have shown positive correlation with all the trace elements excluding Cr.

The analysis has revealed that some of the elements are positively correlated while other has shown negative correlation. Strong positive correlation has been observed between MgO and SiO₂ at each site. Similarly, Al₂O₃ has been positively correlated MnO, TiO₂ and Fe₂O₃. On the other hand, MgO has shown strong negative correlation with Al₂O₃, TiO₂, Fe₂O₃ and MnO.

In general, the concentration of V is positively associated with Co, Cu, Zn, Ba, La, Ce and Nd. It has, however, is negatively correlated with Cr as at EP, JP, KTI, KTII, SP and KK. Peculiarly, at CB and AG which are collected from beach ridge and palaeochannel respectively, the V has shown positive correlation with Cr.

3.4 Discussion and Conclusion

It is apparent from the above analysis that most of the elements are depleted at each location of lower Baitarani basin. However, MnO is enriched in each facie. The enrichment of Cr is generally associated with the sandy facies i.e. EPL4, EPL6, JPL4, JPL5, JPL6 and JPL11 of the riverine zone and SPL5, SPL6, CBL1, CBL3, CBL5, CBL6, AGL3 and KKL3 of the mixing zone. In the mixing zone, V is also enriched considerably in each facies of CB, AG and KK whereas in the riverine zone it is depleted. A higher enrichment of V is marked in CBL3, AGL3 and KKL3. Apart from these, Pb is also enriched in many facies of the riverine and mixing zone. Nevertheless, its enrichment cannot be linked with grain size distribution. Among REEs, only Ce is enriched in JPL1, JPL2, JPL3, and JPL5 of riverine zone. In the mixing zone, La, Ce, and Nd are enriched in CBL3 and AGL3.

The concentration of TOC has been relatively high in the facies of mixing zone. Its content is generally high in clayey facies though in some of the sandy facies also high concentration of TOC is observed as in JPL7, CBL2 and AGL3. Nevertheless, the TOC has varied considerably across the facies. SiO₂ is recognized as the most abundant element in the study region. Silica (SiO₂) is the most abundant material in the Earth crust and it readily goes into

colloidal solution (Henderson, 1998). Nevertheless, its distribution has always remained below the terrestrial mean. In riverine zone other significant elements are Al_2O_3 , Fe_2O_3 , Na_2O , CaO and MgO . In the mixing zone the concentration of MgO has been comparatively higher than the CaO . It may be due to the fact that MgO is usually derived from marine sources in the coastal areas (Comero et al., 2014; Gredilla et al., 2015; Li et al., 2019). In EP, JP, KTI, KTII, SP, CB and AG, content of Fe_2O_3 has exhibited the highest changeability among all the major elements followed by SiO_2 . In KK, however, SiO_2 has been found to be the most variable element followed by Fe_2O_3 . The Na_2O concentration has appeared least variable at EP, JP, KTII, CB and KK while at KTI and AG, the CaO and K_2O have exhibited minimum fluctuation.

The concentration of Al_2O_3 , MnO , TiO_2 , Fe_2O_3 are relatively high in clayey facies while these are low in sand dominated facies. An association of detrital elements (Al_2O_3 , MnO , TiO_2 , Fe_2O_3 and K_2O) with clay can be attributed to their detrital origin (Zhao and Yan, 1994). In contrast, the higher concentration of MgO and SiO_2 is mostly associated with sandy facies such as EPL4, EPL6, JPL4, JPL7, CBL1, CBL2, AGL3 and KKL3. Elevated concentration of MgO can be attributed to the enhanced influence of tidal activity in the study area because the MgO is primarily derived from the biogenic carbonates (Comero et al., 2014). It is mainly contributed by the calcareous organisms such as mollusks, bivalves and foraminifera in coastal regions (Li et al., 2019). The loosely packed coarser particles enable oxygen to mix deep into the sediments promoting the flourishing of the benthic communities (Li et al., 2019). Li et al. (2019) has further explained the higher concentration of CaO and MgO in the coastal environment. According to them, the marine organisms utilize CaO and MgO from seawater and construct their skeleton and shells. Thus, mollusks, bivalves and foraminifera supply sedimentary CaO and MgO in the coastal areas. It has also been recorded that MgO is usually more abundant in the sediments of marine zones than those of the fresh water environment (Gredilla et al., 2015).

Among trace elements and REEs, Ba is the most abundant followed by Zr, Cr, Sr, Ce and V. At CB site the concentration of V has remained higher than the Cr whereas in KK the Zn has been more enriched than the V. Maximum variation in the distribution of major, trace and rare earth elements has been observed in the facies of EP, JP and CB. The concentration of

Zr is highly variable at each location. It has also become clear that trace elements have been highly variable as compared to the major elements. The trace elements are derived from the composition of rocks and soils in the watershed (Koukina et al., 2017). Metal enrichment can occur due to fractionation of the riverine materials. These can be enriched through industrial and agricultural activities. In general, higher Pb concentration has been observed in the lower reaches of Baitarani basin. This might have been derived from agricultural sources as no major industries could be located in the study locations as coastal areas mainly receive contaminants from local sources (Eggleton and Thomas, 2004).

A correlation reveals common source and common mode of accumulation (Banta et al., 2008). Thus, in this study, correlation of Al_2O_3 , P_2O_5 , TiO_2 , MnO and Fe_2O_3 suggests their common source origin. These elements show a negative relationship with MgO and SiO_2 distribution which can be attributed to their distinct origin. Based on the above discussion it can be stated that the source of is different from that of MgO and SiO_2 . The former group of elements (Al_2O_3 , P_2O_5 , TiO_2 , MnO and Fe_2O_3) is supposed to be derived from the detrital flux (Zhao and Yan., 1994). On the hand, the latter group (MgO and SiO_2) is supposed to be contributed from the marine sources (Li et al., 2019). Among trace elements and REEs V, Co, Cu, Zn, Ba and Nd have formed distinct group from Cr as evident from the correlation pattern in the riverine zone. In contrast, in mixing zone there has appeared wide variation in the correlation of trace elements and REEs. For instance, V has shown positive correlation with Co, Zn, Ba and Nd in SP whereas there has existed negative relationship with Cr and Cu. In contrast, in CB and AG distribution of V has positively associated with Cr apart from Ba and Nd. In KK again V has illustrated negative correlation with Cr.

Based on the above discussion, it can be concluded that geochemistry has provided valuable information regarding the environment of deposition and the processes that were operational at different instances. As evident from the above discussion, in the study area, the elements have been deposited from two diverse regions, terrestrial and marine. The Al_2O_3 , Fe_2O_3 , TiO_2 , and MnO have been derived from terrestrial sources while MgO and SiO_2 have come from the marine sources. The enriched concentration of terrestrial elements has indicated increase in terrestrial activity i.e. enhanced river flow. On the other hand, increase in MgO and SiO_2 has demonstrated enhancement in the marine processes. These evidences are

crucial for the reconstruction of palaeoclimate which will be discussed later. Hence, based on sediment geochemistry, it has become clear that the clayey facies (as discussed in the previous chapter) with high concentration of detrital elements have been deposited through fluvial action. On the other hand, sandy facies containing high MgO and SiO₂ have been aggraded through marine processes. Along with this, it is also speculated that the area has experienced a high sea stand in the past influencing the depositional environment which will become more clear with further analysis in subsequent chapters.

The trace elements and REEs (V, Cr, La, Ce, Nd etc.) are considered as redox indicators as their concentration is influenced by the oxygen availability in the sedimentary sequence. With the help of these elements variability in oxygen availability is analyzed. Assessment of redox-sensitive elements reveals the existence of oxic or anoxic conditions. The significance of geochemistry to assess the palaeoredox environment will be discussed in Chapter 4.

Chapter 4

Assessment of Palaeoredox Environment using Geochemistry

4.1 Introduction

Periodic deposition of sediments in the coastal region occurs under the combined interplay of riverine and marine processes. The environment of sedimentation in coastal areas is generally classified into oxic and anoxic based on oxygen concentration. Variation in oxygen content indicates the well-oxygenated (oxic) and poorly oxygenated (anoxic) zones. The sub-oxic zone is a transition region between the oxic and anoxic zones (Murray et al., 1999). However, there are no definite boundaries between oxic, hypoxic, sub-oxic and anoxic environments (Pinti, 2014). The redox-sensitive processes such as detrital input of trace and rare earth elements (REEs), their removal and diagenesis, take place under these conditions resulting in the removal or absorption of elements during the sediment deposition.

The assessment of systematic variations in the distribution of redox-sensitive metals provides the opportunity to examine the environment at the time of sediment deposition. Studies based on redox-sensitive elements assist in the analysis of palaeo-redox environment in diverse geographic settings such as marine and estuarine environment (Morford and Emerson, 1999; Lyons and Severmann, 2006; O'Connor et al, 2015; Cole et al., 2017; Costa et al., 2018; Eltom et al., 2018), fluvial regions (Poulichet et al., 1997; Goldberg and Humayun, 2016; Choi et al., 2016; Natali and Bianchini, 2017), continental environment (Pi et al., 2013; Och et al., 2016; Kumar et al., 2017) and shale deposits (Jiang et al., 2006; Pi et al., 2013; Goldberg and Humayun, 2016).

Metal solubility is usually associated with redox state and hence their enrichment in sediments has the potential to provide significant clues of the palaeoredox environment (Cole et al., 2017). The most extensively studied redox-sensitive elements include Fe_2O_3 , Ni_2O , V, Cr, Mo, Ce, Co, Cu, U and Zn (Poulichet et al., 1997; Tribovillard et al., 2006; Coynel et al., 2016; Goldberg and Hymayun, 2016; Cole et al., 2017; Kumar et al., 2017; Eltom et al., 2018; Parveen and Sreekesh, 2019). The trace metals and REEs are sensitive to redox changes and usually enriched in reducing conditions. Among redox-sensitive elements, V and Cr are easily reduced (Algeo and Maynard, 2004; Li et al., 2015). Hence,

these can offer exclusive clues for the suboxic (weakly reducing) environment (Cole et al., 2017). V/Cr ratio has also been incorporated to assess palaeo-oxygenation (Dill et al., 1988; Nagaraan, 2007; Arsairai and Wannakomol, 2016). Zn and V enrichment has been utilized as an indicator of reducing environment (Costa et al., 2018). The behaviour of Fe is rather complex, however, it is also enriched in the anoxic environment (Lyons and Savemann, 2006). However, Fe, Cr, and V have considerable detrital constituents (Sahoo et al., 2012). Thus, detrital flux can influence their delivery to the sedimentary environment and its response to oxygen availability.

The concentration of TOC also affects the distribution of redox-sensitive indicators (Arsairai et al., 2016). The organic matter exhausts the available oxygen that often leads to generate suboxic conditions. These characteristics potentially make the trace metals and REEs the robust proxies of palaeoredox environment (Tribovillard et al., 2006). Episodes of enhanced primary productivity indicated by high TOC concentration can cause anoxic conditions. The respiration of organic matter consumes the available oxygen hence, producing an anoxic environment of deposition. An elevated concentration of TOC also exhausts dissolved oxygen making it reducing in nature. The anoxia can also develop because of the microbial decomposition of TOC in the sediments (Tribovillard et al., 2006). They consume the dissolved oxygen in the water during sediment deposition and the facie becomes anoxic. Therefore, changes in the TOC concentration affect significantly the oxygen availability in a sediment profile.

Among REEs, Ce and Ce/Ce* is extensively used palaeoredox indicator (German and Henry, 1990; Shen et al., 2012; Pi et al., 2013; Arsairai and Wannakomol, 2016). The enrichment in REEs and hence of La, Ce, Nd, etc. takes place under reducing environment suggesting anoxic conditions.

This study presents an analysis of palaeoredox environment that existed in the area of study. The assessment is based on down-core variability in the concentration of selected redox-sensitive trace elements and REEs in respect to their terrestrial mean as suggested by Rudnick and Gao (2014). Along with this, the utility of these metals to interpret the palaeoredox conditions in the riverine and coastal environment is also investigated.

4.2 Methodology

The present study is conducted using subsurface sediment samples obtained from distinct landforms of the riverine zone (EP, JP, KTI, and KTII) and mixing zone (SP, CB, AG, KK). The distribution of trace and REEs is estimated using Energy Dispersive X-Ray Spectrometry (EDXRF). The concentration of total organic carbon (TOC) is analysed using Walkley-Black method. A detail discussion of the methodology is provided in the previous chapter (Chapter 3).

The trace elements selected included for the assessment of palaeoredox environment are V, Cr, Co, Cu, and Zn. The selected REEs include Ba, Ce, La, and Nd (Table 4.1). These are the most extensively used proxies in palaeoredox studies. In addition, variation in the ratios of V/Cr, V/Al, Fe/Al, and Cu/Zn are also analysed to investigate the oxic and anoxic conditions that existed in the past.

Table 4.1 Selected redox-sensitive trace, rare earth elements (REEs) and ratios

Variables	Selected Elements and Ratios	Redox Environment		References
		Enrichment	Depletion	
Trace Elements	V, Cr, Co, Cu, and Zn	Anoxic/Suboxic	Oxic	Lyons and Severmann, 2006; Madhavaraju et al., 2016; Cole et al., 2017; Costa et al., 2018
REEs	La, Ce and Nd	Anoxic/Suboxic	Oxic	
Ratios	V/Cr, V/Al, Fe/Al, and Cu/Zn	Anoxic/Suboxic	Oxic	

Based on their analysis Ernst (1970) has postulated the V/Cr ratio above two (>2) as an indicator of anoxic environment. Jones and Manning (1994) have suggested a ratio below two (<2) has been considered an indicator of more oxidizing and less reducing environment. V/Cr value approximate to one ($V/Cr=1$) indicates the O_2 - H_2S interface within the stratigraphic profile Jones and Manning (1994). Subsequently, Madhavaraju et al. (2016) have suggested a lower ratio of V/Cr (<2) as the indicator of oxic depositional environment. Its value between two and four (2-4), has been linked with suboxic conditions while a ratio above two (>2) has been considered to represent anoxic conditions. Similarly, a higher ratio of Cu/Zn (>2) has been associated with anoxic environment whereas lower ratio as the tracer of well-oxidized conditions (Hallberg, 1976).

As discussed in the previous chapter, V is depleted while Cr is enriched in most of the facies of the Riverine and Mixing Zone. However, in present study relatively higher and lower concentration of trace elements and REEs has been examined to analyse relative changes in oxygen concentration.

4.3 Analysis

4.3.1 Variability of Redox-Sensitive Trace Elements

4.3.1.1 Riverine Zone

Ezapur (EP)

The concentration of V has varied from 49 ppm in EPL6 to 74 ppm in EPL3 with an average concentration of 64.71 ppm (Table 4.2). It has remained below the crustal mean in each facie. The concentration of Cr has been significantly above the crustal average (Table 4.2). The Cr has remained between 113 ppm in EPL7 and 249 ppm EPL4 with a mean of 182.6 ppm. Elevated concentration of Cr has associated with mafic provenance (Akinyemi et al., 2014). It can also be derived from anthropogenic sources. The ratio of V/Cr has deviated between 0.21 in EPL6 and 0.60 in EPL7 with a mean of 0.39. It has also remained below the crustal mean across the facies. The V/Al ratio has varied from 4.83 in EPL6 to 6.10 in EPL1 with an average of 5.64.

The concentration of Co has fluctuated from 15 ppm to 18 ppm with average content being 16.29 ppm (Table 4.2). Cu has varied between 13 ppm (EPL6) to 46 ppm (EPL1 and EPL2) with a mean of 32.9 ppm. Its concentration has been above the crustal mean in EPL1, EPL2, EPL3, EPL5, and EPL7. In EPL1 and EPL2, significant enrichment in Zn content has occurred. Zn concentration has varied between 6 ppm and 62 ppm in EP. The average concentration has been 17.29 ppm. The ratio of Cu/Zn has varied from 0.74 in EPL2 to 6.17 ppm in EPL3. It has been above the crustal mean in the EPL1, EPL2, EPL3, EPL5, and EPL7. The ratio of Fe/Al has deviated from 0.54 in EPL6 and 1.05 in EPL5 with a mean of 0.85 ppm. It is above the crustal average value in all the facies.

Table 4.2 Distribution of selected trace elements (in ppm) and ratios in Ezapur site

Facies/ Element	V	Cr	Co	Cu	Zn	V/Cr	V/Al	Cu/Zn	Fe/Al
EPL1	72	159	16	46	60	0.45	6.10	0.77	0.93
EPL2	67	148	18	46	62	0.45	5.63	0.74	0.95
EPL3	74	156	15	37	6	0.47	5.94	6.17	0.90
EPL4	54	249	15	16	7.4	0.22	5.31	2.20	0.86
EPL5	69	217	17	35	9	0.32	5.80	3.89	1.05
EPL6	49	236	15	13	14	0.21	4.83	1.10	0.54
EPL7	68	113	18	37	22	0.60	5.86	1.68	0.75
Mean	64.7	182.6	16.3	32.9	17.3	0.39	5.64	1.67	0.85
*Crustal Mean	97	92	17	28	67	1.05	13.28	0.42	0.48

*Crustal Mean value is based on Rudnick and Gao (2014)

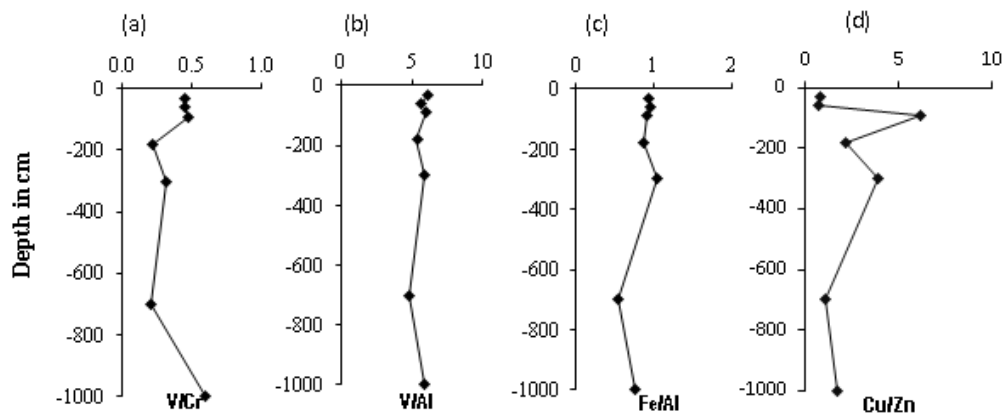


Figure 4.1 Variability of (a) V/Cr, (b) V/Al (c) Fe/Al (d) Cu/Zn at Ezapur site

The concentration of V, Co, Cu, and Zn has always remained below the crustal mean suggesting oxygen abundance. However, Cr has significantly enriched in EPL6, EPL5, and EPL4 suggesting oxygen reduction. Nevertheless, higher Cr content can also be attributed to anthropogenic sources. The ratio of V/Cr and V/Al has always remained below the crustal mean suggesting the oxic depositional environment at this site. However, enrichment Cu/Zn (>2) in EPL3 and EPL5 has suggested oxygen reduction in these facies (Figure 4.1). The ratio of V/Cr and V/Al is also relatively high in these facie which can be associated with an anoxic environment of deposition. In contrast, the ratio of Fe/Al has always remained above the crustal mean. This can be the result of an increase in solid-phase iron (Crusius et al., 1996). A higher detrital flux (Fe, Al) also reduces the oxygen availability in the core leading to the development of anoxia as in EPL5.

Jhumpuri (JP)

The concentration of V has deviated from 43 ppm in JPL4 to 76 ppm in JPL3 with an average of 61.3 ppm (Table 4.3). It has remained below the crustal mean in each facie. The Cr has varied from 177 ppm in JPL11 to 233 ppm in JPL4 with an average distribution of 188.6 ppm. Its concentration has been above the crustal mean across the facies, which can again be the manifestation of its source region which are rich in iron (Fe) and anthropogenic influence. The V/Cr has remained between 0.23 in JPL7 and 0.44 in JPL9. The distribution of V/Al has varied from 3.73 in JPL7 to 6.80 in JPL8. These ratios have always remained below the crustal mean.

Table 4.3 Distribution of selected trace elements (in ppm) and ratios at Jhumpuri site

Facies/ Elements	V	Cr	Co	Cu	Zn	V/Cr	V/Al	Cu/Zn	Fe/Al
JPL1	70	214	23	53	66	0.33	5.98	0.80	1.40
JPL2	74	190	21	49	73	0.39	6.55	0.67	1.46
JPL3	76	185	23	56	79	0.41	6.27	0.71	1.43
JPL4	43	233	17	37	23	0.18	3.84	1.61	0.52
JPL5	63	187	25	67	103	0.34	4.59	0.65	1.13
JPL6	56	198	21	51	63	0.28	4.11	0.81	0.63
JPL7	44	192	17	30	11	0.23	3.73	2.73	0.60
JPL8	73	191	21	41	60	0.38	6.80	0.68	1.01
JPL9	68	153	14	41	7	0.44	5.47	5.86	1.03
JPL10	52	155	13	34	3	0.34	4.45	11.3	1.03
JPL11	55	177	16	26	13	0.31	4.47	2.10	0.47
Mean	61.3	188.6	19.2	44.1	45.6	0.33	5.11	2.53	0.97
*Crustal Mean	97	92	17	28	67	1.05	13.28	0.42	0.48

*Crustal Mean value is based on Rudnick and Gao (2014)

The Co has fluctuated from 13 ppm to 25 ppm with an average of 19.2 ppm. It has been above the crustal mean in JPL1, JPL2, JPL3, JPL5, JPL6, and JPL8. The concentration of Cu has deviated from 26 ppm to 67 ppm with a mean value of 44.1 ppm. It has been above the crustal average in all the facies except JPL11. The Zn has varied significantly from 3 ppm to 103 ppm with an average concentration of 45.6 ppm. Its content is above the crustal average in JPL2, JPL3, and JPL5. The ratio of Cu/Zn has fluctuated from 0.67 ppm in JPL2 to 11.3 ppm in JPL10. It has been above the crustal mean in each facie. The ratio of Fe/Al has varied between 0.47 in JPL11 and 1.46 in JPL2. In most of the facies, this ratio has been above the crustal average of 0.48 (Rudnick and Gao, 2014).

Similar to EP site, V has remained below the crustal average at JP while Cr has enriched in all the facies. The ratios of V/Cr and V/Al have remained below the crustal mean suggesting the oxic environment of deposition up to a depth of 1000 cm (Figure 4.2). However, a higher concentration of Co, in JPL8, JPL6, JPL5, JPL3, JPL2, and JPL1 can be attributed to the higher detrital inflow, which can result in oxygen exhaustion. The ratio of Cu/Zn has indicated lower oxygen concentration during the deposition of JPL10, JPL9, and JPL7 (Table 4.3). Hence, it has been inferred that at this time the environment was anoxic which could not be associated with higher detrital inflow. The value of Fe/Al has always remained above the crustal mean, which can be associated with an increase in solid-phase iron.

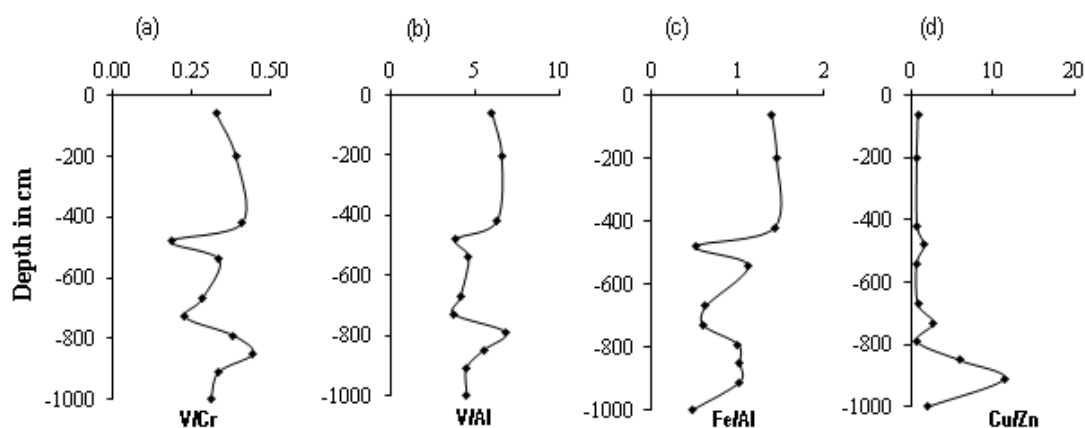


Figure 4.2 Variability of (a) V/Cr, (b) V/Al (c) Fe/Al (d) Cu/Zn at Jhumpuri site

Katia I (KTI)

The concentration of V has fluctuated from 68 ppm in KTIL2 to 79 ppm in KTIL3 with a mean of 72.6 ppm (Table 4.4). Hence, it has always remained below the crustal average. Cr has deviated between 148 ppm in KTIL1 and 215 ppm in KTIL2. Its average concentration has been 169 ppm which is significantly higher than the crustal mean of 92 (Rudnick and Gao, 2014). The V/Cr ratio has varied from 0.32 in KTIL2 to 0.48 in KTIL1, KTIL3, and KTIL5. The V/Al ratio has deviated between 5.84 (KTIL4) and 6.81 (KTIL1). These ratios have been below the crustal mean in each facie of KTI.

The concentration of Co has varied from 16 ppm and 23 ppm with an average of 18.8 ppm (Table 4.4). In KTIL3, KTIL4, and KTIL5 it has been above the crustal average. Cu has fluctuated from 36 ppm to 52 ppm in KTI with an average concentration of 43.8 ppm. It has

remained above the crustal mean across the facies. The concentration of Zn has varied from 10 ppm to 60 ppm with an average distribution of 47 ppm. The ratio of Cu/Zn has deviated from 0.60 ppm in KTIL1 to 4.60 ppm in KTIL5. It has been above the crustal average of 0.42 (Rudnick and Gao, 2014) in all the facies. Fe/Al ratio has varied from 0.99 to 1.49. It has also remained above the crustal mean in each facie.

Table 4.4 Distribution of selected trace elements (in ppm) and ratios at Katia I site

Facies/ Elements	V	Cr	Co	Cu	Zn	V/Cr	V/Al	Cu/Zn	Fe/Al
KTIL1	71	148	16	36	60	0.48	6.81	0.60	0.99
KTIL2	68	215	16	36	48	0.32	5.54	0.75	1.19
KTIL3	79	165	20	52	61	0.48	7.10	0.85	1.49
KTIL4	73	168	23	49	56	0.43	5.89	0.88	1.30
KTIL5	72	149	19	46	10	0.48	6.05	4.60	1.25
Mean	72.6	169	18.8	43.8	47.0	0.44	6.28	1.54	1.24
*Crustal Mean	97	92	17	28	67	1.05	13.28	0.42	0.48

*Crustal Mean value is based on Rudnick and Gao (2014)

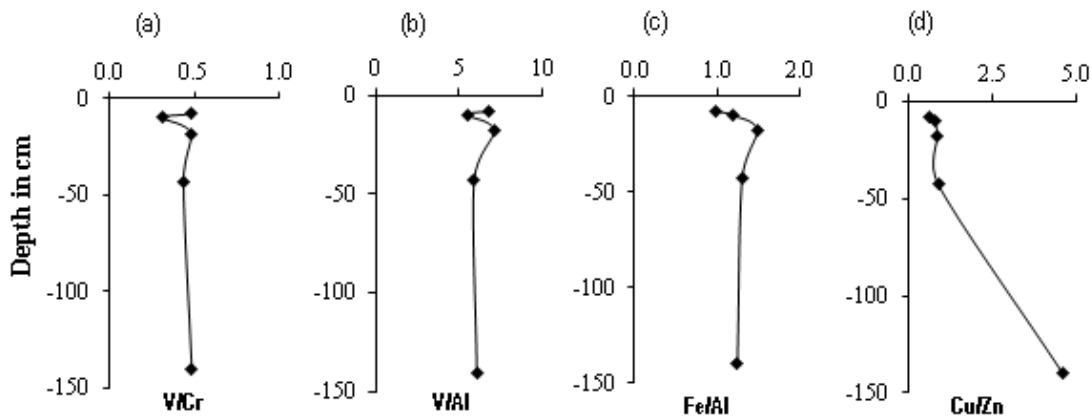


Figure 4.3 Variability of (a) V/Cr, (b) V/Al (c) Fe/Al (d) Cu/Zn at Katia I site

A marginal deviation has been marked in the oxygen availability at KTI location (Figure 4.3). A higher ratio of Cu/Zn has indicated lower oxygen availability in KTIL5 and hence the development of anoxia. This ratio has declined in KTIL4, which can be due to an increase in the oxygen concentration resulting in the development of oxic environment. Afterward, no considerable change in the oxygen concentration has been indicated at the KTI site suggesting the persistence of oxic depositional environment.

Katia II (KTII)

The concentration of V has varied from 60 ppm in KTII3 to 73 ppm in KTII6. Similar to other locations of the Riverine Zone, it has remained below the crustal average in each facie (Table 4.5). Cr has fluctuated from 146 ppm in KTII5 to 221 ppm in KTII8 with a mean being 179.7 ppm. It has remained above the crustal average of 92 ppm (Rudnick and Gao, 2014). The ratio of V/Cr has been recorded between 0.28 in KTII3 and 0.58 in KTII5. The V/Al ratio has deviated from 4.68 in KTII3 to 6.72 in KTII6. These ratios have always remained below the crustal mean at this location.

Co has varied from 15 ppm (KTII4) to 23 ppm (KTII5) with a mean of 18.6 ppm (Table 4.5). Its concentration has been above the crustal mean in KTII2, KTII2, KTII3, KTII5, KTII6, KTII8, and KTII9. The concentration of Cu has remained between 31 ppm (KTII4) and 48 ppm (KTII9) with a mean distribution of 38.9 ppm. In all the facies, Cu has been above the crustal average of 28 ppm (Rudnick and Gao, 2014). The concentration of Zn has fluctuated from 15 ppm in KTII2 to 81 ppm in KTII9 with an average content of 53.1 ppm. In KTII5 and KTII9, it has been above the crustal mean. The ratio of Cu/Zn has varied from 0.56 in KTII7 and 2.27 in KTII2 remaining above the crustal average. The value of Fe/Al has deviated from 0.93 in KTII3 to 1.42 in KTII5. It has also remained above the crustal mean across the sediment sequences.

Table 4.5 Distribution of selected trace elements (in ppm) and ratios at Katia II site

Facies/ Elements	V	Cr	Co	Cu	Zn	V/Cr	V/Al	Cu/Zn	Fe/Al
KTII1	71	159	16	44	44	0.45	5.58	1.00	1.04
KTII2	66	165	18	34	15	0.40	5.89	2.27	1.18
KTII3	60	213	18	32	52	0.28	4.68	0.62	0.93
KTII4	63	213	15	31	42	0.30	5.39	0.74	1.08
KTII5	85	146	23	46	71	0.58	6.46	0.65	1.42
KTII6	73	147	19	42	55	0.50	6.72	0.76	1.19
KTII7	69	171	17	35	62	0.40	5.69	0.56	0.95
KTII8	69	221	20	38	56	0.31	5.58	0.68	0.99
KTII9	68	182	21	48	81	0.37	5.95	0.59	1.41
Mean	69.3	179.7	18.6	38.9	53.1	0.40	5.77	0.87	1.13
*Crustal Mean	97	92	17	28	67	1.05	13.28	0.42	0.48

*Crustal Mean value is based on Rudnick and Gao (2014)

Oxygen concentration has remained quite persistent at this location as suggested by the ratios of V/Cr and V/Al (Table 4.5). The value of Cu/Zn, however, has indicated oxygen reduction during the deposition of KTIIIL2 (Figure 4.4).

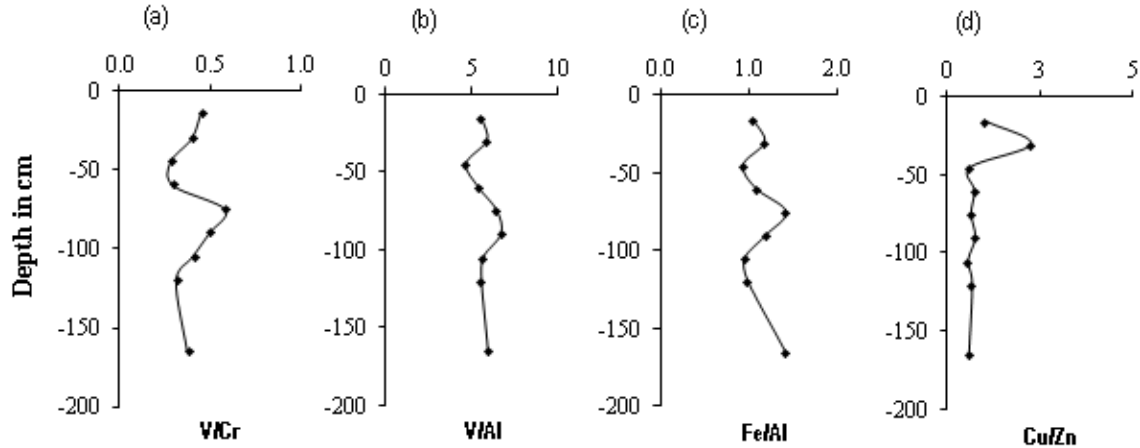


Figure 4.4 Variability of (a) V/Cr, (b) V/Al (c) Fe/Al (d) Cu/Zn at Katia II site

The analysis has indicated the predominance of oxic conditions during the sediment aggradation in the Riverine Zone. Based on the down core variability of Cu/Zn anoxic environment has been reported in EPL6, EPL5, JPL10, JPL9, JPL7, KTIL5 and KTIIIL2. However, the analysis of redox-sensitive trace elements i.e. V, Cr, Co, Cu, and Zn has not provided any significant evidence of palaeoredox conditions.

4.3.1.2 Mixing Zone Sonpanki (SP)

The concentration of V has varied from 33 ppm in SPL6 to 82 ppm in SPL5 with a mean of 67 ppm (Table 4.6). In each facie of SP, it has remained below the crustal mean of 97 ppm (Rudnick and Gao, 2014). Cr content has been between 134 ppm in SPL2 and 218 ppm in SPL6 with a mean distribution of 168.8 ppm. Its concentration has been above the crustal mean in each facie. The V/Cr ratio has been between 0.15 in SPL6 and 0.54 in SPL2. The value of V/Al has deviated from 2.97 in SPL6 to 6.31 in SPL5. Their values have always remained below the crustal average.

Table 4.6 Distribution of selected trace elements (in ppm) and ratios at Sonpanki site

Facies/ Elements	V	Cr	Co	Cu	Zn	V/Cr	V/Al	Cu/Zn	Fe/Al
SPL1	69	177	24	38	72	0.39	5.38	0.52	1.10
SPL2	72	134	23	39	79	0.54	5.33	0.49	1.18
SPL3	75	157	22	39	76	0.48	5.55	0.51	0.83
SPL4	71	169	24	38	75	0.42	5.53	0.51	0.97
SPL5	82	158	23	30	71	0.52	6.31	0.42	0.57
SPL6	33	218	19	37	18	0.15	2.97	2.06	0.39
Mean	67	169	22.5	36.8	65.2	0.42	5.18	0.75	0.84
*Crustal Mean	97	92	17	28	67	1.05	13.28	0.42	0.48

*Crustal Mean value is based on Rudnick and Gao (2014)

Co has varied from 19 ppm in SPL6 to 24 ppm in SPL1 and SPL4 with a mean of 22.5 ppm (Table 4.6). It has remained above the crustal average in each facie. The Cu has fluctuated from 30 ppm in SPL5 to 39 ppm in SPL2 and SPL3. Its mean concentration has been 36.8 ppm, which is significantly higher than the crustal average of 28 ppm (Rudnick and Gao, 2014). The concentration of Zn has varied from 18 ppm in SPL6 to 79 ppm in SPL2 with mean concentration being 65.2 ppm. In most of the facies, it has been above the crustal average except in SPL6. The ratio of Cu/Zn has deviated between 0.42 in SPL5 and 2.06 in SPL6. The value of Cu/Zn has remained below the crustal mean in all the facies except SPL6 where it is above the crustal mean. Fe/Al ratio has fluctuated from 0.39 in SPL6 to 1.18 in SPL2. It has remained above the crustal average in SPL1 and SPL2.

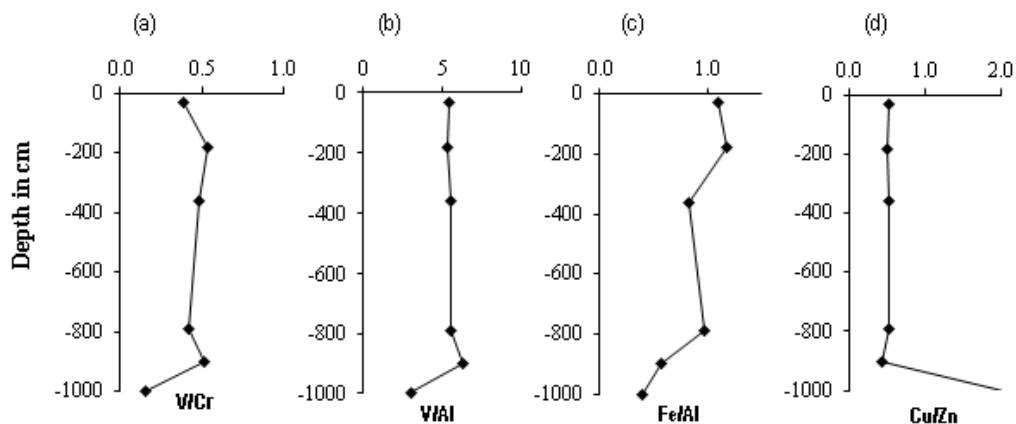


Figure 4.5 Variability of (a) V/Cr, (b) V/Al (c) Fe/Al (d) Cu/Zn at Sonpanki site

The ratio of Cu/Zn has shown a different pattern in comparison to V/Cr, V/Al, and Fe/Al in SP which was collected from the active floodplain (Figure 4.5). This can be attributed to its unique depositional environment as it significantly influenced by tidal activity. This is also the confluence region of Salnadi and Baitarani. The value of other indicators i.e. V/Cr, and V/Al has remained below the crustal mean, suggesting the oxic environment of deposition. However, the Cu/Zn ratio has been relatively high in SPL6 indicating the development of anoxia during the deposition of this facie.

Chandbali (CB)

The V has varied from 66 ppm in CBL2 and CBL4 to 88 ppm in CBL1 (Table 4.7). Its average concentration has been 74.3 ppm, which is below the crustal mean of 92 ppm (Rudnick and Gao, 2014). The distribution of Cr has remained between 115 ppm in CBL2 and 368 ppm in CBL1 with an average of 209.3 ppm. The V/Cr ratio has fluctuated from 0.24 in CBL1 to 0.57 in CBL2. The ratio of V/Al has remained between 5.54 in CBL3 and 9.79 in CBL5. Similar to previous locations, these have remained below the crustal average in each facie of CB.

Table 4.7 Distribution of selected trace elements (in ppm) and ratios at Chandbali site

Facies/ Elements	V	Cr	Co	Cu	Zn	V/Cr	V/Al	Cu/Zn	Fe/Al
CBL1	88	368	18	21	28	0.24	8.11	0.75	1.09
CBL2	66	115	22	40	74	0.57	6.04	0.54	0.68
CBL3	68	199	20	34	40	0.34	5.54	0.85	0.31
CBL4	66	154	25	34	59	0.43	5.77	0.58	0.82
CBL5	73	240	18	29	27	0.30	9.79	1.07	1.43
CBL6	85	180	22	30	50	0.47	6.74	0.60	0.69
Mean	74.3	209	21	31	46.3	0.39	7.00	0.73	0.84
*Crustal Mean	97	92	17	28	67	1.05	13.28	0.42	0.48

*Crustal Mean value is based on Rudnick and Gao (2014)

Co has fluctuated from 18 ppm to 25 ppm with an average distribution of 21 ppm (Table 4.7). In each facie, its concentration is above the crustal mean of 17 ppm (Rudnick and Gao, 2014). Cu has remained between 21 ppm and 40 ppm with an average of 31 ppm. It has been above the crustal mean across the facie except CBL1. Zn has deviated from 27 ppm to 74 ppm with a mean of 46.3 ppm. The ratio of Cu/Zn has varied from 0.54 to 1.07. The value of

Fe/Al has deviated between 0.31 and 1.43. These ratios have remained above the crustal mean.

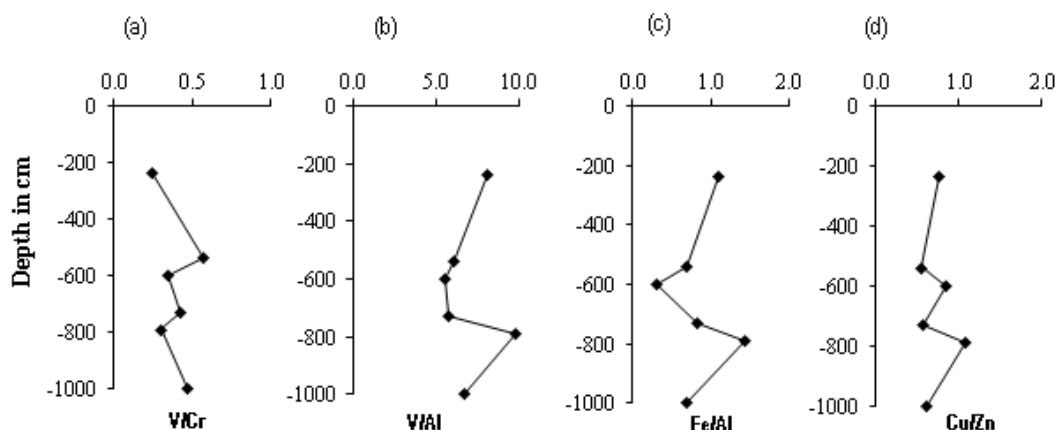


Figure 4.6 Variability of (a) V/Cr, (b) V/Al (c) Fe/Al (d) Cu/Zn at Chandbali site

In CB sample, obtained from the older beach deposit, the ratio of V/Al, Fe/Al, and Cu/Zn ratios have varied in a similar pattern (Figure 4.6). Their ratio has suggested the predominance of oxic environment of deposition up to a depth of 1000 cm.

Ambiligan (AG)

The content of V has deviated from 65 ppm in AGL5 and 79 ppm in AGL1 (Table 4.8). Its mean concentration (71.4 ppm) has remained below the crustal mean of 97 ppm (Rudnick and Gao (2014)). The Cr content has varied from 83 ppm in AGL5 to 153 ppm in AGL1 with mean concentration being 115.2 ppm. It has been below the crustal mean in AGL5 while in other facies it is above the crustal average of 92 ppm (Rudnick and Gao, 2014). The ratio of V/Cr has varied from 0.52 in AGL1 to 0.78 in AGL5, which is markedly higher than the other locations of the Mixing Zone. The V/Al has remained between 4.71 in AGL2 and 6.94 in AGL3. The value of V/Cr and V/Al has always remained below the crustal mean.

Co has varied from 16 ppm in AGL3 to 26 ppm in AGL1 with a mean concentration of 21.6 ppm (Table 4.8). It has remained above the crustal mean in all the facies except AGL3. The Cu has fluctuated between 23 ppm in AGL3 and 49 ppm in AGL2. Its concentration has been above the crustal average in AGL1 and AGL2. The value of Cu/Zn has deviated from 0.45 in AGL2 to 0.92 in AGL3. In all the facies, it has been above the crustal mean. The

ratio of Fe/Al has fluctuated from 0.56 in AGL3 to 0.97 in AGL1. Its mean concentration is 0.77 ppm, which is considerably above the crustal mean of 0.48 ppm (Rudnick and Gao, 2014)

Table 4.8 Distribution of selected trace elements (in ppm) and ratios at Ambiligan site

Facies/ Elements	V	Cr	Co	Cu	Zn	V/Cr	V/Al	Cu/Zn	Fe/Al
AGL1	79	153	26	41	76	0.52	5.80	0.54	0.97
AGL2	68	92	24	49	108	0.74	4.71	0.45	0.86
AGL3	78	139	16	23	25	0.56	6.94	0.92	0.56
AGL4	67	109	20	28	34	0.61	5.77	0.82	0.76
AGL5	65	83	22	28	39	0.78	4.93	0.72	0.72
Mean	71.4	112	21.6	33.8	56.4	0.64	5.63	0.69	0.77
*Crustal Mean	97	92	17	28	67	1.05	13.28	0.42	0.48

*Crustal Mean value is based on Rudnick and Gao (2014)

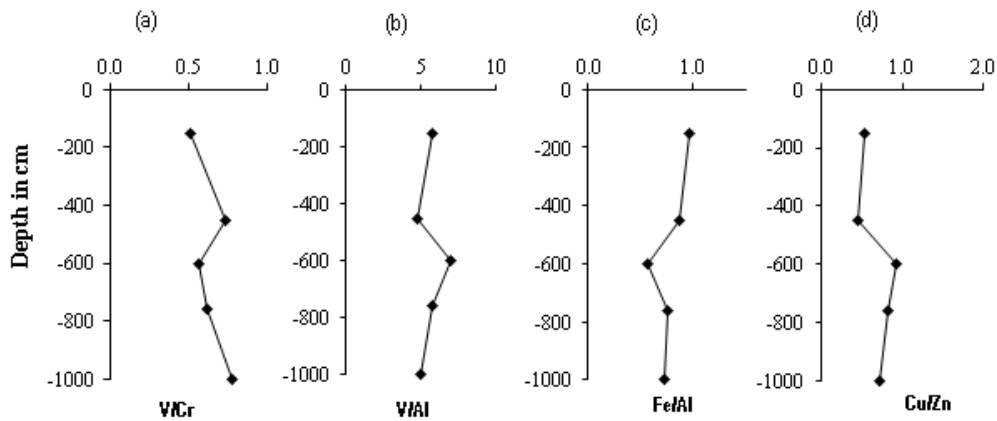


Figure 4.7 Variability of (a) V/Cr, (b) V/Al (c) Fe/Al (d) Cu/Zn at Ambiligan site

The AG sample has been obtained from the palaeochannel of River Baitarani similar to EP; however, owing to its location in the Mixing Zone, selected palaeoredox proxies have behaved uniquely (Figure 4.7). The Cu/Zn has not shown significant variability at this location. It has always remained below one (<1), hence exhibiting the oxic environment of deposition. The ratios of V/Cr and V/Al have also suggested an abundance of oxygen.

Kasturikaran (KK)

The concentration of V has fluctuated from 64 ppm in KKL3 and KKL4 to 68 ppm in KKL1 with a mean distribution of 65.8 ppm (Table 4.9). In each facie it has remained below the

crustal mean. Cr content has varied from 150 ppm in KKL2 to 268 ppm in KKL3. The mean concentration of Cr is 187 ppm, which is considerably above the crustal mean. The V/Cr ratio has been between 0.24 in KKL3 and 0.45 in KKL2. It has depleted in KKL1 while in other facies it has been above the crustal average. The V/Al ratio has varied from 4.83 in KKL4 to 6.07 in KKL3. Its value has been above the crustal mean across the facies.

Table 4.9 Distribution of selected trace elements (in ppm) and ratios at Kasturikaran site

Facies/ Elements	V	Cr	Co	Cu	Zn	V/Cr	V/Al	Cu/Zn	Fe/Al
KKL1	68	168	23	36	98	0.40	5.00	0.37	0.74
KKL2	67	150	23	37	82	0.45	5.34	0.45	0.94
KKL3	64	268	21	28	25	0.24	6.07	1.12	0.74
KKL4	64	162	25	39	84	0.40	4.83	0.46	0.84
Mean	65.8	187	23	35	72.3	0.37	5.31	0.60	0.82
*Crustal Mean	97	92	17	28	67	1.05	13.28	0.42	0.48

*Crustal Mean value is based on Rudnick and Gao (2014)

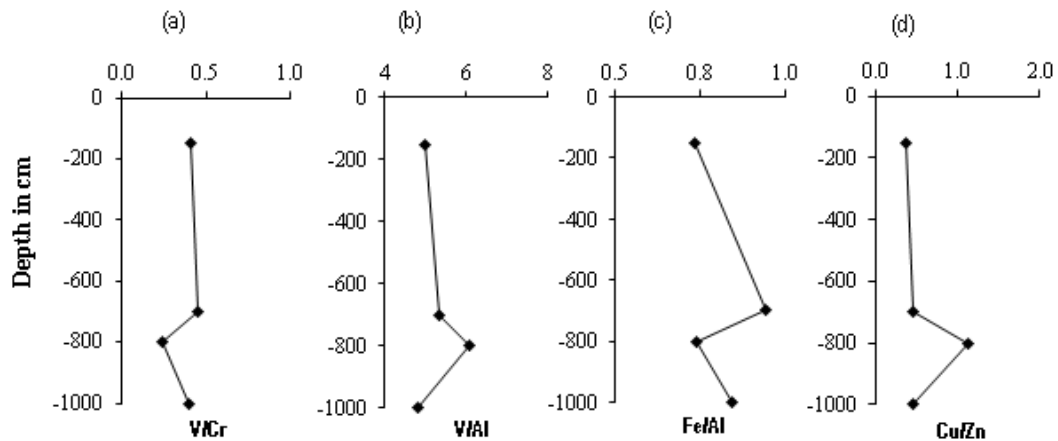


Figure 4.8 Variability of (a) V/Cr, (b) V/Al (c) Fe/Al (d) Cu/Zn at Kasturikaran site

Co has varied between 21 ppm in KKL3 and 25 ppm in KKL4. Its concentration has been above the crustal average in all the facies. The Cu has deviated from 28 ppm in KKL3 to 39 ppm in KKL4. In KKL1, KKL2, and KKL4, it has been above the crustal mean of 28 ppm (Rudnick and Gao, 2014). Zn has varied from 25 ppm in KKL3 to 98 ppm in KKL1. It has been below the crustal mean in KKL3 whereas in other facies its concentration has been above the crustal average of 67 ppm (Rudnick and Gao, 2014). The ratio of Cu/Zn has

deviated from 0.37 in KKL1 to 1.12 in KKL3. The Fe/Al ratio has varied from 0.74 in KKL1 and KKL3 to 0.94 in KKL2.

The ratios of V/Cr, V/Al, Cu/Zn, and Fe/Al have been low at KK location which was also collected from palaeochannel of Baitarani River, in the Mixing Zone. All the indicators have suggested the existence of oxic environment of deposition at this site.

Thus, the selected redox-sensitive trace elements and ratios have indicated that during the sediment aggradation, oxic environment has prevailed in the Mixing Zone. During the deposition of SPL6, the ratio of Cu/Zn has suggested oxygen reduction. However, moving towards the coast this ratio has declined markedly illustrating the abundance of oxygen.

4.3.2 Variability of Redox-Sensitive Rare Earth Elements (REEs) and TOC

4.3.2.1 Riverine Zone

Ezapur (EP)

The concentration of Ce has varied between 10 ppm in EPL6 to 44 ppm in EPL3 with an average of 29.9 ppm (Table 4.10). It has been above the crustal mean in EPL2, EPL3, and EPL7. The distribution of La has deviated from 28 ppm in EPL7 to 90 ppm in EPL1. The average content is 66.6 ppm. It has remained above the crustal mean in EPL1, EPL2, EPL3 and EPL7. Nd has fluctuated between 8 ppm in EPL6 and 34 ppm in EPL3 with a mean distribution of 23 ppm. In EPL3 and EPL7 it has been above the crustal mean of 27 ppm (Rudnick and Gao, 2014). The concentration of TOC has deviated from 0.11% in EPL3 to 0.53 in EPL4 with an average distribution of 0.31%.

Table 4.10 Distribution of selected REEs (in ppm) and TOC (in %) at Ezapur site

Proxies/Facie	Ce	La	Nd	TOC
EPL1	31	90	24	0.18
EPL2	37	79	27	0.36
EPL3	44	83	34	0.11
EPL4	16	50	12	0.53
EPL5	31	63	24	0.48
EPL6	10	28	08	0.24
EPL7	40	73	32	0.30
Mean	29.9	66.6	23	0.31
*Crustal Mean	31	63	27	-

*Crustal Mean value is based on Rudnick and Gao (2014)

The content of selected proxies, Ce, La, Nd, and TOC has remained high in EPL7 depicting oxygen reduction (Figure 4.9). In EPL6, the concentration of Ce, La, Nd, and TOC has reduced markedly suggesting increased oxygen availability and hence the oxic environment.

Nevertheless, all the proxies have exhibited a rise in EPL5 suggesting the development of anoxia during the sedimentation. In EPL4, lower concentration of Ce, La, Nd, and TOC has pointed towards oxic environment of deposition. A marginal increase in REEs and TOC has been marked in EPL3, which can be attributed to oxygen reduction. In EPL2, all the REEs have depleted again suggesting enrichment of oxygen. Ce and Nd have declined further in EPL1 along with TOC, depicting an increase in oxygen availability.

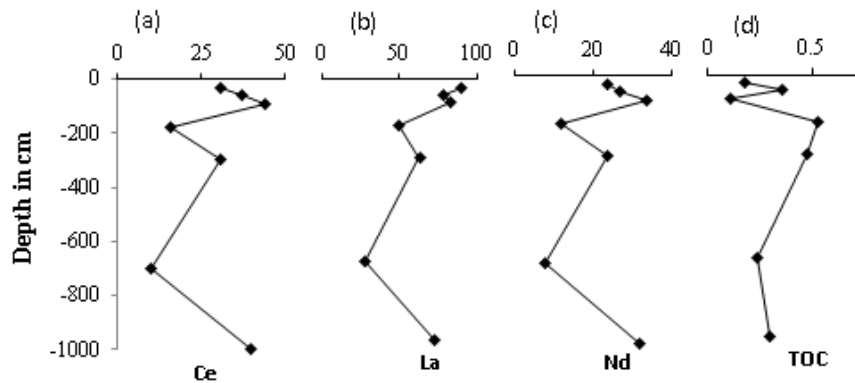


Figure 4.9 Variability of selected REEs (ppm) and TOC (%) in facies of Ezapur

Jhumpuri (JP)

The concentration of Ce has deviated from 10 ppm in JPL4 to 53 ppm in JPL2 (Table 4.11). The average content of Ce has been 36.5 ppm, which is above the crustal mean. La has varied between 25 ppm in JPL4 and 108 ppm in JPL2 with a mean concentration of 70.2 ppm. The Nd content has deviated from 10 ppm in JPL4 and 39 ppm in JPL3 with an average distribution of 24 ppm. The REEs have remained relatively high in JPL1, JPL2, JPL3, JPL5, and JPL6. The concentration of TOC has deviated from 0.08% in JPL10 to 0.75% in JPL7. It has been comparatively high in JPL1, JPL5, JPL6, JPL7, JPL8, and JPL9.

The concentration of REEs and TOC has been relatively low in the bottom facies, shown as JPL11 and JPL10 depicting oxic environment of deposition (Figure 4.10). The selected proxies have revealed marginal variability up to JPL6 and JPL5 wherein their concentration has increased significantly suggesting oxygen reduction. In JPL4, a considerable decline has

occurred in all the selected REEs revealing an increase in oxygen availability. Higher content of Ce, La, and Nd in JPL3 has indicated oxygen reduction. During the deposition of JPL1, lower content of Ba, Ce, La, and Nd has indicated the existence of oxic conditions.

Table 4.11 Distribution of TOC and selected REEs in sub-surface facies of JP

Proxies/Facies	Ce	La	Nd	TOC
JPL1	50	84	31	0.33
JPL2	53	108	38	0.11
JPL3	49	101	39	0.06
JPL4	10	25	10	0.26
JPL5	45	84	30	0.63
JPL6	52	91	30	0.33
JPL7	38	64	19	0.75
JPL8	24	60	17	0.56
JPL9	35	60	22	0.54
JPL10	25	48	13	0.08
JPL11	20	47	15	0.09
Mean	36.5	70.2	24	0.34
*Crustal Mean	31	63	27	-

*Crustal Mean value is based on Rudnick and Gao (2014)

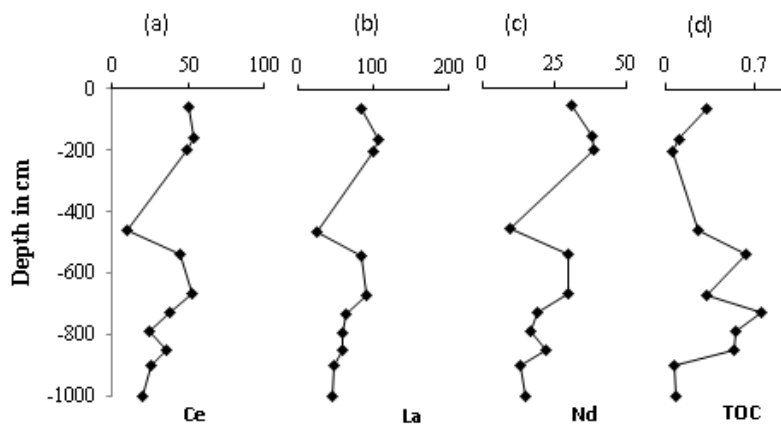


Figure 4.10 Variability of selected REEs (ppm) and TOC (in %) in facies of Jhumpuri Katia I (KTI)

The concentration of Ce has fluctuated from 69 ppm in KTIL2 to 97 ppm in KTIL3 with the average distribution of 88.3 ppm (Table 4.12). It has been above the crustal mean of 31 ppm (Rudnick and Gao, 2014) in all the facie. La has varied from 34 ppm in KTIL2 to 54 ppm in KTIL3. The concentration of Nd has remained between 24 ppm in KTIL2 and 35 ppm in KTIL3 with average content being 31 ppm. Concentration of TOC has varied from 0.24% in

KTIL5 to 0.59% in KTIL1. The distribution of Ce, La, Nd, and TOC has been relatively high in KTIL1, KTIL3, and KTIL4.

Table 4.12 Distribution of TOC and selected REEs in sub-surface facies of KTI

Proxies/Facies	Ce	La	Nd	TOC
KTIL1	95	52	35	0.59
KTIL2	69	34	24	0.26
KTIL3	97	54	35	0.42
KTIL4	96	48	32	0.51
KTIL5	84	50	33	0.24
Mean	88.2	47.6	31.8	0.40
*Crustal Mean	31	63	27	-

*Crustal Mean value is based on Rudnick and Gao (2014)

The selected REEs and TOC have remained almost unchanged between KTIL5 and KTIL4 depicting insignificant deviation in oxygen availability (Figure 4.11). However, these have shown a noticeable rise in KTIL4 and KTIL3 indicating the relative reduction in oxygen availability. The REEs and TOC have been low in suggesting a relative rise in the oxygen concentration. Opposite to this, in KTIL1 higher concentration of REEs and TOC can be associated with a comparative reduction in oxygen concentration.

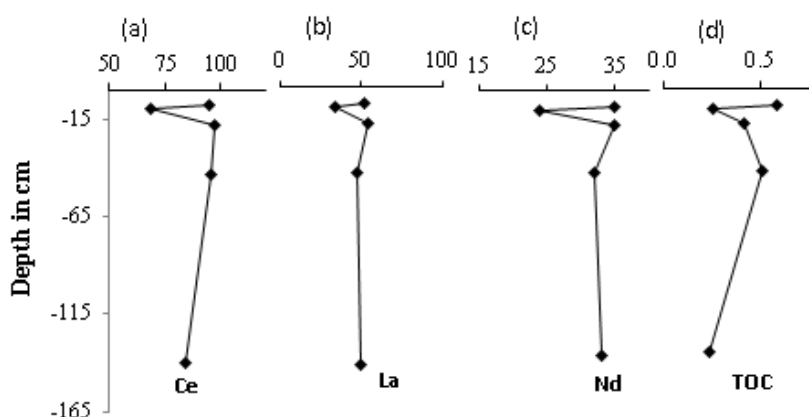


Figure 4.11 Variability of selected REEs in (ppm) and TOC (in %) in facies of Katia I

Katia II (KTII)

Ce content has varied between 60 ppm in KTIL3 and 187 ppm in KTIL5 with an average concentration of 91 ppm (Table 4.13). The distribution of La has fluctuated from 31 ppm in KTIL3 to 53 ppm in KTIL5 with average being 42.2 ppm. The concentration of Nd has

varied between 19 ppm in KTII2 and 38 ppm in KTII5 with a mean of 28.2 ppm. Distribution of TOC has remained between 0.08% in KTII6 and 1.38% in KTII3.

Table 4.13 Distribution of TOC and selected REEs in sub-surface facies of KTII

Proxies/facie	Ce	La	Nd	TOC
KTII1	88	47	31	0.50
KTII2	65	32	23	0.32
KTII3	60	31	19	0.20
KTII4	65	40	22	0.29
KTII5	187	53	38	1.38
KTII6	127	49	33	0.08
KTII7	74	45	31	1.28
KTII8	71	38	27	0.24
KTII9	82	45	30	0.15
Mean	91.0	42.2	28.2	0.49
*Crustal Mean	31	63	27	-

*Crustal Mean value is based on Rudnick and Gao (2014)

The selected REEs have remained low between KTII9 and KTII6 indicating an abundance of oxygen (Figure 4.12). In KTII5, a higher concentration in Ce, La, Nd, and TOC has suggested a relative reduction in oxygen availability during the deposition of this facie. Contrary to this, the concentration of REEs and TOC has declined in KTII4 pointing towards increased availability of oxygen. Another oxygen reduction phase has appeared in KTII1 as the content of Ce, La, Nd, and TOC have marginally increased.

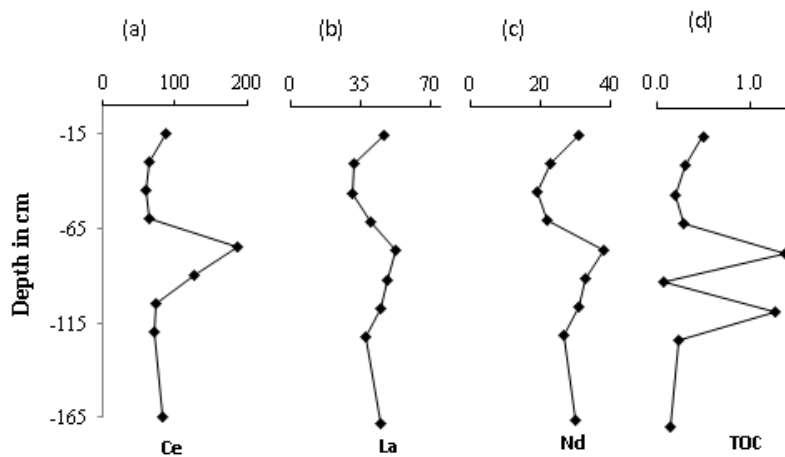


Figure 4.12 Variability of selected REEs (ppm) in facies of KTII

Therefore, based on the above analysis it can be stated that the selected REEs and TOC have indicated considerable variability in the oxygen availability during sediment deposition in

the Riverine Zone. In facies with relatively lower oxygen concentrations, the concentration of TOC has been relatively high. This has indicated the influence of organic matter on the reduced availability of oxygen.

4.3.2.2 Mixing Zone

Sonpanki (SP)

The concentration of Ce has shown large variations from 29 ppm in SPL6 to 104 ppm in SPL3 with a mean concentration of 83.5 ppm (Table 4.14). It has always remained above the crustal mean of 31 ppm (Rudnick and Gao, 2014). The concentration of La has varied between 7 ppm in SPL6 to 55 ppm in SPL3 with an average of 40.8 ppm. The Nd has deviated between 6 ppm in SPL6 and 38 ppm in SPL3 with mean value remaining 29 ppm. TOC content has deviated from 0.33% in SPL2 to 1.16% in SPL3.

Table 4.14 Distribution of TOC and selected REEs in sub-surface facies of SP

Proxies/Facies	Ce	La	Nd	TOC
SPL1	91	42	32	0.99
SPL2	94	50	33	0.33
SPL3	104	55	38	1.16
SPL4	95	49	34	0.71
SPL5	88	42	31	0.39
SPL6	29	07	06	0.42
Mean	83.5	40.8	29.0	0.7
*Crustal Mean	31	63	27	-

*Crustal Mean value is based on Rudnick and Gao (2014)

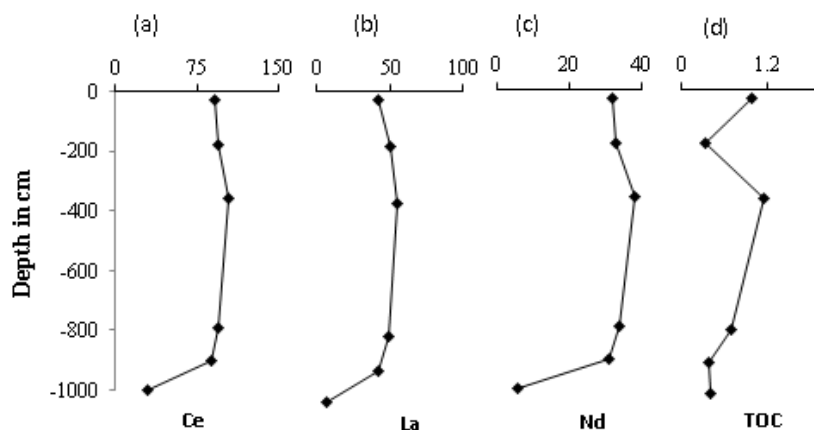


Figure 4.13 Variability of selected REEs (ppm) and TOC (%) in facies of SP

The concentration of all the selected REEs and TOC has been lower in SPL6 (Figure 4.13). Their relatively higher value in SPL5 and SPL4 has suggested a lower oxygen availability. However, in this facie the TOC content is relatively low in SPL5. The REEs along with TOC have increased considerably in SPL3 suggesting a reducing environment of deposition. Afterward, a marginal depletion has occurred in their concentration, which can be attributed to an increase in oxygen availability.

Chandbali (CB)

The concentration of Ce has fluctuated from 43 ppm in CBL1 to 87 ppm in CBL2 with an average distribution of 67 ppm (Table 4.15). La has varied from 17 ppm in CBL1 to 43 ppm in CBL2 with a mean value of 27.5 ppm. The concentration of Nd has remained between 15 ppm in CBL1 to 34 ppm in CBL2 with an average being 22.8 ppm. The concentration of TOC has varied remarkably in CB. It has fluctuated from 0.06% in CBL6 to 3.9% in CBL3.

Table 4.15 Distribution of TOC and selected REEs in sub-surface facies of CB

Proxies/Facies	Ce	La	Nd	TOC
CBL1	43	17	15	0.11
CBL2	87	43	34	0.65
CBL3	66	29	23	3.90
CBL4	82	32	25	0.56
CBL5	55	20	20	0.20
CBL6	69	24	20	0.06
Mean	67	28	23	0.9
*Crustal Mean	31	63	27	-

*Crustal Mean value is based on Rudnick and Gao (2014)

The concentration of Ce, La, and Nd has been relatively high in CBL6 indicating reduced availability of oxygen (Figure 4.14). In this facie, however, the TOC content has been low. A lower concentration of REEs and TOC has indicated increased oxygen availability in CBL5. Ce, La, Nd, and TOC have further enriched in CBL4 indicating oxygen reduction. In CBL3, the lower concentration of REEs has revealed enhanced oxygen availability. Nevertheless, in this facie, TOC has enriched considerably indicating a higher synthesis of organic carbon. The concentration of Ce, La, and Nd has increased in CBL2 suggesting lower oxygen availability. These have declined in CBL1 revealing increased oxygen

availability. It has been apparent, that unlike other locations the TOC has an inverse relationship with selected redox-sensitive REEs at this location.

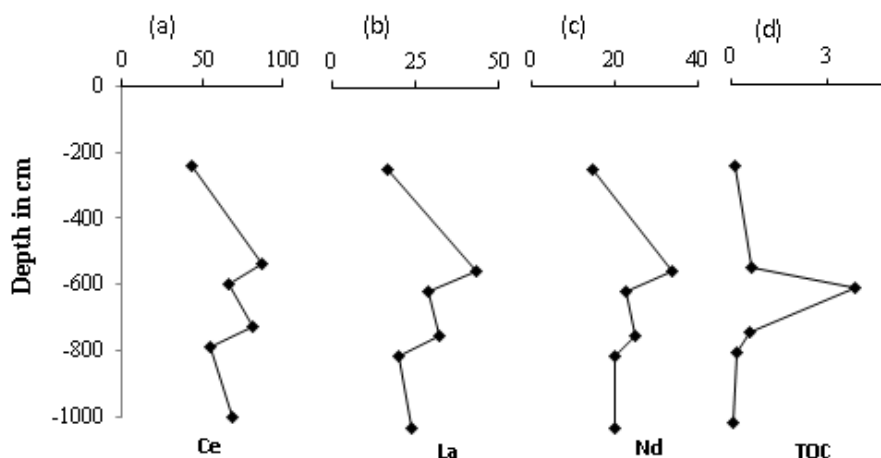


Figure 4.14 Variability of selected REEs (ppm) and TOC (%) in CB

Ambiligan (AG)

The concentration of Ce has fluctuated between 74 ppm in AGL5 and 103 ppm in AGL1 with mean being 91.8 ppm (Table 4.16). The La content has recorded between 34 ppm in AGL5 and 50 ppm in AGL2 with an average of 45.2 ppm. The distribution of Nd has varied between 28 ppm in AGL5 and 42 ppm in AGL1. The TOC has shown a marked deviation from 0.18% in AGL1 to 6.6% in AGL4.

Table 4.16 Distribution of TOC and selected REEs in sub-surface facies of AG

Proxies/Facie	Ce	La	Nd	TOC
AGL1	103	49	42	0.18
AGL2	96	50	36	1.65
AGL3	93	46	34	1.68
AGL4	93	47	35	6.6
AGL5	74	34	28	1.02
Mean	91.8	45.2	35	2.2
*Crustal Mean	31	63	27	-

*Crustal Mean value is based on Rudnick and Gao (2014)

Distribution of the selected REEs and TOC has been low in AGL5 suggesting higher availability of oxygen (Figure 4.15). In succeeding facie (AGL4) a higher concentration of REEs and TOC has indicated a reducing depositional environment. In AGL3, relatively

lower concentration of REEs and TOC have suggested a rise in oxygen concentration. In AGL2 and AGL1, the indicators have not shown remarkable variation.

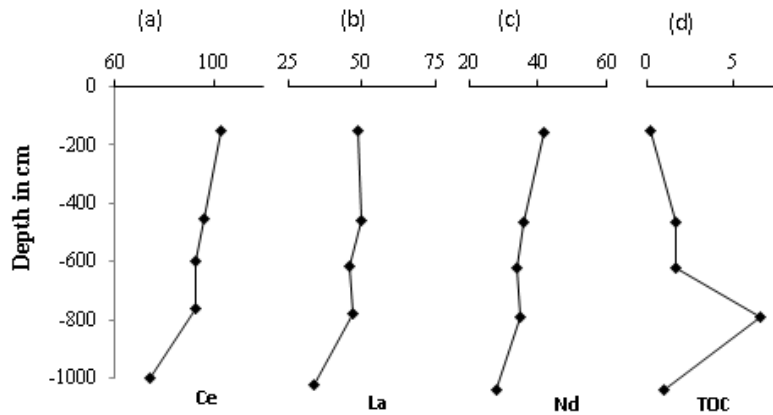


Figure 4.15 Variability of selected REEs (ppm) and TOC (%) in AG

Kasturikaran (KK)

The distribution of Ce has varied from 71 ppm in KKL3 to 95 ppm in KKL1 with the average being 84.8 ppm (Table 4.17). The concentration of La has deviated between 32 ppm in KKL3 and 50 ppm in KKL1 with mean concentration being 41.5 ppm. Nd has fluctuated from 26 ppm in KKL3 to 35 ppm in KKL1 and KKL2. The concentration of TOC has remained between 0.08% in KKL3 and 0.53% in KKL2.

Table 4.17 Distribution of TOC and selected REEs in sub-surface facies of KK

Proxies/Facies	Ce	La	Nd	TOC
KKL1	95	50	35	0.33
KKL2	92	46	35	0.53
KKL3	71	32	26	0.08
KKL4	81	38	27	0.50
Mean	84.8	41.5	30.8	0.40
*Crustal Mean	31	63	27	-

*Crustal Mean value is based on Rudnick and Gao (2014)

The selected REEs and TOC have been relatively high in KKL4 suggesting a reducing depositional environment (Figure 4.16). In KKL3, the REEs have declined along with TOC indicating a relative increase in oxygen availability and hence, oxic environment. In KKL2,

Ce, La, Nd, and TOC have increased revealing reduced oxygen availability. These have remained almost unchanged in KKL1.

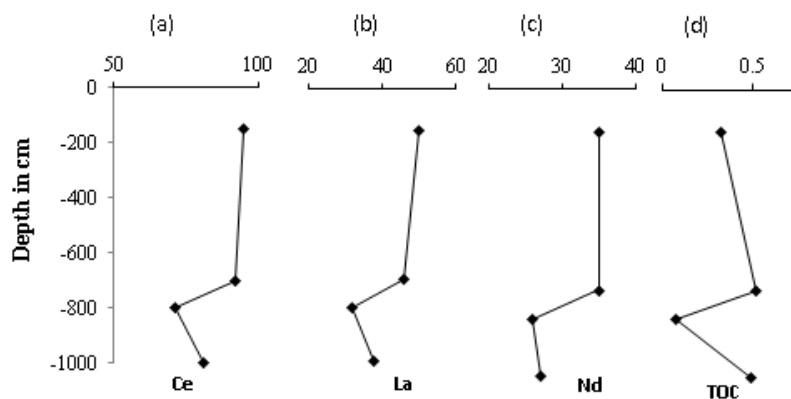


Figure 4.16 Variability of selected REEs (ppm) and TOC (%) in KK

Therefore, the selected redox-sensitive REEs have shown considerable variability in the Mixing Zone. They have suggested sediment accumulation under both oxic and reducing conditions. The analysis has also revealed a strong relationship between organic carbon production and the concentration of REEs as the facies with relatively high TOC concentration have been marked with relatively higher REEs content.

4.3.3 Correlation between TOC and Elemental Ratios

4.3.3.1 Riverine Zone

The influence of TOC on the concentration of REEs has already been analysed in the previous segment (4.3.4). It has been observed that the concentration of organic carbon has considerable influence on REEs concentration across the facies. As discussed before, organic matters consume the available oxygen and result in the development of anoxia. Thus, here the relationship between TOC and selected redox-sensitive ratios has been analysed to examine the impact of down-core variability of TOC on the ratios of V/Cr, V/Al, Fe/Al, and Cu/Zn.

Ezapur (EP)

The change in the concentration of TOC has influenced the ratios of V/Cr (Figure 4.17a). It has indicated that a higher ratio of V/Cr has a negative association with TOC concentration whereas a decline in TOC has been linked with an increasing value of V/Cr. Similarly, a

higher concentration of TOC has manifested into a declining ratio of V/Al (Figure 4.17b). Hence, the ratio of V/Al has also been negatively associated with TOC. In contrast, the ratios of Fe/Al and Cu/Zn have shown a strong influence of TOC concentration (Figure 4.17c and d). Therefore, the variation in TOC content has affected the ratios of Fe/Al and Cu/Zn across the stratigraphic sequences.

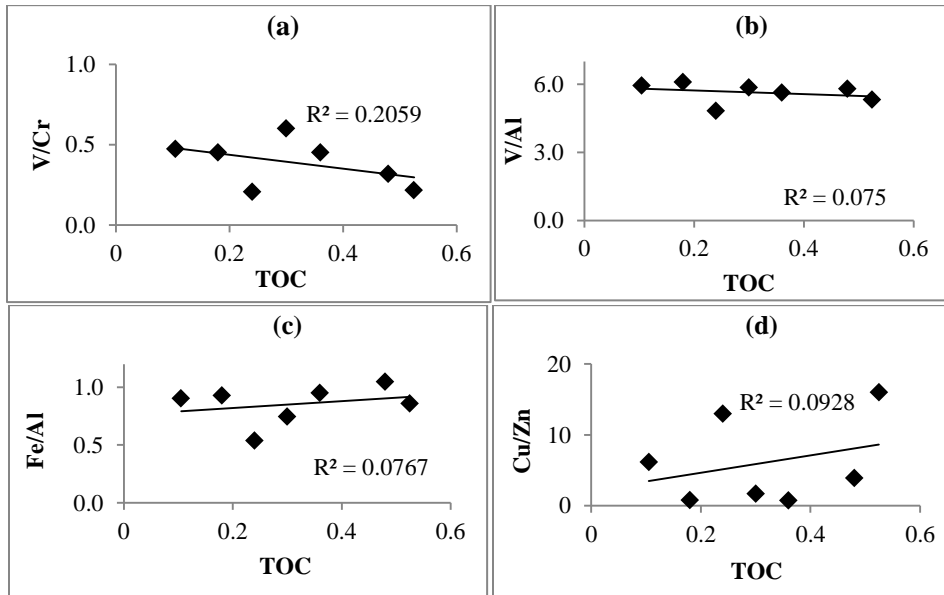


Figure 4.17 Correlation of between TOC and (a) V/Cr, b) V/Al (c) Fe/Al, (d) Cu/Zn at Ezapur site

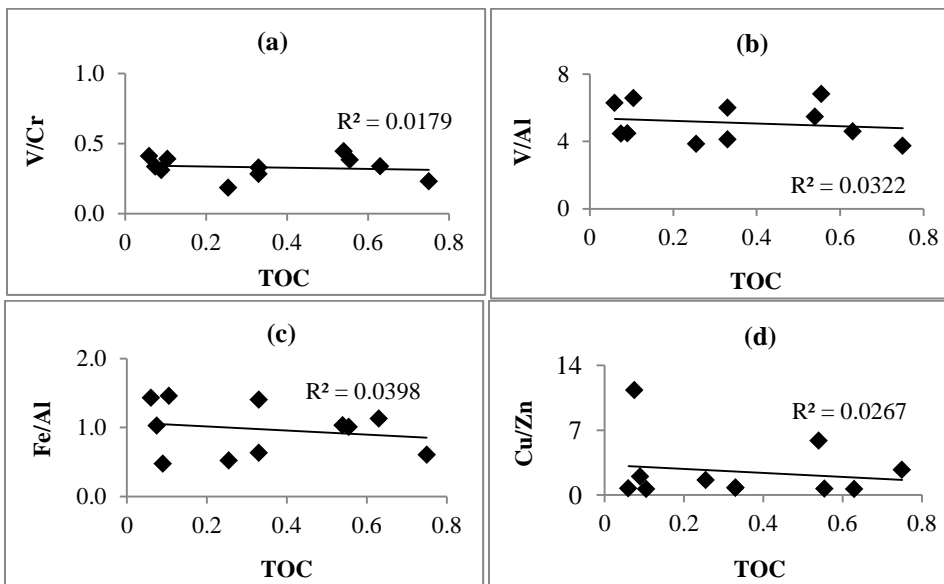


Figure 4.18 Correlation of between TOC and (a) V/Cr, b) V/Al (c) Fe/Al, (d) Cu/Zn at Jhumpuri site

Jhumpuri (JP)

The ratios of V/Cr, V/Al, Fe/Al, and Cu/Zn have not exhibited any correlation with the distribution of TOC (Figure 4.18a, b, c, and d). Thus, these ratios have not been affected by the increased availability of TOC at this location.

Katia I (KTI)

In contrast to the previous locations, the variation of TOC has influenced the ratios of V/Cr and V/Al (Figure 4.19a and b). It can be inferred that at the KTI site, the higher ratios of V/Cr and V/Al have been driven by an increase in TOC content. On the contrary, Fe/Al and Cu/Zn have not been affected by the TOC distribution (Figure 4.19c and d). Hence, at the KTI site, the TOC has only influenced V/Cr ratio.

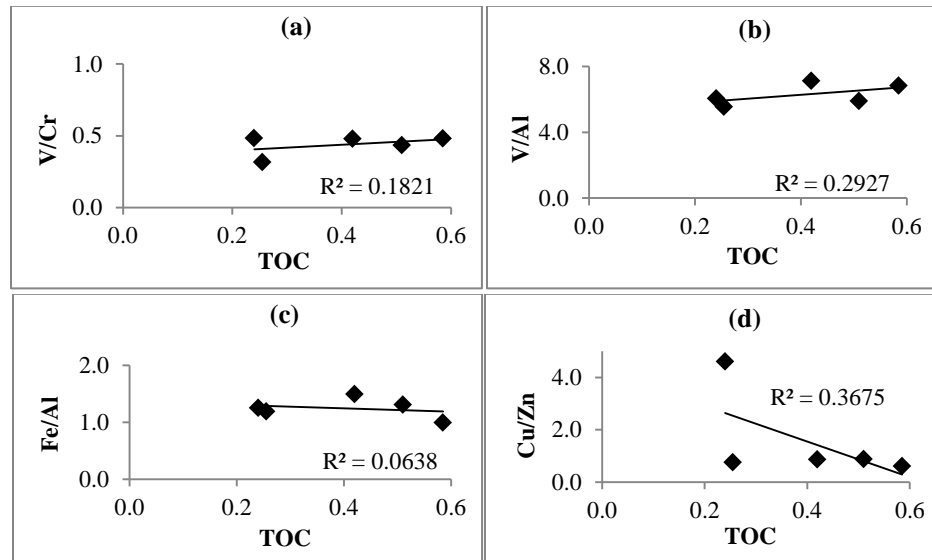


Figure 4.19 Correlation of between TOC and (a) V/Cr, b) V/Al (c) Fe/Al, (d) Cu/Zn at Katia I site

Katia II (KTII)

At this site, similarly, the TOC has shown a positive influence on the ratios of V/Cr and V/Al (Figure 4.20a and b). Among these, V/Cr has shown a strong positive correlation with TOC. On the other hand, the Fe/Al and Cu/Zn have revealed a negative influence of TOC distribution (Figure 4.20c and d). Hence, it can be elucidated that an increase in TOC content has resulted in the higher ratio of V/Cr and V/Al whereas Fe/Al and Cu/Zn have lower ratios in the facies with higher carbon concentration.

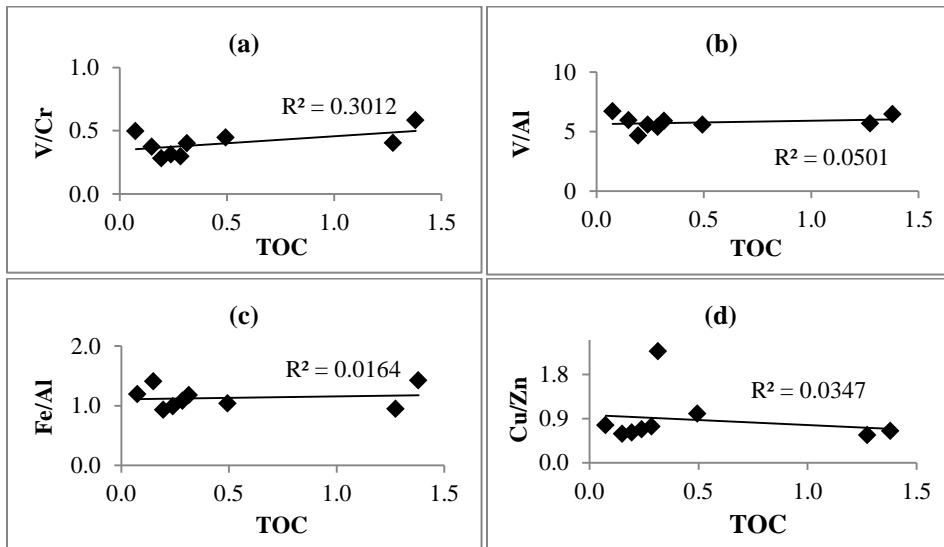


Figure 4.20 Correlation of between TOC and (a) V/Cr, b) V/Al (c) Fe/Al, (d) Cu/Zn at Katia II site

4.3.3.2 Mixing Zone Sonpanki (SP)

The influence of TOC distribution has a lesser influence on V/Cr ratio at this location (Figure 4.21a). However, the ratio of V/Al has shown a positive association with TOC concentration (Figure 4.21b). TOC content has also influenced the value of Fe/Al (Figure 4.21c). Hence, facies with higher TOC has exhibited a higher ratio of Fe/Al. In contrast, facies with higher TOC concentration have shown a lower Cu/Zn ratio (Figure 4.21d). It has suggested that TOC has influenced the ratios of V/Cr, V/Al, and Fe/Al.

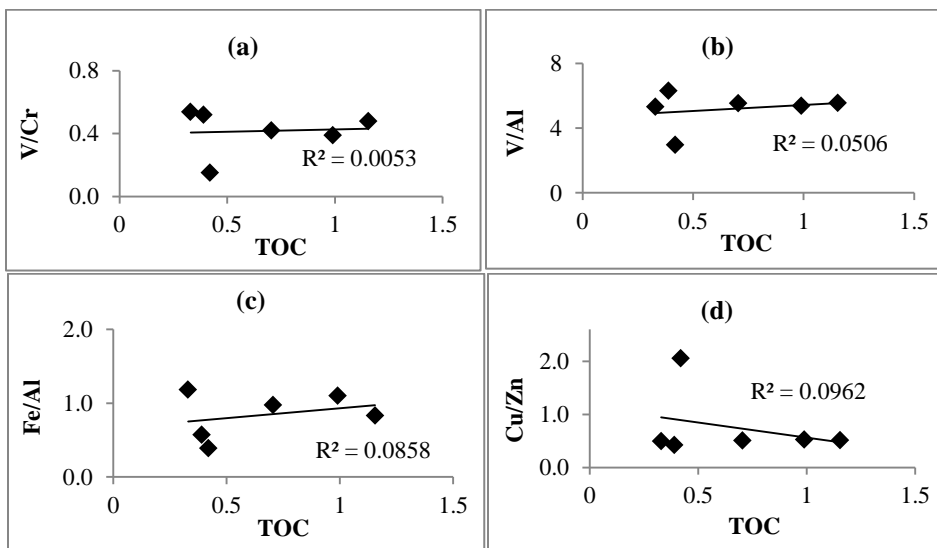


Figure 4.21 Correlation of between TOC and (a) V/Cr, b) V/Al (c) Fe/Al, (d) Cu/Zn at Sonpanki site

Chandbali (CB)

The distribution of TOC has no considerable influence on the distribution of V/Cr at CB site (Figure 4.22a). Nevertheless, the ratio of V/Al has shown a strong correlation with TOC (Figure 4.22b). TOC has been negatively associated with Fe/Al (Figure 4.22c). hence, the facies with higher Fe/Al ratio has lesser TOC concentration. However, TOC has influenced the ratio of Cu/Zn. Therefore, it has become clear that TOC concentration has only influenced the Cu/Zn ratio.

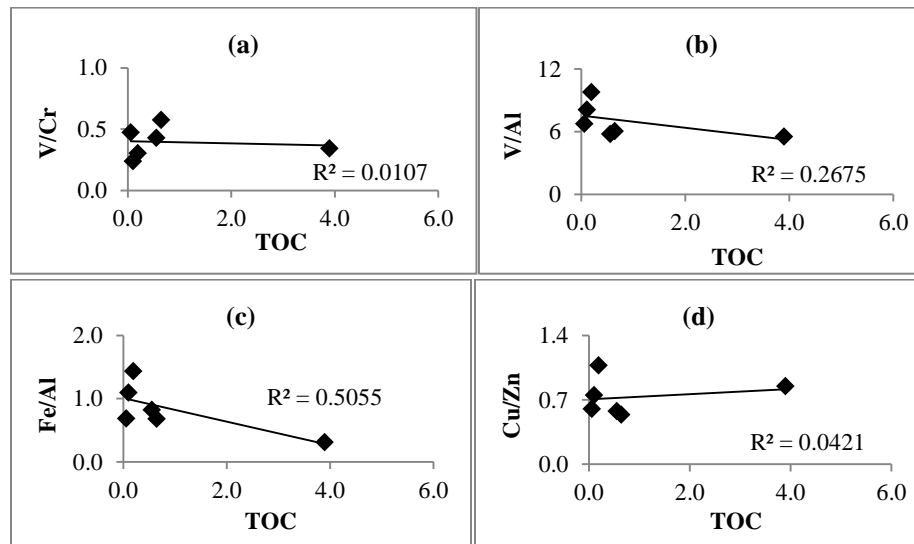


Figure 4.22 Correlation of between TOC and (a) V/Cr, b) V/Al (c) Fe/Al, (d) Cu/Zn at Chandbali site

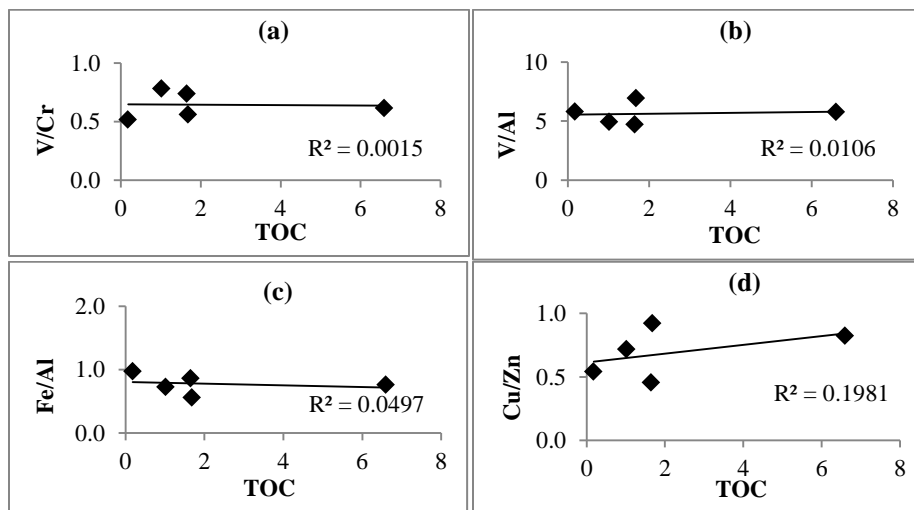


Figure 4.23 Correlation of between TOC and (a) V/Cr, b) V/Al (c) Fe/Al, (d) Cu/Zn at Ambiligan site

Ambiligan (AG)

The concentration of TOC has no considerable influence on the ratio of V/Cr at this site (Figure 4.23a). However, V/Al has been affected by the distribution of TOC across the facies (Figure 4.23b). TOC has shown a strong influence on the ratio of Cu/Zn at this site (Figure 4.23c). Thus, it has become apparent that the concentration of TOC has influenced the ratios of V/Al and Cu/Zn.

Kasturikaran (KK)

The TOC has strongly influenced the ratio of V/Cr (Figure 4.24a). However, it has no influence on the V/Al ratio (Figure 4.24b). The ratio of V/Al has been affected by the distribution of TOC while Cu/Zn has shown no association with TOC content at this location (Figure 4.24c and d). Thus, it can be stated that the distribution of TOC has influenced the ratios of V/Cr and Fe/Al across the stratigraphic sequences.

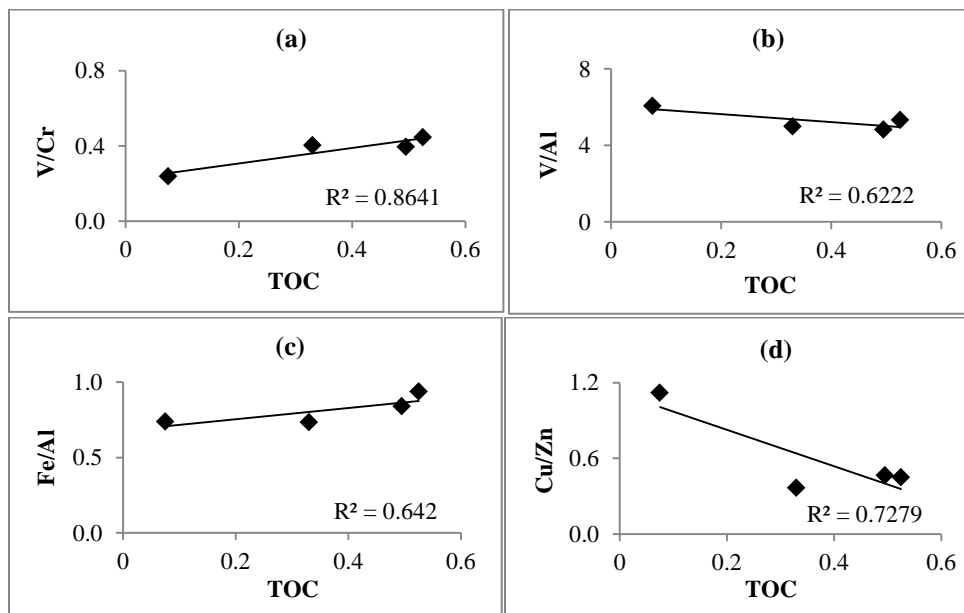


Figure 4.24 Correlation between TOC and (a) V/Cr, b) V/Al (c) Fe/Al, (d) Cu/Zn at Kasturikaran site

Therefore, it has become obvious that the selected ratios have been influenced by the TOC concentration at some of the locations of Riverine and Mixing Zone. However, there has not emerged any consistency in their association with TOC. For instance, TOC has affected V/Cr ratio at KTI, KTII, and KK which is absent at other locations. Similarly, the ratio of V/Al has shown the influence of TOC at KTI, KTII, SP, and AG. Subsequently, the

distribution of TOC has been associated with Fe/Al at EP, SP, and KK. The ratio of Cu/Zn has exhibited a correlation with TOC concentration at EP, CB, and AG locations. Thus, the reducing environment suggested by the Cu/Zn ratio might be the outcome of higher TOC concentration that results in the removal of oxygen.

4.4 Discussion and Conclusion

In this chapter, the analysis of palaeoredox conditions has been carried on the basis of selected palaeoredox proxies. These proxies include trace and REEs i.e. V, Cr, Co, Cu, Zn, Ce, La, Nd. Furthermore, along with these metals the concentration of TOC and the ratios of V/Cr, V/Al, Fe/Al, Cu/Zn were also analysed to distinct between oxic and anoxic environment. The variability of V has been analysed along with Al₂O₃, which is one of the most crucial detrital tracers (Taylor, et al., 2011), and Cr. The selected elements and ratios have been extensively utilized to analyse the palaeoredox conditions (Poulichet et al., 1997; Tribovillard et al., 2006; Coynel et al., 2016; Goldberg and Humayun, 2016; Cole et al., 2017; Kumar et al., 2017; Eltom et al., 2018). The V/Cr ratio is the most commonly used indicator of palaeoredox conditions (Ernst, 1970; Bjorlykke, 1974; Dill et al., 1988; Jones and Manning, 1994; Nagarjan, 2007; Madhavraju et al., 2016). The V/Cr ratio above two is considered as the representative of anoxic conditions while the ratio below two suggests oxic depositional environment (Ernst, 1970; Dill et al., 1988; Madhavraju et al., 2016).

An increase in the concentration of selected trace elements and REEs has depicted a relative reduction in the oxygen availability while their lower content has been associated with anoxic environment of deposition. In this study, however, the ratio of V/Cr has remained below two (<2) in both riverine and mixing zones. The value of V/Cr, hence, has indicated an abundance of oxygen during the aggradation of all the facies. A higher ratio of V/Al is also attributed to the reducing environment (Lyons and Severmann, 2006; Cole et al., 2017). In this study, similar to V/Cr, the ratio of V/Al has always remained below the crustal mean. Thus, it has also suggested a prevalent oxic depositional setting.

The Fe/Al ratio, contrary to this, has illustrated occurrence of anoxic environment during the deposition of most of the facies. This ratio is low only in SPL6 and CBL3, indicating sedimentation under oxic conditions. However, it is quite complicated to utilize Fe as a redox proxy. It is usually presumed that under reducing conditions Fe concentration

increases due to scavenging of iron. It is generally believed that Fe/Al ratios could help resolve this confusion by unravelling enrichment in comparison to the crustal mean (Lyons and Severmann, 2006; Cole et al., 2017). Therefore, the ratios of V/Cr, V/Al and Fe/Al are not reliable redox indicators in present scenario.

The ratio of Cu/Zn is also significant indicator of palaeoredox environment. The ratio above two (>2) is generally associated with reducing conditions (Hallberg, 1976). In this analysis, the ratio of Cu/Zn has suggested existence of anoxic conditions during the deposition of EPL3, EPL4, EPL5, JPL7, JPL9, JPL10, JPL11, KTIL5 and KTIL2 in the riverine zone. In the mixing zone, reducing condition has been marked in SPL6 while at other locations Cu/Zn ratio has indicated oxic environment of deposition.

The selected REEs indicate anoxic conditions during the aggradation of EPL3, EPL7, JPL2, JPL3, JPL6, KTIL1, KTIL3, KTIL4, KTIL1, KTIL5 and KTIL6 in the riverine zone. In the mixing zone, these have demonstrated reducing environment in SPL1, SPL2, SPL3, SPL4, CBL2, AGL1, AGL2, AGL3, AGL4, KKL1, and KKL2.

As mentioned earlier, a higher concentration of TOC can also develop anoxia due to higher oxygen consumption. In the riverine zone, TOC content is relatively high in EPL4, JPL5, JPL7, JPL8, JPL9, KTIL1, KTIL4, KTIL1, KTIL5 and KTIL7 depicting lower oxygen concentration. In the mixing zone, higher TOC concentration is recorded in SPL1, SPL3, SPL4, CBL2, CBL3, CBL4, AGL2, AGL3, AGL4, AGL5, KKL2, and KKL4 indicating reducing environment during their deposition.

The above discussion suggests that in this study the dependable redox-sensitive indicators are Cu/Zn, REEs and TOC. However, it is crucial to note that the availability, as well as the mobility of elements in sediment sequences, can be reduced or enhanced due to the chemical and biological processes that begin to operate as soon as the sediments are deposited. These include detrital input, depositional environment, and diagenic conditions. The elements can also reduce due to the formation of sulphide under anoxic conditions. Contrary to this, increasing salinity may promote the concentration of elements.

The determination of palaeoredox environment, therefore, should be based on the combination of indicators. While assessing oxygen reduction scenarios, other indicators

such as colour of the sub-surface sediment sequence and TOC concentration should also be incorporated. In this regard, as discussed in the previous chapter (Chapter 2), the darker colours i.e. black and dark gray with higher TOC and REEs content can be associated with reducing environment. The black colour of the sediment sequences indicates lower oxygen availability due to impartial oxidation of carbon during the deposition (Jacobsson et al., 2000; Sayem et al., 2018). Similarly, dark gray colour in deeper layers suggests reducing environment during sediment deposition (Jacobsson et al., 2000). Black and dark gray colours were observed in JPL4, JPL5, JPL6, JPL7, KTIL2, KTIL5, KTIL2, KTIL5 and KTIL9 in the Riverine Zone. In the Mixing Zone, the black and dark gray colours have appeared in SPL4, SPL5, CBL1, CBL2, CBL3, CBL4, CBL5, AGL1, AGL3, AGL4, AGL5, KKL3 and KKL4. Thus, based on the colour scheme, these facies can be linked with anoxic environment. On the other hand, the facies with red and brown colour can be associated with oxic depositional environment.

Therefore, based on the above discussion it can be concluded that the redox-sensitive elements (basically TOC, Cu/Zn, and REEs) have indicated considerable deviation in the oxygen concentration during sediment accumulation. Other proxies i.e. V/Cr, V/Al and Fe/Al have not exhibited any consistency and hence, that cannot be used as the indicators of oxic and anoxic conditions in this study. Finally, by combining the Cu/Zn ratio, REEs, TOC, and sediment colour, the aggradation of EPL4, JPL5, JPL7, JPL8, and KTIL5 of the riverine zone and SPL1, SPL3, CBL2, AGL3, AGL4, KKL2 of mixing zone has been associated with reducing environment, hence suggesting anoxic conditions during their deposition.

Chapter 5

Chronology of Landforms

5.1 Introduction

The coastal landforms are the products of the coastal processes caused by climatic variations, sea level oscillations and tectonics (Lalbiakzuali et al., 2013; Limaye et al., 2017). The coasts are considered to be carved out during the Quaternary (Allu and Priju, 2006). Since the mid-Holocene, the regional perturbations in sea level have brought profound changes to the coastal configuration and associated landforms. Each cycle of sea level fluctuation during the Holocene has resulted in the gain or loss of land surface (Table 5.1).

Table 5.1 Reconstruction of sea level changes in the Indian Ocean region during the Holocene

Holocene Sea-rise	Sea Retreat	References	Region	Reconstruction Techniques	Type of Sample
6000 yr BP	2,500 yr BP	Banerjee (1993)	South India	14C dating	Peat, geological Records
7,300 cal yr BP	2,500 cal yr BP	Banerjee (2000)	East Coast of India	U/Th dating	Corals and shell
9,000 cal yr BP	1,800 cal yr BP	Hameed et al. (2006)	South India	14C dating	Shell, organic matter
7,000 cal yr BP	2,500 cal yr BP	Hashmi et al. (1995)	Western India	14 C dating	Wood, sediment, shell, and limestone
7,000 cal yr BP	NA	Islam and Tooley (1999)	Bangladesh	14C dating	Pollen
7,900 cal yr BP	2,500 cal yr BP	Khandelwal et al. (2008)	East Coast of India (Chilika Lake)	14C dating	Pollen
10,900-8.800 cal yr BP	NA	Rao et al. (2015)	East Coast of India	14 C dating	Shell, plants
11000-7000 yr BP	7000-5000 yr BP	Narayana et al. (2017)	South-west coast of India	14 C dating	Pollen
5600 yr BP	11000 yr BP	Jayagondaperu mal et al. (2012)	South-east coast of India	OSL dating	Sediments

The freshwater-saltwater interface was pushed landward during transgression (Khandelwal et al., 2008). On the other hand, during regression, this interface was shifted seaward. Due to this shift, the predominant geomorphic processes were also modified from fluvial to marine and vice-versa. Along with this, intensification and weakening of monsoon rainfall that is reported during the Holocene (Basavaiah and Khadkikar, 2004; Limaye et al., 2014; Banerji et al., 2017; Limaye et al., 2017; Band et al., 2018; Kumaran et al., 2018) also influences

landforms aggradation in coastal areas (Table 5.2). The episode of enhanced monsoon manifested into elevated river discharge whereas weak monsoon causes a reduction in river flow. These clues are archived in the coastal sedimentary deposits and landforms. By examining the response of the sedimentary environment to the predominant geomorphic process, the climatic and eustatic perturbations can be inferred (Gao et al., 2007; Mial, 1985; Resmi et al., 2017). Therefore, the chronological inspection of sedimentary archives provides crucial clues to the Holocene climate and sea level changes.

Table 5.2 Palaeomonsoon reconstruction in Indian sub-continent during the Holocene

Enhanced Monsoon	Weak monsoon	References	Region	Dating technique	Type of sample
8500-6500 yr BP	6500-5600 yr BP	Band et al., 2018	Central India	²³⁰ Th dating	Stalagmite
9000-6000 cal yr BP	6000 cal yr BP	Limaye et al., 2017	South-west India	¹⁴ C dating	Pollen, sediments
5800-4300 yr BP	3200-1800 yr BP	Tripathi et al., 2014	Western Odisha	¹⁴ C dating	Sediments
7200-3800 yr BP	3500 yr BP	Limaye et al., 2014	South-west coast	¹⁴ C, OSL dating	Shell, sediments
2000 yr BP	3000-2000 yr BP	Farooqui and Naidu, 2010	South-east coast	¹⁴ C dating	Sediments, pollen

Furthermore, the construction of chronology is crucial to understand the evolutionary history of landforms and the exact timing of sediment aggradation. It is also required for correlating diverse proxy evidence so that inferences about climate change can be tested. Earlier, palaeoclimate reconstruction was mainly based on examining the position of changes within the stratigraphic records for working out the relative episode of deposition. These relative methods were based on the ‘*law of superposition*’ which presumes that the sediments deposited at the bottom of the sedimentary sequence must have been deposited prior to those on the top of the stratigraphic sequence (Lowe and Walker, 1984). However, often these approaches led to imprecise information about the palaeoclimate as similar looking facies may not necessarily be deposited at the same time. A drastic change has been brought in the field of palaeoclimate studies by the development of radiocarbon dating (Roberts, 1998). This technique has applied independent assumptions about the stratigraphic relation of

events based on absolute age and thereby, global correlations have been drawn on a much steadier basis.

Radiocarbon or ^{14}C dating has evolved steadily since 1949 when it was first implied by Libby (Libby et al., 1955) providing a chronology for approximately the last 50,000 years. Earlier organic carbonates, wood, peat, bone, etc. were used. However, at present, it has been expanded for a wider range of material including soil carbonates. One of the problems associated with obtaining enough organic carbon for dating the chosen facie has been resolved by the invention of accelerator mass spectrometry (AMS) method of radiocarbon dating. In AMS ^{14}C dating $^{14}\text{C}/^{12}\text{C}$ ratio is directly measured for which required sample size is quite smaller (Vahila et al., 2016). It is also significant to make a distinction between 'radiocarbon years' and 'calendar years' as the correlation of results can be affected by using different radiocarbon dates. The age provided by radiocarbon dating is generally not corresponding with the real or calendar age derived from the dendrochronology (Roberts, 1998). This is because in the past substantial changes have occurred in the production of the atmospheric carbon (^{14}C). The temporal variability in atmospheric ^{14}C has been caused by changes in solar activity, geomagnetism, radiocarbon plateau, etc. (Roberts, 1998). By convention, dates are given in the years before present (BP) needs to be interpreted as raw, uncalibrated radiocarbon years. In contrast, dates expressed as 'cal BP' reflect calibrated radiocarbon age with the dates obtained from the dendrochronology. The BP is actually set at years before 1950 AD (Vahila et al., 2016).

The climatic conditions exert a powerful influence over geomorphic processes and landforms. However, not all landforms are harmoniously adjusted to the prevailing climate because some were produced in the past when climatic conditions were different (older beach ridges). The coastal landforms can be classified into a series of geomorphological regimes such as fluvial, marine and aeolian (Roberts, 1998), each with its own characteristic depositional environment (Table 5.3). Available information about the surface processes are applied to fossil landforms (palaeodelta, palaeochannel, relict beach ridge, etc.) and sediments, first to assign them a particular geomorphological regime, and secondly, to interpret their origin in terms of past processes and climate.

Table 5.3 Characteristics of geomorphic regimes along the coast

Geomorphic Regime	Sedimentation	Sediments	Landforms
Fluvial	Semi-continuous	River gravel	Palaeochannels
Coastal marine	Semi-continuous	Beach sand	Raised beach
Aeolian	Semi-continuous	Dune sand	Fossil dune

Based on Roberts, (1998).

The landforms identified in the study region include- floodplain, older beach deposits, and palaeochannels. In coastal areas, the energy of river flow declines greatly and hence the river changes its course frequently giving way to the palaeochannels. The sedimentation in palaeochannels is governed by both riverine and marine processes as through these channels the freshwater and seawater interact. Beach deposits can be formed slowly, mainly by multi-depositional events rather than in single events i.e. storm. These are constructed primarily by wave run-up from swell rather than the strong, storm waves (Narayana and Priju, 2006). One of the most usual prerequisites for beach deposits is onshore transport of sediment along with sufficient sediment supply (Morton et al., 1995). The older beach deposits may indicate the sea highstand in the past. However, anthropogenic influence cannot be ignored in the modification of landforms. In the area of study, agriculture and pisciculture are the most dominant economic activities which might modify and alter the existing landforms.

The present analysis is based on the reconstruction of landform chronology which is one of the major objectives of this research. During the review of literature, there has appeared a gap in the knowledge regarding the signatures of monsoon driven fluvial actions and tidal processes attributed to sea level changes that have influenced the formation of archives and their role in the evolution of coastal landforms. Physical characteristics and geochemistry of subsurface sediment deposits along with ^{14}C dates have been taken into account while distinguishing the significant aspects of sedimentation processes.

5.2 Methodology

To fulfill the objective, the study area was broadly delineated into the riverine and mixing zones (Chapter 1, Section 1.9). The major landforms were identified using satellite images, geological and geomorphic maps of Jajpur and Bhadrak districts of Odisha. In the mixing zone active floodplain (SP), older beach deposits (CB) and palaeochannels (AG and KK)

were recognized and samples were collected by digging 10 m deep bore-well at these locations. The chronology of landforms is constructed using AMS ^{14}C dating University Acceleration Centre (IUAC), New Delhi, India. The radiocarbon dates were obtained for the landforms of the mixing zone. It is significant to mention here, that samples recovered from the riverine zone could not be dated using AMS facility, as required percentage of organic matter ($>0.5\%$) for AMS ^{14}C dating was not available for most of the sites of the riverine zone. For instance, among 7 distinct facies of EP, only EPL4 has carbon content around 0.5%. Similarly, amongst 11 facies of JP, only JPL5, JPL7 and JPL8 have required carbon concentration. Therefore, no sample from EP and JP was selected for the AMS ^{14}C dating. At the same time, KTI and KTII were omitted from the analysis owing to their shallower depth. Apart from this, permission for dating only 12 samples was granted using the AMS facility at IUAC, New Delhi. Nevertheless, the chronology is constructed for all the landforms located in the mixing zone that have shown remarkable variation in their depositional environment.

The radiocarbon dates have been obtained in the following steps-

(a) Sample Preparation

The sediment samples selected for ^{14}C dating were kept in the oven at 50°C overnight. After they were dried completely, each sample was ground finely using pestle mortar. The wash tubes were cleaned using the tap water, soap solution, exile water, and MQ water and then properly dried. Then, the samples were kept in these tubes. To remove the contaminants having carbonaceous material of recent times, such as rootlets, dry leaves, etc. the samples were inspected under the microscope and then each of them was pre-treated using acid-base-acid (ABA) treatment.

ABA treatment is required to remove the impurities from sediment samples. For ABA treatment 2 g of sediment sample was mixed with 8 ml of Hydrochloric acid (HCl-0.5 m). This mixture was shaken well in the wash tube so that the entire sample gets immersed in the acid. Subsequently, this solution was kept in Thermoshaker at 60°C for about 8 hrs. Afterward, the solution was kept in the Centrifuge (3000 rpm for 3-5 min) to remove the acid from the samples. For this, the samples were washed using MQ water for 6 to 7 times until the pH becomes neutral (7).

Subsequent to neutralization, each of the samples was mixed with 6 ml of Sodium Hydroxide (NaOH-0.1 m) and kept in Thermoshaker for 3 hrs. The same procedure was repeated to neutralize each sample. Afterwards, the samples were again treated with Hydrochloric acid (HCl-0.5 m) in the same manner to remove absorbed CO₂. Following this, the samples were freeze-dried to make them ready for graphitization. The graphitized samples were used for AMS ¹⁴C dating.

(b) AMS ¹⁴C dating

Radiocarbon (¹⁴C) ages of four samples were determined using AMS ¹⁴C dating based on 500 kV Pelletron’s accelerator. AMS ¹⁴C ages were obtained for the sub-samples with carbon concentration above 0.5 %. The uncalibrated radiocarbon dates were converted into the calendar ages using OxCal 4.3 (Bronk and Lee, 2013; Bronk, 2017). In the figures, the median of the date range (2 σ date range) has been used while the analysis has been based on date ranges.

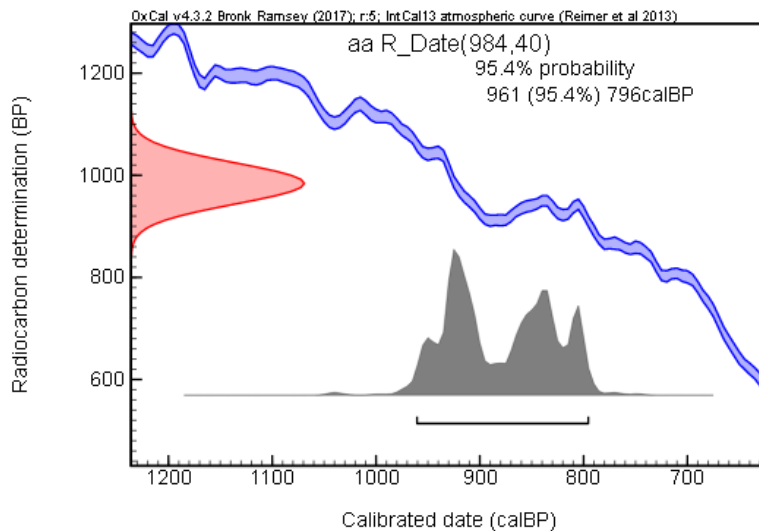


Figure 5.1 Calibration of radiocarbon dates using OxCal 4.3

Samples for ¹⁴C dating were collected from SP site at the depth of 800 cm, 350 cm and 30 cm providing age ranges (2 σ date range) of 1740-1541, 1415-1296 and 961-769 cal yr BP respectively. From CB location, samples from 750 cm, 550 cm, and 250 cm depth were recovered giving dates of 7764-7595, 7759-7575 and 4766-4615 cal yr BP (2σ date range). From AG site, samples from the depth of 1000 cm, 760 cm, 600 cm, and 450 cm yielded radiocarbon ages of 7790-7610, 7634-7469, 6283-6095 and 2851-2738 cal yr BP (2σ date

range). From KK, ^{14}C samples were obtained from 1000 cm and 700 cm depth providing dates of 7792-7608 and 2441-2301 cal yr BP (2σ date range). Further details regarding ^{14}C dates are listed in the following table (Table 5.2).

Table 5.4 Details of ^{14}C AMS dates from the organic content of sediment samples

Sample Id	Lab Id	Depth (cm)	^{14}C dates (yr BP)	Cal yr range (cal yr BP)	Median of the interval 2σ (cal yr BP)
SPL1	IUACD#18C1635	-30	984 \pm 40	961-796	882
SPL3	IUACD#18C1673	-350	1469 \pm 39	1415-1296	1356
SPL4	IUACD#18C1636	-800	1734 \pm 45	1740-1541	1647
CBL2	IUACD#18C1639	-550	4210 \pm 42	4766-4615	4736
CBL3	IUACD#18C1672	-600	6817 \pm 53	7759-7575	7652
CBL4	IUACD#18C1640	-750	6847 \pm 44	7764-7595	7677
AGL2	IUACD#18C1641	-450	2656 \pm 42	2851-2738	2773
AGL3	IUACD#18C1670	-600	5373 \pm 50	6283-6095	6174
AGL4	IUACD#18C1642	-760	6686 \pm 47	7634-7469	7555
AGL5	IUACD#18C1671	-1000	6858 \pm 44	7790-7610	7689
KKL2	IUACD#18C1637	-700	2316 \pm 40	2441-2301	2336
KKL4	IUACD#18C1638	-1000	6859 \pm 45	7792-7608	7690

Note:

- Measured results for all the samples are normalized to the standard sample OX II.
- Background value during the measurement was (0.455 \pm 0.018) pMC (Percentage modern carbon) and that corresponds to $^{14}\text{C}/^{12}\text{C}$ ratio (4.3543 \pm 0.168) $\times 10^{-15}$.
- Data quality is monitored with a secondary standard sample (IAEA-C8). Its consensus values (pMC = 15.03 \pm 0.17) was matching with its experimental result (pMC= 14.96 \pm 0.09) within the error.

5.3 Analysis

The response of each landform to climatic and sea level perturbation is distinct owing to their location and dominance of geomorphic processes, fluvial or marine. Even very similar facies could have been deposited during different time intervals while distinct facies in appearance could have been aggraded at the same event (Figure 5.2). Therefore, the depositional history of landforms has been discussed considering each landform as distinct units.

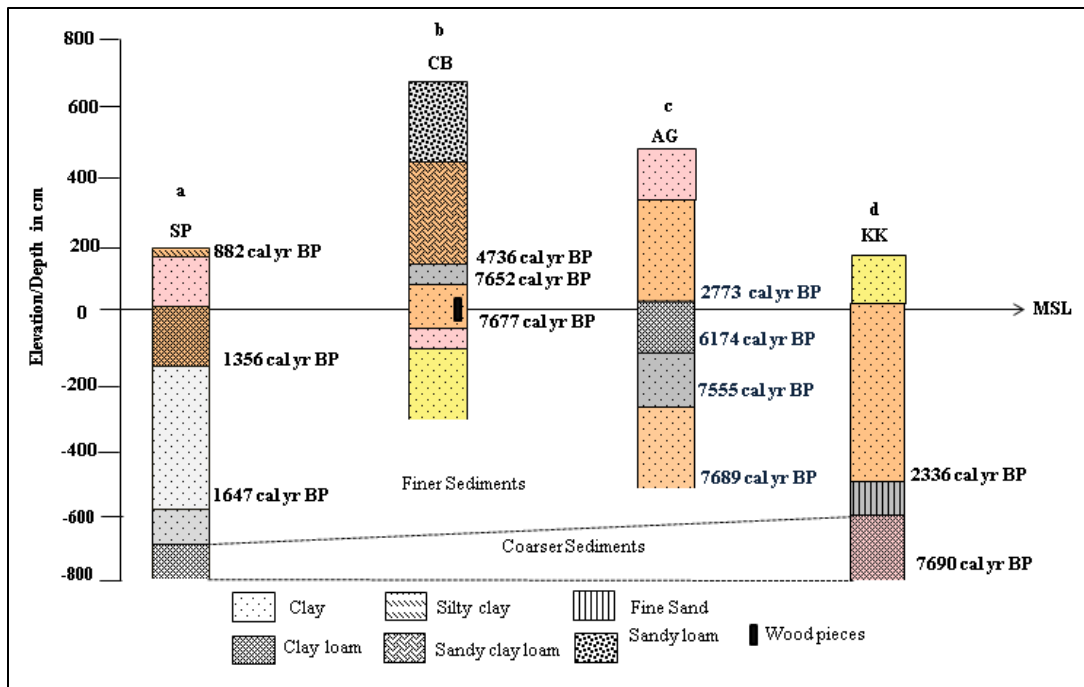


Figure 5.2 Stratigraphy and chronology of landforms (a) Active floodplain, (b) Older beach deposits, (c) Palaeochannel of AG and (d) palaeochannel of KK

Note: ^{14}C ages are shown as the median of the 2σ range in cal yr BP. The index is showing textural classes.

5.3.1 Chronology of the Active Floodplain (SP)

The SP sample is retrieved from the active floodplain located near the confluence of river Baitarani and Salnadi in Sonpanki village. At this site rich sediments mainly constituted of fine-grained clay, clay loam and sandy loam have been brought by the rivers. In recent times, the river bulges markedly during the high tide indicating the influence of tidal activity, nearly 31 km away from the Odisha coast. This also suggests that the sediment aggradation at this location has been influenced by both fluvial and marine processes. The deposits at the floodplain are more recent in comparison to the other landforms of the mixing zone. This characteristic might be attributed to its location near rivers that deposit rich sediments during heavy precipitation.

The lowermost sequence of the floodplain, SPL6 has a total thickness of about 100 cm (Figure 5.3). It was deposited prior to 1740-1541 cal yr BP (Table 5.4). The colour of SPL6 is grayish and the texture is relatively coarser. This has been categorized under the clay loam category. The higher concentration of coarser sediments has been associated with the high

energy of the river flow. A decline in the sea level has also been reported since 2500 cal yr BP in the Indian coast (Banerjee, 2000; Hameed et al., 2006; Khandelwal et al., 2008). This episode of enhanced river flow might have coincided with enhanced rainfall reported during around 2000 yr BP leading to enhanced weathering in the catchment region. The texture of the subsequent facie, SPL5 has changed to clay. It is also roughly 100 cm thick. The decline in coarser particles has indicated a reduction in the intensity of fluvial activity attributed to the decline in river flow. The SPL4 is remarkably thick facie (around 350 cm). It was deposited between 1740-1541 and 1415-1296 cal yr BP. The main constituent of this facie is also clay which has indicated the persistence of low intensity fluvial action and hence, low energy of river flow. Khandelwal et al. (2008) have also reported the existence of drier climate around 1600 cal yr BP in coastal Odisha. The succeeding facie SPL3 has a total thickness of approximately 200 cm. Its sedimentation has occurred during 1415-1296 cal yr BP (2 σ range). The clay loam texture of SPL3 has indicated a relative increase in the intensity of fluvial activity that can be attributed to enhanced river flow during its aggradation.

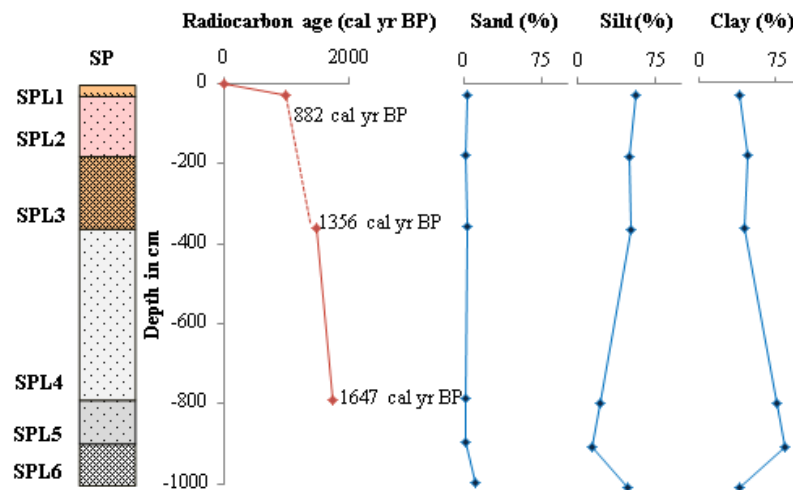


Figure 5.3 Lithostratigraph, age-depth curve and concentration of sand, silt and clay in the facies of active floodplain deposits collected from Sonpanki

Note: the radiocarbon ages are shown as the median of the ^{14}C age (2 σ range)

The SPL2 was deposited prior to 961-796 cal yr BP. The fine-grained clay is the predominant ingredient of this facie. The clayey texture has suggested a decline in the energy of fluvial activity. The surface sequence of the floodplain, SPL1 is 30 cm thick. Its

aggradation took place between 961-796 and the present. This sequence is dominated by silty clay which has demonstrated a relative increase in the energy of riverine processes that might have been caused by elevated river flow. The red and brown colours of SPL3, SPL2, and SPL1 have suggested that during their deposition mainly freshwater environment existed at this location. On the other hand, the grayish facies (SPL6, SPL5, and SPL4) has pointed towards the existence of damp, stagnated or high salinity conditions as these segments are located below the current sea level.

5.3.2 Chronology of the Older Beach Deposits

Older beach deposits are the markers of palaeo-shoreline depicting sea transgression that occurred in the past. These are supposed to be formed gradually by wave action (Allu and Priju, 2006). The CB was collected from the older beach ridge located at Chandbali village of Bhadrak. At present, it is approximately 24 km away from the. The elevation of this location is markedly high 700 cm MSL demonstrating a rise in relative height from the SP.

The CBL6 was deposited before 7677 cal yr BP most probably during the early-Holocene (Table 5.4). The total thickness of this facies is around 200 cm which is primarily clayey in nature indicating the dominance of riverine processes (Figure 5.4). The yellow colour of this facie has also indicated deposition under the freshwater environment. This episode of deposition might have coincided with the wetter period of the early-Holocene (Lezine, 1989). The thickness of the succeeding facie, CBL5 has declined markedly. It is also categorized as clay. However, the concentration of sand has increased in comparison to the CBL6. A higher concentration of coarser particles has been attributed to the elevated tidal action during sea regression as reported by Khandelwal et al. (2008) during 7900 cal yr BP. The CBL4 was accumulated between 7764-7595 and 7759-7575 cal yr BP. It is primarily constituted of fine gray clay which has been associated with the predominance of fluvial action during its deposition. This phase might have occurred during the enhanced monsoon that was experienced in the south-eastern coast around 8500-6500 yr BP (Band et al., 2018). The brownish colour has also depicted deposition through fluvial action. The aggradation of CBL3 took place between 7759-7575 and 4766-4615 cal yr BP. This is markedly thin indicating a considerable reduction in the sediment accumulation. This facie is also clayey suggesting the predominance of river action during its deposition. The black colour,

however, has indicated a swampy environment of deposition. This might have deposited during the transition phase when monsoon was weakening and tidal processes were strengthening. Some wood pieces were also collected from this facie giving it a black colour and higher content of TOC (Chapter 2 and 3).

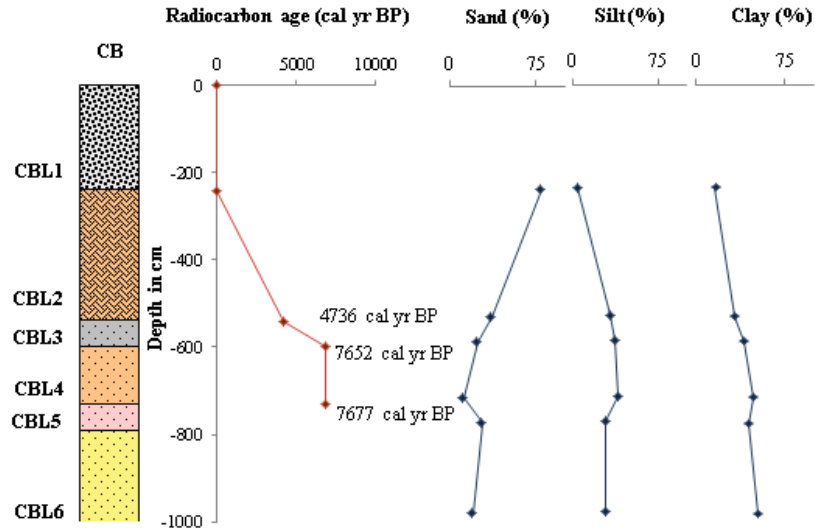


Figure 5.4 Lithostratigraph, age-depth curve and concentration of sand, silt and clay in the facies of active floodplain deposits collected from Chandbali

Note: the radiocarbon ages are shown as the median of the ^{14}C age (2σ range)

The succeeding facie, CBL2 was deposited after 4766-4615 cal yr BP. A surge in the concentration of coarser grains has indicated the predominance of marine processes. The percentage of coarser particles has declined in CBL1 revealing a relative reduction in tidal activity. This phase of sedimentation most probably has occurred during sea retreat as reported during 2500 cal yr BP in the eastern coast (Banerjee, 1993; Banerjee, 2000; Khandelwal et al., 2008). Most of the sequences i.e. CBL5, CBL4, CBL3, CBL2, and CBL1 are of gray and black colour illustrating prevalent swampy conditions during the sedimentation. This could have been due to its location in the transition zone that might have experienced cycles of sea transgression and regression.

5.3.3 Chronology of the Palaeochannels

Samples AG and KK were obtained from the palaeochannels of river Baitarani (Figure 5.5). These were located in Ambiligan and Kasturikaran villages of Bhadrak district very approximate to the Dhamra estuary (Chapter 1, area of study). AG is situated nearly 20 km

inland from the coast with a general elevation of 5 m above MSL showing a decline in the relative height from CB site.

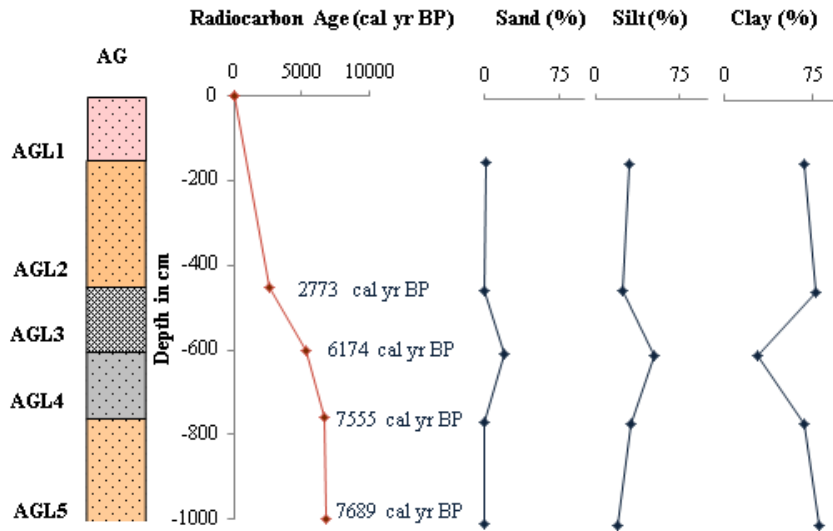


Figure 5.5 Lithostratigraph, age-depth curve and concentration of sand, silt and clay in the facies of active floodplain deposits collected from Ambiligan

Note: the radiocarbon ages are shown as the median of the ^{14}C age (2σ range)

The lower-most sequence of AG, represented as AGL5 has a total thickness of about 200 cm. This thick facie was deposited during 7790-7610 and 7634-7469 cal yr B.P (Figure 5.5, Table 5.4). This is aggraded by fine-grained clay suggesting deposition through fluvial processes. This phase might have coincided with elevated precipitation as reported by Band et al. (2018) in the south-eastern coast around 8500-6500 yr BP The brownish-gray colour has indicated stagnated and marshy depositional environment. The total thickness of AGL4 is approximately 150 cm. Its sedimentation has occurred during 7634-7469 and 6283-6095 cal yr BP (Table 5.4). Clay is the predominant constituent in both these sequences demonstrating deposition through fluvial action. The AGL3 has a thickness of nearly 150 cm. It was deposited between 6283-6095 and 2851-2738 cal yr BP. An increase in the concentration of coarser particles has illustrated a shift in the depositional environment from riverine to marine. This facie might have deposited before the sea regression that occurred since 2500 cal yr BP (Banerjee, 1999; Banerjee 2000; Khandelwal et a., 2008). The predominant gray colour of these sequences has indicated deposition under the stagnated conditions. The sedimentation of AGL2 began during 2851-2738 cal yr BP. This 250 cm

thick sequence is predominantly fine-grained clay suggesting deposition through fluvial processes. The reddish-brown colour has indicated the well oxidized fluvial environment during its deposition. The surface facie, represented as AGL1 is also clayey indicating the persistence of fluvial activity.

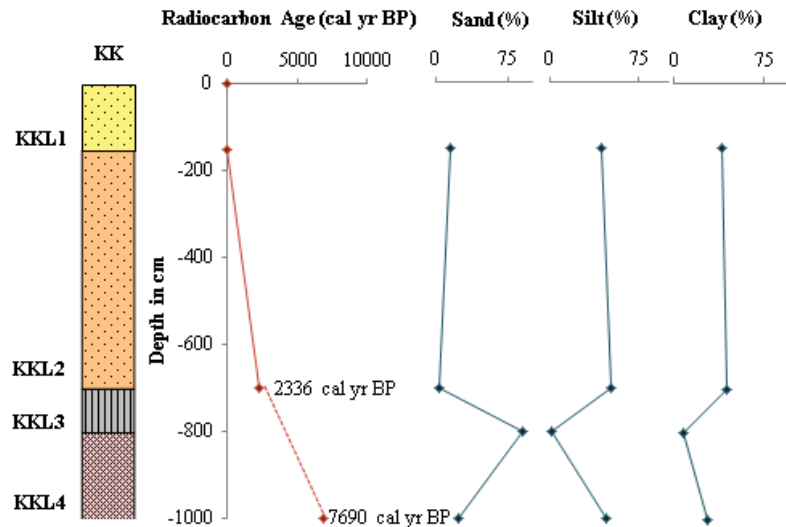


Figure 5.6 Lithostratigraph, age-depth curve and concentration of sand, silt and clay in the facies of active floodplain deposits collected from Kasturikaran

Note: the radiocarbon ages are shown as the median of the ^{14}C age (2σ range)

The site KK is located nearly 17 km far from the present coast. The general elevation at this site is 2 m above MSL exhibiting a further reduction in the relative height. The basal part, KKL4 was deposited during 7792-7608 cal yr BP (Table 5.4). This 200 cm thick sequence of clay loam is indicating deposition through fluvial activity (Figure 5.5). The 100 cm thick succeeding facie, KKL3 has a markedly high concentration of fine sand indicating deposition under the dominance of tidal action that might have coincided with sea transgression episode. The gray colour of this facie has illustrated deposition under a swampy environment. Sequence, KKL2 is markedly thick (540 cm) clay which began to be aggraded during 2441-2301 cal yr BP. Fine texture has suggested sediment accumulation primarily through riverine processes, unlike the KKL3. The KKL1 is the most recent sequence of this site. The predominance of fine clay has illustrated the continuation of fluvial dominance in the sedimentation process. The red and yellow colours of KKL2 and KKL1 have been attributed to the well-oxygenated environment of deposition.

5.4 Discussion and Conclusion

In a river catchment, sediments are transported from source to mouth through river action. Thus, floodplains and palaeochannels are formed under dominant fluvial action. Nevertheless, the presence of older beach deposits, aggraded mainly by wave action, itself has indicated high sea level in the past. During sea transgression accompanied by lower precipitation, the sediments are likely to enter the depositional environment through elevated tide and wave action. In contrast, during sea regression along with enhanced precipitation, the sediments are accumulated mainly through fluvial processes. Subsequently, the coastal landforms, apart from climate and sea level fluctuations, can also be influenced by tectonic activities. As discussed earlier (Chapter 1), a fault line runs almost parallel to the Baitarani river in this region that must have influenced landform development processes.

The analysis done so far suggests that different landforms, floodplain, beach deposit, and palaeochannel have been influenced by both riverine and tidal activities during the Holocene. It has been observed that the total number of facies, identified on the basis of distinct colour and texture, has declined from floodplain (SP with 6 facies) to palaeochannel (KK with 4 facies). The SP has represented the fining of sediments upwards till SPL4. The aggradation of SP up to 800 cm depth began during the late-Holocene that is relatively younger in origin in comparison to CB, AG, and KK. This has indicated active sediment accumulation at this site by the rivers. Contrary to this, the lower-most sequence of CB was formed during the early-Holocene, prior to 7700 cal yr BP, representing the oldest facie among all the selected landforms. It has shown an upwards coarsening of sediment particles. Sedimentation of the lowermost sequence of the palaeochannels, AG and KK occurred during the mid-Holocene around 7700 cal yr BP.

The SP location is aggraded by both finer and coarser particles indicating considerable shift in the depositional environment. The colour scheme of SP has suggested the formation of SPL6 and SPL5 under a damp environment. On the other hand, remaining sequences have been deposited under well-oxygenated conditions as suggested by red and brown colour. The CB was also formed by both fine and coarser sediments; however, the sandy particles are predominant in the upper stratigraphic sequences. The colour has demonstrated the formation of CBL6 under well-oxygenated or fluvial conditions while the concentration of

oxygen reduced during the sedimentation of succeeding facies. In contrast, AG and KK are primarily deposited by the fine-grained sediments. Nevertheless, the AGL3 and KKL3 are sandy sequences suggesting deposition under enhanced tidal action during the sea transgression.

The assessment of landforms chronology and stratigraphy during the Holocene provides insight into the climatic variations and sea level oscillations in the region (Rao et al., 2012). Here, the analysis has suggested that till 7700 cal yr BP fluvial processes have dominated the area, transporting mainly fine-grained sediments from the catchment area and depositing them towards the mouth of the river. Hence, the facies formed during this period has fine clayey texture i.e. AGL5, KKL4. The colour (mainly red and brown) has also demonstrated a well-oxygenated environment. The concentration of detrital metals such as Al_2O_3 , Fe_2O_3 , TiO_2 , MnO , etc. is also high in these facies which can be associated with higher terrestrial flux. Between 7700 and 6100 cal yr BP the influence of fluvial processes began to decline in the area. On the other hand, marine processes began to dominate. This has been recognized as the period of higher sea level. Thus, till 6100 cal yr BP, the tidal processes dominated the sedimentation processes depositing mainly grayish coarser particles such as in facies AGL3 and KKL3. The concentration of detrital elements has declined considerably in these facies while MgO and CaO have increased which are mostly contributed from the marine biogenic sources in the coastal areas. On the basis of the above discussion, it has been inferred that both fluvial and marine processes have dominated the accumulation at different time intervals offering distinct colour, texture and geochemical characteristics to the facies.

The ^{14}C dates have provided a temporal framework to the events occurred in the past. It has also become apparent that by linking physic-chemical characteristics with radiocarbon ages crucial information about the past climate can be deduced. The geochemical proxies also yield crucial information about the palaeoclimate. Hence, detailed analysis and discussion about the palaeoclimate are presented in the preceding chapter (Chapter 6) by combining geochemical proxies and ^{14}C ages.

Chapter 6

Reconstruction of Palaeoclimate using Geochemical Proxies and AMS ^{14}C dating

6.1 Introduction

Reconstruction of palaeoclimate is mandatory in order to analyze the changes in geomorphic processes and their intensities throughout the geological past. These processes have operated since the formation of the Earth and will be shaping the landscape in the future. In the absence of direct instrument based records, reconstruction of palaeoclimate has to rely on proxy sources such as sedimentary records, tree rings, pollen, etc. (Roberts et al., 1998; Anderson et al., 2007). The sub-surface sedimentary records are considered as rich archives of the Earth history expanding over longer periods in comparison to the instrumental data. The sedimentary sources also yield continuous records of past climate (Roberts et al., 1998; Hofer et al., 2013). Thus, sediment sequences are amongst the most preferred proxies to identify the processes of deposition and palaeoclimate under which the present landforms have been carved.

The studies illustrate that the climate of the Earth has changed throughout the geological time. It has incorporated major and drastic changes over millions of years as well as minor fluctuations (Juyal et al., 2003; Jayalakshmi et al., 2004; Kumaran et al., 2005; Anderson et al., 2007; Nair et al., 2010). Earlier it was believed that during the Holocene climate has remained fairly stable that resulted in the remarkable advancement of human civilization. However, the Pleistocene has been considered as the period of crucial climatic and sea level changes. Nevertheless, recent studies have reported that since 11,000 yr BP, significant alteration in the climate such as warming, cooling as well as changes in the humidity conditions have been experienced around the globe (Roberts, 1998). Therefore, unlike the previous understanding, substantial climatic and eustatic changes have been reported during the Holocene (Vaz and Banerjee, 1997; Jayalakshmi et al., 2004; Alappat et al., 2011; Jayangondaperumal et al., 2012; Tyagi et al., 2012; Srivastava and Farooqui, 2013; Quamar and Bera, 2014; Limaye et al., 2014; Tripathi et al., 2014; Malik et al., 2015; Rao et al., 2015; Govil et al., 2016; Makwana et al., 2019). However, there has been a marked deviation in these changes across the regions (Roberts, 1998).

The Holocene climate in coastal region can be reconstructed by cautious examination of landforms stratigraphy and their depositional history (Babu, 1975; Banerjee et al., 1993; Chauhan et al., 1993; Agnihotri et al., 2003; Banerjee, 2000; Kumaran et al., 2005;

Dillenburg, 2007; Khandelwal et al., 2008; Coltorti et al., 2010; Farooqui and Naidu, 2010; Rao et al., 2012; Selvakumar et al., 2012; Singh et al., 2014; Alappat et al., 2015; Basaviah et al., 2015; Malik et al., 2015; Das et al., 2017; Narayana et al., 2017). Sedimentation in these areas is governed by both terrestrial and marine processes. Hence, the evolution of the coastal landforms i.e. beach ridges, palaeochannels, coastal plain, dunes, lagoons bear the consequences of oscillating climate and sea level which has been experienced in the selected region as well (Chapter 5). One process, however, dominated the other at different periods under a distinct climatic setup. These details make the coastal sedimentary environment a robust proxies for not only infer the past climate but also to reconstruct the palaeo-monsoon variability (Basavaiah and Khadkikar, 2004; Banerji et al., 2017; Limaye et al., 2017), sea level perturbations (Banerjee, 1993; Vaz and Banerjee, 1997; Khandelwal et al., 2008) and evolution of landforms (Juyal et al., 2003; Mukherjee et al., 2009; Nair et al., 2010; Alappat et al., 2011; Tyagi et al., 2012; Rao et al., 2015).

The analysis of stratigraphic archives is a relative method for inferring the palaeoclimate. Even though this approach does not yield the exact age, it remains crucial for cross-checking on absolute dating. It becomes even more pivotal in the cases where absolute age is impossible to obtain such as lack of organic matter for ^{14}C dating. However, these relative methods can also lead to faulty correlations by assuming that similar-looking strata at different locations were deposited at the same time while this may not actually be the case. It is known as '*homotaxial error*' (Alexanderson et al., 2007). Nevertheless, in recent times relative methods have experienced much advancement through quantifying the degree of weathering, rate of sedimentation and break-down of organic compounds or palaeoproductivity using geochemical signatures. Along with this, the implementation of absolute dating techniques i.e. ^{14}C dating has made it viable to achieve the much accurate and precise age estimates.

There are certain assumptions that are made while examining the stratigraphic records or proxy sources for palaeoclimatic reconstruction. Firstly, it is anticipated that the materials at the bottom of the stratigraphic sequences were deposited earlier while those towards the top were deposited later. This is also known as the '*law of superposition*.' Another very crucial postulation is that the physical, chemical and biological properties of the deposit are the

products of the past environment when the deposition took place. And lastly, the region has remained tectonically stable during this depositional period. That means there were no geological over-turns that took place in the past.

The growing concern about the global climatic changes has provided prominent attention to the analysis of regional climatic variations (Meng et al., 2017). These are also vital to estimate the consequences of future climate change. Marked variation in regional climate during the mid-late Holocene period has made such analyses even more pressing.

The broader idea behind this research was the reconstruction of the palaeoclimate. Hence, in this chapter, an attempt has been made to reconstruct the palaeoclimate of lower Baitarani Basin, Odisha and examine variation in the depositional processes (riverine or marine). This has been carried out using both relative methods such as variation in the geochemical proxies depicting changes in the terrestrial flux, palaeoproductivity, weathering, and salinity. In addition, the absolute dates (AMS ^{14}C ages) have been used to provide an exact date to the past event. In the riverine zone (EP, JP, KTI, and KTII), the reconstruction of palaeoclimate is done only using the geochemical proxies. However, for the samples obtained from the mixing zone (SP, CB, AG, and KK), the inferences of palaeoclimate have been derived by both relative and absolute approaches. The results have also been compared with the existing literature to validate the findings. However, pronounced deviation in the occurrence of events has been reported across the Indian subcontinent that might be due to the variation in techniques applied for the reconstruction. These irregularities in the findings might also be attributed to the regional and local perturbations in climate, sea level and tectonics which is one of the basic characteristics of the Holocene period (Roberts, 1998).

6.2 Methodology

6.2.1 Geochemical Proxies

The geochemical properties of sediments have been utilized as vital tracers of the provenance, transportation process and weathering conditions (Makwana et al., 2018). Down-core variations in the concentration of oxides have often been applied as the surrogacy for changes in palaeo-monsoon intensity (Agnihotri et al., 2003; Kemp and Izumi, 2014; Banerji et al., 2017; Das et al., 2017; Makwana et al., 2018). In the present study

selected geochemical proxies were used to assess the indicators on which basis palaeoclimate can be inferred (Table 6.1).

Table 6.1 Geochemical proxies used to analyze palaeoclimate

Palaeoclimate Indicators	Geochemical Proxies
Terrestrial Flux	Al ₂ O ₃ , Fe ₂ O ₃ , TiO ₂ , MgO, Co, Cu, Zn, and Ba
Palaeoproductivity	TOC, CaO/Al ₂ O ₃ , Cu/Al ₂ O ₃ , Sr/Al ₂ O ₃ , Zn/Al ₂ O ₃ , and Ba/Al ₂ O ₃
Weathering	TiO ₂ /Al ₂ O ₃ , Fe ₂ O ₃ / Al ₂ O ₃ , MgO/Al ₂ O ₃
Salinity	[(MgO)/(CaO+MgO)]

(a) Terrestrial Flux

The deviation in the concentration of Al₂O₃, FeO, TiO₂, CaO, MgO, Co, Cu, Zn and Ba in different sub-surface sediment facies is used as tracers of changes in the terrestrial flux (Table 6.1). Terrestrial flux is one of the proxies illustrating perturbation in rainfall intensity influencing the depositional environment (Agnihotri et al., 2003; Kemp and Izumi, 2014; Banerji et al., 2017). Metals such as Al₂O₃, Fe₂O₃, TiO₂, Co, Cu, and Zn are considered as detrital that are derived from non-biogenic sources whereas the prime source of Ba, MgO and CaO are biogenic. In general belief, the concentration of detrital elements (Al₂O₃, Fe₂O₃, TiO₂, Co, and Zn) increases due to elevated fluvial action in the catchment area under humid climate. Their concentration tends to decline during arid episodes when sediment supply is restricted. In contrast, the concentration of Ba, CaO and MgO tends to increase under the enhanced marine influence (Peek and Clementz, 2012; Gredilla et al., 2015; Li et al., 2019). Subsequently, these proxies also provide traces of the changes in palaeo-monsoon intensity and sea level (Agnihotri et al., 2003; Kemp and Izumi, 2014; Banerji et al., 2017; Narayana et al., 2017).

(a) Palaeoproductivity

Down core variation in TOC and ratios of $\text{CaO}/\text{Al}_2\text{O}_3$, $\text{Cu}/\text{Al}_2\text{O}_3$, $\text{Sr}/\text{Al}_2\text{O}_3$, $\text{Zn}/\text{Al}_2\text{O}_3$, and $\text{Ba}/\text{Al}_2\text{O}_3$ have been selected to assess the changes in the palaeoproductivity (Goldberg and Arrhenius, 1958; Dymond et al., 1992; Agnihotri et al., 2002; Tribovillard et al., 2006; Banerji et al., 2017). The palaeoproductivity represents the primary productivity of organic matter. If the microbial concentration is high in a particular facie it may result into enhanced production of organic elements. Variation in the palaeoproductivity is related to the changes in climatic conditions making it a common relative method to reconstruct the palaeoclimate (Barcena et al., 2001; Sageman and Lyons, 2003). The $\text{CaO}/\text{Al}_2\text{O}_3$, $\text{Cu}/\text{Al}_2\text{O}_3$, $\text{Sr}/\text{Al}_2\text{O}_3$, and $\text{Ba}/\text{Al}_2\text{O}_3$ demonstrate the ratio of biological productivity (CaO, Cu, Sr, and Ba) in comparison to the detrital flux (Al_2O_3). CaO and Ba are considered to be derived from marine sources in the coastal environment. The organisms utilize the available Cu and when they are dead or molted, the Cu is released in the depositional environment. Sr is also fixed by biogenic activities. The Ca, MgO and Sr are highly mobile under the weathering environment (Buggle et al., 2011). Thus, the increase in their ratio suggests an elevated biological activity that has been associated with higher palaeoproductivity. Hence, sufficient nutrient supply is a prerequisite for higher palaeoproductivity. Under arid climate, an increase in palaeoproductivity has been linked to the existence of mangrove vegetation (Banerji et al., 2015, Banerji et al., 2017). Nevertheless, the Al_2O_3 content can also be altered by the biogenic processes affecting the outcomes of palaeoproductivity (Sageman and Lyons, 2003). A strong correlation between Ba and Al_2O_3 has been reported that can also influence the results (Dymond, 1992). Since the source of Al_2O_3 is non-biogenic while that of Ba is biogenic, a strong relationship between Ba and Al_2O_3 is not the representative of the palaeoproductivity (Dymond, 1992).

(b) Weathering and Salinity

The ratios of $\text{TiO}_2/\text{Al}_2\text{O}_3$, $\text{Fe}_2\text{O}_3/\text{Al}_2\text{O}_3$ and $\text{MgO}/\text{Al}_2\text{O}_3$ have been used to examine the palaeo-weathering conditions (Banerje et al., 2017). Chemical weathering alters the composition of siliciclastic sediments (Nesbitt et al., 1980; Selvaraj et al., 2004). The review of past weathering conditions mainly reckons on the selective removal of relatively soluble and mobile elements (TiO_2 , Fe_2O , and MgO) from a weathering profile in relation to the

comparative enrichment of rather immobile and non-soluble metals i.e. Al_2O_3 (Buggle et al., 2011). These chemical changes recorded in the sediments that can be used as the tracer of palaeoclimate (Benson et al., 1996; Banerji et al., 2017; Makwana et al., 2018). Here, Al is basically used for normalizing TiO_2 , Fe_2O_3 , and MgO.

The fluctuations in salinity have been examined through the ratio of $\text{MgO}/\text{CaO}+\text{MgO}$ (Table 6.1). This ratio has been suggested by Sinha et al., (2006) and Banerji et al. (2017). The response of these biogenic metals varies with the changes in salinity (Nash et al., 1994). A higher MgO content within the individual sample is usually attributed to elevated salinity levels during MgO precipitation (Watts, 1980).

6.2.2 Radiocarbon (^{14}C) dating

AMS ^{14}C ages were determined using Accelerator Mass Spectrometry (AMS) based on 500 kV Pelletron accelerator at Inter-University Acceleration Centre (IUAC), New Delhi, India. The details of the methodology have been provided in the previous chapter (Chapter 5).

6.3 Analysis

The samples for ^{14}C dating were obtained from SP at the depth of 800 cm, 350 cm and 30 cm providing age ranges of 1740-1541, 1415-1296 and 961-769 cal yr BP (2σ date range) respectively. From CB location, samples from 750 cm, 550 cm, and 250 cm depth were recovered giving dates of 7764-7595, 7759-7575 and 4766-4615 cal yr BP (2σ date range). From AG site, samples from the depth of 1000 cm, 760 cm, 600 cm, and 450 cm yielded radiocarbon ages of 7790-7610, 7634-7469, 6283-6095 and 2851-2738 cal yr BP (2σ date range). From the KK site, ^{14}C samples were obtained from 1000 and 700 cm depth providing dates of 7792-7608 and 2441-2301 cal yr BP (2σ date range).

6.3.1 Reconstruction of Palaeoclimate in the Riverine Zone

Ezapur (EP)

In this palaeochannel site, the higher concentration of Al_2O_3 , TiO, Fe_2O_3 , Co, Cu, and Zn have suggested an episode of elevated terrestrial flux during the deposition of basal sequence, EPL7 (Figure 6.1). At the same time, the concentration of Ba and MgO was low indicating lower tidal influence. The concentration of detrital elements has declined in EPL6 revealing a reduction in the terrestrial flux. On the other hand, a higher MgO has revealed an

increase in marine influence. In EPL5 the signals of enhanced terrestrial flux have been marked by the increasing content of Al_2O_3 , TiO_2 , Fe_2O_3 , Co, Cu, and Zn. Lower MgO has demonstrated the declining impact of tidal activity. Another period of reduced terrestrial flux has been observed during the sedimentation of EPL4 which has coincided with increasing tidal influence (higher MgO content). In EPL3 the concentration of detrital proxies has increased again indicating enhanced terrestrial flux. In recent deposits, towards the top of the stratigraphic sequence (60 cm to the surface), a marginal decline in the terrestrial flux has been inferred due to a decline in detrital metals.

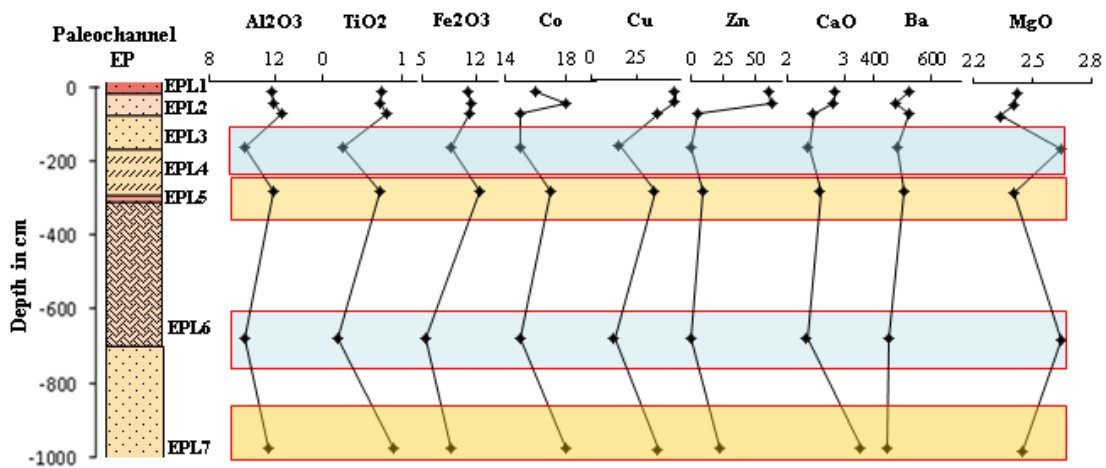


Figure 6.1 Variability in the proxies selected for terrestrial flux at the EP site. The yellow rectangles are showing higher terrestrial flux while blue rectangles are showing lower terrestrial flux

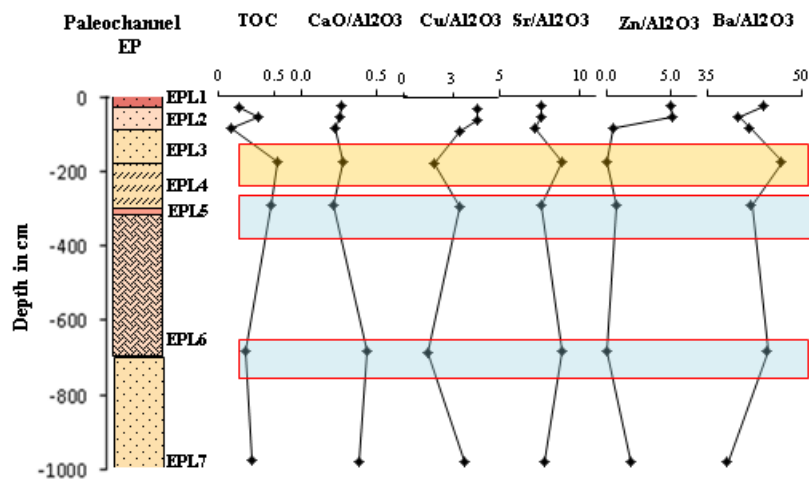


Figure 6.2 Variation in the proxies selected for palaeoproductivity at EP site. The yellow rectangles are showing higher palaeoproductivity while blue rectangles are showing lower palaeoproductivity

Corresponding to the terrestrial flux, the primary productivity (TOC) was relatively higher in the earlier deposits shown as EPL7. A higher palaeoproductivity during the deposition of EPL7 has been inferred due to the elevated TOC, Cu/Al₂O₃ and Zn/Al₂O₃ content (Figure 6.2). The lower concentration of Sr and Ba might be the result of lower fixation in the sediments. Subsequently, the productivity of organic carbon has declined marginally during the deposition of EPL6. Another incident of higher primary production (TOC) has been marked in EPL5. In EPL4 significant rise in the palaeoproductivity has been inferred due to the higher concentration of proxies. In the recent deposits, EPL2 and EPL1 the proxies have indicated no significant change in palaeoproductivity.

The geochemical proxies have revealed higher weathering during the deposition of EPL7 (Figure 6.3). Higher weathering has been associated with the elevated river flow during which it corrodes more material in the catchment area and transports them to its mouth region. In the succeeding facie EPL6, weathering has declined significantly indicating declining stream energy. Another episode of elevated weathering has been marked during the sedimentation of EPL5 demonstrating an episode of enhanced river flow. In EPL4, in contrast, a reduction in weathering has appeared. Higher weathering has taken place during EPL3 deposition. In the recent deposits, represented by EPL2 and EPL1 the weathering condition has appeared to decline.

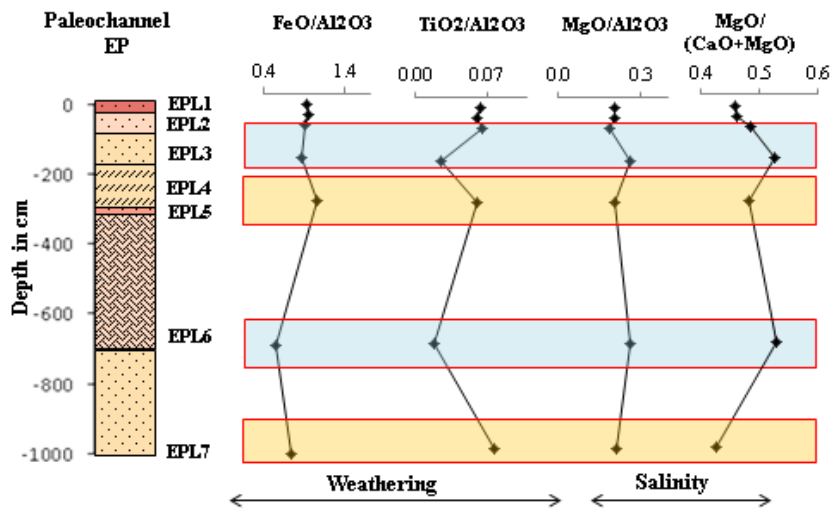


Figure 6.3 Variability in the proxies of weathering and salinity at the EP site. The yellow rectangles are showing higher weathering and low salinity while the blue rectangles are showing lower weathering and higher salinity

The MgO/CaO+MgO ratio has indicated fluctuation in salinity levels from low to moderate at this location (Figure 6.3). During the deposition of EPL7, the salinity was lower suggesting lower inflow of saline water. It has increased significantly during the sedimentation of EPL6 showing a surge in tidal influence. Afterward, another phase of declining salinity has been marked in EPL5 facie that can be attributed to another episode of higher marine inflow. An episode of higher salinity conditions has been observed in EPL4 exhibiting an elevated influence of tidal activity. In the succeeding facies, salinity has declined. The decreasing salinity has been associated with a decline in tidal influence due to which the inflow of saline water is low.

The analysis done so far for the EP site located in the palaeochannel has illustrated elevated fluvial process during the sedimentation of EPL7. This has been attributed to the enhanced rainfall condition resulting in a rise in the river erosion and carrying capacity. The decline in the stream flow has occurred during the deposition phase of EPL6 referring to the weakening of rainfall that led to the reduction in the stream energy. This episode has corresponded with the increasing influence of tidal activity. Another period of increased river flow under the enhanced rainfall conditions has been marked in EPL5. At this time, the tidal influence declined. In EPL4 signals of the reducing rainfall intensity have been marked. This has resulted in declining river flow. This has also been identified as the period of higher tidal action. The episode of elevated rainfall has been marked again in EPL3 which coincided with reduced tidal influence. During the deposition of EPL2 and EPL1, no remarkable change in fluvial and tidal processes has occurred. The episodes of enhanced rainfall have corresponded with the increased tidal influence as suggested by a lower concentration of MgO and reduced salinity.

Jhumpuri (JP)

The terrestrial flux has not varied significantly during the deposition of JPL11 and JPL10(Figure 6.4). During the accumulation episodes of JPL9 relatively higher terrestrial flux has been indicated by the increased concentration of Al₂O₃, TiO₂, Co, and Zn. It has been attributed to an increase in stream energy. At this time the content of Ba and MgO has been low illustrating a lower influence of the tidal process. The terrestrial flux has declined significantly during the deposition of JPL8 and JPL7 as revealed by the declining

concentration of Al_2O_3 , TiO_2 , Fe_2O_3 , Co, Cu, and Zn. This has suggested a decline in the river flow velocity that can be attributed to the lower rainfall. At this time, the tidal influence has been high as indicated by the increasing content of Ba and MgO. The terrestrial flux has increased markedly during the deposition of JPL6 and JPL5 that can be associated with the elevated energy of the river. During this period, the tidal influence has declined. Another remarkable decline in the terrestrial flux has been detected in JPL4. This might have been caused by the decline in streamflow. During the sedimentation of JPL3 signs of higher terrestrial flux has been observed along with the lower tidal influence. In JPL2 slight decline in terrestrial flux has occurred which has been coincided with a marginal rise in tidal influences. Overall, in JPL2 and JPL1 no significant change in fluvial or marine processes has been detected.

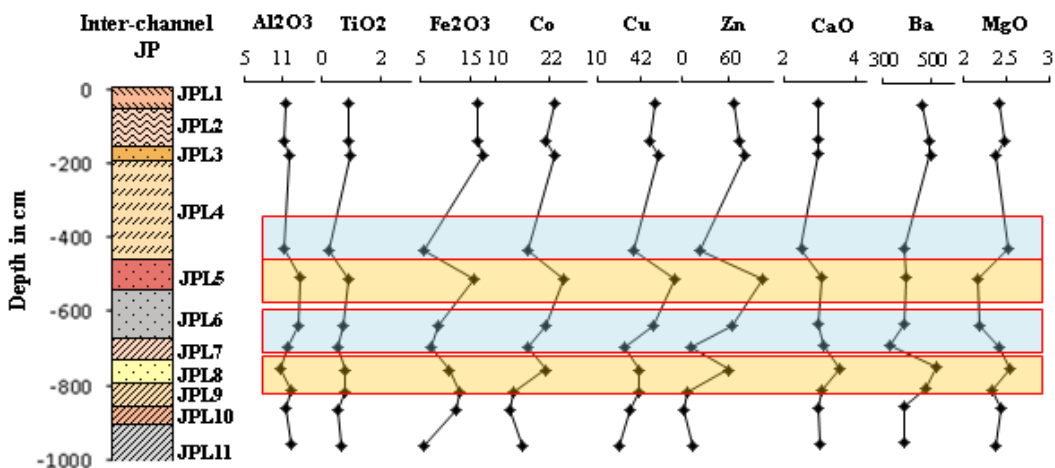


Figure 6.4 Variability in the proxies indicating terrestrial flux at JP site. The yellow rectangles are showing higher terrestrial flux while blue rectangles are showing lower terrestrial flux

The palaeoproductivity, in general, has been lower in JPL11 and JPL10 as indicated by TOC, $\text{CaO}/\text{Al}_2\text{O}_3$, $\text{Cu}/\text{Al}_2\text{O}_3$, $\text{Zn}/\text{Al}_2\text{O}_3$, and $\text{Ba}/\text{Al}_2\text{O}_3$. It has increased markedly during the deposition of JPL8 (Figure 6.5). At this time, higher terrestrial flux has also been recorded at this location (Figure 6.4). Higher palaeoproductivity has indicated that the environment was suitable for a rise in primary production. Afterward, the palaeoproductivity has declined as represented by the depletion of TOC, $\text{CaO}/\text{Al}_2\text{O}_3$, $\text{Cu}/\text{Al}_2\text{O}_3$, $\text{Sr}/\text{Al}_2\text{O}_3$, $\text{Zn}/\text{Al}_2\text{O}_3$, and $\text{Ba}/\text{Al}_2\text{O}_3$ in JPL7 and JPL6. In JPL5, higher values of TOC, $\text{Cu}/\text{Al}_2\text{O}_3$, $\text{Sr}/\text{Al}_2\text{O}_3$, and $\text{Zn}/\text{Al}_2\text{O}_3$ has indicated a period of elevated primary production during its deposition. TOC

and Zn/Al_2O_3 has suggested another period of declining palaeoproductivity in JPL4. The decreasing concentration of TOC has suggested reduced productivity of organic carbon in JPL3. At this time, a relative rise in the ratios of Cu/Al_2O_3 , Sr/Al_2O_3 , Zn/Al_2O_3 , and Ba/Al_2O_3 might be attributed to the enhanced detrital flux. In facies JPL2 and JPL1, no remarkable changes in palaeoproductivity have been detected. Thus, it can be inferred that during the deposition of JPL2 and JPL1 the palaeoproductivity has remained almost stable.

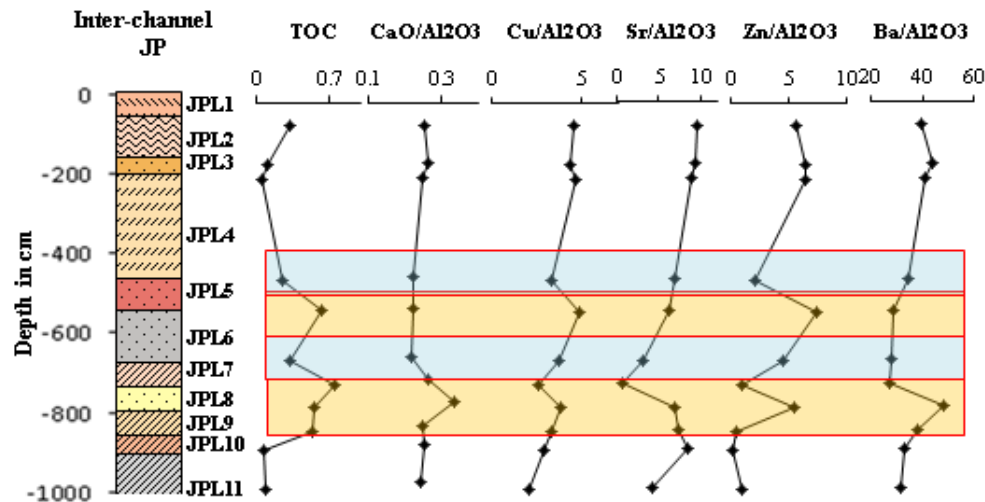


Figure 6.5 Variability in the proxies indicating palaeoproductivity at JP site. The yellow rectangles are showing higher palaeoproductivity while blue rectangles are showing lower palaeoproductivity

During the deposition of JPL10 and JPL9, relatively low weathering has been observed that might be attributed to the lower capacity of the stream to erode the materials in the catchment region. An increase in the ratio of FeO/Al_2O_3 , TiO/Al_2O_3 , and MgO/Al_2O_3 has indicated markedly higher weathering in JPL8. Relative rise in weathering has been marked in JPL5. FeO/Al_2O_3 and TiO_2/Al_2O_3 have illustrated a decline in weathering in the catchment as these metals have been derived from the catchment area. At this time a relatively higher ratio of MgO/Al_2O_3 might be associated with higher weathering under the tidal influence as MgO is considered to be derived by marine processes. In JPL3 another phase of elevated weathering has occurred as ratios of FeO/Al_2O_3 and TiO_2/Al_2O_3 has increased. This has revealed a rise in upper catchment weathering whereas the decline in MgO/Al_2O_3 has been attributed to a decline in marine weathering or lower influence of tidal activities when it's unable to bring metals from marine sources. In recent deposits (JPL2 and JPL1), however, no significant change in the weathering environment can be observed.

The salinity indicator has revealed low to moderate levels of salinity that have occurred at this location (Figure 6.6). In JPL11, lower salinity has been reported which has marginally increased during the deposition of JPL10. Thereafter, the salinity has declined until the deposition of JPL8. In JPL7, the salinity has increased slightly. A remarkable decline in salinity has occurred during the deposition of JPL5. In JPL4 considerable rise in salinity has been recorded. Thereafter, the salinity has declined perpetually at this site.

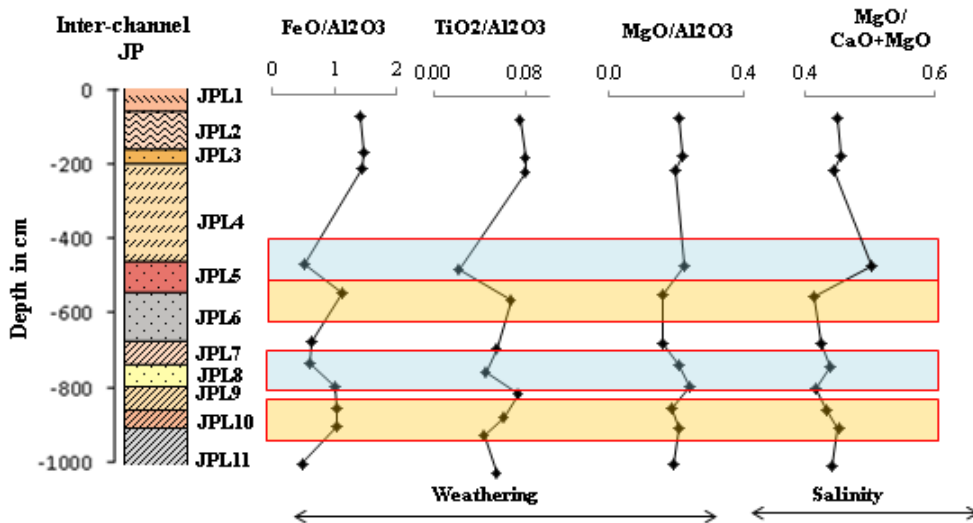


Figure 6.6 Variability in the proxies indicating weathering and salinity at JP site. The yellow rectangles are showing higher weathering and low salinity while the blue rectangles are showing lower weathering and higher salinity

The analysis done for JP site, which has been collected from the older flood plains located between two palaeochannels of Baitarani, has revealed low rainfall intensity manifested into lower river flow during the sedimentation of JPL11, JPL10 and JPL9. The influence of tidal activity was relatively high during this phase. The intensity of rainfall has increased marginally during the deposition of JPL8, corresponding to the environment during the deposition of EPL7. A decline in river flow has been marked in JPL7 suggesting a decline in rainfall intensity. In JPL5, the significant rise in river flow has appeared indicating a surge in rainfall. During this episode, a notable decline in tidal activity and salinity were also marked. A subsequent period of weak rainfall intensity and elevated tidal influence has occurred during the deposition of JPL4. Enhanced rainfall condition has been suggested by the selected proxies during the sedimentation of JPL3. Similar to EP, no remarkable

variation in fluvial or marine influence has been detected during the aggradation of JPL2 and JPL1.

Katia I (KTI)

The indicators representing terrestrial flux have not exhibited noticeable change during the deposition of KTIL5 and KTIL4 (Figure 6.8). Here, Al_2O_3 which is relatively stable has exhibited unique patterns in comparison to the other mobile metals i.e. TiO, Cu and Zn. The higher concentration of TiO_2 , Fe_2O_3 , Cu, and Zn has indicated a minor increase in the terrestrial flux during the deposition of KTIL3. At the same time, a rise in tidal influence has been inferred from higher Ba and MgO content. In KTIL2, a decline in the concentration of TiO_2 , Fe_2O_3 , Co, Cu, and Zn has indicated lower terrestrial flux. A marginal drop in the terrestrial flux and increasing tidal influence has been suggested in KTIL1.

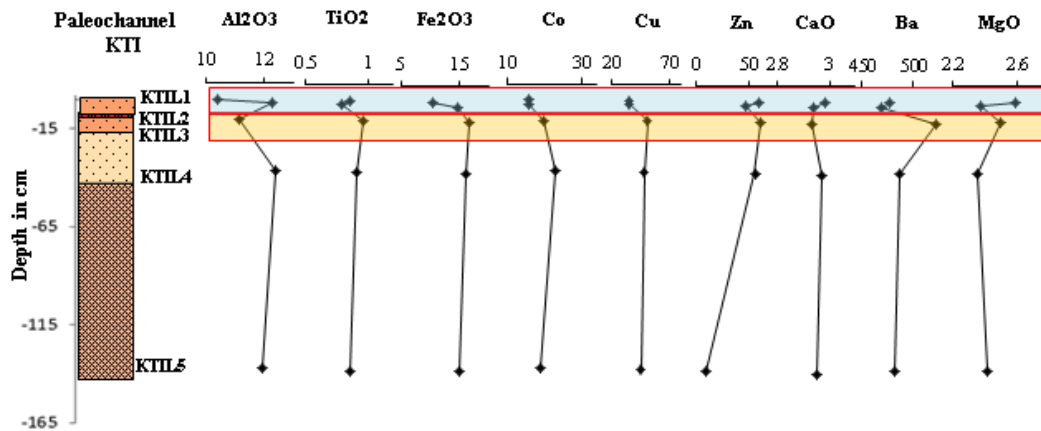


Figure 6.7 Variability in the proxies indicating terrestrial flux at KTI. The yellow rectangles are showing higher terrestrial flux while blue rectangles are showing lower terrestrial flux

Similar to the terrestrial flux, no noticeable variation in the palaeoproductivity has been observed in KTIL5 and KTIL4 (Figure 6.8). The proxies have suggested an increase in palaeoproductivity in KTIL3. In KTIL2 the palaeoproductivity has declined as suggested by lower TOC, $\text{CaO}/\text{Al}_2\text{O}_3$, $\text{Cu}/\text{Al}_2\text{O}_3$, $\text{Sr}/\text{Al}_2\text{O}_3$, $\text{Zn}/\text{Al}_2\text{O}_3$, and $\text{Ba}/\text{Al}_2\text{O}_3$. During the deposition of KTIL1, all the indicators have suggested an increase in palaeoproductivity.

Weathering and salinity have also not shown significant variability in KTIL5 and KTIL4 (Figure 6.9). However, during the deposition of KTIL3, a marginal rise in weathering has

occurred. In KTIL2, the weathering has declined. A marginal increase in weathering has been reported in KTIL1.

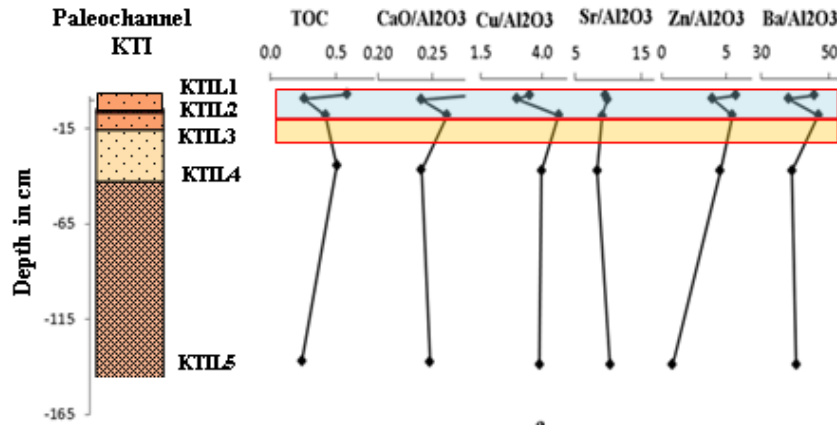


Figure 6.8 Variability in the proxies indicating palaeoproductivity at KTI site. The yellow rectangles are showing higher palaeoproductivity while blue rectangles are showing lower palaeoproductivity

The $MgO/CaO+MgO$ ratio has revealed that the level of salinity has varied from low to moderate at this site (Figure 6.9). The ratio has relatively increased during the deposition episode of KTIL3 corresponding to the rise in MgO concentration suggesting a higher salinity. A marginal decline has occurred during KTIL2 deposition that can be attributed to lower tidal influence. It has been followed by a marginal rise in KTIL1 indicating a higher level of salinity.

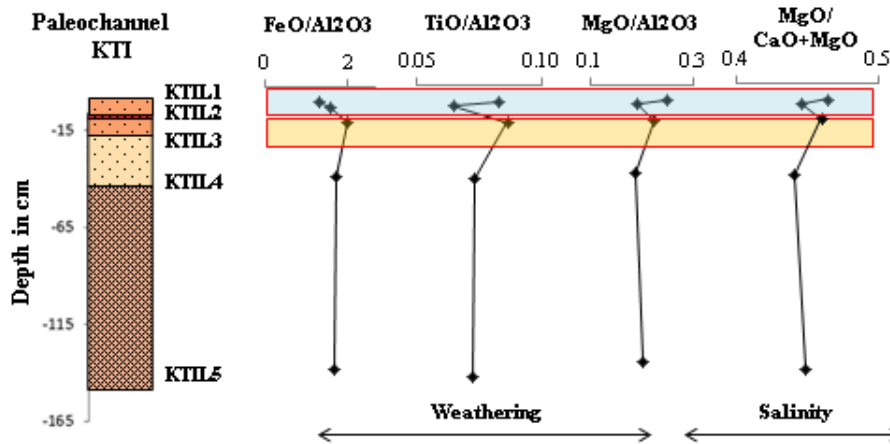


Figure 6.9 Variability in the proxies indicating weathering and salinity at KTI site. The yellow rectangles are showing higher weathering and low salinity while the blue rectangles are showing lower weathering and higher salinity

Based on the above analysis it can be stated that no remarkable variation in the pattern of riverine or tidal activities has been marked during the deposition episode of KTIL5 and KTIL4. The riverine influence has declined marginally during the deposition of KTIL3 which can be attributed to lower rainfall. At the same time, the influence of tidal activity has increased. In KTIL2, signals of higher river flow and reduced tidal influence have been observed suggesting the dominance of fluvial activity. An episode of marginal decline in the river flow has been marked in KTIL1 that has coincided with the relative rise in tidal influence.

Katia II (KTII)

During the deposition of KTIL9, KTIL8, and KTIL7, no significant change in the terrestrial flux has been recorded (Figure 6.10). A considerable increase in the terrestrial flux has been marked by a higher concentration of Al_2O_3 , TiO, Fe_2O_3 , Co, Cu, and Zn in KTIL5. During this episode, the decline in MgO content has suggested a decrease in tidal influence. A lower concentration of geochemical proxies has indicated a reduction in the terrestrial flux during the sedimentation of KTIL4. This has coincided with higher tidal influence as suggested by higher MgO content. No considerable variation in the terrestrial flux has occurred during the deposition of KTIL3, KTIL2, and KTIL1.

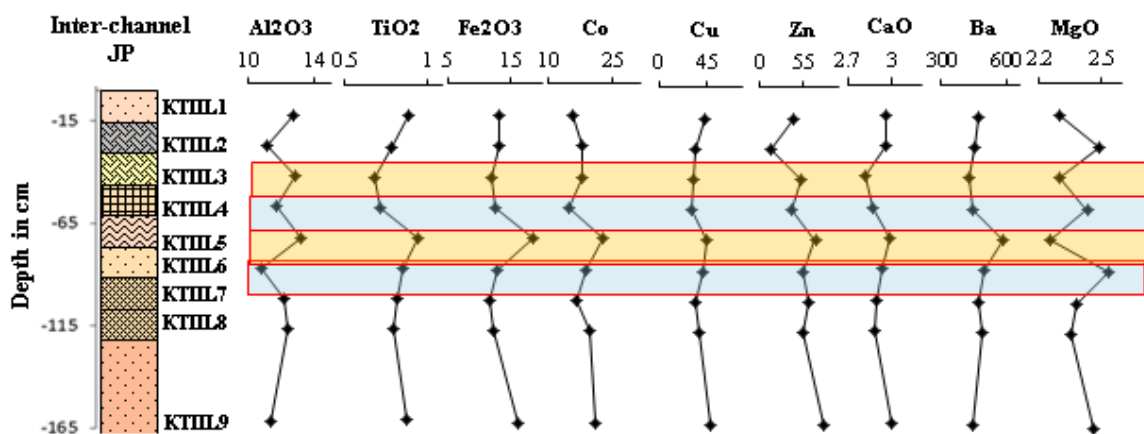


Figure 6.10 Variability in the proxies indicating terrestrial flux at KTII site. The yellow rectangles are showing higher terrestrial flux while blue rectangles are showing lower terrestrial flux

Indicators of palaeoproductivity have remained almost unchanged during the deposition of KTIL9 and KTIL8 (Figure 6.11). The concentration of TOC has increased significantly in

KTIL7 showing higher primary productivity while other indicators have remained almost unchanged. The TOC has declined in KTIL6 indicating lower primary production. During the deposition of KTIL5, higher TOC, Cu/Al₂O₃, Zn/Al₂O₃ and Ba/Al₂O₃ have revealed an increase in palaeoproductivity. The proxies have suggested lower palaeoproductivity during the deposition of KTIL4 and KTIL3. No significant fluctuation in palaeoproductivity has been demonstrated during the sedimentation of KTIL2 and KTIL1.

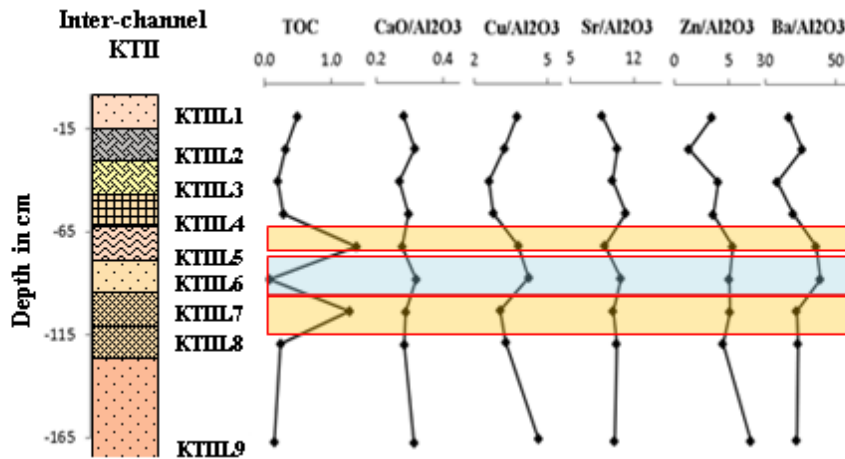


Figure 6.11 Variability in the proxies indicating palaeoproductivity at KTII site. The yellow rectangles are showing higher palaeoproductivity while blue rectangles are showing lower palaeoproductivity

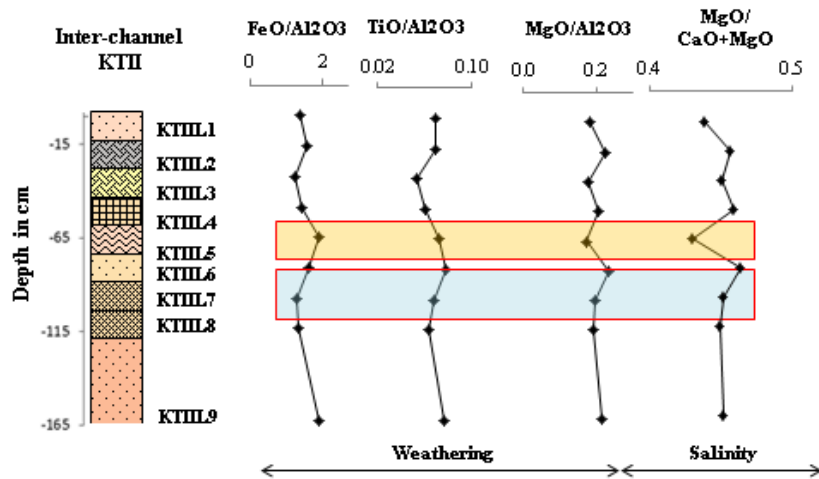


Figure 6.12 Variability in the proxies indicating weathering and salinity at KTII site. The yellow rectangles are showing higher weathering and low salinity while the blue rectangles are showing lower weathering and higher salinity

A relatively higher weathering has been suggested by $\text{FeO}/\text{Al}_2\text{O}_3$, $\text{TiO}_2/\text{Al}_2\text{O}_3$, and $\text{MgO}/\text{Al}_2\text{O}_3$ during the aggradation of KTIL9 (Figure 6.12). However, a significant decline in weathering has been marked in KTIL6. During the deposition of KTIL5, weathering has increased marginally followed by a lower weathering during the sedimentation of KTIL4. Weathering has declined marginally in KTIL3 while a marginal increase has been recorded in KTIL2. During the deposition episode of KTIL1, evidence of lower weathering has appeared.

Salinity has varied from low to moderate at this site as well (Figure 6.12). In most of the facies, however, it has remained low. In KTIL6, relatively high salinity has been observed. Traces of lower salinity have appeared in KTIL5 followed by a rise in KTIL4. A marginal decline has been reported in KTIL3 followed by a marginal increase in KTIL2. The salinity has appeared to decline marginally in KTIL1 as suggested by $\text{MgO}/\text{CaO}+\text{MgO}$ ratio.

The analysis has revealed the occurrence of low intensity rainfall during the sedimentation of KTIL7 along with higher tidal influence. An episode of enhanced rainfall has been indicated during the deposition of KTIL5. At this time the marine processes declined. This was followed by another phase of low rainfall intensity during the accumulation of KTIL4. This period has coincided with higher tidal influence.

6.3.2 Palaeoclimate Reconstruction in the Mixing Zone

Sonpanki (SP)

The sedimentary records are rather newer at SP site owing to its location in the active flood plain. The selected proxies i.e. Al_2O_3 , TiO_2 , Fe_2O_3 , Co, and Zn have demonstrated lower terrestrial flux in the bottom sediment sequence shown as (Figure 6.13). This has suggested low energy of river flow under weak rainfall conditions. On the other hand, the higher concentration of CaO and MgO has revealed a surge in tidal influence. At this location positive correlation between CaO and MgO (Chapter 3) has suggested that CaO must have been contributed from biogenic marine sources. The terrestrial flux has increased significantly during the deposition episode of SPL5 suggesting enhanced flow condition under higher rainfall. This period has coincided with lower tidal activity under weak tidal influence. The terrestrial flux has declined marginally. Afterward, no considerable change

has been detected in the terrestrial flux. Nevertheless, during the deposition of SPL1 insignificant decrease in terrestrial flux has been indicated by lower Al_2O_3 , TiO_2 , Fe_2O_3 , Cu and Zn. Relatively high content of CaO and MgO in SPL1 has demonstrated a marginal rise in tidal activity in recent times.

The lower concentration of TOC has indicated a lower synthesis of organic carbon during the deposition of SPL6 and SPL5 (Figure 6.14). Along with this, lower palaeoproductivity has been suggested by $\text{Sr}/\text{Al}_2\text{O}_3$, $\text{Zn}/\text{Al}_2\text{O}_3$ and $\text{Ba}/\text{Al}_2\text{O}_3$ in SPL6. Higher microbial activities might have resulted in the reduced concentration of nutrients i.e. Sr, Zn, and Ba. During the sedimentation of SPL4 palaeoproductivity has further increased. The TOC concentration has increased in SPL3 revealing higher productivity. However, no major changes have been observed in other indicators. During the deposition episode of SPL2, TOC and $\text{Ba}/\text{Al}_2\text{O}_3$ has declined which has been attributed to the reduced palaeoproductivity followed by an increase in SPL1.

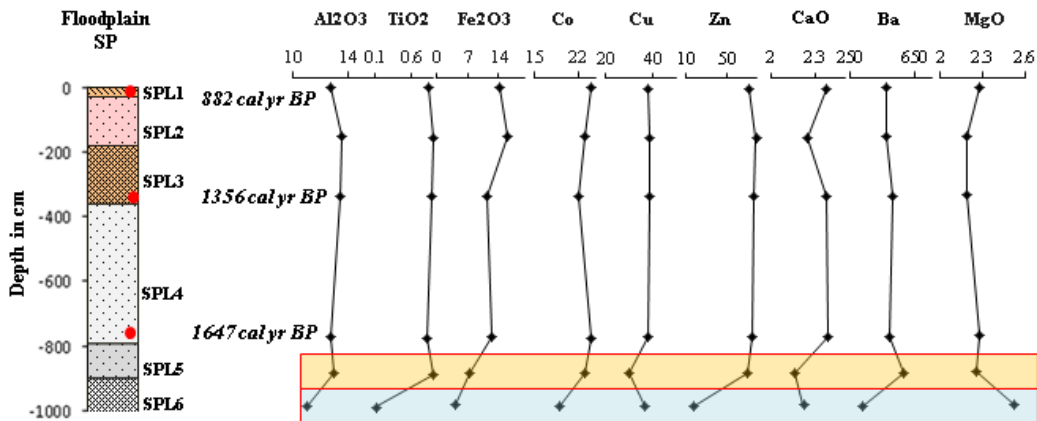


Figure 6.13 Variability in the proxies indicating terrestrial flux at SP site. The yellow rectangles are showing higher terrestrial flux while blue rectangles are showing lower terrestrial flux

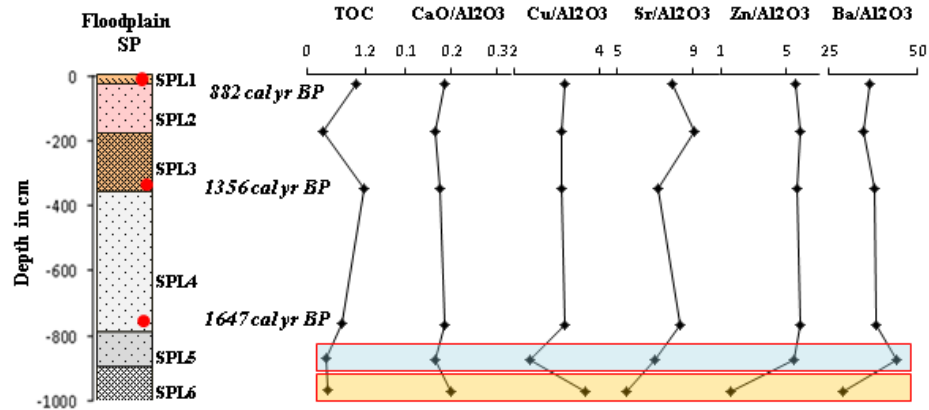


Figure 6.14 Variability in the proxies indicating palaeoproductivity at SP site. The yellow rectangles are showing higher palaeoproductivity while blue rectangles are showing lower palaeoproductivity

The geochemical proxies have suggested relatively lower weathering during the sedimentation of SPL6 as exhibited by lower ratios of $\text{FeO}/\text{Al}_2\text{O}_3$, $\text{TiO}_2/\text{Al}_2\text{O}_3$ (Figure 6.15). A higher concentration of MgO in this facie might be associated with higher tidal influence in comparison to detrital input (Al_2O_3). This period has been followed by an enhanced weathering episode as detected in SPL5 and SPL4. Thereafter, no substantial change in the weathering condition has been observed for this location.

The salinity has remained moderate in SPL6 (Figure 6.15). During the aggradation of SPL6, lower salinity has been marked. A gradual decline in salinity has been recorded till SPL4. The salinity has increased marginally in SPL2. However, in SPL1, no considerable deviation has been recorded.

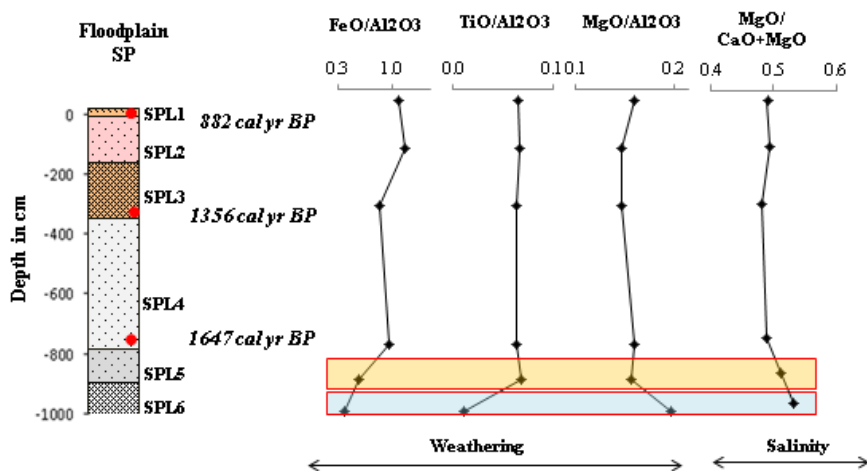


Figure 6.15 Variability in the proxies indicating weathering and salinity at SP site. The yellow rectangles are showing higher weathering and low salinity while the blue rectangles are showing lower weathering and higher salinity

The geochemical proxies have illustrated a period of weak rainfall during the deposition of SPL6. This was followed by enhanced rainfall intensity during the sedimentation of SPL5. The marginal decline in rainfall intensity has been recorded in SPL4 deposited during 1647 cal yr BP. During this phase, tidal activity was relatively high. No significant change in rainfall intensity has been detected in SPL3, deposited during 1356 cal yr BP. Similarly, during the accumulation of SPL2 (882 cal yr BP), no significant perturbation could be observed.

Chandbali (CB)

The site CB was located at older beach deposits of Chandbali which are basically aggraded by gradual wave action, unlike the palaeochannels or floodplains which are considered to be primarily developed by the fluvial action. The existence of these landforms far away from the coast, itself suggests the occurrence of sea transgression in the past. At present, this location is very approximate to the river Baitarani, hence fluvial processes have also influenced its evolution in recent times as discussed in the previous analysis (Chapter 5).

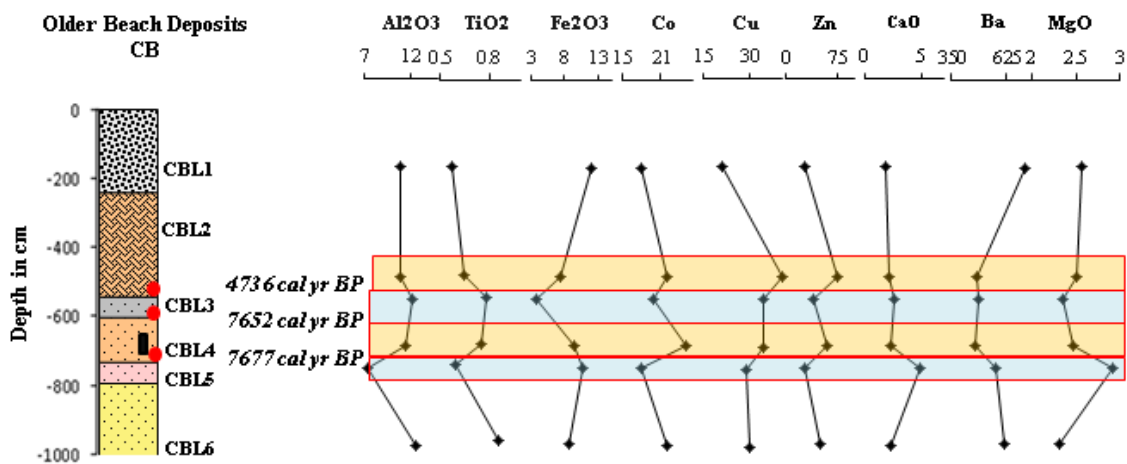


Figure 6.16 Variability in the proxies indicating terrestrial flux at CB site. The yellow rectangles are showing higher terrestrial flux while blue rectangles are showing lower terrestrial flux. The higher detrital input i.e. Al₂O₃, TiO₂, Co, and Zn have suggested higher terrestrial flux during the deposition of CBL6 (Figure 6.16). This higher terrestrial flux has been associated with the intensified depositional process. At this time, the indication of weak tidal action has been provided by the lower content of CaO and MgO. The depletion of Al₂O₃, TiO₂, Co, Cu, and Zn during the aggradation of CBL5 has demonstrated a considerable decline in the terrestrial flux. Reduced terrestrial flux has depicted weakening fluvial energy. During this

period the tidal process has dominated this location. Another period of higher detrital flux has been marked during the deposition of CBL4 suggesting a surge in the intensity of the riverine process. At this time, a lower concentration of CaO and MgO has illustrated a decline in the tidal influence. No significant perturbation in the terrestrial flux has been noticed in CBL3. A lower concentration of Al₂O₃ and TiO₂ has revealed a marginal rise in terrestrial flux in CBL2. This has coincided with a fall in tidal influence. In CBL1 a marginal decline in the terrestrial flux has been suggested by relatively low content of Al₂O₃, TiO₂, Co, Cu, and Zn.

The palaeoproductivity has been low during the deposition of CBL6 (Figure 6.17). A higher ratio of CaO/Al₂O₃, Cu/Al₂O₃, Sr/Al₂O₃, and Ba/Al₂O₃ in CBL5 along with lower TOC might be attributed to low scavenging of these metals by organism resulting into their increased concentration. In CBL3 remarkably high primary productivity has been observed resulting in lower ratios of CaO/Al₂O₃, Cu/Al₂O₃, Sr/Al₂O₃, and Ba/Al₂O₃ due to increased utilization.

The lower ratios of Fe₂O₃/Al₂O₃, TiO₂/Al₂O₃, and MgO/Al₂O₃ have suggested lower weathering during the deposition of CBL6 (Figure 6.18). However, a rise in weathering has been marked in CBL5. The subsequent period of lower weathering has been recorded during the deposition of CBL4 and CBL3. However, no remarkable deviation in weathering has been indicated during the deposition of CBL2 and CBL1.

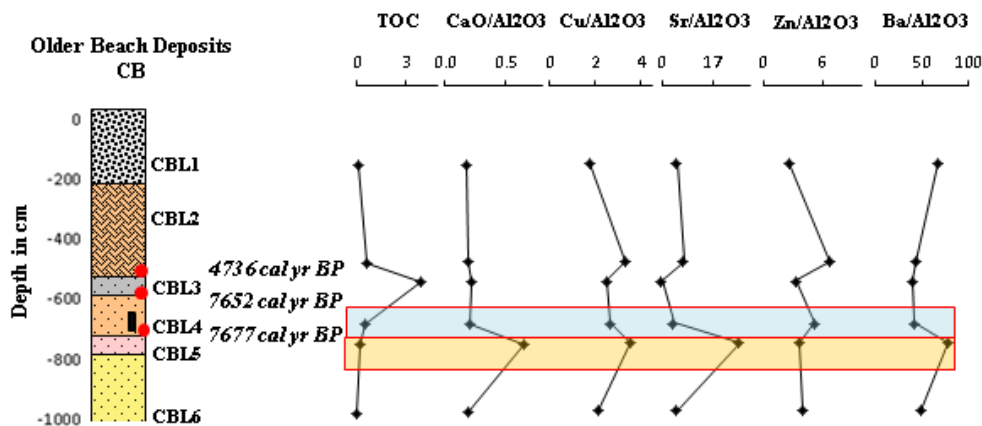


Figure 6.17 Variability in the proxies indicating palaeoproductivity at CB site. The yellow rectangles are showing higher palaeoproductivity while blue rectangles are showing lower palaeoproductivity

The salinity has remained higher at this location in comparison to the riverine zone. A higher salinity has been recorded in CBL6 which declined in CBL5 (Figure 6.18). Another phase of elevated salinity has occurred during the deposition of CBL4. The salinity has reduced again in CBL3. The next episode of higher salinity has been found in CBL2 which further increased in CBL1.

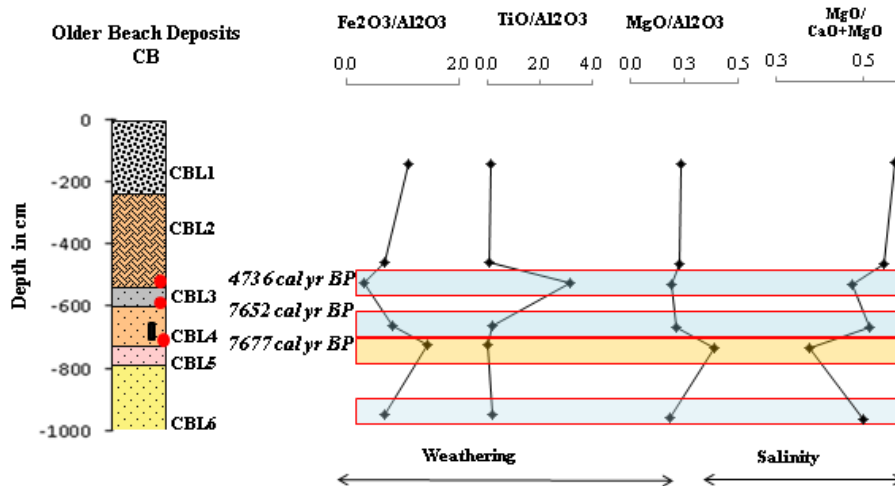


Figure 6.18 Variability in the proxies indicating weathering and salinity at CB site. The yellow rectangles are showing higher weathering and low salinity while the blue rectangles are showing lower weathering and higher salinity

From the above analysis, it has become clear that the intensity of fluvial processes was high during the deposition of CBL6. At this point in time, the tidal influence was low. The energy of river flow was weakening during the accumulation of CBL5 while in this phase the tidal processes were gaining dominance. This was followed by a period of intensified depositional activity under higher flow as evident in CBL4 deposited during 7677 cal yr BP. This can be associated with higher rainfall in the catchment area. It has coincided with lower tidal influence. A marginal decline in the intensity of fluvial activity has occurred during the deposition of CBL3 around 7652 cal yr BP. At this time, the influence of tidal activity increased. In the recent deposits represented as CBL2 (4736 cal yr BP) and CBL1, no considerable variation has been recorded in fluvial and marine processes.

Ambiligan (AG)

During the deposition of the basal sequence of palaeochannel AG (AGL5), a higher terrestrial flux has been indicated by the higher content of Al_2O_3 , TiO_2 , Fe_2O_3 , Co and Zn (Figure 6.19). This has suggested higher river flow under elevated rainfall conditions. The lower concentration of CaO and MgO has depicted an insignificant influence of tidal processes. In AGL4 traces of reduced terrestrial flux have been marked as the concentration of Al_2O_3 , TiO_2 , Fe_2O_3 , Co , and Zn has declined. The terrestrial flux has continued to decline until the deposition of AGL3 as the concentration of Al_2O_3 , Fe_2O_3 , Co , Cu , and Zn has further declined. These episodes have coincided with a surge in tidal activity as revealed by the higher content of CaO and MgO . However, in AGL2 the terrestrial flux has increased significantly as suggested by detrital tracers- Al_2O_3 , TiO_2 , Fe_2O_3 , Co , Cu , and Zn while the tidal influence declined. During the deposition of AGL1, a decline in the terrestrial flux has been demonstrated by the lower concentration of Al_2O_3 , Cu and Zn . At this time, an increase in tidal influence has also been recorded.

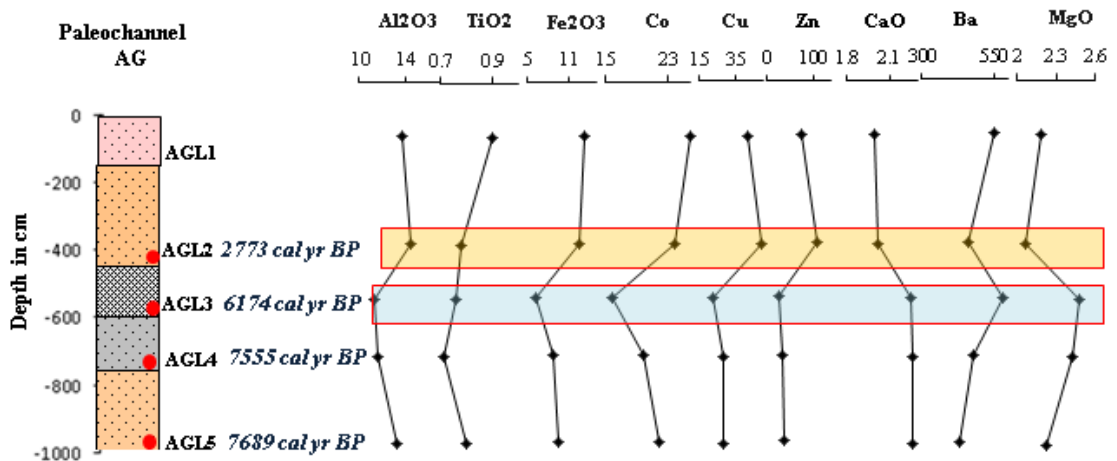


Figure 6.19 Variability in the proxies indicating terrestrial flux at AG site. The yellow rectangles are showing higher terrestrial flux while blue rectangles are showing lower terrestrial flux

The TOC has been lower in AGL5 in comparison to $\text{CaO}/\text{Al}_2\text{O}_3$, $\text{Cu}/\text{Al}_2\text{O}_3$, $\text{Sr}/\text{Al}_2\text{O}_3$, $\text{Zn}/\text{Al}_2\text{O}_3$, and $\text{Ba}/\text{Al}_2\text{O}_3$ (Figure 6.20). A lower primary production might have led to their higher concentration. In AGL4, the indication of increased palaeoproductivity has been marked by higher TOC concentration. However, no remarkable change in other indicators has been marked. Another episode of lower palaeoproductivity has occurred during the deposition of AGL3. Here, TOC, $\text{Cu}/\text{Al}_2\text{O}_3$, $\text{Sr}/\text{Al}_2\text{O}_3$, and $\text{Zn}/\text{Al}_2\text{O}_3$ have declined

significantly while Sr/Al₂O₃ and Ba/Al₂O₃ have increased. During the deposition of AGL2, a marginal rise in the palaeoproductivity has been suggested by TOC, Cu/Al₂O₃, Sr/Al₂O₃, and Zn/Al₂O₃. The palaeoproductivity has appeared to decline in AGL1.

Enhanced weathering conditions has been suggested by relatively higher values of FeO/Al₂O₃ and TiO₂/Al₂O₃ in AGL5 (Figure 6.21). This has been associated with the higher rainfall resulting in elevated weathering in the catchment region. A considerable reduction in the weathering process has been observed during the deposition of AGL3 revealing lower energy of river flow. In AGL2 and AGL1 the weathering has appeared to increase suggesting an increase in river erosion capacity.

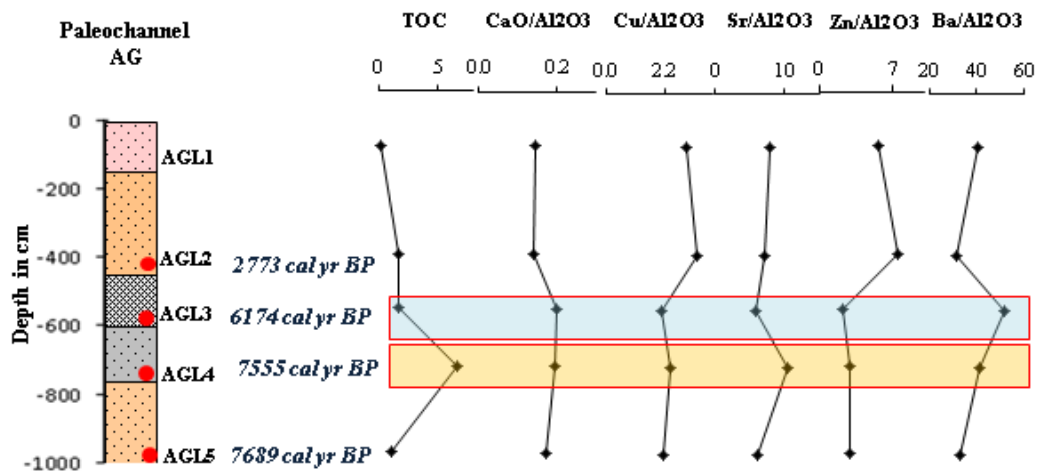


Figure 6.20 Variability in the proxies indicating palaeoproductivity at AG site. The yellow rectangles are showing higher palaeoproductivity while blue rectangles are showing lower palaeoproductivity

The salinity has remained around 0.60, however, no remarkable variation in the salinity condition has been observed till 1000 cm depth (Figure 6.21). Comparatively lower salinity has existed in AGL5 which has increased perpetually until the deposition of AGL3. A marginal decline in the salinity has been marked in AGL2 whereas it has increased marginally in AGL1.

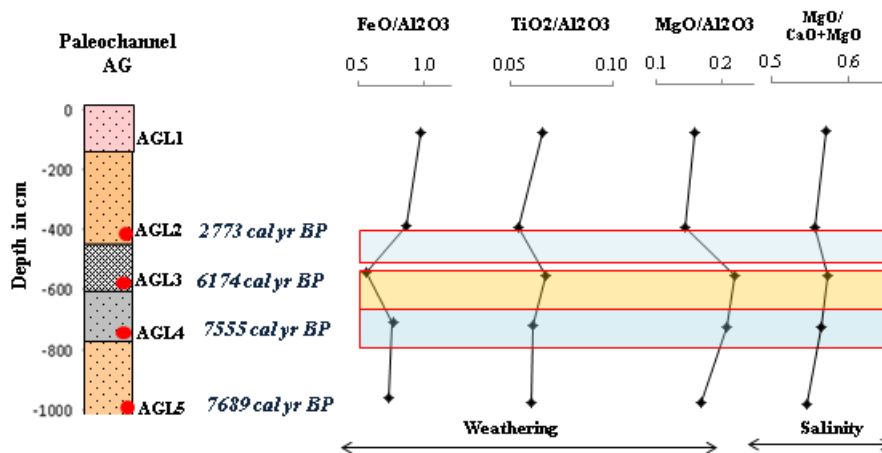


Figure 6.21 Variability in the proxies indicating weathering and salinity at AG site. The yellow rectangles are showing higher weathering and low salinity while the blue rectangles are showing lower weathering and higher salinity

The analysis has indicated a period of enhanced rainfall during the deposition of AGL5 around 7689 cal yr BP. Higher turbidity due to higher river flow might have resulted in the lower synthesis of organic materials during this episode. During the sedimentation of AGL4, the environment might have been stable and more favorable for the organisms to flourish. This humid period has been followed by an arid climate around 6174 cal yr BP (as indicated in AGL3). At this time, the influence of marine processes was also escalated as suggested by the higher concentration of sand, MgO, Ba, and CaO along with salinity. This also resulted in lower carbon productivity. Many great civilizations of the world have also collapsed owing to enhanced aridity around 6000 yr BP (Tripathi et al., 2014). Another episode of enhanced rainfall condition has occurred around 2773 cal yr BP as illustrated by enhanced terrestrial input and higher weathering resulting in lower productivity. During this episode again the impact of the tidal process declined.

Kasturikaran (KK)

The terrestrial flux has been higher during the deposition of KKL4 as suggested by the higher concentration of Al_2O_3 , TiO, Fe_2O_3 , Co, Cu and Zn (Figure 6.22). This has been attributed to the increase in river flow under increased rainfall. During this period the tidal processes have been less effective as revealed by the lower content of CaO, Ba, and MgO. In KKL3 notable decline in the terrestrial flux has occurred as revealed by the lower content of

Al₂O₃, TiO, Fe₂O₃, Co, Cu and Zn which can be attributed to the weakening of rainfall. At the same time, the tidal processes have gained predominance as represented by the higher content of CaO, Ba, and MgO. The terrestrial flux has appeared to increase again during the aggradation of KKL2 as the concentration of Al₂O₃, TiO₂, Fe₂O₃, Co, Cu, and Zn has increased considerably. The river flow must have increased during this period under enhanced rainfall. This period has coincided with the weakening influence of marine processes. In recent deposits represented by KKL1, the terrestrial flux has further increased as illustrated by higher Al₂O₃, TiO₂ Co and Zn. On the other hand, lower content of CaO, Ba, and MgO has suggested a decline in tidal influence.

The palaeoproductivity has remained high during the sedimentation of KKL4 as suggested by higher TOC, Cu/Al₂O₃, Sr/Al₂O₃, and Zn/Al₂O₃ (Figure 6.23). It has indicated that this period was relatively stable and less turbidity might have resulted in an increase in primary production. In KKL3, clues of declining palaeoproductivity have been marked which have coincided with higher detrital flux and lower marine influence. Another episode of elevated palaeoproductivity has been marked during the sedimentation of KKL2. In KKL1, the palaeoproductivity has declined again as suggested by the lower content of TOC, CaO/Al₂O₃, Cu/Al₂O₃, and Sr/Al₂O₃.

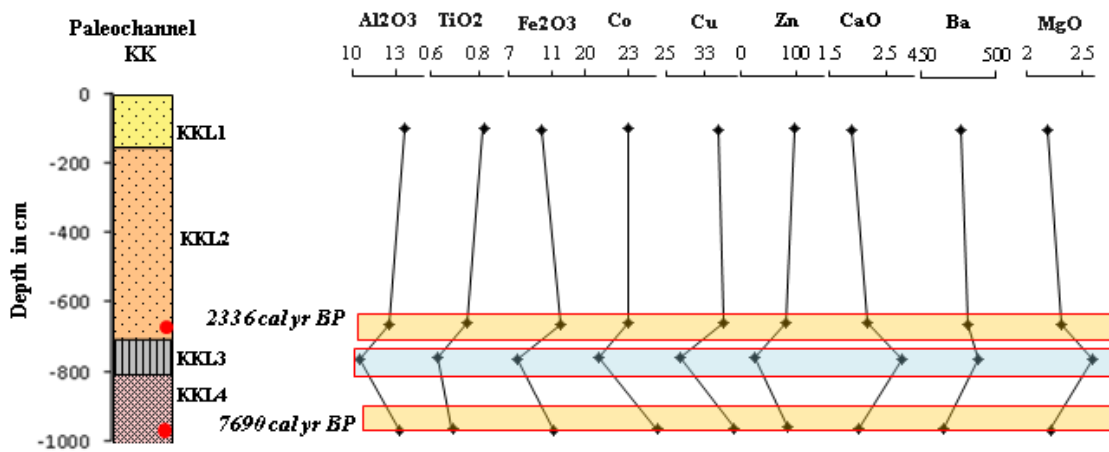


Figure 6.22 Variability in the proxies indicating terrestrial flux at KK site. The yellow rectangles are showing higher terrestrial flux while blue rectangles are showing lower terrestrial flux

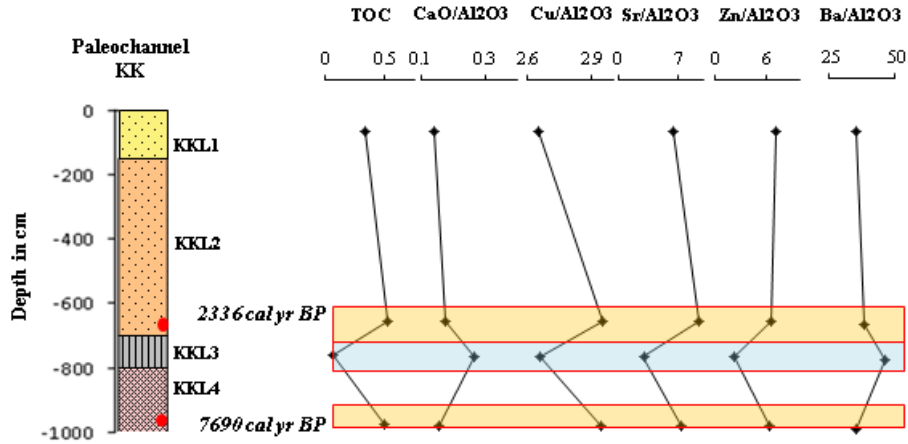


Figure 6.23 Variability in the proxies indicating palaeoproductivity at KK site. The yellow rectangles are showing higher palaeoproductivity while blue rectangles are showing lower palaeoproductivity

A higher weathering under enhanced fluvial action has been marked in KKL4 suggested by the higher ratio of Fe₂O₃/Al₂O₃ (Figure 6.24). A lower weathering by marine influence has been suggested by lower MgO/Al₂O₃ ratio. It has appeared that the weathering in this facie has been mainly governed by the fluvial action. The flux of detrital elements has declined in KKL3 indicating lower weathering in the catchment area. At this time, weathering has been governed by tidal influence and not by the fluvial action. In KKL2 a rise in weathering has been marked in the catchment region resulting in a higher inflow of Fe₂O₃. In KKL1, the weathering has declined as suggested by the geochemical proxies.

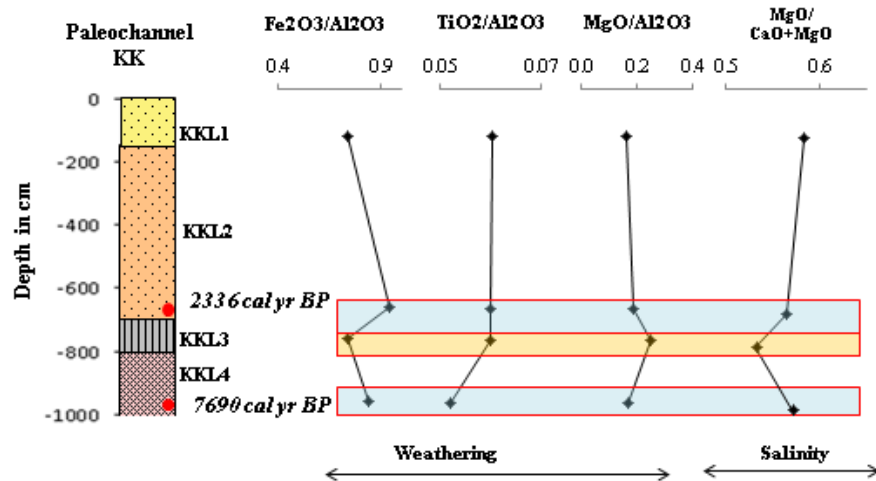


Figure 6.24 Variability in the proxies indicating weathering and salinity at KK site. The yellow rectangles are showing higher weathering and low salinity while the blue rectangles are showing lower weathering and higher salinity

The salinity has remained approximate to 0.60 in all the facies (Figure 6.24). At this location, relatively higher salinity has been recorded along with higher detrital flux. Along with this, during decreasing terrestrial flux the salinity has also declined marginally. This might have been attributed to its location very close to the Dhamara estuary. In the past, this location might have been under greater influence of marine processes.

Thus, it is apparent that the rainfall has been higher during the deposition of KKL4 around 7690 cal yr BP. It has declined during the deposition of KKL3 when the tidal processes were predominant. Another increase in the rainfall intensity has occurred during the deposition of KKL2 around 2336 cal yr BP coinciding with the reduced tidal influence at this location.

On the basis of the above discussion, it can be stated that prior to 7700 cal yr BP the rainfall intensity was high in the coastal Odisha manifesting into elevated terrestrial flux and weathering. Higher turbidity has led to a lower synthesis of organic carbon during this period. At this point in time, the influence of the tidal process was also low. The rainfall was weakened between 7700 and 6100 cal yr BP when the terrestrial flux, as well as weathering, have declined. The tidal activity gained predominance as suggested by higher salinity and inflow of biogenic elements. Another episode of enhanced rainfall intensity existed between 2700 and 2300 cal yr BP in the region. This was also the period of declining impact of tidal action.

6.5 Discussion and Conclusion

The analysis of palaeoclimate has been based on inferring the changes in depositional processes the basis of relative method i.e. variations in terrestrial flux, palaeoproductivity, weathering and salinity conditions and arrange these events into chronological order using radiocarbon (^{14}C) ages. In recent time, the tidal water generally does not reach to the riverine zone while it continuously affected the mixing zone. The study has also aimed to analyze the variability in humidity/rainfall conditions during the Holocene using geochemical proxies. However, it was realized that the area has experienced sea transgression and regression in the past that must have also affected the evolution of landforms as well as the environment of deposition which is also recorded in other literatures (Banerjee, 1993; Islam and Toolet, 1999; Banerjee, 2000; Hameed et al., 2006; Khandelwal et al., 2008; Narayana et al., 2017).

It is well established that climate has altered between humid and arid episodes during the Holocene which are the manifestations of changes in rainfall intensity (Roberts, 1998; Banerji et al., 2017). Here, the periods of enhanced and weakened rainfall during the Holocene have been inferred through deviation in terrestrial flux, primary productivity, weathering, and salinity. Their variability, in addition, has also demonstrated variation in tidal/marine influence in the region. The terrestrial flux represents the amount of sediment load being transferred from continents to the oceans. Therefore it has been regarded as a function of changes in climatic conditions i.e. humidity and aridity affecting the intensity of sediment transportation. Sediment accumulation is affected by weathering. As during higher weathering, more materials are available for transportation. In turn, higher weathering is assisted by higher rainfall and enhanced humidity. The palaeoproductivity is generally influenced by the presence or absence of turbidity where the synthesis of organic carbon can take place without disturbance. The level of salinity is also the manifestation of the fluvial and marine processes. Under enhanced monsoon condition the salinity is likely to decline owing to the higher concentration of freshwater. In contrast, during arid periods the salinity is likely to increase. A higher inflow of saline water can also result in a higher level of salinity. Thus, the selected geochemical proxies are directly linked with rainfall intensity and tidal influence.

Remarkable changes in rainfall intensity are apparent in the riverine zone as indicated by variability in terrestrial flux, palaeoproductivity, weathering, and salinity. The elevated intensity of rainfall has been marked during the deposition of EPL7 while in JPL7 indication of low rainfall has appeared. During the deposition of EPL6 weakening in rainfall intensity has occurred. On the other hand, the intensity of rainfall began to increase in JPL6 as suggested by the selected proxies. In EPL5 and JPL5 signal of enhanced rainfall has been detected. This is followed by the weakening of rainfall during the sedimentation of EPL4 and JPL4. During the deposition episode of EPL3 and JPL3 rainfall intensity increased again. Owing to their shallow depth no considerable change in rainfall pattern could be observed at KTI and KTII locations. Nevertheless, during the deposition of KTIII5 considerable increase in rainfall has been marked. The elevation of these locations (MSL) has varied providing facies with distinct physical and geochemical characteristics (Chapter 2). The period of rainfall enhancement has intersected well with reduced tidal influence in

the riverine zone. In contrast, during rainfall weakening, an increase in tidal activity has been marked.

In the mixing zone, substantial inferences about the past climate have been drawn by combining the geochemical proxies with AMS ^{14}C ages. The sedimentary history of SP, up to the depth of 1000 cm is comparatively newer than the other locations. Here, no significant change in rainfall intensity was suggested by the geochemical proxies between 1600 and 880 cal yr BP. At CB site, higher terrestrial flux has been recorded during 7677 cal yr BP probably coinciding with a humid episode during the mid-Holocene period (Banerji et al., 2017; Narayana et al., 2017; Makwana et al., 2019). In CBL3 deposited during 7652 cal yr BP, again the terrestrial flux has remained high with declined MgO content. A lower terrestrial flux was reported in CBL2 during 4736 cal yr BP.

At AG and KK locations, both collected from palaeochannel, the terrestrial flux has been higher during 7689 cal yr BP followed by a reduced flux during around 6174 cal yr BP. Another episode of elevated terrestrial flux recorded around 2773 cal yr BP. In KK, similarly, terrestrial flux has been higher during 7690 cal yr BP. It declined during KKL3 deposition and increased again during 2336 cal yr BP.

The productivity of organic carbon at the CB site, indicated by TOC was low around 7677 cal yr BP. It increased during 7652 cal yr BP followed by a decrease around 4736 cal yr BP. The lower primary productivity in AG has occurred during 7689 cal yr BP. However, during around 7555 cal yr BP, the palaeoproductivity increased abruptly. It declined during around 6174 cal yr BP. In KK during 7690 cal yr BP, the palaeoproductivity was high followed by a decrease during the deposition of KKL3. This episode gave way to declined palaeoproductivity condition during 2336 cal yr BP and continued to be low till the recent deposits. The weathering has increased in comparison to the riverine zone suggesting higher weathering by marine processes. In CB, weathering was relatively high during 7677 cal yr BP. No remarkable change has occurred thereafter. In AG, traces of higher weathering is shown during 7689 cal yr BP which declined considerably around 6174 cal yr BP. The increase in weathering has been recorded around 2773 cal yr BP at AG site. In KK, higher weathering has occurred around 7690 cal yr BP under elevated rainfall conditions. It declined during the aggradation of KKL3 and increased again around 2336 cal yr BP.

It has been observed that comparatively higher salinity level has prevailed in the tide-dominated region around 7600 cal yr BP as indicated in AG and KK. Around 6174 cal yr BP, the salinity has marginally declined. It increased slightly around 2700 and 2300 cal yr BP in the region. In the mixing zone also, the episodes of enhanced rainfall intensity have coincided with lower tidal influence. On the contrary, periods of rainfall weakening have associated with an augmented tidal activity.

The above discussion has illustrated that the intensity of rainfall has declined since 7700 cal yr BP in the study area and the climate began to shift to sub-humid and semi-arid conditions. During this episode, the terrestrial flux declined while marine processes began to dominate. This phase has been marked CBL4, AGL5 and KKL4. The salinity level, on the other hand, was perpetually increasing. The production of organic carbon, (TOC) began to increase during 7600 cal yr BP as observed in CBL3 and AGL4 suggesting low turbidity that helped in synthesis of organic carbon. Higher palaeoproductivity has also been associated with mangrove forests that flourished under freshwater-saltwater interface (Banerji et al., 2015; Banerji et al., 2017). Hence, it can be elucidated on the basis of geochemical proxies and radiocarbon dates that since 7700 cal yr BP that rainfall began to decline. At this time, the sea level started to increase that led to the flourishing of mangrove vegetation at these locations. However, at present the zone of mangrove vegetation has shifted seaward.

The rainfall reached to its minimum level and the climate became drier during 6174 cal yr BP. This episode was indicated by the least concentration of detrital elements in AGL3, and KKL3. The supply of terrestrial flux was the minimum while marine activities increased remarkably. The AGL3 and KKL3, deposited during this period are predominantly grayish sandy facie. This has indicated a higher influence of marine activity and lower influence of fluvial processes. This episode has also been marked in CBL2 which was deposited around 4736 cal yr BP indicating that this drier phase existed till 4736 cal yr BP. The palaeoproductivity declined during this period suggesting unfavorable conditions for mangrove vegetation. The level of weathering also declined while salinity increased. Hence, based on the geochemical proxies it can be stated that the rainfall declined and attained its minimum level around 6174-4736 cal yr BP (CBL2 and AGL3). At this time, the sea level reached to its maximum in the area of study.

Band et al (2018) has also reported an episode of weak monsoon that existed in central India during 6500-5600 yr BP. This episode has also been recorded on the south-west coast of India during 6000 cal yr BP by Limaye et al., (2017). In northern Africa also, since mid-Holocene (7000 and 5700 cal yr BP), less humid climate has been observed (Lezine, 1989). Researches also provide examples of societal collapse that occurred during 6000 yr BP associated with the abrupt shifts to drier and/or colder climate (Weiss et al., 1993; Weiss and Bradely, 2001; Tripathy et al., 2014).

A sea transgression has been reported in the southern coast during 6000 yr BP (Banerjee, 1993); western coast during 7000 cal yr BP (Hashmi et al., 1995) and south-eastern coast during 5600 yr BP (Jayangondaperumal et al., 2012). In Odisha coast, a higher sea level is registered by Khandelwal et al. (2008) during 7900 cal yr BP using pollen. However, this finding has not appeared in the present study might be because here, the time period started since 7700 cal yr BP which is younger. CBL5, in this study, suggesting higher tidal influence might have been deposited during this phase. Furthermore, the deviation in the result can also be due to reconstruction based on different proxies, pollen and sediment records. Nevertheless, different parts of the world experienced their own local sea level oscillations over the last 6000 years (Roberts, 1998).

The intensity of rainfall began to increase since 4736 cal yr BP, as marked in CBL1, AGL2 and KKL2. During this episode, the terrestrial flux and weathering increased considerably. Elevated terrestrial flux has suggested an increase in river runoff that led to the dominance of fluvial activity in the coastal Odisha. The influence of marine activity declined as indicated by lower concentration of MgO, Ba and CaO. The palaeoproductivity also declined that can be attributed to higher turbidity due to elevated river flow. Hence, this phase was dominated by a comparatively humid period and weak tidal activity.

Another period of weak rainfall intensity occurred during 2700 cal yr BP as recorded in AGL1. Srivastava and Farooqui (2013) have also suggested a dry and arid climate coupled with weakened monsoon between 2600 and 1300 cal BP in the Cauvery delta region. Similarly, Farooqui and Naidu, (2010) have reported a drier climate around 3000-2000 yr BP after which the rainfall began to increase. At the same time, Khandelwal et al. (2008) have illustrated a fall in sea level after 2700 cal yr BP near the Odisha coast. The period of

low rainfall is also recorded around 1647 cal yr BP in SPL4 when the terrestrial flux declined and marine influence increased marginally. However, during 1356-882 cal yr BP no significant change in rainfall is detected (SPL3 and SPL2).

Therefore, by compiling the results of different sites, it can be concluded that a period of enhanced rainfall has occurred during around 7700 cal yr BP. Higher turbidity due to higher river flow might have resulted in the lower synthesis of organic materials during this episode. Around 7500 cal yr BP, the environment became more favorable for the organisms to flourish. At this time the rainfall intensity began to decline while tidal activity started to dominate. This period was followed by a predominantly semi-arid climate that existed around 6000-4700 cal yr BP. During this period, the influence of marine processes also escalated. Several great civilizations across the world were also collapsed owing to enhanced aridity around 6000 yr BP (Tripathy et al., 2014). Another episode of enhanced rainfall condition has occurred between 6000-2700 cal yr BP. During this episode again the impact of the tidal process declined while fluvial activities dominated. Since 2700 cal yr BP, the geochemical proxies have indicated another phase of weak rainfall.

Chapter 7

Summary and Conclusion

The analysis of palaeoclimate is essential to have a broader idea about the past climate which was never static on the Earth. It has an intense influence on each and every aspect of human life, be it agriculture, economy or health. Thus, changing climate is going to have severe ramifications for society. The coasts are considered more vulnerable due to their intense relationship with both climatic and eustatic perturbations. Hence, any change in climate or/and sea level is going to directly affect these coastal locations and the population. A remarkable array of evidence is used to reconstruct the palaeoclimate. These traces of past climate range from tree rings, speleotherms, and sedimentary archives to floral and faunal remains over the land and under the sea. The coastal environment represents the amalgamation of landforms e.g. older beach deposits, deltaic plains, ox-bow lakes, palaeochannels. These landforms are the repository of rich Quaternary sediments. Thus, some of the most crucial traces of past climate, especially the Holocene and processes are well preserved in the coastal sedimentary environments. These sediment sequences are frequently utilized as a tool to investigate the perturbations in the past climate and sea level. The east coast of India has experienced significant climatic and eustatic oscillations. A number of studies are based on the palaeoclimate of the east coast using proxy sources. However, very few studies have been conducted to reconstruct palaeoclimate using conjunctive application of textural, geochemical, and geochronological interpretation. Besides, the palaeoclimatic studies were not carried out earlier for Lower Baitarani basin, coastal Odisha. Thus, one of the main objectives of this work was to improve the existing methodological approach and fill the research gap in palaeoclimatic reconstruction in the study area. This study has also incorporated a multi-proxy approach to reconstruct the palaeoclimate which is generally scanty in this region. This work also meant to investigate the utility of geochemical proxies in unraveling the palaeoclimate.

For this work, first of all, the selected area was divided into two distinct zones- 1) Riverine Zone and 2) Marine Zone. This categorization is based on the dominating geomorphic process operating in the study region at present. As the name suggests the fluvial processes are predominant in the riverine zone while the mixing zone is influenced by both fluvial and marine activities. Subsequently, major landforms were identified in each zone which includes- 1) Palaeochannels from where EP and KTI (in the riverine zone,) as well as AG and KK (in the mixing zone) samples were collected, 2) Inter-channel regions lying

between palaeochannels from where JP and KTII were obtained, 3) Active floodplain from where SP was collected and 4) Older beach deposits from where CB was obtained. The geological evidence demonstrates a fault line running almost parallel to the river, bifurcate the study area into northern and southern transects. The EP, JP, KTI, and KTII located in the riverine zone fall under the southern transect while SP, CB, AG, and KK located in the mixing zone fall under the northern transect. The samples were collected through trenching and bore-welling. KTI and KTII were collected through digging trench. These are shallower with the depth ranging from 140 cm to 165 cm respectively. Remaining sub-surface samples were collected by bore-welling up to a depth of 1000 cm. Sub-sampling is based on visible colour and textural variations at different depths.

The colour and texture of the sub-surface samples were primarily determined for facie identification (Chapter 2). Subsequently, these characteristics also illustrate changes in the depositional environment in the past. In the riverine zone, brown and red colours are the most abundant which are indicative of well-oxidized and freshwater environment. In the mixing zone gray, black and grayish-white colours are predominant indicating the prevalence of reducing, swampy and stagnated environment. The particle sizes i.e. sand, silt, and clay also influence colour of the particular strata by absorbing certain metals more than the other. The texture has varied significantly in the region selected for the study (Chapter 2). In general, facies of the riverine zone are coarser than the mixing zone. For instance, in EPL4, EPL6, JPL4, KTII2, KTII3, and KTII4 clay and silt particles are predominant. In the mixing zone, however, clay is the most abundant. In this zone only CBL1, CBL2, AGL3 and KKL3 are sandy.

In this study, it has been observed that red, brown and yellow colours are usually associated with clay particles i.e. EPL1, EPL2, EPL5, JPL1, JPL5, KTIL1, KTIL3 and KTII1 in the riverine zone. In the mixing zone, in general, black and gray colours are associated with clayey facies such as SPL4, SPL5, CBL3, CBL4, CBL5, AGL1, AGL4, and AGL5. Nevertheless, in some cases, gray colour is also observed in sandy facies like JPL4, JPL11, KTIL2, KTII2, CBL2, AGL3, and KKL3.

The inspection of colour and textural variations has provided crucial information about the past depositional environment and the processes that have operated at the time of sedimentation. For instance, red and brown colour of EP, KTI and KTII are associated with

freshwater, well-oxidized environment i.e. riverine in which the deposition took place. Nevertheless, in KTIIIL2, KTIIIL5, KTIIIL9, JPL4, JPL6, JPL8, and JPL11 shades of gray were observed indicating oxygen-reduction conditions in which the deposition occurred. In the mixing zone, at SP site brown and red colours are prevalent in the upper segments of the stratigraphy while in the lower sequences gray colour is abundant. At CB most of the facies are gray or black and only the basal sequence is of yellow colour. Similarly, at AG and KK gray colours were predominant. These colours are the indicators of the swampy, stagnated and reducing environment of deposition. Thus, red and brown colours have suggested sediment aggradation mainly under oxygen abundance in the riverine zone while in the mixing zone shades of gray has illustrated the prevalence of the stagnated and oxygen-reduction environment.

The variations in colour and texture have revealed the involvement of two distinct processes that have operated in the past. In general, in a river basin, coarser facie can be associated with the high magnitude fluvial processes while clayey facie can be attributed to the low magnitude fluvial action that might have occurred in the past. However, for coastal locations, palaeoclimate analyses are rather complex. The study area constitutes a part of the eastern coastal plain of India. Thereby, it contains thick stratigraphic records of the Quaternary period suggesting that it was under the marine influence at some instance of time. Even at present, the mixing zone is influenced by both fluvial and marine processes. During the high tide the saline water is carried far inland through the river channel. This phenomenon affects and must have influenced the configuration of the sedimentary environment in the past. Hence, analysis based on only sediment physical properties is likely to lead to some faulty assumptions. In this regard, the geochemistry of the sub-surface sediments has provided crucial assistance.

The concentration of major, trace and REEs in each facie are identified using EDXRF (Chapter 3). It is apparent that among the selected major elements only MnO is enriched above the UCC level while all the other metals are depleted. Among the trace elements Cr, Cu, and Pb are enriched demonstrating anthropogenic influence in the coastal zone. The depletion of elements is usually the result of their higher mobility and low preservation. On the other hand, enrichment can be attributed to natural or anthropogenic influences i.e. pesticides, industrial waste etc.

In addition, certain elements such as Fe_2O_3 , Al_2O_3 , Cu, Co, Zn, and La are considered as detrital tracers. Hence, an increase in their concentration can be associated with the enhanced magnitude of the transportation process. In contrast reduction in their concentration can be linked to reduced flow conditions. In this study, it has been observed that the concentration of MgO, CaO, and Ba was low during the enhanced flow condition while during reduced flow their concentration was higher. It was inferred that tidal activity must have increased during the low flow condition whereas it reduced during the higher flow. At the same time, sea transgression and regression as reported in this analysis has affected the sediment deposition.

A strong correlation among Al_2O_3 , Fe_2O_3 , MnO, TiO_2 , and SiO_2 suggests that these major elements are derived from a common source. These are considered as detrital elements and hence mostly contributed from the catchment region. On the other hand, these elements show a negative correlation with MgO and Ba. In some cases, MgO, Ba, and CaO have a strong correlation that indicates their common origin. The latter group is regarded as the marine biogenic product and hence mainly derived from the marine sources. The geochemical analysis indicates that clay and silt dominated facies are rich in detrital elements in which the concentration of biogenic elements is low. In contrast, the sandy facies are rich in biogenic deposits and low in terrestrial metals. Thus, it is evident that the clay dominated facies are contributed from the terrestrial sources under the influence of fluvial processes. On the other hand, an increase in marine activity and sea-transgression has led to the deposition of sandy facies. Thus, it can be elucidated that sedimentary proxies can reveal important information about the changes in the processes that were operating in the past. The analysis of colour, texture, and geochemistry has also provided insight to the palaeoclimate.

The analysis of redox-sensitive element has yielded information about the palaeoredox environment (Chapter 4). In this study, V, Cr, Co, Cu, Zn, La, Ce, Nd, and TOC were selected as redox indicators. Along with this, the ratios of V/Cr, V/Al, Fe/Al, and Cu/Zn were used to examine oxic and anoxic conditions. However, among selected redox-sensitive metals and ratios only TOC, Cu/Zn, and REEs. They have revealed that in the riverine zone, during sediment aggradation primarily oxic conditions have prevailed. On the contrary, in the mixing zone during sedimentation anoxic conditions has been predominant. The blackish and yellow facies are usually associated with reducing or anoxic environment whereas the

red and brown facies are the indicators of oxic and well-oxygenated conditions. The analysis has indicated that sandy facies were deposited under low oxygen conditions that might be associated with higher salinity during high sea stand. In contrast, the facies with red and brown colour were deposited primarily through fluvial processes. Therefore, it has become obvious that the physical and chemical attributes of the sediments are crucial tracers of the palaeoclimate and processes that have operated in the past.

These physical characteristics along with ^{14}C dates were used to construct the chronology of the landforms (Chapter 5). The SP represents the younger, active floodplain deposits located at the confluence of Baitarani and Salnadi. The CB collected from older beach deposits, on the other hand, revealed the oldest sedimentary deposits up to 1000 cm depth. It is apparent that the evolution of active floodplain is dominated by riverine processes. Nevertheless, at SP site the basal sequence, SPL6 was deposited through enhanced marine action suggesting that in the past, it was under marine influence. The older beach deposit was aggraded through wave action during the sea transgression. However, the deposition of CBL4 (7652 cal yr BP) and CBL3 (4736 cal yr BP) took place under fluvial dominance. The palaeochannels AG and KK were influenced by both fluvial and marine processes. For instance, the aggradation of AGL5 and KKL4 took place during 7600 cal yr BP under the prevalence of fluvial processes whereas AGL3 was deposited through marine processes around 6174 cal yr BP.

The reconstruction of the palaeoclimate of the lower Baitarani basin is conducted by utilizing the physico-chemical characteristics of sediments along with radiocarbon dates (Chapter 6). These indications have also been used to distinguish the processes that have operated in the region during the mid-Holocene. It has appeared that around 7700 cal yr BP the area has experienced higher fluvial action. At this time, the climate was humid with higher precipitation lengthening the course of the river. However, since 7700 cal yr BP, the rainfall began to decline and around 6100 cal yr BP it became sub-humid or semi-arid. This resulted in lower fluvial activity. At the same time, the marine processes began to dominate leaving their footprints in the sedimentary archives. The climate again became predominantly humid during 2500 cal yr BP when the influence of riverine processes increased. A marginal reduction in the rainfall has been inferred during 1350 cal yr BP.

Thus, it can be established that all the research questions (discussed in Chapter 1, Section 1.4) have been answered through the present analysis. The physical and geochemical

characteristics of the sediments, indeed have disclosed hidden treasures about the past climate in coastal Odisha.

Based on the above discussion, distinct episodes of rainfall enhancement and weakening have been identified during the mid-late Holocene period demonstrating characteristic influence of fluvial activity under a humid environment. Along with this, significant changes in the marine influence are also marked under the semi-arid climate. The mid-Holocene climate, therefore, has been classified in distinct periods with characteristic fluvial and marine influences. This characterization is based on the geochemical proxies and radiocarbon dates -

7.1 Period of enhanced rainfall (till 7700 cal yr BP)

The episode of enhanced rainfall is marked in CBL4, AGL5, and KKL4. These facies indicate higher terrestrial flux and weathering under elevated river flow. However, the proxies have suggested lower palaeoproductivity in CBL4 and AGL5 which can be the result of higher turbidity. In contrast, in KKL4 higher primary production is marked. The higher palaeoproductivity at this site can be associated with low turbidity that assisted in primary production. At this time, there are signs of lower salinity level. The continental flux is primarily controlled by the river discharge which in turn is governed by the rainfall. Thus, on the basis of geochemical proxies and ^{14}C dates, it has been inferred that the region was experiencing a comparatively humid period dominated by the intense fluvial activity till 7700 cal yr BP. At this time, the influence of marine processes was weak as suggested by lower concentration of marine biogenic deposits i.e. Ba and MgO as well as lower salinity in these facies.

The episode of enhanced runoff has also been observed in the central India during 8500-6500 cal yr BP (Band et al., 2018). Higher river flow has been associated with a surge in rainfall during the mid-Holocene period. Limaye et al. (2017) have observed signatures of enhanced monsoon rainfall on the south-west coast of India during 9000-6000 cal yr BP.

At global scale, the phenomenon of enhanced precipitation has been registered during early-mid Holocene period. It is because the rapid rise in temperature at the Pleistocene-Holocene transition manifested into enhanced humidity (Roberts, 1998). In the desert environment, higher summer rainfall during the early-Holocene has been associated with higher lake level

(Singh et al., 1974). Similarly, in the Tibetan plateau, higher precipitation has been reported during the mid-Holocene (Gasse and Campo, 1994). These evidence demonstrate that the entire Asian monsoon system was strengthened during the early-mid Holocene period (Roberts, 1998). Apart from the monsoon regions, warm and humid early-mid Holocene climates have been found in other parts of the Tropics such as the Caribbean and Northern Australia (Leyden, 1987; Hodell et al., 1991). Enhanced early-mid Holocene precipitation is also recorded in the Mediterranean-type regions such as South Australia (Luly, 1993; Chappell and Grindrod, 1983). The existence of a wetter period has also been recorded in northern Africa during the early-Holocene period (Petit-Maire and Riser, 1981).

It is established now that between 10,000 and 5500 cal yr BP level of lake water increased leading to water surplus conditions in the semi-arid Sahel and the Sahara desert (Fontes and Gasse, 1991). Moreover, the Sahara desert did not exist effectively during the early-Holocene humid period marked between 10,000 and 5500 cal yr BP (Roberts, 1998). Thus, during the early-mid Holocene, the climate was milder and more humid not only in India but in different parts of the world.

7.2 Period of rainfall weakening (since 7700-4736 cal yr BP)

In the study region since 7700 cal yr BP, the rainfall began to decline and the climate started to shift from humid to sub-humid and semi-arid conditions. This period is marked by the diminishing concentration of terrestrial flux and increase in the marine biogenic supply in form of Ba and MgO during the deposition of CBL3 and AGL4. At this time, the salinity was also perpetually declining. The production of organic carbon, (TOC) began to increase during 7600 cal yr BP as observed in CBL3 and AGL4 suggesting low turbidity that helped in the synthesis of organic carbon. Increase in the primary production under weakening of humidity can also be attributed to the occurrence of mangrove vegetation as reported by Banerji et al., (2015) and Banerji et al. (2017), as it flourishes under the saline environment. Thus, it can be elucidated on the basis of geochemical proxies that since 7700 cal yr BP rainfall intensity began to decline. At this time, the sea level began to increase that led to the flourishing of mangrove vegetation at these locations.

Around 6174 cal yr BP, the rainfall reached to its minimum level and the climate became predominantly semi-arid to arid. This episode was indicated by the lower concentration of

terrestrial elements in AGL3, and KKL3. The supply of terrestrial flux was the minimum while marine activities increased markedly. The AGL3, deposited during this period is predominantly a sandy facie. This has indicated a higher influence of marine activity and lower fluvial influence. This episode has been marked in CBL2 that was deposited around 4736 cal yr BP indicating that this relatively drier phase existed till 4736 cal yr BP. The palaeoproductivity declined during this period suggesting unfavorable conditions mangrove vegetation to grow. The level of weathering also declined while salinity increased. Hence, based on the geochemical proxies and ^{14}C dates it can be stated that since 7700 cal yr BP the rainfall began to decline which attained its minimum around 6174-4736 cal yr BP (CBL2 and AGL3). At this time, the sea level reached to its maximum suggesting a sea transgression in The Lower Baitarani Basin.

Band et al (2018) have also reported an episode of weak monsoon that existed in central India during 6500-5600 yr BP. This episode has also been recorded on the south-west coast of India during 6000 cal yr BP by Limaye et al., (2017). Apart from the Indian subcontinent, in northern Africa also, since mid-Holocene (7000 and 5700 cal yr BP), less humid climate has been observed (Lezine, 1989). Researches also provide examples of societal collapse that has occurred during 6000 yr BP synchronous with the abrupt shifts to drier and/or colder climate (Weiss and Bradely, 2001; Tripathy et al., 2014).

A sea transgression has also been reported in the southern coast during 6000 yr BP (Banerjee, 1993); western coast during 7000 cal yr BP (Hashimi et al., 1995) and south-eastern coast during 5600 yr BP (Jayangondaperumal et al., 2012). In Odisha coast, a higher sea level is registered by Khandelwal et al. (2008) during 7900 cal yr BP using pollen. However, this finding has not appeared in the present study might be because here, the time period started since 7700 cal yr BP which is younger. The CBL5, in this study, suggesting higher tidal influence might have been deposited during this phase. Furthermore, the deviation in the result can also be due to reconstruction based on different proxies, pollen and sediment records.

7.3 Period of enhanced Rainfall (around 4736-2700 cal yr BP)

The rainfall began to increase since 4736 cal yr BP, as suggested by geochemical proxies in CBL1, AGL2 and KKL2 which were deposited during this time. During this period, the

terrestrial flux and weathering increased considerably. Elevated terrestrial flux has suggested an increase in the river runoff that led to the dominance of fluvial activity in the coastal Odisha. The influence of marine activity declined as indicated by a lower concentration of MgO, Ba, and CaO. The palaeoproductivity also declined that can be attributed to higher turbidity due to the elevated river flow. The freshwater-saline water interface also migrated seaward resulting in loss of mangrove vegetation. Hence, this phase was dominated by a comparatively humid period along with the weak tidal activity.

7.4 Period of Rainfall weakening (Since 2700 cal yr BP)

The rainfall intensity declined again since 2700 cal yr BP as recorded in AGL1. Srivastava and Farooqui (2013) have also suggested the occurrence of dry and arid climate coupled with weakened monsoon between about 2600 and 1300 cal BP in the Cauvery delta region. Similarly, Farooqui and Naidu, (2010) have reported a drier climate around 3000-2000 yr BP after which the rainfall began to increase. At the same time, Khandelwal et al. (2008) have illustrated a fall in sea level after 2700 cal yr BP near the Odisha coast.

A weak rainfall is also recorded around 1647 cal yr BP as marked in SPL4 when the terrestrial flux declined and marine influence increased marginally. However, during 1356-882 cal yr BP no significant change in rainfall is detected (SPL3 and SPL2).

In summary, it can be stated that a period of enhanced rainfall has occurred around 7700 cal yr BP. Higher turbidity due to higher river flow might have resulted in the lower synthesis of organic materials during this episode. Around 7500 cal yr BP, the environment became more favorable for the organisms and mangroves to flourish. At this time the rainfall intensity began to decline while tidal activity started to dominate. This period was followed by a predominantly semi-arid climate that existed around 6100-4700 cal yr BP. During this period, the influence of marine processes escalated. Several great civilizations across the world were also collapsed owing to enhanced aridity around 6000 yr BP (Tripathy et al., 2014). Another episode of enhanced rainfall condition has occurred between 4700-2700 cal yr BP. During this episode again the impact of the tidal process declined while fluvial activities dominated. Since 2700 cal yr BP, the geochemical proxies have indicated another phase of rainfall weakening.

The analyses of physico-chemical characteristics of the sub-surface sediments have unraveled remarkable clues to the past climate and shift in the geomorphic processes. The depositional environment, in the present study, is recognized on the basis of spatio-temporal association of lithofacies and through the interpretation of physical and chemical characteristics of the subsurface sedimentary facies. The colour and textural variations of sediments have unraveled some of the most crucial signatures of the past climate under which the transportation and deposition of sediments took place.

The colour, texture and geochemical analyses have suggested a predominance of fluvial and marine processes during distinct depositional episodes. It was speculated based on physical properties of the sub-surface sediments that the deposition of fine-grained facies has occurred during fluvial dominance as in the lower reaches the carrying capacity of the rivers declines and it mainly deposits fine particles. Contrary to this, the sandy facies were supposed to be aggraded through marine processes during the mid-Holocene due to a higher sea level has been reported in the area. The geochemistry of sub-surface sediments has validated this presumption as the concentration of detrital elements Al_2O_3 , Fe_2O_3 , TiO_2 , MnO , etc. is high in the clayey facies while the concentration MgO , CaO and Ba is low. In contrast, in sandy facies the concentration of MgO , CaO and Ba which are primarily derived from marine biogenic sources, is high while detrital elements are low. The geochemical proxies have also indicated distinct periods of enhanced terrestrial flux and high weathering along with low salinity level and episodes of lower terrestrial flux and low weathering linked along with increased salinity. These events have been organized in a chronological order using radiocarbon ^{14}C dates.

Thus, it can be concluded that the geochemical proxies, along with colour and textural characteristics of sediment deposits can be used as a crucial proxy to unravel the past climate. The selected geochemical proxies have indicated a remarkable shift the climate and depositional environment. Furthermore, the use of ^{14}C dates has provided a temporal framework to these events that occurred in the past. The study has revealed a cyclic pattern of climate in the Lower Baitarani Basin.

The present work was started following the footsteps of Hutton's principle of '*uniformitarianism*'. To conclude this study it can be added that the present is not only the key to the past but also a key to the future. This research work offers an insight to the past

events and suggests that such climatic and sea level perturbations can occur in the future as well. The study also discloses a marginal sea rise in recent times that can affect the coastal communities in future. Thus, future strategies in coastal areas should be developed accordingly to cope up with the changing climate and sea level.

Bibliography

- Agnihotri, R., Sarin, M., Somayajulu, B., Jull, A., Burr, G. (2003). Late-Quaternary biogenic productivity and organic carbon deposition in the eastern Arabian Sea. *Palaeogeography, Palaeoclimatology, Palaeoecology*, 197 (1), 43-60.
- Agrawal, D.P., (1987). Environmental changes in India during last 4 million years. *Journal of Palaeontology Society of India*, 32, 1-4.
- Agrawal, D.P., Guzder, S., (1972). Quaternary studies on the west coast of India: Preliminary observations. *Palaeobotanist*, 21(2), 216-222.
- Akinyemi, S.A., Adebayo, O.F., Ojol, A.O., Gitari, W.M. (2014). Geochemistry and mineralogy of the Campanian sandstone of Lokoja-Basange formation, middle Niger basin (Lokoja sub-basin), Nigeria: Implications for provenance, weathering, tectonic setting and paleo-redox condition. *Journal of Natural Sciences Research*, 14 (16), 65-89.
- Alappat, L., Frechen, M., Ramesh, R., Tsukamoto, S., Srinivasalu, S. (2011). Evolution of late Holocene coastal dunes in the Cauvery delta region of Tamil Nadu, India. *Journal of Asian Earth Sciences*, 42, 381-397.
- Alappat, L., Frechen, M., Sree Kumar, S., Suresh Babu, D.S., Ravur, R., Tsukamoto, S. (2015). Evidence of late Holocene shoreline progradation in the coast of Kerala, south India obtained from OSL dating of palaeo beach ridges. *Geomorphology*, 245, 73-86.
- Alexanderson, H., Backman, J., Cronin, T.M., Funder, S., Ingólfsson, Ó., Jakobsson, M., Landvik, J. Y., Löwemark, L., Mangerud, J., März, C., Möller, P., O'Regan, M., Spielhagen, R. F. (2014). An arctic perspective on dating mid-late Pleistocene environmental history. *Quaternary Science Reviews*, 92, 9-31.
- Algarsamy, R., Zhang, J. (2010). Geochemical characterization of major and trace elements in the coastal sediments of India. *Environment Monitoring Assessment*, 161, 161-176.
- Algeo, T.J., Maynard, J.B. (2004). Trace-elements behavior and redox facies in core shale of Upper Pennsylvanian Kansas-type cyclothems. *Chemical Geology*, 206, 289-318.
- Allison, M.A., Khan, S.R., Goodbred Jr, S.L., Kuehl, S.A. (2003). Stratigraphic evolution of the late Holocene Ganges-Brahmaputra lower delta plain. *Sedimentary Geology* 155, 317-342.
- Allu, N.C., Priju, C.P. (2006). Evolution of coastal landforms and sedimentary environments of the Late Quaternary period along central Kerala, southwest coast of India. *Journal of Coastal Research*, 39, 1898-1902.
- Amoros, C., van Urk, G. (1989). *Palaeoecological analysis of large rivers: some principles and methods*, in G.E. Petts, H. Moller and A.L. Roux (eds), Historical change of large alluvial rivers. Chichester: John Wiley, 143-165.
- Amorosi, A., Centineo, M.C., Colalongo, M.L., Pasini, G., Satri, G., Vaiani, S.C. (2003). Facies architecture and Late Pleistocene-Holocene depositional history of the Po delta (Comacchio Area), Italy. *The Journal of Geology*, 111, 39-56.
- Anderson, D.E., Goudie, A.S., Parker, A.G. (2007). *Global Environments through the Quaternary Exploring Environmental change*. Oxford University Press, UK.

- Anderson, R., Winckler, G. (2005). Problems with paleoproductivity proxies. *Paleoceanography*, 20(3), PA 3012, doi:10.1029/2004PA001107.
- Andreu, B., Colin, J.P., Singh, J. (2012). Middle and Upper Jurassic Ostracods from Western Kachchh, Gujarat, India. *Gondwana Research*, 22, 1110-1124.
- Andrews, J.E., Singhvi, A.K., Kailath, A.J., Kuhn, R., Dennis, F.P., Tandon, S.K. Dhir, R.P. (1998). Do stable isotope data from calcrete record Late Pleistocene monsoonal climate variation in the Thar desert of India? *Quaternary Research*, 50, 240-251.
- Arsairai, B., Wannakomol, A. Feng, Q., Chonglakmani, C. (2016). Paleoproductivity and paleoredox condition of the Huai Hin Lat Formation in northeastern Thailand. *Journal of Earth Sciences*, 27(3), 350-364.
- Asa, S.C., Rath, P., Panda, U.C., Parhi, P.K., Bramha, S. (2013). Application of sequential leaching, risk indices and multivariate statistics to evaluate heavy metal contamination of estuarine sediments: Dhamara Estuary, East Coast of India. *Environment Monitoring Assessment*, 185, 6719-6737.
- Atiken, M.J., Tite, M.S., Reid J. (1964). Thermoluminescent dating of ancient ceramics. *Nature*, 202 (4936), 1032-1033.
- Babeesh, C., Achyuthan, H., Resmi, M.R., Nautiyal., C.M., Shah, R.A. (2019). Late Holocene paleoenvironmental changes inferred from Manasbal Lake sediments, Kashmir Valley, India. *Quaternary International*, 507, 156-171.
- Babu, P.V.L.P. (1975). Morphological evolution of the Krishna delta. *Photonorvachak*, 3, 21-27.
- Band, S., Yadava, M.G., Lone, M.A., Shen, C. (2018). High resolution mid-Holocene Indian Summer monsoon recorded in a stalagmite from the Kotumsar Cave, Central India. *Quaternary International*, 1-6.
- Bandopadhyay, P.C., Eriksson, P.G., Roberts, R.J. (2010). A vertic paleosol at the Archean-Proterozoic contact from the Singhbhum- Orissa craton, Eastern India. *Precambrian Research*, 177, 277-290.
- Banerjee, P.K. (1993). Imprints of late Quaternary climate and sea level changes on east coast and south Indian coast. *Geo- marine letters*, 13, 56-60.
- Banerjee, P.K. (2000). Holocene and late Pleistocene relative sea level fluctuations along the east coast of India. *Marine Geology*, 167, 243-260.
- Banerji, U.S., Pandey, S., Bhushan, R., Juyal, N. (2015). Mid-Holocene climate and land-sea interaction along the southern coast of Saurashtra, western India. *Journal of Asian Earth Sciences*, 111, 428-487.
- Banerji U. S., Bhushan R., Jull A.J.T. (2017). Mid-Late Holocene monsoonal records from the partially active mudflats of Diu island, southern Saurashtra Gujarat, western India. *Quaternary International*, 443 (B), 200-210.
- Banta, J.R., McConnell, J.R., Edwards, R., Engelbrecht, J.P. (2008). Delineation of carbonate dust, aluminous dust, and sea salt deposition in Greenland glaciochemical array using positive matrix factorization. *Geochemistry, Geophysics, Geosystems*, 9(7), 1-19.

- Barcena, M.A., Cacho, I., Abrantes, F., Sierro, F.J., Grimalt, J.O., Flores, J.A. (2001). Paleoproductivity variations related to climatic conditions in the Alboran Sea (western Mediterranean) during the last glacial-interglacial transition: the diatom record. *Palaeogeography, Palaeoclimatology, Palaeoecology*, 167, 337-357.
- Barett, M.T., Brown, D., Plunkett, G. (2019). Refining the statistical parameters for constructing tree-ring chronologies using short-lived species: Alder (*Alnus glutinosa* Gaertn). *Dendrochronologia*, 55, 16-24.
- Basavaiah, N. Mahesh Babu, J.L.V., Gawali, P.B., Naga Kumar, K.Ch.V., Demudu, G., Prizomwala, S.P., Hanamgond, P.T., Rao, K.N. (2015). Late quaternary environmental and sea level changes from Kolleru lake, SE India: influences from mineral magnetic, geochemical and texture analysis. *Quaternary International*, 371, 197-208.
- Basavaiah, N., Khadkikar, A.S. (2004). Environmental magnetism and its application towards paleomonsoon reconstruction. *India Geophysical Union*, 8 (1), 1-14.
- Bronk, R.C., Lee, S. (2013). Recent and planned developments of the programme OxCal. *Radiocarbon*, 55, 720-730.
- Basu S., Anoop A., Sanyal P., Singh P. (2017). Lipid distribution in the lake Ennamangalam, South India: Indicators of organic matter sources and paleoclimatic history. *Quaternary International*, 443, 238-247.
- Basavaiah, N., Beukema, S., Krishnamurthy, R., Singh, A.K., Juyal., N. (2011). Monsoon variability and chemical weathering during the Late Pleistocene in the Goriganga basin, higher central Himalaya, India. *Quaternary Research*, 75, 597-604.
- Belhadj, H., Aubert, D., Youcef, N.D. (2017). Geochemistry of major and trace elements in sediments of Ghazaouet Bay (western Algeria): An assessment of metal pollution. *Comptes Rendus Geoscience*, 349, 412-421.
- Benson, L., White, L.D., Rye, R. (1996). Carbonate deposition, Pyramid lake Subbasin, Nevada: 4. Comparison of the stable values of carbonate deposits (tufas) and the Lahontan lake-level record. *Palaeogeography, Palaeoclimatology, Palaeoecology*, 122, 45-76.
- Birks, H. H., Ammann, B. (2000). Two terrestrial records of rapid climatic change during the glacial Holocene transition (14,000-9000 calendar year B.P.) from Europe. *Proceedings of the National Academy of Sciences of the United States of America*, 94 (4), 1390-1394.
- Bishop, P. S., David, C.W., Stark, M. T. (2004). OSL and radiocarbon dating of a pre-Angkorian canal in the Mekong delta, southern Cambodia. *Journal of Archaeological Science*, 31, 319-336.
- Bister, H., Mermanns, Y.M., Cortizas, A.M. (2012). The influence of organic matter decay on the distribution of major and trace elements in ombrotrophic mires- a case study of from the Hartz Mountains. *Geochimica et Cosmochimica Acta*, 84(1), 126-136.
- Bjorlykke, K. (1974). Geochemical and mineralogical influence of Ordovician island arcs on epicontinental clastic sediments: a study of Lower Palaeozoic sedimentation in the Oslo region. *Sedimentology*, 21, 251-272.

- Blum, M. D., Tornqvist, T. E. (2000). Fluvial response to climate change: a review and look forward. *Sedimentology*, 47(1), 2-48.
- Bounakhla, M., Embarch, K., Zahry, F., Bilal, E., Kump, P. (2008). Capabilities of elemental analysis by EDXRF for geochemistry. *Journal of Radioanalytical and Nuclear Chemistry* 275 (3), 467-478.
- Briggs, D. (1977). *Sources and methods in Geography: Sediments*. Butterworths, London.
- Bronk, R.C. (2017). Methods for summarizing radiocarbon datasets. *Radiocarbon*, 59 (2), 1809-1833.
- Brook, M.S., Kirbride, M.P. (2018). Reconstruction and paleoclimatic significance of late Quaternary glaciers in the Tararua Range, North Island, New Zealand. *Quaternary International*, 470, 53-66.
- Bryson, R.A., Swain, A.M. (1981). Holocene variations of monsoon rainfall in Rajasthan. *Quaternary Research*, 16(2), 135-145.
- Bufarale, G., O'Leary, M., Stevens, A., Collins, L.B. (2017). Sea level controls on palaeochannel development within the Swan River estuary during the Late Pleistocene to Holocene. *Catena*, 153, 131-142.
- Buggle, B., Glaser, B., Hambach, U., Gerasimenko, N., Markovic, S. (2009). Stratigraphy and spatial and temporal paleoclimatic trends in southeast/eastern Europe loess paleosol sequences. *Quaternary International*, 196 (1-2), 86-106.
- Buggle, B., Glaser, B., Hambach, U.F., Gerasimenko, N., Morkovic, S. (2011). An evaluation of geochemical weathering indices in loess-paleosol studies. *Quaternary International*, 240(1-2), 12-21.
- Burbank, D.W., Fort, M.B. (1985). Bedrock control on glacial limits: Examples from the Ladakh and Zaskar ranges, North-Western Himalaya, India. *Journal of Glaciology*, 31(108), 143-149.
- Butola Y.D., Cornelis, M.W., Baert, G., Mafuka, P., Van Ranst, E. (2013) Particle size distribution models for soils of the humid tropics. *Journal of Soils Sediments*, 13: 686-698.
- Campbell, C. (1998). Late Holocene Lake sedimentology and climate change in southern Alberta, Canada. *Quaternary Research*, 49, 96-101.
- Caran, S. (1998). Quaternary paleoenvironmental and plaeoclimatic reconstruction: A discussion and critique with examples from the southern high plains. *Plant Anthropologist*, 43 (164): 111-124.
- Carvalho, L., Figueira, P., Monteiro, R., Reis, A.T., Almeida, J., Catry, T., Lourenco, P.M., Catry, P., Barbosa, C., Catry, I., Pereira, E., Granadeiro, J.P., Vale, C. (2018). Major, minor, trace and rare earth elements in sediments of the Bijagos archipelago, Guinea-Bissau. *Marine Pollution Bulletin*, 129, 829-834.
- Chand, P., Acharya, P. (2010). Shoreline change and sea level rise along coast of Bhitarkanika wildlife sanctuary, Orissa: an analytical approach of remote sensing and statistical techniques. *International Journal of Geomatics and Geosciences*, 1 (3), 436-455.

- Chappell, J.M.A., Grindrod, A. (eds). (1983). *Proceedings of the first CLIMANZ conference*, (2) Canberra: Department of Biogeography and Geomorphology, Australian National University.
- Chauhan, O.S., Borole, D.V., Gujar, A.R., Mascarenhas, A., Mislankar, P.G., Rao, Ch. M. (1993). Evidence of climatic variations during Late Pleistocene-Holocene in the eastern Bay of Bengal. *Current Science*, 65, 558-562.
- Choi, B.Y., Yun, S.T., Kim, K.H. (2016). Role of oxbow lakes in controlling redox geochemistry of shallow groundwater under a heterogeneous fluvial sedimentary environment in an agriculture field: Coexistence of iron and sulfate reduction. *Journal of Contaminant Hydrology*, 185-186, 28-41.
- Cochrane, S. (2014). The Munsell color system: A scientific compromise from the world of art. *Studies in History and Philosophy of Science*, 47, 26-41.
- Cole, D.B., Zhang, S., Planavsky, N.J. (2017). A new estimate of detrital redox-sensitive metal concentration and variability in fluxes to marine sediments. *Geochimica et Cosmochimica Acta*, 215, 337-353.
- Coltorti, M., Melis, E., Patta, D. (2010). Geomorphology, stratigraphy and facies analysis of some Late Pleistocene and Holocene key deposits along the coast of Sardinia (Italy). *Quaternary International*, 222, 19-35.
- Costa, K.M., Anderson, R.F., McManus, J.F., Winckler, G., Middleton, J.L., Langmuir, C.H. (2018). Trace elements (Mn, Zn, Ni, V) and authigenic uranium (aU) geochemistry reveal sedimentary redox history on the Juan de Fuca Ridge, North Pacific Ocean. *Geochimica et Cosmochimica Acta* (in press).
- Coyne, A., Gorse, L., Curti, C., Schafer, J., Grosbois, C., Morelli, G., Ducassou, E., Blanc, G., Maillet, G.M., Mojtahid, M. (2016). Spatial distribution of trace elements in the surface sediments of major European estuary (Loire Estuary, France): Source identification and evaluation of anthropogenic contribution. *Journal of Sea Research* (in press).
- Crucius, J., Calvert, S., Pedersen, T., Sage, D. (1996). Rhenium and molybdenum enrichments in sediments as indicators of oxic, suboxic and sulfidic conditions of deposition. *Earth and Planetary Sciences Letters* 145, 65-78.
- Das, S. (2014). Palaeo-palynology of late Quaternary peat deposit from Lower Bengal Basin, India: A palaeoecological approach. *Quaternary International*, 325, 197-204.
- Das, A., Prizomwala, S., Makwana, N., Thakkar, M. (2017). Late Pleistocene-Holocene climate and sea level changes inferred based on the tidal terrace sequence, Kachchh, Western India. *Palaeogeography, Palaeoclimatology, Palaeogeography*, 473, 82-93.
- Davies, C. P. (2006). Holocene paleoclimates of southern Arabia from lacustrine deposits of the Dhamar highlands, Yemen. *Quaternary Research*, 66, 454-464
- deMenocal, P.B. (1995). Plio-Pleistocene African climate. *Science*, 270, 53-59.
- De Terra H., Paterson, T.T. (1939). *Studies on the ice age in India and associated human cultural* Carnegie, Washington.

- De Terra H., Teilhard de Chardin, P. (1936). Observations on the upper shivalik formation and later Pleistocene deposits in India. *Proceedings of the American Philosophical Society*, 76 (6), 791-822.
- Diaz-de Alba, M., Galindo-Riano, M.D., Casanueva-Marenco, M.J., Garcia-Vargas, M., Kosore, C.M. (2011). Assessment of the metal pollution, potential toxicity and speciation of sediment from Algeciras Bay (South of Spain) using chemometric tools. *Journal of Hazardous Materials*, 192, 177-187.
- Dill, H. (1986). Metallogenesis of early Paleozoic graptolite shales from the Graefenthal Horst (northern Bavaria-Federal Republic of Germany). *Economic Geology*, 81, 889-903.
- Dill, H., Teshner, M., Wehner, H. (1988). Petrography, inorganic and organic geochemistry of Lower Permian Carboniferous fan sequences ("Brandshiefer Series") FRG: constraints to their palaeogeography and assessment of their source rock potential. *Chemical Geology*, 67,307-325.
- Dou, Y., Li, J., Zhao, J., Hu, B., and Yang, S. (2013). Distribution, enrichment and source of heavy metals in surface sediments of the eastern Beibu Bay, South China Sea. *Marine Pollution Bulletin*, 67, 137-145.
- Durand, N., Gunnell, Y. C. P., Ahmad, M. (2007). Pedogenic carbonates on Precambrian silicate rocks in south India: origin and paleoclimatic significance. *Quaternary International*, 162-163, 35-49.
- Dyer, K.R. (1986). *Coastal and Estuarine Sediment Dynamics*. John Wiley and Sons, Toronto.
- Dymond, J., Suess, E., Lyle, M. (1992). Barium in deep-sea sediment: a geochemical proxy for Paleoproductivity. *Paleoceanography*, 7 (2), 163-181.
- Eggleton, J., Thomas, K.V. (2004). A review of factors affecting the release and bioavailability of contaminants during sediment distribution events. *Environmental International*, 30, 973-980.
- Einsele, G., Herm, D., Schwartz, H.U. (1974). Sea level fluctuations during the past 6000 yr at the coast of Mauritania. *Quaternary Research*, 4, 282-289.
- Eltom, H.A., Abdullatif, O., Babalola, L.O. (2018). The elemental geochemistry of Lower Triassic shallow-marine carbonates from central Saudi Arabia: Implications for redox conditions in the immediate aftermath of the latest Permian mass extinction. *Journal of African Earth Sciences*, 139, 283-306.
- Erashin, S., Gunal, H., Kutlu, T., Yetgin, B., Coban, S. (2006) Estimating specific surface area and cation exchange capacity in soil using fractal dimension of particle-size-distribution. *Geoderma*, 136(3), 588-597.
- Ericson, D.B., Broecker, W.S., Kulp, J.L., Wollin, G. (1956). Late-Pleistocene climates and deep-sea sediments. *Science*, 124, 385-389.
- Ergin, M., Saydam, A.C., Basturk, O., Erdem, E., Yoruk, R. (1991). Heavy metal concentrations in surface sediments from the two coastal inlets (Golden Horn Estuary and Izmit Bay) of the northeastern sea of Marmara. *Chemical Geology*, 91, 269-285.
- Ernst, T.W. (1970). *Geochemical Facies Analysis*. Elsevier Publications, Amsterdam.

- Esmaelnejad, L., Siavashi, F., Seyedmohammadi, J., Shabanpour, M. (2016). The best mathematical models describing particle size distribution of soils. *Modelling Earth Systems and Environment*, 2 (4): 1-11.
- Farooqui, A., Naidu T.Y. (2010). Thecamoebians and palaeonological assemblage in Gautami-Godavari river mouth, India: environment and sea level since 3000 years. *Journal of geological society of India*, 75, 841-850.
- Faure, P., Volkoff, B. (1998). Some factors affecting regional differentiation of the soils in the Republic of Benin (West Africa). *CATENA*, 32 (3-4), 281-306.
- Ferrat, M., Weiss, D.J., Strekopytov, S., Dong, S., Chen, H., Najorka, J., Sun, Y., Gupta, S., Tada, R., Sinha, R. (2011). Improved provenance tracing of Asian dust source using rare earth elements and selected trace elements for palaeomonsoon studies on the eastern Tibetan Plateau. *Geochimica et Cosmochimica Acta*, 75, 6374-6399.
- Filho et al. (2006). Using mangroves as a geological indicator of coastal changes in the Braganca macrotidal flat, Brazilian Amazon: A remote sensing data approach. *Ocean and Coastal Management*, 49(7), 462-475.
- Fritts, H.C. (1965). Tree-ring evidence for climatic changes in Western North America. *Monthly Weather Review*, 93(7), 421-443.
- Fritts, H.C., Blasing, T.J., Hayden, B.P., Kutzach, J.E. (1971). Multivariate techniques for specifying Tree-Growth and climate relationships and for reconstructing anomalies in Paleoclimate. *Journal of Applied Meteorology* 10(5), 845-864.
- Folk, R.L. (1966). A Review of grain-size parameters. *Sedimentology*, 6(2), 73-93.
- Fontes, J. C., Gasse, F. (1991). PALYDAF (Palaeohydrology in Africa) program: objectives, methods, major results. *Palaeogeography Palaeoclimatology Palaeoecology* 84, 191-215.
- Fukumoto, M.M., Mahiquet, M.M., Tessler, M.G. (2004). Reconstruction of the Late Holocene history of Santos bay (Southern Brazil) based on bulk organic matter characteristics. *Journal of Coastal Research, Special Issue (39). Proceedings of the 8th International Coastal Symposium (ICS 2004)*, 1, 259-261.
- Gao, C., Boreham, S., Preece, R.C., Gibbard, P.L., Briant, R.M. (2007). Fluvial response to rapid climate change during the Devensian (Weichselian) lateglacial in the river Great Ouse, southern England, UK. *Sedimentary Geology*, 202, 193-210.
- Gao, S. (2010). Chemical composition of the continental crust: A perspective from China. *Geochemical News*, 143, 1-16.
- Gautam, P.K., Narayana, A.C., Band, S.T., Yadava, M.G., Ramesh, R., Wu, C.C., Shen, C.C. (2019). High resolution reconstruction of Indian summer monsoon during Bolling-Allerod from a central Indian stalagmite. *Palaeogeography Palaeoclimatology Palaeoecology*, 514, 567-576.
- Gasse, F., van Campo, E. (1994). Abrupt post-glacial climatic events in West Asia and North Africa monsoon domains. *Earth and Planetary Science Letters*, 126, 435-456.
- Gattolin, G., Preto, N., Breda, A., Franceschi, M. Isotton, M., Gianolla, P., Gattolin, G., Preto, N., Breda, A., Franceschi, M. (2015). Sequence stratigraphy after the demise of a high relief

- carbonate platform (cranium of the dolomites): sea level and climate disentangled. *Palaeogeography, Palaeoclimatology, Palaeoecology*, 423, 1-17.
- Gayantha, K., Routh, J., Chandrajith, R. (2017). A multi-proxy reconstruction of the late Holocene climate evolution in Lake Bolgoda, Sri Lanka. *Palaeogeography, Palaeoclimatology, Palaeoecology*, 473, 16-25.
- Gebrekirstos, A., Mitlohner, R., Teketay, D., Worbes, M. (2008). Climate-growth relationships of the dominant tree species from semi-arid savanna woodland in Ethiopia. 22:631. [Http://doi.org/10.1007/s00468-008-0221-z](http://doi.org/10.1007/s00468-008-0221-z).
- German, C.R., Henry, E. (1990). Application of the Ce- anomaly as a paleoredox indicator: The ground rules. *Paleoceanography*, 5(5), 823-833.
- Goldberg, E.D., Arrhenius, G. (1958). Chemistry of Pacific pelagic sediments. *Geochimica et Cosmochimica Acta*, 13 (2), 253-362.
- Goldberg, K., Humayun, M. (2016). Geochemical paleoredox indicators in organic-rich shales of the Irati Formation, Permian of the Parana Basin, southern Brazil. *Brazilian Journal of Geology*, 46(3), 377-393.
- Goldschmidt, V.M. (1954). *Geochemistry*. Clarendon Press, Oxford, UK.
- Govil, P., Mazumder, A., Tiwari, A., Kumar. S. (2016). Holocene climate variability from lake sediment core in Larsemann Hills, Antarctica. *Journal of the Geological Society of India*, 78 (1), 453-463.
- Gredilla, A., Stoichev, T., de Vallejuelo, F.O., Iruretagoiena, A.R. (2015). Spatial distribution of some trace and major elements in sediments of the Cavado estuary (Esposende, Portugal). *Marine Pollution Bulletin*, 99, 305-311.
- Grette, J. B., Hopkins, D. M. (1995). Emergent marine record and palaeoclimate of the last interglaciation along the northwest Alaskan coast. *Quaternary Research*, 43, 159-173.
- Gupta, A., 2007b. Large rivers: Geomorphology and management. John Wiley and Sons, 75-96.
- Hallberg, R.O. (1976). A geochemical method for investigation of palaeoredox conditions in sediments: *Ambio. Special Report*, 4: 139-147.
- Hamer, J.M.M., Sheldon, N.D., Nichols G. J. (2007). Global aridity during the early Miocene? A terrestrial paleoclimate record from Ebro Basin, Spain. *The Journal of Geology*, 115(5), 601-608.
- Hameed, A., Achyuthan, H., Sekhar, B. (2006). Radiocarbon dates and Holocene sea level change along the Cuddalore and Odinur coast, Tamil Nadu. *Research Communications*, 91(3), 362-367.
- Hanh, P.T.T., Furukawa, M. (2007). Impact of sea level rise on coastal zone of Vietnam. *Bulletin of the Faculty of Science*, University of Ryukyu, 84, 45-59.
- Hari, K., Saito, Y. (2007). *Classification, architecture, and evolution of large river deltas* in Gupta A. (eds).

- Harnois, L. (1988). The CIW index: a new chemical index of weathering. *Sedimentary Geology*, 55, 319-322.
- Hartnett, H.E., Keil, R.G., Hedges, J.I., Devol, A.H. (1998). Influence of oxygen exposure time on organic carbon preservation in continental margin sediments. *Nature*, 391, 572-574.
- Hashimi, N.H., Nigam, R., Nair, R., Rajagopalan, G. (1995). Holocene sea level fluctuations on western Indian continental margin: an update. *Journal of Geological Society of India*, 46(1), 157-162.
- Hass, A., Fine, P. (2010). Sequential selective extraction procedure for the study of heavy metals in soils, sediments, and waste materials- a critical review. *Critical Review of Environmental Science and Technology*, 40(5), 365-399.
- Henderson, P. (1984). Rare earth element geochemistry (Developments in Geochemistry), Elsevier, Oxford.
- Hodell, D.A., Curtis, J.H., Jones, G.A., Higuera-Gundy, A., Brenner, M., Binford, M.W., Dorsey, K. (1991). Reconstruction of Caribbean climate change over the past 10500 years. *Nature*, 52, 790-793.
- Hofer, G., Wagreich M., Neuhuber S. (2013). Geochemistry of fine grained sediments of the upper Cretaceous to Paleogene Gosau group (Austria, Slovakia): Implications for paleoenvironment and provenance studies. *Geoscience Frontiers*, 4, 449-468.
- Hughen, K.A. (2007). Radiocarbon dating of deep sea sediments. *Developments in Marine Geology*, 185-210.
- Huntley, B. (2012). Reconstructing paleoclimates from biological proxies: some often overlooked sources of uncertainty. *Quaternary Science Reviews*, 31, 1-16.
- IPCC, (2007). *Climate Change 2007: Impacts, adaptation and vulnerability. Contribution of Working Group II to the Fourth Assessment Report of the Intergovernmental Panel on Climate Change*, M.L. Parry, O.F., Canziani, J.P. Palutik, van der Linden, C.E. Hanson Eds., Cambridge University Press, Cambridge, UK.
- Islam, M.S., Tooley, M.J. (1999). Coastal and sea-level changes during the Holocene in Bangladesh. *Quaternary International*, 55(1), 61-75.
- Islam, M.A., Al-mamum, A., Hossain, F., Quraishi, S.B., Naher, K., Khan, R., Das, S., Tamim, U., Hossain, S.M., Nahid, F. (2017). Contamination and ecological risk assessment of trace elements in the sediments of the rivers of Sunderbans mangrove forest, Bangladesh. *Marine Pollution Bulletin*, 124, 356-366.
- Ito, L., Omori, T., Yoneda, M., Yamaguchi, T., Kobayashi, R., Takahashi, Y. (2018). Origin and migration of trace elements in the surface sediments of Majuro Atoll, Marshall Island. *Chemosphere* 202, 65-75.
- Jakobsson, M., Lovlie, R., Al-Hanbali, H., Arnold, E., Backman, J., Morth, M. (2000). Manganese and color cycles in Arctic Ocean sediments constrain Pleistocene chronology. *Geology*, 28, 23-26.

- Jana, A., Biswas, A., Sabyasachi, M., Amit K. B. (2014). Shoreline changes in response to sea level rise along Digha coast, eastern India: an analytical approach of remote sensing, GIS and statistical techniques. *Journal of Coastal Conservation*, 18(3), 145-155.
- Jayangondaperumal, R., Murari, M.K., Sivasubramanian, P., Chandrasekar, N. (2012). Luminescence dating of fluvial and coastal red sediments in the SE coast, India, and implications for palaeoenvironmental changes and dune reddening. *Quaternary Research*, 77 (3), 468-481.
- Jayalakshmi, K., Nair, K.M., Santosh, M. (2004). Late Pleistocene-Holocene paleoclimatic history of the southern Kerala Basin, southwest India, *Gondwana Research*, 7 (2), 585-594.
- Jiang, S.Y., Chen, Y.Q., Liang, H.F., Yang, J.H., Feng, H.Z., Ni, P. (2006). Trace and rare-earth element geochemistry and Pb-Pb dating of black shale and intercalated Ni-Mo-PGE-Au sulfide ores in Lower Cambrian strata, Yangtze Platform, South China. *Miner Deposita*, 41, 453-467.
- Jones, B., Manning, D.A.C. (1994). Comparison of geological indices used for the interpretation of palaeoredox conditions in ancient mudstones. *Chemical Geology*, 111, 111-129.
- Juyal, N., Kar, A., Rajaguru, S.N., Singhvi, A.K. (2003). Luminescence chronology of Aeolian deposition during the Late Quaternary on the southern margin of Thar Desert, India. *Quaternary International*, 104, 87-98.
- Kale, V.S., Hire, P., Baker, V.R. (1997). Flood hydrology and geomorphology of monsoon dominated rivers: the Indian peninsula. *Water International*, 22 (4), 259-265.
- Karim, M.F., Mimura, N. (2008). Impacts of climate change and sea level rise on cyclonic storm surge flood in Bangladesh. *Global Environmental Change*, 18, 490-500.
- Kern A.K., Harzhauser, M., Reuter, M., Kroh, A., Piller, W.E. (2013). The Miocene coastal vegetation of southwestern India and its climatic significance. *Palaeoworld*, 22 (3-4), 119-132.
- Kemp, D.B., Izumi, K. (2014). Multiproxy geochemical analysis of a Panthalassic margin record of the early Toarcian oceanic anoxic event (Toyora area, Japan). *Palaeogeography, Palaeoclimatology, Palaeoecology*, 414 (0), 332-341.
- Kettler, T.A., Doran, J.W., Gilbert, T.L. (2001). Simplified method for soil particle-size determination to accompany soil-quality analysis. *Soil Science Society of America*, 65, 849-852.
- Khandelwal, A., Mohanti, M., Rodrigues, F.G., Schrf, B.W. (2008). Vegetation history and sea level variations during the last 13,500 years inferred from a pollen record at Chilika Lake, Orissa, India. *Vegetation History Archaeobotanist*, 17: 335-344.
- Khatri, D., Zhang, W., Fang, X., Paudyal, K.N. (2017). Review of late Cenozoic climatic fingerprints in the Nepal Himalaya. *Bulletin of Nepal Geological Society*, 34, 87-96.
- Khokhlova, O.S. Sedov, S., Khokhlov, A.A., Belyaeva, E.V., Lyubin, V.P. (2018). Indications of pedogenesis in lower Pleistocene tool bearing sediments in North America and regional paleoclimatic reconstruction. *Quaternary International*, 469, 68-84.
- Kobayashi, D., Yamamoto, M., Irino, T., Nam, S., Park, Y., Harada, N., Nagashima, K., Chikita, K., Saitoh, S. (2016). Distribution of detrital minerals and sediment color in western Arctic

- Ocean and northern Bering Sea sediments: Changes in the provenance of western Arctic Ocean sediments since the last glacial period. *Polar Science*, 10 (4), 519-531.
- Kochel, R.C., Baker, V.R., 1982. Paleoflood Hydrology. *Science*, 215, 353-361.
- Konhauser, K.O., Powell, M.A., Fyfe, W.S., Longstaffe, F.J., Tripathy, S. (1997). Trace element geochemistry of river sediment, Orissa state, India. *Journal of Hydrology*, 193, 258-269.
- Kumar, K., Tewari, R., Agnihotri, D., Sharma, A., Pandit, S.K., Pillai, S.S.K., Singh, V., Bhat, G.D. (2017). Geochemistry of the Permian-Triassic sequences of the Guryul Ravine section, Jammu and Kashmir, India: Implications for oceanic redox conditions. *Geo Research Journal*, 13, 114-125.
- Kumaran, K.P.N., Nair, K.M., Shindikar, M., Limaye, R.B., Padmalal, D. (2005). Stratigraphical and palynological appraisal of the late Quaternary mangrove deposits of the west coast of India. *Quaternary Research*, 64, 418-431.
- Kumaran, K.P.N., Padmalal, D., Limaye, R.B., Mohan, S.V. (2018). Signatures of Holocene hydrological processes from sedimentary archives in southwestern India: case studies from wetland of Kerala coast. *Journal of Geological Society of India*, 92, 569-606.
- Koukina, S.E., Lobus, N.V., Peresykin, V.I., Dara, O.M., Smurov, A.V. (2017). Abundance, distribution and biodiversity of major and trace elements in surface sediments from the Cai River estuary and Nha Trang Bay (South China Sea, Vietnam). *Estuarine, Coastal and Shelf Science*, 198, 450-460.
- Krishna, J. (2017). *The Indian Mesozoic chronicle*. Springer Publications, Singapore.
- Kumaran, K.P.N. Limaye, R. B., Padmalal D. (2013). Mangrove response to climate change along the southwestern coast of India during Holocene: evidence from palynology and geochronology in *Climate Change and Island and Coastal Vulnerabilities*. Sundaresan, J. et al. (eds.) Capital publishing company, New Delhi, Kolkata.
- Kumar, M. (2015). Remote sensing and GIS based SLR inundation assessment of Bhitarkanika forest and adjacent eco- fragile area, Odisha. *International Journal of Geomatics and Geosciences*, 5(4), 684-696.
- LaMarche Jr, V.C. (1974). Paleoclimatic inferences from long tree-ring records. *Science*, 183(4129), 1043-1048.
- LaMarche Jr, V.C. (1978). Tree-ring evidence of past climatic variability. *Nature*, 276, 334-338.
- Laing, G.D., Rinklebe, J., Vandecasteele, B., Meers, E., Tack, F.M.G. (2009). Trace metal behavior in estuarine and riverine floodplain soils and sediment: A review. *Science of the total Environment*, 407, 3972-3985.
- Lal, N.K., Siwal, A., Kaul, A.K. (2009). Evolution of East Coast of India - A plate tectonic reconstruction. *Journal of the Geological society of India*, 73, 249-260.
- Lalbiakzuali, C., Suresh Gandhi, M.S., Mohan, V.R. (2013). Geomorphology and evolution of coastal landforms between Mimisal and Rajamadam, Palk Strait, east coast of India. *Current Science*, 105, 1730-1735.

- Lambeck, K., East, T. M., Potter, Emma-Kate. (2002). Links between climate and sea level for the past three million years. *Nature*, 419, 199-207.
- Leeder, M. R., Harris, T., Kirkby, M. J. (1998). Sediment supply and climate change: implications for basin stratigraphy. *Basin Research*, 10, 7-18.
- Lezine, A.M. (1989). Late Quaternary vegetation and climate of the Sahel. *Quaternary Research*, 32, 317-334.
- Leyden, B.W. (1987). Man and climate in the Maya lowlands. *Quaternary Research*, 28, 407-415.
- Li, C., Planavsky, N.J., Love, G.D., Reinhard, C.T., Hardisty, D., Feng, L., Bates, S.M., Huang, J., Zhang, Q., Chu, X., Lyons, T.W. (2015). Marine redox conditions in the middle Proterozoic ocean and isotopic constraints on authigenic carbonate formation: Insight from the Chuanlinggou Formations, Yanshan Basin, North China. *Geochimica et Cosmochimica Acta*, 150, 90-105.
- Li, T., Sun, G., Yang, C., Liang, K., Ma, S., Huang, L., Luo, W. (2019). Source apportionment and source to sink transport of major and trace elements in coastal sediments: Combining positive matrix factorization and sediment trend analysis. *Science of the Total Environment*, 651, 344-356.
- Libby, W.F., (1955). *Radiocarbon dating (2nd edition)*. University of Chicago press, Chicago.
- Limaye, R.B., Padmalal, D., Kumaran, K.P.N. (2014). Mangrove habitat dynamics in response to Holocene sea level and climate change along southwest coast of India. *Quaternary International*, 325, 116-125.
- Limaye, R.B., Padmalal, D., Kumaran, K.P.N. (2017). Late Pleistocene-Holocene monsoon variations on climate, landforms and vegetation cover in southwestern India: An overview. *Quaternary International*, 443, 143-154.
- Liu, S., Shi, X., Yang, G., Khokiattiwong, S., Kornkanitnan, N. (2016). Distribution of major and trace elements in surface sediments of the western Gulf of Thailand: Implications to modern sedimentation. *Continental Shelf Research*, 117, 81-91.
- Liu, Y.Y., He, S., Zhao, F., Zhu, J., Wang, H., Liu, G., Wu, X. (2011). Patterns of local and regional grain size distribution and their application to Holocene climate reconstruction in semi-arid Inner Mongolia, China. *Palaogeography, Palaeoclimatology, Palaeoecology*, 307, 168-176
- Liu, D., Lin, B., Kandasamy, S., Wang, H., Liu, Q., Zou, W., Zou, J., Shi, X. (2019). Geochemical appraisal of chemical weathering and metal contamination in coastal surface sediments, off northwest Hainan island, the Gulf of Tonkin. *Frontiers in Marine Sciences*, doi.org/10.3389/fmars.2019.00363.
- Lowe, J.J., Walker, M.J. (1984). *Reconstructing Quaternary Environments*. Longman, London.
- Lulu, Z., Hanlie, H., Jiacheng, L., Qian, F., Yuzeng, Y., Wei, T., Ke, Y., Chaowen, W., Mi, C., Thomas J.A. (2018). Assessing the utility of visible to shortwave infrared reflectance spectroscopy for analysis of soil weathering intensity and paleoclimatic reconstruction. *Palaogeography, Palaeoclimatology, Palaeoecology*, 512, 80-94.
- Luly, J. (1993). Holocene palaeoenvironments near Lake Tyrrell, semi-arid northwestern Victoria. *Journal of Biogeography*, 20, 587-598.

- Lyons, T.W., Severmann, S. (2006). A critical look at iron paleoredox proxies: New insights from modern euxinic marine basins. *Geochimica et Cosmochimica Acta*, 70, 5698-5722.
- Lyons, R.P., Scholz, C.A., Buoniconti, M.R., Martin, M.R. (2011). Late Quaternary stratigraphic analysis of the lake Malawi rift, east Africa: an integration of drill core and seismic-reflection data. *Palaeogeography, Palaeoclimatology, Palaeoecology*, 303, 20-37.
- McCarthy, F.M.G., Collins, E. S., McAndrews, J.H., Kerr, H.A., Scott, D.B., Medioli, F.S. (1995). A comparison of postglacial arcellacean (“Thecamoebian”) and pollen succession in Atlantic Canada, illustrating the potential of arcellaceans for paleoclimatic reconstruction. *Journal of Paleontology*, 69 (5), 980-993.
- McClure, H.A. (1976). Radiocarbon chronology of late Quaternary lakes in the Arabian Desert. *Nature*, 263, 755-756.
- McDonald, R., Edge, R.A. (1970). Trace element distribution in alkaline dykes from the Tugtutoq region, south Greenland. *Bulletin of the Geological Society of Denmark*, 20, 38-58.
- Madhavaraju, J., Loser, H., Lee, Y.I., Santacruz, R.L., Puig, T.P. (2016). Geochemistry of Lower Cretaceous limestones of the Alisitos Formation, Baja California, Mexico: Implications for REE source and paleo-redox conditions. *Journal of the South American Earth Sciences*, 66, 149-165.
- Madsen, A.T., Murray, A.S. (2009). OSL dating of young sediments: A review. *Geomorphology*, 109 (1-2), 3-16.
- Mahalik, N.K. (2013). Coastal Tract of Odisha: geology, Resources and Environment. *Journal of the Geological Society of India*, 81(1), 142-143.
- Makwana, N., Prizomwala, S.P., Chauhan, G., Phartiyal, B., Thakkar, M.G. (2019). Late Holocene paleo-environmental change in the Banni plains, Kachchh, Western India. *Quaternary International*, 507, 197-205.
- Malik, J.N., Banerjee, C., Khan, A., Johnson, F.C., Shishikura, M., Satake, K., Singhvi, A.K. (2015). Stratigraphic evidence for earthquakes and tsunami on the west coast of South Andaman Island, India during past 1000 years. *Tectonophysics*, 661, 49-65.
- Mazumdar, A., Kocherla, M., Carvalho, M.A., Peketi, A., Joshi, R.J., Mahalakshmi, P., Joao, M.H. (2015). Geochemical characterization of the Krishna-Godavari and Mahanadi offshore basin (Bay of Bengal) sediments: A comparative study of provenance. *Marine and Petroleum Geology*, 60, 18-33.
- Meng, Q., Bruch, A.A., Sun, G., Liu, Z., Hu, F., Sun, P. (2017). Quantitative reconstruction of Middle and Late Eocene paleoclimate based on palynological records from the Huadian basin, northeastern China: Evidence for monsoonal influence on oil shale formation. *Palaeogeography, Palaeoclimatology, Palaeoecology*, DOI: 10.1016/j.palaeo.2017.11.036.
- Meyers, P.A. (1994). Preservation of elemental and isotopic source identification of sedimentary organic matter. *Chemical Geology*, 114, 289-302.
- Mial, A.D. (1985). Architectural element analyses: a new method of analyses applied to fluvial deposits. *Earth Science Review*, 22, 261-308.

- Milliman, J.D., Farnsworth, K. (2011). River discharge to the coastal oceans- A global synthesis. Cambridge University Press, UK.
- Misra, S., Bhattacharya, A. (2014). Analysis of the Late Holocene climate vis a vis vegetation dynamics along the southwest coast of India, Thrissur (Kerala). *Quaternary International*, 325, 150-161.
- Mohanty, A.K., Das, S., Vijayan, V., Sengupta, D., Saha, S. (2003). Geochemical studies of monazite sands of Chhatrapur beach placer deposit of Orissa, India by PIXE and EDXRF method. *Nuclear Instruments and Methods in Physics Research*, 211, 145-154.
- Mohapatra, P. (2006). Sequence stratigraphic approach for identification of hydrocarbon plays in Mahanadi offshore basin. 6th International conference and exposition on petroleum geophysics. "Kolkata", 672-677.
- Morford, J.L., Emerson, S. (1999). The geochemistry of redox sensitive trace metals in sediments. *Geochimica et Cosmochimica Acta*, 63, 1735-1750.
- Morozova, T.D. (1995). Identification of paleosol types and their applicability for paleoclimatic reconstruction. *Geological Journal*, 36 (2/3), 199-205.
- Morton, R.A., Gibeaut, J.C., Paine, J.G. (1995). Meso-scale transfer of sand during and after storms: Implications for prediction of shoreline movement. *Marine Geology*, 126, 161-179.
- Mukherjee, A., Fryar, A.E., Thomas, W.A. (2009). Geologic, geomorphic and hydrologic framework and evolution of the Bengal basin, India and Bangladesh. *Journal of Asian Earth Sciences* 34, 227-244.
- Munsell, A.H. (1947). A colour notation (10th ed.). Munsell Color Company, Baltimore.
- Murray, J.W., Lee, B.S., Bullister, J., Luther, G.W. (1999). The suboxic zones of the Black Sea. In: Besiktepe, S.T., Unluata, U., Bologa, A.S. (eds) *Environmental Degradation of the black sea: Challenges and Remedies*. NATO Science Series (2), (Environmental Security), 56. Dordrecht.
- Murray, A.S., Mohanti, M. (2006). Luminescence dating of the barrier spit at Chilika lake, Orissa, India. *Radiation Protection Dosimetry*, 119 (1-4), 442-445.
- Murthy, K.S.R., Subrahmanyam, A.S., Lakshminarayana, S., Chandrasekhar, D.V., Rao, T.C.S. (1995). Some geodynamic aspects of the Krishna-Godavari basin, east coast of India. *Continental Shelf Research*, 15, 779-788.
- Nagarajan, R., Madhavaraju, J., Armstrong-Altrin, J.S., Moutte, J. (2007). Geochemistry of Neoproterozoic shales of the Rabanpalli Formations, Bhima Basin, Northern Karnataka, Southern India: implications for provenance and paleoredox conditions. *Review of Mex. Cienc. Geology*, 24, 150-160.
- Narayana A.C., Prakash V., Gautam P.K., Tripathi S. (2017). Holocene environmental changes as recorded in sediments of a paleodelta, southwest coast of India. *Quaternary International*, 443 (3), 115-123.
- Nair, K.M., Padmalal, D., Kumaran, K.P.N., Sreeja, R., Limaye, R.B., Srinivas, R. (2010). Late quaternary evolution of Ashtamudi-Sasthamkotta lake systems of Kerala, south west India. *Journal of Asian Earth Sciences*, 37, 361-372.

- Nash, D., Thomas, D.S.G., Shaw, P.A. (1994). Siliceous duricrusts as Palaeoclimatic indicators: evidence from the Kalahari Desert of Botswana. *Palaeogeography, Palaeoclimatology, Palaeoecology*, 112: 279-295.
- Natali, C., Bianchini, G. (2017). Geochemical proxies of sediment provenance in alluvial plains with interfering fluvial systems: A study case from NE Italy. *Catena*, 157, 67-74.
- Nesbitt, H.W., Young, G.M. (1982). Early Proterozoic climates and plate motions inferred from major element chemistry of lutites. *Nature*, 299, 715-717.
- Nesbitt, H.W., Markovics, G., Price, R.C. (1980). Chemical processes affecting alkalies and alkaline earths during continental weathering. *Geochimica et Cosmochimica Acta*, 44, 1659-1666.
- Nesbitt, H.W., Young, G.M., McLennan, S.M., Keays, R.R. (1996). Effects of chemical weathering and sorting on the petrogenesis of siliclastic sediments, with implications for provenance studies. *Journal of Geology*, 104, 525-542.
- Nichols, G. (2009). *Sedimentology and stratigraphy*. Wiley-Blackwell.
- O'Connor, A., Luek, J.L., McIntosh, H., Beck, A.J. (2015). Geochemistry of redox-sensitive trace elements in a shallow subterranean estuary. *Marine Chemistry*, 172, 70-81.
- Och, L.M., Cremonese, L., Zhou, G.A.S., Poulton, S.W., Ling, U.S.H., Li, D., Chen, X.I., Manning, C., Thirlwall, M., Strauss, H., Zhu, M. (2016). Palaeoceanographic controls on spatial redox distribution over the Yangtze Platform during the Ediacaran-Cambrian transition. *Sedimentology*, 63, 378-410.
- Om, Z.B., Ozeren, M.S. (2019). Temperature and precipitation variability in eastern Anatolia: Results from independent component analysis of Lake Van sediment data spanning the last 250 kyr BP. *Quaternary International*, 514, 119-129.
- Owen, L.A. (2008). Late Pleistocene and Holocene glacier fluctuations in the Himalaya and Tibet. *Quaternary Science Research* (in press), 1-15.
- Padmalal, D., Nair, K.M., Kumaran, K.P.N., Sajan, K., Mohan, S.V., Maya, K., Santhosh, V., Anooja, S., Limaye, R.B. (2013). Climate and sea level changes in a Holocene bay head delta, Kerala, Southwest coast of India in *Climate Change and Island and Coastal Vulnerabilities*. Sundaresan, J. et al. ed. Capital publishing company, New Delhi, Kolkata.
- Palanisamy, H., Cazenave, A., Meyssignac, B., Wöppelmann, G., Soudarin, L., Becker, M. (2014). Regional sea level variability, total relative sea level rise and its impacts on islands and coastal zones of Indian Ocean over last sixty years. *Global and planetary change*, 116, 54-67.
- Pan, B., Guan, Gao, Q., Guan, H., Liu, D., Li, F., Su, H. (2014). The origin and sources of loess-like sediments in the Jinsha River Valley, SW China. *Boreas*, 43, 121-131.
- Pandey, S., Scharf, U.W., Mohanti, M. (2014). Palynological studies on mangrove ecosystem of the Chilka lake lagoon, east coast of India during the last 4165 years BP. *Quaternary International*, 325, 126-135.
- Parker, A.G., Goudie, A.S., Stokes, S., White, K. (2006). A record of Holocene climate change from lake geochemical analysis in southern Arabia. *Quaternary Research*, 66, 465-476.

- Parveen, U., Sreekesh, S. (2019). Elemental geochemistry of subsurface sediments of lower Baitarani Basin, East coast of India: Implications for paleoredox conditions in *Petrogenesis and Explorations of the Earth's interior: Proceedings of the 1st Springer Conference of the Arabian Journal of Geosciences*, Springer Publications, Tunisia.
- Pattan, J.N., Pearce, N.J.G., Mislankar, P.G. (2005). Constraints in using Cerium-anomaly of bulk sediments as an indicator of paleo bottom water redox environment: A case study of the Central Indian Ocean Basin. *Chemical Geology*, 221, 260-278.
- Peek, S., Clementz, M.T. (2012). Sr/Ca and Ba/Ca variations in environmental and biological sources: A survey of marine and terrestrial systems. *Geochimica et Cosmochimica Acta*, 95, 36-52.
- Penk, A., Bruckner, E. (1909). Die alpen im eiszeitalter in Blum, Michael D. and Tornqvist, Torbjorn E. 2000. Fluvial response to climate change: A review and look forward. *Sedimentology*, 47(1), 2-48.
- Pennington, B.T., Hamdan, M.A., Pears, B.R., Sameh, H.I. (2019). Aridification of the Egyptian Sahara 5000-4000 cal BP revealed from x-ray fluorescence analysis of Nile Delta sediments at Kom al-Ahmer/Kom Wasit. *Quaternary International*, 514, 108-118.
- Petit-Marire, N., Riser, J. (1981). Holocene lake deposits and palaeoenvironment in central Sahara, northeastern Mali. *Palaeogeography, Palaeoclimatology, Palaeoecology*, 35, 45-61.
- Pi, D.H., Liu, C.Q., Zhou, G.A.S., Jiang, S.Y. (2013). Trace and rare element geochemistry of black shale and kerogen in the early Cambrian Niutitang Formation in Ghizhou province, South China: Constraints for redox environments and origin of metal enrichments. *Precambrian Research*, 225, 218-229.
- Pinta, M. (1982). *Modern methods for trace element analysis*. Ann Arbor Science Publisher, United States of America.
- Pinti, D. L. (2014). *Sub-oxic definition*. *Encyclopedia of Astrobiology*, GEOTOP Research Center for Geochemistry and Geodynamics, University of Quebec, Montreal, Canada.
- Pokrovsky, O.S., Dupre, B., Scott, J. (2005). Fe-Al-organic colloids control of trace elements in peat soil solutions: Results of ultrafiltration and dialysis. *Aquatic Geochemistry*, 11(3), 241-278.
- Polanski, S., Fallah, B., Befort, D.J., Prasad, S., Cubasch, U. (2014). Regional moisture change over India during the past millennium: A comparison of multi-proxy reconstructions and climate model simulations. *Global and Planetary Changes*, 122, 176-185.
- Poulichet, F.E., Nagy, A., Cserny, T. (1997). The distribution of redox sensitive elements (U, As, Sb, V and Mo) along a river-wetland-lake system (Balatin Region, Hungary). *Aquatic Geochemistry*, 3, 267-282.
- Prasad, S., Enzel, Y. (2006). Holocene paleoclimate of India. *Quaternary Research*, 66(3), 442-453.
- Prasad, V., Farooqui, A., Sharma, A., Phartiyal, B., Chakraborty, S., Bhandari, S., Raj, R., Singh, A. (2014). Mid-Late Holocene monsoonal variations from mainland Gujarat, India: A multi proxy study for evaluating climate culture relationship. *Palaeogeography, Palaeoclimatology, Palaeoecology*, 397, 38-51.

- Prasad, V., Utescher, T., Sharma, A., Singh, I.B., Garg, R., Gogoi, B., Srivastava, J., Uddandam, P.R., Joachimski, M.M. (2018). Low-latitude vegetation and climate dynamics at the Paleocene-Eocene transition from the Jathang section in northeastern India. *Palaeogeography, Palaeoclimatology, Palaeoecology*, 497, 139-156.
- Quamar, M.F., Chauhan, M.S. (2014). Signals of Medieval warm period and Little Ice Age from southwestern Madhya Pradesh (India): A pollen-inferred Late Holocene vegetation and climate change. *Quaternary International*, 325, 74-82.
- Quamar, M.F., Bera, S.K. (2014). Vegetation and climate change during mid and late Holocene in northern Chhattisgarh (central India) inferred from pollen records. *Quaternary International*, 349, 357-366.
- Raikesh, R. (1967). *Water, Weather and Prehistory*. London: John Baker.
- Ram, S.S., Aich, A., Sengupta, P., Chakraborty, A., Sudarshan, M. (2018). Assessment of trace metal contamination of wetland sediments from eastern and western coastal regions of India dominated with mangrove forest. *Chemosphere*, 211, 1113-1122.
- Ramesh, R., Bhattacharya, S.K., Gopalan, K. (1985). Dendroclimatological implications of isotope coherence in trees from Kashmir Valley, India. *Nature*, 317, 802-804.
- Rao, N., Vaidyanadhan, R. (1978). Geomorphic features in the Krishna delta and its evolution. *Proceedings of the symposium on morphology and evolution of landforms*. University of Delhi. Delhi, 120-130.
- Rao, G.N. (2001). Sedimentation, stratigraphy and petroleum potential of Krishna-Godavari basin, east coast of India. *AAPG Bulletin*, 85, 1623-1643.
- Rao, K.N., Sadakata, N. (1985). Evolution of landforms in the area between the Krishna and Godavari deltas. *Indian Geomorphic Journal*, 60, 30-36.
- Rao, K.N., Sadakata, N., Malini, B.H., Takayasu, K. (2005). Sedimentation processes and asymmetric development of the Godavari delta, India. *Society for Sedimentary Geology*, 113 (8), 433-449.
- Rao, K.N., Saito, Y., Nagakumar, K.C.V., Demudu, G., Basavaiah, N., Rajawat, A.S., Tokanai, F., Kato, K., Nakashima, R. (2012). Holocene environmental changes of the Godavari delta, east coast of India, inferred from sediment core analysis and AMS ¹⁴C dating. *Geomorphology*, 44, 47-66.
- Rao, K.N., Saito, Y., Nagakumar, K.Ch.V., Demudu, G., Rajawat, A.S., Sumiko Kubo, S., Zhen Li, Z. (2015). Palaeogeography and evolution of the Godavari delta, east coast of India during the Holocene: An example of wave dominated and fan delta setting. *Palaeogeography, Palaeoclimatology, Palaeoecology*, 440, 213-233.
- Rao, S.M. (1964). Some aspects of continental shelf sediments off the east coast of India. *Marine Geology*, 1, 59-87.
- Rashid, S.A., Ganai, J.A. (2018). Depositional environments, provenance and paleoclimatic implications of Ordovician clastic rocks of the Thango formation, Spity Valley, Tethys Himalaya, northern India. *Journal of Asian Earth Sciences*, 157, 371-386.

- Rath, P., Panda, U.C., Bhatta, D., Sahu, K.C. (2009). Use of sequential leaching, mineralogy, morphology and multivariate statistical technique for quantifying metal pollution in highly polluted aquatic sediment- a case study: Brahmani Nandira rivers, India. *Journal of Hazardous Materials*, 163, 632-644.
- Rathore, V.S., Nalhawat, M.S., Champatiray, P.K. (2010). Paleochannel detection and aquifer performance assessment in Mendha river catchment, Western India. *Journal of Hydrology*, 395, 216-225.
- Reddy, D.V., Singaraju, V., Mishra, R., Kumar, D., Thomas, P.J., Rao, K.K., Singhvi, A.K. (2013). Luminescence chronology of the sand dunes from SE India. *Quaternary Research*, 80, 265-273.
- Resmi, M.R., Achyuthan, H., Jaiswal, M.K. (2017). Middle to late Holocene paleochannels and migration of the Palar River, Tamil Nadu: Implications of neotectonic activity. *Quaternary International*, 443, 211-222.
- Retallack, G.J. (1999). Postapocalyptic greenhouse paleoclimate revealed by earliest Triassic paleosols in the Sydney basin, Australia. *Geological Science World Bulletin*, 111(1), 52-70.
- Riddle, C. (1993). *Analysis of Geological Materials* (eds). Marcel Dekker, Inc. New York.
- Rizea, N., Radul, L., Rodica, L., Store, V.M., Aldae, M.M. (2009) Reaction buffering capacity of soils in the Zlatna area. *Science papers of the University of Pardubice, A LII*, 70-75.
- Roalsdet, E. (1975). Rare earth elements distributions in some Precambrians rocks and their phyllosilicates, Numedal, Norway. *Geochimica et Cosmochimica Acta*, 39, 455-469.
- Roberts, N. (1998). *The Holocene: An environmental History*. Blackwell Publishers, UK.
- Rodriguez, A.B., Yu, W., Theuerkauf, E.J. (2018). Abrupt increase in washover deposition along e transgressive Barrier Island during the Late nineteenth century acceleration in sea-level rise. *Barrier Dynamics and Response to Changing Climate*, 121-145.
- Romano, S., Mugnai, C., Giuliani, S., Turetta, C., Huu, C.N., Belucci, L.G., Nhon, D.H., Caporaglio, G., Frignani, M. (2012). Metals in sediment cores from nine coastal lagoons in central Vietnam. *American Journal of Environmental Sciences*, 8, 130-142.
- Royer, A., De Angelis, M., Petit, J.R. (1983). A 3000 year record of physical and optical properties of microparticles from an East Antarctic ice core and implications for paleoclimate reconstruction models. *Climate Change*, 5(4), 381-412.
- Rudnick, R.L., Gao, S. (2014). *Composition of the Continental Crust*. Elsevier Publications, USA.
- Russ, J., Loyd, D.H., Boutton, T.W. (2000). A paleoclimate reconstruction for southwestern Texas using oxalate residue from lichen as a paleoclimate proxy. *Quaternary International*, 67, 29-36.
- Sageman, B.B., Lyons, T.W. (2003). Geochemistry of fine grained sediments and sedimentary rocks in *Sediments, Diagenesis and Sedimentary Rocks*. Elsevier, 115-158. DOI: <https://doi.org/10.1016/B0-08-043751-6/07157-7>.

- Sahoo, S., Planavsky, N.J., Kendall, B., Wang, X., Shi, X., Scott, C., Anbar, A.D., Lyons, T.W., Jiang, G. (2012). Ocean oxygenation in the wake of the Marinoan glaciation. *Nature*, 489(7417), 546-549.
- Saxena, A., Trivedi, A., Chauhan, M.S., Sharma, A. (2015). Holocene vegetation and climate change in Central Ganga Plain : A study based on multiproxy records from Chaudhary-Ka-Tal, Raebareli District, Uttar Pradesh, India. *Quaternary International*, 371, 164-174.
- Sayem, A.S.M., Guo, Z., Wu, H., Zhang, C., Yang, F., Xiao, G., He, Z. (2018). Sedimentary and geochemical evidence of Eocene climate change in the Xining Basin, northeastern Tibetan Plateau. *Science China Earth Sciences*, 61(9), 1292-1305.
- Selvakumar, V., Rajaguru, S.N., Jhaldiyal, R. (2012). Palaeolithic occupation of southern Tamil Nadu, India: New evidence from south of the river Kaveri. *Quaternary International*, 2012, 74-86.
- Selvaraj, K., Mohan, V.R., Szefer, P. (2004). Evaluation of metal contamination in coastal sediments of the Bay of Bengal, India: geochemical and statistical approaches. *Marine Pollution Bulletin*, 49, 174-185.
- Shaltout, A.A., Welz, B., Ibrahim, M.A. (2011). Influence of the grain size on the quality of standard less WDXRF analysis of river Nile sediments. *Microchemical Journal*, 99, 356-363.
- Shen, J., Algeo, T.J., Zhou, L., et al. (2012). Volcanic perturbations of the marine environment in South China preceding the Latest Permian mass extinction and their biotic effects. *Geobiology*, 10(1), 82-103.
- Shulmeister, J. (1992). A Holocene pollen record from lowland tropical Australia. *The Holocene*, 2, 107-116.
- Simms, M.J., Ruffell, A. H. (1990). Climatic and biotic change in the late Triassic. *Journal of Geological Society, London*, 147, 321-327.
- Singh, G., Joshi, R.D., Chopra, S.K., Singh, A.B. (1974). Quaternary history of vegetation and climate of the Rajasthan desert, India, *Philosophical Transactions of the Royal Society of London, Series B*, 267, 467-501.
- Singer, A. (1984). The paleoclimatic interpretation of clay minerals in sediments- A review. *Earth science Reviews*, 21(4), 251-293.
- Singh, H., Prasad, M., Kumar, K., Singh, S.K. (2011). Paleobotanical remains from the Paleocene-lower Eocene Vagadkhol formation, Western India and their Paleoclimatic and phytographic implications. *Palaeoworld*, 20 (4), 332-356.
- Singh, S., Prakash, B., Awasthi, A.K., Kumar, S. (2014). Do stable isotopes in carbonate cement of Nio-Pleistocene Himalayan sediments record paleogeological and paleoclimatic changes? *Palaeogeography, Palaeoclimatology, Palaeoecology*, 399, 363-372.
- Singh, K.T., Nayak, G.N., Fernandes, L.L., Borole, D., Basavaiah, N. (2014). Changing environmental conditions in recent past- Reading through the study of geochemical characteristics, magnetic parameters and sedimentation rate of mudflats, central west coast of India. *Palaeogeography, Palaeoclimatology, Palaeoecology*, 397, 61-74.

- Singh, A., Paul, Debjyoti, Sinha, Rajiv, Thomsen, K.J., Gupta, S. (2016). Geochemistry of buried river sediments from Ghaggar plains, NW India: Multi-proxy records of variations in provenance, paleoclimate, and paleovegetation patterns in the Late Quaternary. *Palaeogeography, Palaeoclimatology, Palaeoecology*, 449, 85-100.
- Sinha, R., Smykatz-Kloss, W., Stuben, D., Harrison, S.P., Berner, Z., Kramar, U. (2006). Late Quaternary paleoclimatic reconstruction from the lacustrine sediments of the Sambhar playa core, Thar Desert margin, India. *Palaeogeography, Palaeoclimatology, Palaeoecology*, 233 (3-4), 252-270.
- Springer, A.M., McRoy, C.P., Flint, M.V. (1996). The Bering Sea Green Belt: shelf-edge processes and ecosystem production. *Fish Oceanography*, 5, 205-223.
- Srivastava, J., Farooqui, A. (2013). Late Holocene mangrove dynamics and coastal environmental changes in the Northeastern Cauvery River Delta, India. *Quaternary International*, 298, 45-56.
- Swain, A.M., Kutzbach, J.E., Hastenrath, S. (1983). Estimates of Holocene precipitation for Rajasthan, India, based on pollen and lake-level data. *Quaternary Research*, 19(1), 1-17.
- Stanley, S.M., Yang, X. (1994). A double mass extinction at the end of the paleozoic era. *Science*, 1340-1344.
- Stern, L.A., Camberlain, C.P., Reynolds, R.C., Johnson, G.D. (1997). Oxygen isotope evidence of climate change from pedogenic clay minerals in the Himalayan molasses. *Geochimica et Cosmochimica Acta* 61(4), 731-744.
- Sterckeman, T., Douay, F., Baize, D., Fourrier, H., Proix, N., Schwartz, C. (2004). Factors affecting trace elements concentration in soils developed on recent marine deposits from northern France. *Applied Geochemistry*, 19, 89-103.
- Steinnes, E., Lierhagen, S. (2018). Geographical distribution of trace elements in natural surface soils: Atmospheric influence from natural and anthropogenic sources. *Applied Geochemistry*, 88, 2-9.
- Taylor, S.R., McLennan, S.M. (1985). *The continental Crust: Its Composition and Evolution*. Blackwell, London.
- Taylor, K., Konhauser, K. (2011). Iron in Earth surface systems: A major player in chemical and biological processes. *Elements*, 7 (2), 83-88.
- Tingley, M.P., Craigmile, P.F., Haran, M., Li, B., Mannshardt, E., Rajaratnam, B. (2012). Piecing together the past: statistical insights into paleoclimatic reconstructions. *Quaternary Science Reviews*, 35, 1-22.
- Tiwari, M., Sahu, S.K., Bhangare, R.C., Ajmal, P.Y., Pandit, G.G. (2013). Depth profile of major and trace elements in estuarine core sediments using the EDXRF technique. *Applied Radiation and Isotopes*, 80, 78-83.
- Thomas, P.J. (2009). Luminescence dating of beachrock in the southeast coast of India- potential for Holocene shoreline reconstruction. *Journal of Coastal Research*, 25 (1), 1-7.

- Thomson, L.G., Mosley-Thompson, E., Davis, M.E., Bolzan, J.F., Dai, J., Yao, T., Gundestrup, N., Wu, X., Klein, L., Xie, Z. 1989. Late Pleistocene climatic ice core records from Qinghai-Tibetan Plateau. *Science*, 246, 474-477.
- Tomazelli, L. J., Dillenburg, S. R. (2007). Sedimentary facies and stratigraphy of a last interglacial coastal barrier in south Brazil. *Marine Geology*, 244, 33-45.
- Tribovillard, N., Algeo, T.J., Lyons, T., Riboulleau, A. (2006). Trace metal as paleoredox and paleoproductivity proxies: an update. *Chemical Geology*, 232 (1), 12-32.
- Tripathi, S., Basumatary, S.K., Singh, V.K., Bera, S.K., Nautiyal, C.M., Thakur, B. (2014). Palaeovegetation and climate oscillation of western Odisha, India: a pollen data-based synthesis for the Mid-Late Holocene. *Quaternary International*, 325, 83-92.
- Tripathi, G.R., Singh, S.K., Ramaswamy, V. (2014). Major and trace element geochemistry of Bay of Bengal sediments: implications to provenances and their controlling factors. *Palaeogeography, Palaeoclimatology, Palaeoecology*, 397, 20-30.
- Tucker, M.E. (2003). *Sedimentary rocks in the field* (3rd edition). John Wiley and Sons, England.
- Turekian, K. K., Wedepohl, K.H. (1961). Distribution of the elements in some major units of the earth crust. *Geological Society of American Bulletin*, 72, 175-192.
- Tyagi, A.K., Shukla, A.D., Bhushan, R., Thakker, P.S., Thakkar, M.G., Juyal, N. (2012). Mid-Holocene sedimentation and landscape evolution in the western Great Runn of Kachchh, India. *Geomorphology*, 151, 89-98.
- Van, B. P., Polk, J.S., Asmerom, Y., Polyak, V. (2017). Late Pleistocene and mid-Holocene climate change derived from a Florida speleothem. *Quaternary International*, 449, 75-82.
- Vaidyanadhan, R., Ghosh, R.N. (1993). Quaternary of the east coast of India. *Current Science*, 64, 804-816.
- Vahila, M.N., Kumar, P., Bhogale, A., Chopra, S., Shinde, V., Jadhav, N., Shastri, R. (2016). Radiocarbon dating of charcoal samples from Rakhigarhi, Haryana using Accelerator Mass Spectrometer. *Current Science*, 3 (1), 27-28.
- Van Campo, E. (1986). Monsoon fluctuations in two 20,000 B.P. oxygen isotope/pollen Records off southwest India. *Quaternary Research*, 26 (3), 376-388.
- Vaz, G.G., Banerjee, P.K. (1997). Middle and Late Holocene sea level changes in and around Pulicat lagoon, Bay of Bengal, India. *Marine Geology*, 138, 261-271.
- Venkatrathnam, K. (1970). Formation of the barrier spit and other sand ridges near Chilka Lake on the east coast of India. *Marine Geology*, 9 (2), 101-116.
- Vuba, S., Farnaaz, S., Sagar, N., Ahmad, M. (2013). Geochemical and Mineralogical Characteristics of Recent Clastic Sediments from Lower Godavari River: Implications of Source Rock Weathering. *Journal Geological Society of India*, 82, 217-226.
- Wang, H., Shao, X., Li, M. (2019). A 2917-year tree-ring-based reconstruction of precipitation for the Buerhanbuda Mts., Southern Qaidam Basin, China. *Dendrochronologia*, 55, 80-92.

- Walkley, A., Black, I.A. (1934). Chemical soil tests. Cornell University. *Agricultural Expedition Experiment Station Buletine*,. 960, 34-36.
- Warrick, R. A., Barrow, E. M., Wigley, T. M. L. (1993). *Climate and Sea Level Change: Observations, Projections and Implications*. Wiley Publications, Cambridge.
- Warrier, A.K., Pednekar, H., Mahesh, B.S., Mohan, R., Gazi, S. (2016). Sediment grain size and surface textural observations of quartz grains in late quaternary lacustrine sediments from Schirmacher Oasis, East Antarctica: Paleoenvironmental significance. *Polar Science*, 10 (1), 89-100.
- Watts, N.L. (1980). Quaternary pedogenic calcretes from Kalahari (southern Africa), mineralogy, genesis, and diagenesis. *Sedimentology*, 27: 661-686.
- Weiss, H., Bradley, R.S. (2001). Archaeology, what drives societal collapse? *Science*, 291, 988.
- Yadav, A., Kumar, P., Anoop, A., Mishra, P.K., Varghese, S. (2017). Mid-late Holocene climate variability in the Indian monsoon: Evidences from continental shelf sediments adjacent to Rushikulya river, eastern India. *Quaternary International*, 443, 155-163.
- Zhao, Y.Y., Yan, M.C. (1994). *Geochemistry of sediments of the China shelf sea*. Science Press, Beijing.
- Zwolsman, G., vanEck, B., derWeijden, C.H. (1997). Geochemistry of dissolved trace metals (cadmium, copper, zink) in the Scheldt Estuary, southwestern Netherlands: Impact of seasonal variability. *Geochimica et Cosmochimica Acta*, 61(8), 1635-1652.